Development of innovative approaches for characterizations of magnetic particles and target (bio)molecules

Ngoc-Van-Thanh Nguyen

THESE DE DOCTORAT

NNT : 2023UPASF025

université PARIS-SACLAY

Development of innovative approaches for characterizations of magnetic particles and target (bio)molecules

Développement d'approches innovantes pour la caractérisation de particules magnétiques et de (bio)molécules cibles

Thèse de doctorat de l'université Paris-Saclay

École doctorale n° 571 : sciences chimiques : molécules, matériaux, instrumentation et biosystème (2MIB)
Spécialité de doctorat : chimie
Graduate School : Chimie. Référent : Faculté des Sciences d'Orsay

Thèse préparée dans l'unité de recherche **IGPS (Université Paris-Saclay, CNRS)**, sous la direction de **Claire SMADJA**, Professeure, le co-encadrement de **Thanh Duc MAI**, Maître de conférences

Thèse soutenue à Paris-Saclay, le 13 avril 2023, par

Ngoc-Van-Thanh NGUYEN

Composition du Jury

(Membres du jury avec voix délibérative)

Anne VARENNE Professeure, i-CLeHS, Chimie ParisTech	Président du jury
Emmanuelle LIPKA Professeure, Université de Lille	Rapportrice & Examinatrice
Farid OUKACINE Maître de conférences, HDR Université de Grenoble	Rapporteur & Examinateur
Bruno LE PIOUFLE Professeur, Université Paris-Saclay (CNRS FR3242)	Examinateur
Thibaut DEVILLERS Maître de conférences, Institut Néel Université de Grenoble	Examinateur

université PARIS-SACLAY

ÉCOLE DOCTORALE
Sciences Chimiques: Molécules, Matériaux, Instrumentation et Biosystèmes (2MIB)

Titre : Développement d'approches innovantes pour la caractérisation de particules magnétiques et de (bio)molécules cibles.

Mots clés : Électrophorèse capillaire, billes magnétiques, ADN, anticorps, peptide bêta-Amyloïde 1-42.

Abstrait : Les particules magnétiques de taille micro/nanométriques, plus particulièrement à base d'oxyde de Fer (Fe_2O_3, Fe_3O_4) sont très utilisées dans le domaine biomédical. Dans le cadre de ma thèse nous nous sommes intéressés aux méthodes exploitant les particules magnétiques pour la détection de biomarqueurs présents dans les fluides biologiques à très faibles taux. Mes travaux ont porté sur trois axes.

Le premier axe a visé à contrôler la densité et l'orientation des anticorps greffés de manière covalente sur des billes. Ceci en réalisant une digestion enzymatique préalable de l'anticorps et en analysant le digestat par chromatographie d'exclusion stérique. Cette approche a été appliquée à la capture du peptide bêta-amyloïde 1-42 (Aβ1-42), biomarqueur de la maladie d'Alzheimer.

Le deuxième axe a consisté à développer une méthode innovante d'électrophorèse capillaire couplée à la détection par fluorescence induite par laser (CE-LIF) permettant la préconcentration électrocinétique des nanoparticules. Cette méthode a été utilisée pour caractériser l'interaction des billes à très faibles concentrations (µM) avec des antibiotiques (kanamycine, amikacine).

Dans la dernière partie de ma thèse, les deux étapes: magnéto-extraction, à l'aide de nanoparticules magnétiques, et préconcentration électrocinétique ont été réalisées en ligne au sein du même capillaire. Cette combinaison réalisée pour la première fois a été utilisées pour extraire, préconcentrer et séparer un ADN double brin dans une capillaire unique. Pour cette expérience, un instrument dédié a été développé au laboratoire.

Title : Development of innovative approaches for characterizations of magnetic particles and target (bio)molecules

Keywords : Capillary electrophoresis, magnetic beads, dsDNA, antibodies, amyloid-beta peptides.

Abstract : The micro/nanometric magnetic particles, especially the beads constituted by Fe_3O_4 and Fe_2O_3 are widely used today for diverse applications in the biomedical. In my thesis, I focused on the application of magnetic beads for the biomarker detection in biofluids and their interaction. Hence, I propose three innovative analytical methods for this purpose.

The first strategy relies on controlling the density and orientation of antibodies covalently grafted on beads, using enzymatic digestion, followed by size exclusion chromatography-fluorescent detector (SEC-FLD) analysis. This approach was then applied for magneto-immunoassays of amyloid-beta peptide 1-42 (Aβ1-42), an established biomarker of Alzheimer's disease.

The second strategy is to develop a new capillary electrophoresis method coupled with- laser induced fluorescent detection (CE- LIF) to characterize the interaction of beads at very low concentrations with antibiotics (kanamycin and amikacin) during electrokinetic preconcentration and separation processes.

In the last strategy, a new on-line dual-stage of enrichment via magneto-extraction and electrokinetic preconcentration are developed to capture, label, elute and separate dsDNA in the same capillary. A home-made instrument was also built for the concept.

RÉSUMÉ DE LA THÈSE EN FRANÇAIS

Les particules magnétiques (PMs) de taille micro/nanométrique sont fréquemment employées dans le domaine biomédical, notamment pour extraire des biomarqueurs d'un milieu complexe, ou pour le développement de dispositifs miniaturisés (laboratoires sur puce, biocapteurs, etc). Cependant, il est important de noter que le développement d'outils de diagnostic liés aux particules magnétiques repose sur leur interaction avec des molécules cibles. Celles-ci dépendent notamment des propriétés physico-chimiques des PMs. Aussi leur caractérisation est primordiale. Les objectifs de cette thèse sont de développer deux nouvelles techniques pour caractériser (i) l'orientation et la densité d'anticorps greffés sur des billes magnétiques et (ii) l'interaction entre ces particules avec des antibiotiques. De plus, une approche d'extraction et préconcentration de l'ADN en utilisant des PMs a été également démontrée.

Par ailleurs, l'électrophorèse capillaire (EC) est une technique séparative qui présente de nombreux avantages tels que le faible volume d'échantillon consommé, un temps d'analyse court ainsi qu'une haute résolution. En outre, elle peut être couplée à plusieurs modes de détection comme le détecteur à ultraviolet (UV), la fluorescence induite par laser (FIL) et la spectrométrie de masse (SM). Cependant, c'est une méthode peu sensible et les macromolécules biologiques tels que les peptides ou les protéines peuvent s'adsorber sur les parois du capillaire. Au vu de ces limitations, des stratégies pour améliorer la sensibilité de détection ont été développées. La première approche a visé à caractériser l'orientation et la densité d'anticorps anti bêta-Amyloïde Aβ 1-42 immobilisés sur trois groupes de billes magnétiques. Deux groupes présentant à leur surface des groupements : Tosyls, ou Carboxylique. Le troisième groupe est constitué par des billes présentant à leur surface des Protéine G qui permettent une immobilisation orientée des anticorps. Cette étude a été réalisée à l'aide d'un enzyme de digestion l'IdeZ, clivant les anticorps en deux fragments de taille différent ($F(ab)_2$ et Fc). Le digestat obtenu a ensuite été analysé par la chromatographie d'exclusion stérique (SEC) couplée à une détection à fluorescence. En se basant sur le ratio des

fragments digérés $F(ab)_2$/Fc, les deux billes, Tosylé et Protéine G, montrent une meilleure orientation et densité d'anticorps immobilisés à leur surface. Elles ont donc été utilisées pour capturer le peptide bêta-Amyloïde Aβ1-42.

La deuxième stratégie a visé à caractériser l'interaction des billes à très faibles concentration avec les antibiotiques en utilisant une nouvelle méthode d'EC couplée à la détection FIL. Une nouvelle méthode de préconcentration électrocinétique, en utilisant des molécules organiques ayant des charges très faibles, a également été développée afin d'augmenter la sensibilité de détection de l'EC.

Le troisième axe a porté sur l'extraction et l'enrichissement de fragments d'ADN en combinant : une capture dynamique par les PMs circulant au sein du capillaire, et avec la préconcentration électrocinétique développée précedemment.

En conclusion, ces travaux ont contribué à l'amélioration des connaissances de l'interaction des PMs (fonctionnalisées ou non avec des anticorps) et des (bio)molécules, et de leur application potentielle dans le domaine de l'analyse et biomédical.

ACKNOWLEDGEMENTS

First of all, I would like to thank my thesis director, Professor Claire SMADJA, for accepting and giving me an opportunity to follow Ph.D. program in PNAS team, supporting as well as helping me in many difficult situations, both scientifically and personally. Her kindness, generosity, comprehension, and listening are precious motivation for me to overcome the challenges and finish the project. A big thank you to my thesis co-supervisor, Doctor Thanh Duc MAI, for his valuable advices, unfailing optimism, and unending motivation every day during more than three years. Thanks to your extensive scientific knowledge and skills, I learned a lot and able to work independently or challenge myself in many projects and daily work now. It is a great pleasure to work for those years under both of your supervisors. We are always a great team!

A particular thanks to Professor Myriam TAVERNA for welcoming me to the team and her precious advices for my thesis, my publications and lab life also. Thank you to Dr. Thuy Tran, a special team member, a big friend, who shared amazing ideas with me for scientific and personal life projects, who encourage me through a rough time. After 3 years, I still do not understand all the french words you say, Thuy!

I would like to thank Professor Emmanuel LIPKA, Farid OUKACINE, Professor Bruno LE PIOUFLE, Thibault DEVILLERS, and Professor Anne VARENNE who give me the honor of being members of my thesis jury. I would also like to thank Doctor Jean-Michel SIAUGUE for agreeing to be the external member of my thesis committee, for advising me throughout this project and for his collaboration.

I also want to express my appreciation to Professor Isabelle TURBICA and Dr. Myriam Nahban with whom we had the chance to collaborate and participate their interesting class of therapeutic antibodies. I would like to express my gratitude to Dr Frederic HALGAND for his invaluable assistance with mass spectrometry and to Professor Stephanie DECROIX for her collaboration.

Thank you also to the PNAS (Proteins and Nanotechnology in Analytical Sciences) team members: Marie-Claude, Sylvie Z., Patricia, Fatiah, Maria, Lynda and Orane for their daily logistical assistance. Thank you very much for the countless delicious cakes and other goodies.

I would also like to express my gratitude to the former and new doctoral students as well as the interns and postdocs, I had the chance to meet during my thesis: Seray, Etienne, Ayoub, Camille, Clara, Lucile, Théo, Marco, Joanie, Cécile, Bin, Delaram, Sameh, Charlotte, Mathilde, Emilie. You all make my three years so special and unforgettable. Thank you for sharing food, culture, helping me to adapt to daily life, joking, hanging out, keeping me away from troubles. It is so lucky to work in an international team.

Thank you to all my Vietnamese friends in France, chị Trâm, Thành, Quỳnh Anh, Chí Hồng, Hải, Hòa, Hà, Linh, Duy, Thảo. We spent amazing weekends and vacations altogether. You give me the support and encouragement I need to overcome the most difficult days as well as share the happiness with me in the most special day of my life. Far from our country, we had a lot of blasts.

I also want to thank my family in Vietnam and in France, especially, my parents and the family of my cousin who love me unconditionally, witness my growth from the very first days and give me the strength to finish the thesis as well as other projects. Although I cannot see one of them again, I know he is still watching and taking care of me from somewhere.

Last but not least, thanks to my husband, Dr. Minh-Thang LE, who always stands by me through 3 years, and tolerates all my childishness, stubbornness, laziness, and "chiante" sometimes. You are a strict, unpleasant tutor who never gives me directly the answers without making me search and think about it. It was annoying but frankly, I learned a lot of skills. Thanks for being a great partner with much patience, love, and tenderness that nobody can imagine. However, the rule is always the same:

''NO ANALYTICAL CHEMISTRY AT HOME, CHÉRI!''

CURRICULUM VITAE

Education:

• M.Sc. Drug Sciences at Université Claude Bernard Lyon 1, Specialized in Innovative Pharmaceutics and Analytical Development

• Ph.D. at Université Paris-Saclay Analytical Chemistry, Institut Galien Paris-Saclay.

Oral communications:

• "Novel Strategies for Elucidation of the Interaction Between Functionalized Magnetic Beads-Pharmaceutical and Diagnostic Molecules", 37th International Symposium on Microscale Separations and Bioanalysis (MSB2021), online.

• "2D in-line enrichment by circulating magnetic beads and electrokinetic preconcentration: a new concept and instrumentation for dsDNA analysis by capillary electrophoresis", Analytics 2022, Nantes, France.

Publications:

• Nguyen, N.V.T., Smadja, C., Taverna, M., Halgand, F., & Mai, T. D. (2023). Immuno-capture of biomolecules on functionalized magnetic beads: from characterization to application for a biomarker of Alzheimer's disease. (Talanta Open- Submitted)

• Nguyen, N.V.T., Smadja, C., Taverna, Nguyen, H.L.T., Descroix, S., & Mai, T. D. (2022). On-line dual-stage enrichment via magneto-extraction and electrokinetic preconcentration: a new concept and instrumentation for capillary electrophoresis. Analytica Chimica Acta 1225, 341141.
DOI: https://doi.org/10.1016/j.aca.2023.341141

• Nguyen, N.V.T., Smadja, C., Taverna, Nguyen, H.L.T., & Mai, T. D. (2021). Electroosmotic flow modulation for improved electrokinetic preconcentration : application to capillary electrophoresis of fluorescent magnetic nanoparticles. Analytica Chimica Acta 1161, 338466.
DOI: https://doi.org/10.1016/j.aca.2021.338466

• Nguyen, N.V.T., Smadja, C., Taverna, Nguyen, H.L.T., & Mai, T. D. (2020). Recent Electrokinetic and Microfluidic Strategies for Detection of Amyloid Beta Peptide Biomarkers: Towards Molecular Diagnosis of Alzheimer Disease. (Review) Chemical Record 21, 149–161.
DOI: https://doi.org/10.1002/tcr.202000103

LIST OF ABBREVIATIONS

AAB	4-aminoazobenzene
AD	Alzheimer disease
Anti-EpCAM	Antibody anti-epithelial cell adhesion
APP	Amyloid precursor protein
APTS	1-aminopyrene-3,6,8-trisulfonic acid
ASAPs	Actuatable surface attached posts
Aβ 1-42	Amyloid beta 1-42 peptide
BGE	Background electrolyte
BHB	Bovine hemoglobin
BSA	Bovine serum albumin
C4D	Capacitively-Coupled Contactless Conductivity Detectors
CAPS	N-cyclohexyl-3-aminopropanesulfonic acid
CE	Capillary electrophoresis
CGE	Capillary gel electrophoresis
CHES	N-Cyclohexyl-2-aminoethanesulfonic acid
CMCS	Carboxymethylated chitosan
Con-A	Concanavalin A
CSF	Cerebrospinal fluid
MCE	Microchip electrophoresis
CRM	Certified reference material
POC	Point-of-care
IPA	Isopropanol
EDC	N-(3-Dimethylaminopropyl)-N'-ethylcarbodiimide hydrochloride
S-NHS	N-Hydroxysulfosuccinimide sodium salt
PBS	Phosphate buffer saline
CSMNPs	Core-shell magnetic nanoparticles
FITC	Fluorescein isothiocyanate
GBI	Good buffer index
PDI	Polydispersity index
CTC	Circulating tumor cells
CTMA	Cetyltrimethylammonium bromide
cyt C	Cytokine C
CZE	Capillary zone electrophoresis

DEA	Diethanolamine
DLS	Dynamic light scattering
DMSO	Dimethyl sulfoxide
DNA	Deoxyribonucleic Acid
EA	Ethanolamine
EAE	Autoimmune encephalomyelitis
EDC	3-ethyl-carbodiimide
EDTA	Ethylenediaminetetraacetic acid
EKC	Electrokinetic supercharging
ELISA	Enzyme-linked immunoassay
EOF	Electroosmotic flow
F127	Pluronic
FASI	Field-amplified sample injection
FASS	Field-amplified sample stacking
FDA	Food and drug administration
FDG	Fluorodeoxyglucose
FLD	Fluorescent detector
FS- NPs	Functionalized nanoparticles
FTIR	Fourier transform infrared spectroscopy
GO	Graphene oxide nanosheets
HEC	Hydroxyethylcellulose
HEPES	2-[4-(2-hydroxyethyl)piperazin-1-yl]ethanesulfonic acid
HER2	Human Epidermal Growth Factor Receptor-2
HER3	Human Epidermal Growth Factor Receptor-3
hIgG	Human Immunoglobulin G
HPMC	Hydroxypropylmethylcellulose
HRP	Horseradish peroxidase
ICP	Inductively coupled plasma
ID	Inner diameter
IdeS	Immunoglobulin G degrading enzymes (FabRICATOR S)
IdeZ	Immunoglobulin G degrading enzymes (FabRICATOR Z)
IEP	Isoelectrical point
IR	Infrared spectroscopy
IS	Ionic strength

ITP	Isotachophoresis
LE	Leading electrolyte
LEDIF	LED-induced fluorescence detector
LIF	Laser-induced fluorescence detector
LOC	Lab-on-chip
LOD	Limit of detection
LOQ	Limit of quantification
LPA	Linear polyacrylamide
LVSEP	Large volume sample stacking with electroosmotic pump
LVSS	Large volume sample stacking
LYZ	Lysozyme
MALDI-TOF	Matrix-assisted laser desorption/ionization-time of flight
MALS	Multi angles light scattering
MES	2-(N-morpholino)ethanesulfonic acid
mIgG	Mouse Immunoglobulin G
MNPs	Magnetic nanoparticles
MOPS	3-(N-Morpholino)propane sulfonic acid
MPs	Magnetic particles
MRI	Magnetic resonance imaging
MS	Mass spectrometry
NHS	N-Hydroxysuccinimide
NPs	Nanoparticles
NTA	Nanoparticle tracking analysis
PAA	Poly acrylic acid
PBS	Phosphate buffered saline
PDDA	Poly(diallyldimethylamonium chloride)
PEG	Polyethylene glycol
PEI	Polyethylene imide
PEO	Polyethylene oxide
PET	Positron emission tomography
PGMA	Poly (glycidyl methacrylate)
PMG	Poly(N,N′-methylenebisacryla-mide-co-glycidyl methacrylate)
PMMA	Poly methyl methacrylate
PPO	Poly(phenylene oxide)

ProG	Protein G
PS_{250}-*b*-PAA_{13}	Poly($styrene_{250}$-block-$acrylic\ acid_{13}$)
PVA	Polyvinyl alcohol
PVP	Polyvinylpyrrolidone
RGO	Reduced graphene oxide
RNA	Ribonucleic acid
SARS-CoV-2	Severe acute respiratory syndrome coronavirus 2
SC	Spycatcher
SEC	Size exclusion chromatography
SEM	Scanning electron microscope
SMBs	Silica-coated magnetic beads functionalized with carboxylic group
SNPs	Superparamagnetic Fe_3O_4 nanoparticles
SQUID	Superconducting quantum interference device
TAM	Tumor-associated macrophages
TAPS	Tris(hydroxymethyl)methylamino] propanesulfonic acid
TBE	Tris-borate-EDTA buffer
TBS	Tris buffer saline
TE	Terminating electrolyte
TEA	Triethanolamine
TEM	Transmission electron microscope
Tris	2-Amino-2-hydroxymethyl-propane-1,3-diol
TRT	Apo-transferrin
Ts	Tosyl-activated
UV	Ultraviolet
β CD	Beta cyclodextrin

CONTENT

GENERAL INTRODUCTION

Micrometric and nanometric magnetic particles (MPs) are widely used nowadays in biomolecule analysis, and magnetic resonance imaging (MRI). These MPs have a common core-shell structure, covered by an optional surface layer. Among the particles, the beads made by magnetite (Fe_3O_4) or maghemite (Fe_2O_3) attract much attention of scientist since they have the unique superparamagnetic properties as well as the capacity for surface modification to provide multifunctional design. Since these particles are normally manipulated in biological fluids and used in patients as the contrast agents for MRI, their performance and toxicity are taken into account. Interestingly, they are related to the stability, size, morphology, surface properties of MPs and their interaction with (bio)molecules. Therefore, the characterizations that allow to assess the MPs' properties are highly necessary.

So far, there are several established methods to analyze the size and morphology (e.g., electron microscope, etc.), hydrodynamic radius (e.g., dynamic light scattering, etc.) and functionalized surface groups of beads (e.g., infrared spectroscopy, etc.). Particularly, for characterizing the MPs' interaction with (bio)molecules, capillary electrophoresis (CE) is commonly used. CE, one of the separative techniques based on the migration of charged molecules under an electrical field, can also characterize the surface charge and size of particles. The technique has some advantages such as high selectivity, small volume sample requirement and short time analysis. Moreover, CE can couple to many detectors (e.g., ultraviolet, fluorescent, etc.) to give diverse MPs' information. Nevertheless, the low sensitivity is emphasized as its limitation, leading the difficulty in detecting analytes which exist at low abundance in biosample. Consequently, many forefronts electrokinetic preconcentration strategies are developed to optimize the sensitivity detection of CE such as isotachophoresis, field-amplified sample stacking, etc. The second consideration of CE is the adsorption of analyte on capillary wall and the precipitation of MPs inside narrow capillary during separation.

Regarding the context, the main objective of the thesis is to develop innovative analytical methods to characterize (i) the MPs and their interaction with aminoglycoside antibodies; (ii) the orientation and density of antibody immobilized on MPs. The second aim is to perform a new approach to extract and enrich DNA target by combining CE with MPs. The strategies to optimize the CE sensitivity are also investigated in our project.

The bibliography part includes two chapters. **The first chapter** presents the overview of common MPs' structure, their applications in diagnosis imaging and especially in biomolecule analysis as a solid support. **The second chapter** describes the working principles of CE and some electrokinetic

preconcentration techniques. Various applications of CE to analyze amyloid beta peptide, DNA and MPs as well as the preconcentration approaches for enrichment of these targets are also presented in this chapter.

The experimental part of the manuscript is divided into three chapters that describe three developed strategies to achieve two main objectives of our project.

The third chapter focuses on the method development of Size Exclusion Chromatography (SEC) coupled to fluorescent detector (FLD) and enzymatic strategy to control the interaction between three types of MPs with antibodies grafted on beads. The beads have better grafted antibody density and orientation are selected for magneto-immunoassays of amyloid beta peptide.

The fourth chapter was put on a new EOF-assisted preconcentration method in CE coupled to laser-induced fluorescent detector to increase the detection sensitivity. The technique is based on the utilization of weakly charged ions as buffer separation. It is successfully demonstrated to enrich and characterize MPs and MPs 'interaction with antibiotics (kanamycin and amikacin) as well as amyloid beta peptide preconcentration in silica capillary without recourse any coating.

The combination of the new EOF-assisted preconcentration method CE (presented in chapter 4) and MPs for an extraction and enrichment approach is described in **chapter 5.** A home-made system with two pairs of tweezers were installed, allowing the MPs to circulate forth-and-back inside the capillary. This novel concept was successfully demonstrated for extracting and preconcentrating DNA target prior the CE separation.

BIBLIOGRAPHY PART

Chapter 1: MAGNETIC BEADS FROM CHARACTERIZATION TO THEIR BIOMEDICAL APPLICATIONS

Over the years, micro/nano magnetic particles have found a growing interest in biomedical field. This is related to their easy synthesis, tunable size and structure as well as high specific areas. In addition, their magnetic properties allow easy manipulation under an external magnetic field. Among magnetic particles (MPs), particularly iron oxide, magnetite (Fe_3O_4) or maghemite (Fe_2O_3), offer a great potential thanks to their unique superparamagnetic properties and capacity for surface modification to provide multifunctional design [1]. As a result, these iron oxide magnetic particles have attracted much attention in the scientific community [2]. This chapter will present the magnetic particles' structure, their applications in the biomedical field, and the analytical methods to characterize them.

1.1 MICRO/NANOMAGNETIC PARTICLES

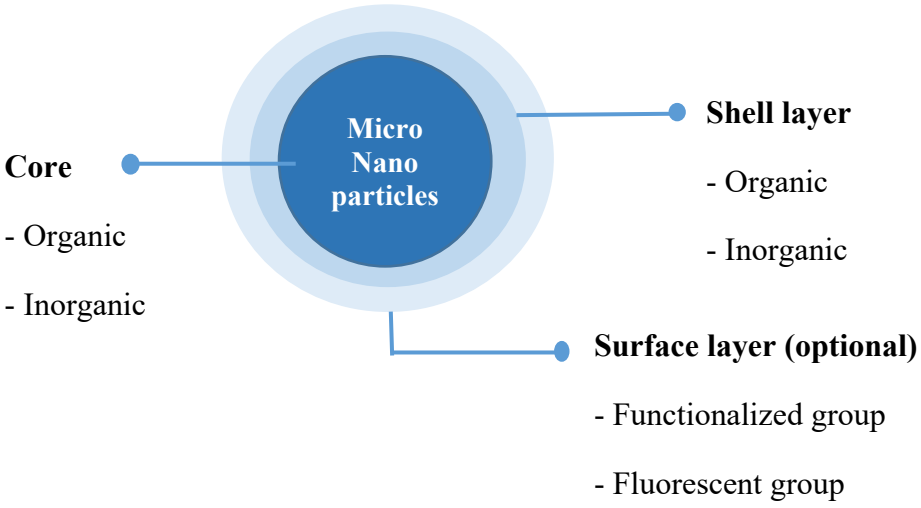

Figure 1: The core-shell structure of micro/nanoparticles [3].

Micro (diameter from 1 µm to hundred micrometers) and nanoparticles (from 1 nm to hundred nanometers) have a common principal structure composed by three layers *(Figure 1)* [3, 4]. A magnetic core covered by a shell layer made from inorganic, organic or hybrid materials bounded covalently or non-covalently (through physical interactions). The third layer (surface) is optional, depending on the purposes (e.g., fluorescent dye for detection or bioreceptor for bioseparation). The stability, biocompatibility, and biodegradation of particles relies mainly on the shell layer [5]. Different types of coating commonly used will be presented in the following parts.

1.1.1 Core

Metallic cores are made of transition metals (Fe, Co, Ni) or metal oxide such as Fe_2O_3, Fe_3O_4, etc. Indeed, pure metals such as Fe or Co are prone to oxidize and are highly toxic. As a result, iron oxide particles are preferred, even though pure metals possess the highest saturation magnetism. The Fe_2O_3, Fe_3O_4 particles have high magnetic susceptibility, non-toxicity and chemical stability [6]. These ferrite colloids are synthesized under various forms (spherical, cylindrical, tubular, hollow core, spiral, etc.) and by different methods [7, 8]. However, bare magnetic nanoparticles are prone to aggregate in solution due to their nanoscale size, large specific area, high specific surface energy and magnetic dipole interactions [6]. Therefore, numerous strategies to modify the surface layer of MPs have been investigated.

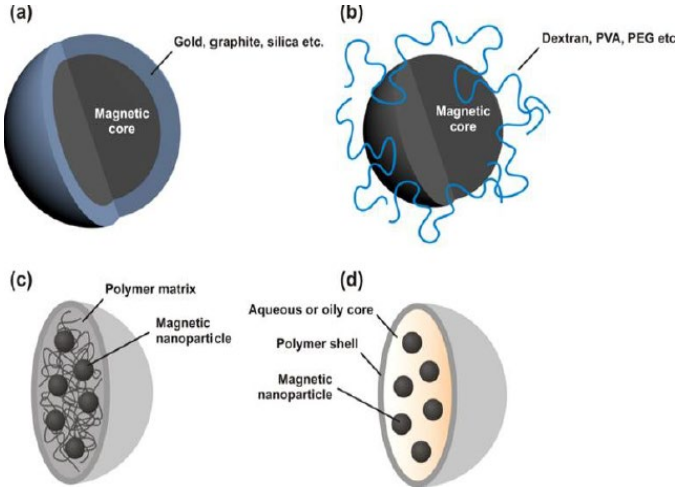

Figure 2: Some core-shell structures of micro/nano magnetic particles. Surface coating with a) Inorganic metals (gold, silver, silica); b) Natural /Synthetic polymer; or polymeric shells surround an aqueous or oily core, making c) nanosphere; d) nanocapsule [9].

1.1.2 Shell surface's modifications

MPs surface modifications by organic compounds are an important step regarding magnetic particles stability during their synthesis and storage. Surface modifications could also provide functionalization for further conjugation with bioactive molecules or targeting ligands, to obtained multifunctional MPs [3].

Several approaches could be proposed to achieve the coating surface *(Figure 2):*

1. Coating with natural polymers (e.g., dextran, chitosan) or synthetic polymers (e.g., polyvinyl alcohol (PVA) or polyethylene glycol (PEG), polyethylene imine (PEI)) *(Figure 2b)*

2. Generating polymeric shells surrounding aqueous or oily core to avoid cluster growth after nucleation *(Figure 2c, d).*

3. Deposing the layers of inorganics metal, gold, silver, or silica *(Figure 2a).*

Stabilization of MPs is of paramount importance considering their broad application. Compared to other coating materials presented above (e.g., silica, gold, etc.), polymeric coatings offer excellent colloidal stability. They also prevent the core from oxidation, could ensure core protection under physiological conditions and render the beads more permeable. However, it should be carefully monitored as they can be altered by temperature and pH variation [10, 11].

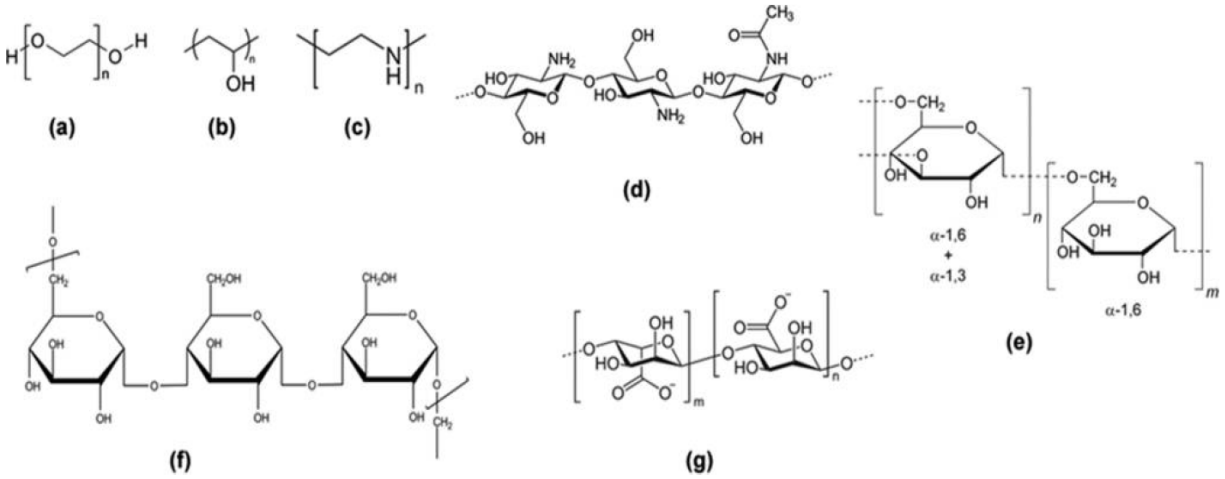

Figure 3: Structures of polymers for magnetic particles coating a) PEG, b) PVA, c) PEI, d) chitosan, e) dextran, f) pullulan, and g) alginate [9].

More importantly, these shell surface modifications allow the immobilization of various functional groups such as amine, carboxyl, epoxy, tosyl, hydroxyl, N-hydroxysuccinimide as well as biological molecules such as biotin, streptavidin, protein A, protein G, and antibodies [12]. Conjugation of antibodies to the surface of beads can occur through various chemical functions, such as bioconjugation reactions [13] or through streptavidin-biotin [14] or Protein A/G type bioaffinity interactions (specifically capture antibodies through their Fc fragment) [15]. The immobilization of biomolecules such as antibodies on the surface of beads has opened the way to several applications in biomedical, notably in the separation and preconcentration of analytes [16].

However, taking into account that MPs are often manipulated in biological fluids, characterizations assessing their stability, size, morphology and surface properties are essential. The main methods employed to characterize MPs will be presented hereafter.

1.2 CHARACTERIZATION METHODS FOR MPS

The changes in size and morphology of MPs can alter their physicochemical properties while changes in surface's charge, or functionalized group can modify their performance. Hence, many characterization techniques are employed to analyze the physical and chemical properties of beads. These established methods are summarized in *Table 1* below.

Table 1: Methods of magnetic particles's characterization

Techniques	Provided information	References
Electron microscopes	TEM: Morphology, size, structure, aggregation SEM: Morphology, size, surface topography	[17-19]
X-ray technologies	Morphology, crystallinity, size, aggregation state	[20, 21]
Dynamic light scattering (DLS)	Hydrodynamic radius, size distribution, colloidal stability, aggregation state	[22-24]
Nanoparticle tracking analysis (NTA)	Hydrodynamic radius, size distribution, aggregation state, particle's mouvement	[25, 26]
Zeta potential	Surface' charge in term of pH, colloidal stability	[27, 28]
Superconducting quantum interference device (SQUID)	Magnetic moment	[29, 30]
Infrared spectroscopy (IR)	Chemical identification of binding groups on MP's surface	[31-33]
Capillary electrophoresis (CE)	Size, charge, interaction between MPs and (bio)molecules, structure	To be discussed in chapter 2

In this part, the most commonly employed methods in the field of magnetic bioseparation and diagnosis will be presented, such as electronic microscopies, DLS, zeta potential and IR.

1.2.1 MPs morphology, crystallinity, size

Electron microscopes

Transmission electron microscope (TEM) and scanning electron microscope (SEM) are often employed to study the morphology of micro/nano particles. Although both methods use electron

source for imaging, TEM provides information regarding the structure, morphology, and size of MPs while SEM gives information regarding surface topography. The important difference between them is that in an SEM experiment, the electron emitted from the irradiated sample is detected. In TEM, the electron beam passes through the sample, and the transmission change is recorded (*Figure 4*) [34].

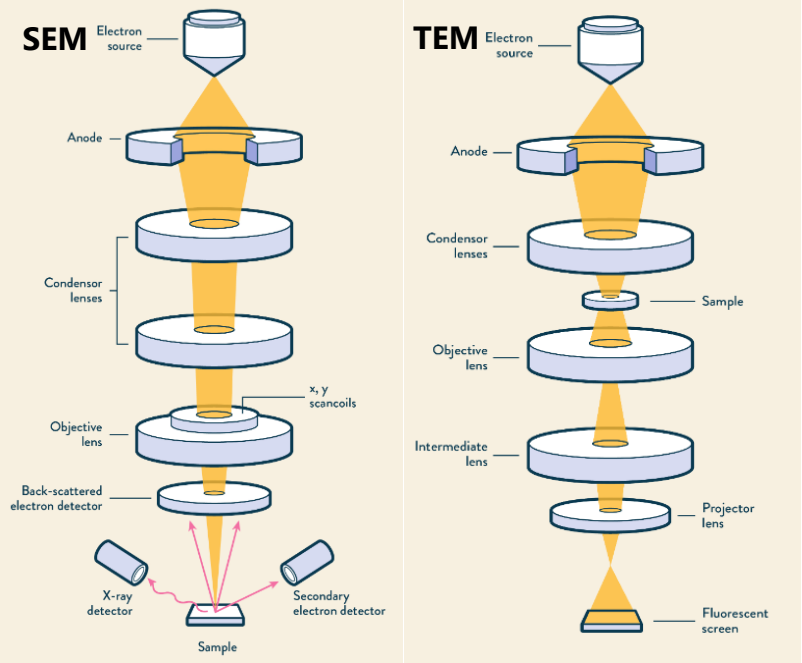

Figure 4: Illustration of working mechanism of SEM and TEM [34].

Imaging provided by electron microscopies is related to the contrast due to the absorption, scattering, and diffraction of the electrons from the target. It depends greatly on the composition, but also on the thickness of the material studied. Thus, MPs, which are often high-mass and highly crystalline, will appear darker than the surrounding media. Conversely, the matrix and small molecules will appear in the brighter zone due to the lack of scattered electron to camera [35]. Consequently, morphology, size (down to 1 nm), as well as bonding information of magnetic beads and target molecule could be revealed. However, it is important to note that the samples are analyzed in a vacuum which can require a time-consuming preparation.

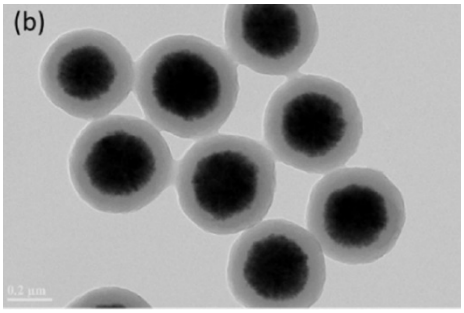

Figure 5: TEM image of Fe_3O_4/PMG microspheres [17].

TEM reveals the core-shell structure, morphology, and size of MPs. For instance, we can see from *Figure 5* that the magnetic colloid nanocrystal cluster (Fe_3O_4, hydrodynamic diameter 290 nm) is covered by a thick poly (N,N′-methylenebisacrylamide-co-glycidyl methacrylate) (PMG) layer. The measured hydrodynamic diameter after coating is from 600-800 nm, depending on the amount of glycidyl methacrylate added. *Figure 5* shows also the uniform shape of Fe_3O_4/PMG [17].

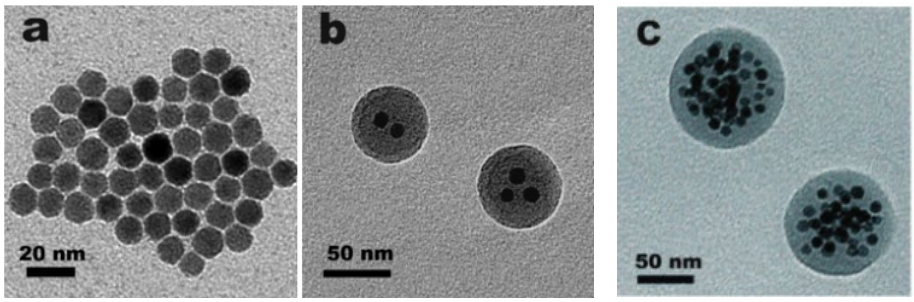

Figure 6: TEM images of 10.9 nm γ-Fe_2O_3 nanoparticles (a) before and after encapsulation within PS250-b-PAA13 micelles with the initial concentration of particles at (a) 0.1 mg/mL; (b) 0.3 mg/mL and (c) 0.5 mg/mL [18].

We can observe from *Figure 6* the images of γ-Fe_2O_3 nanoparticles before and after encapsulation within amphiphilic block copolymer poly(styrene250-block-acrylic acid13) (PS_{250}-*b*-PAA_{13}) recorded by TEM. An increase of the magnetomicelles microsphere size from 40 nm to more than 120 nm is observed related to the number of incorporated Fe_2O_3 nanoparticles (diameter 10.9 nm). Indeed, the number of nanoparticles incorporated into each micelle increased when the initial concentration of γ-Fe_2O_3 nanoparticles rose from 0.1 mg/mL to 0.5 mg/mL. No aggregation was found as the magnetomicelles are stable for months thanks to the encapsulation of PS_{250}-*b*-PAA_{13} [18].

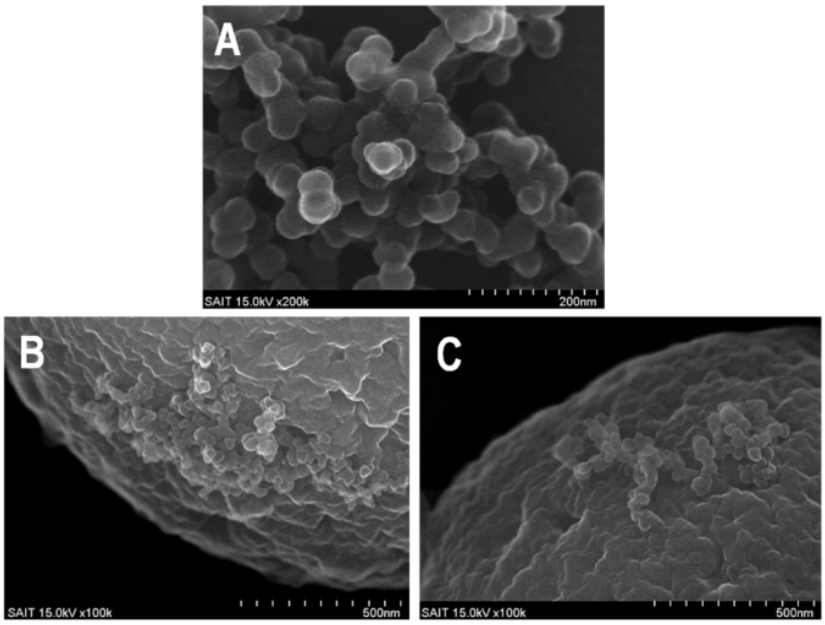

Figure 7: SEM image of (A) Free exosome, (B) and (C) MPs' surface after successfully capturing exosome in buffer and in undiluted human serum, respectively [19].

SEM images provide data about surface topography besides shape and size. For example, free exosomes and captured ones by MPs in buffer and undiluted human serum can be observed by SEM as depicted in *Figure 7*. These MPs were specifically designed including three parts: 1) particles coated by polyacrylic acid to increase the biorecognition sites of protein G and by sylfobetaine to decrease non-specific bonding, 2) protein G to control the antibody orientation, and 3) antibody anti-epithelial cell adhesion molecule (anti-EpCAM) for exosome recognition/capture [19].

1.2.2 MPs hydrodynamic size

Dynamic light scattering (DLS)

Dynamic light scattering, also known as photon correlation spectroscopy, is one of the most popular techniques mainly used to tailor the hydrodynamic size (Z-average), size distribution and polydispersity index of particles ranging from 1 nm to approximately 5 μm [22]. The light perpendicularly projects through the MPs suspension and the scattered light will be detected depending on the angle of detector, normally at 135° and 90°. Since the particles move continuously in solution based on the Brownian's law, the obtained result is measured at one given time.

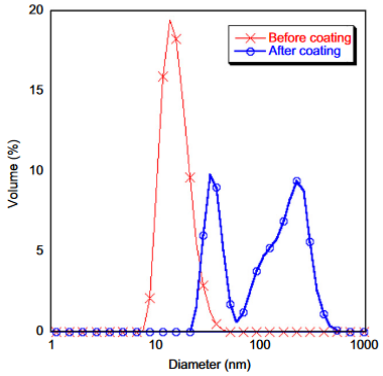

Figure 8: Hydrodynamic diameters of nanoparticles measured with DLS before and after coating with F127 [23].

In addition to, some organic compounds on particle' surface are electron transparent such as oleic acid, pluronic coating, that cannot be detected by TEM. Therefore, when TEM is employed to measure the size of these particles, il shows a different result with DLS. For example, *Gonzales et al* employed DLS and TEM to measure the size of their synthetized oleic-acid-coated iron oxide nanoparticles before and after coating with copolymer Pluronic (F127). As shown in *Figure 8*, the initial hydrodynamic radio of particles is 13 nm, slightly higher than that measured by TEM (10 nm). The difference is due to the presence of oleic acid coating that could not be detected by TEM. After coating with F127, the hydrodynamic diameter increased from 13 nm to 36 nm. This increase could be due to the dynamic association of the F127 on the nanoparticles [23].

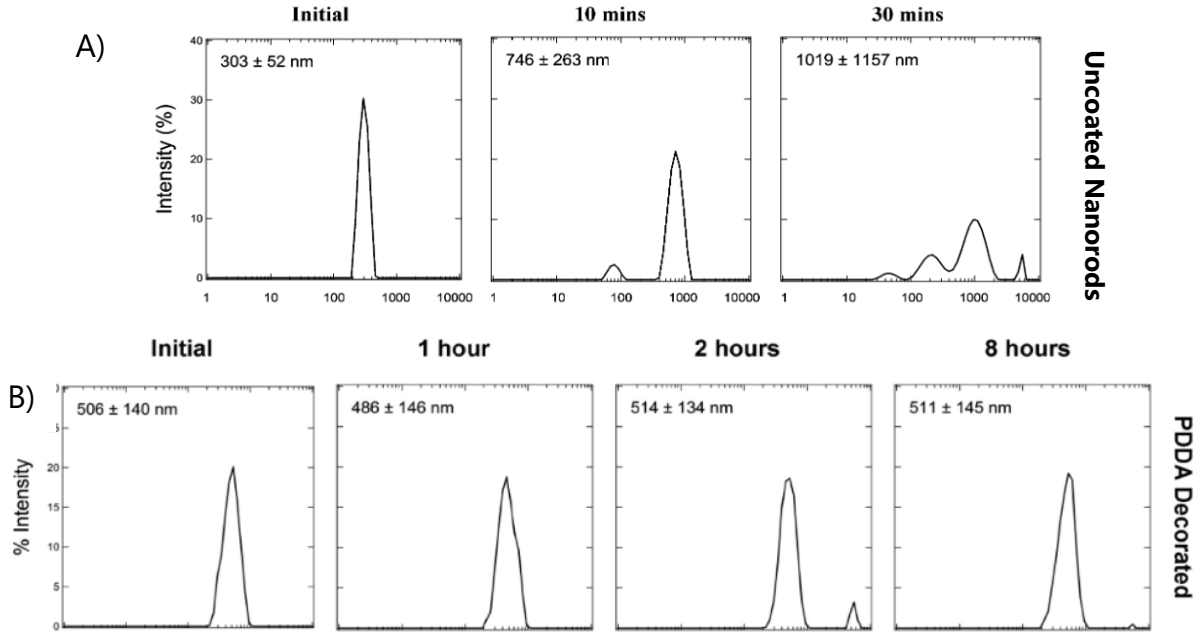

Figure 9: A) Hydrodynamic diameter of uncoated gold-coated nanorods at 10 mg/L and (B) after decorating with PDDA overtime in PBS, measured by DLS [24].

DLS can also be employed to monitor the colloidal stability of MP's suspension. For instance, gold-coated iron oxide nanorods at 10 mg/L (length 380 nm x diameter 40 nm), flocculate immediately in PBS in 10 minutes and the diameter of flocculated nanorods increased up to 1000 nm in 30 minutes. However, MPs' coating by poly(diallyldimethylamonium chloride) (PDDA) at same concentration can prevent flocculation phenomenon after 8h in PBS [24]. Moreover, the hydrodynamic diameter of nanorods decorated with PDDA increased from 300 nm to 500 nm since the hydrodynamic diameter of this material coating was more than 100 nm *(Figure 9)*.

In conclusion, DLS is a powerful method to characterize MPs' hydrodynamic size and colloidal stability due to its simple manipulation, fast time analysis, non-invasive and sample recycling after measurement. Nevertheless, the MPs' concentration has to be adapted as when the suspension is too diluted, there are not enough scattered light for the detector. Conversely, at too high concentration, multiple scatters may occur including both Brownian movement and particle's interaction, especially particles at bigger size (such as the hydrodynamic diameter of MNPs 18 nm in deionized water raised more rapidly than smaller one at 6 nm when their concentration increases > 100 mg/L) [22].

1.2.3 Colloidal stability and surface' charge

Zeta potential (ζ-potential)

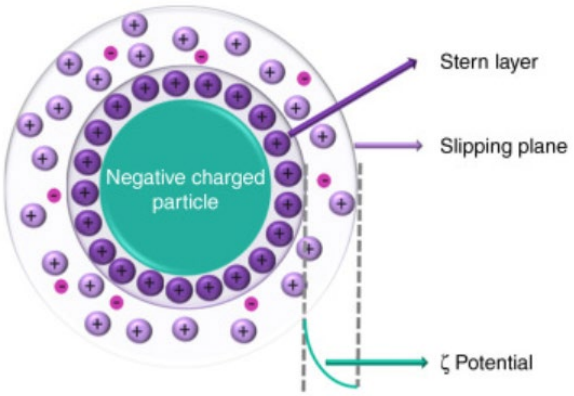

Figure 10: Illustration of ζ-potential of MPs [36].

ζ-potential is an electromagnetic potential of the double layers surrounding electrically charged particles in a colloidal dispersion. When the particles are exposed to the surrounding area, their surface are charged due to the ionization. A double layer is formed between the particle and the suspending medium to balance the surface' charge. The first layer, named Stern-layer, binds strictly

to particles 'surface. The second layer, surrounding the first one, composed by diffused counterions is called diffusion or Gouy-Chapman layer *(Figure 10).* Within the diffuse layer, there is a hypothetical boundary inside of which the ions and particles form a stable/rigid entity. Thus, under the application of an electric field, the ions within this boundary move together with the particle, and ions outside the boundary migrate separately in the dispersing fluid. The zeta-potential is the different electrostatic potential value of the double layer [36].

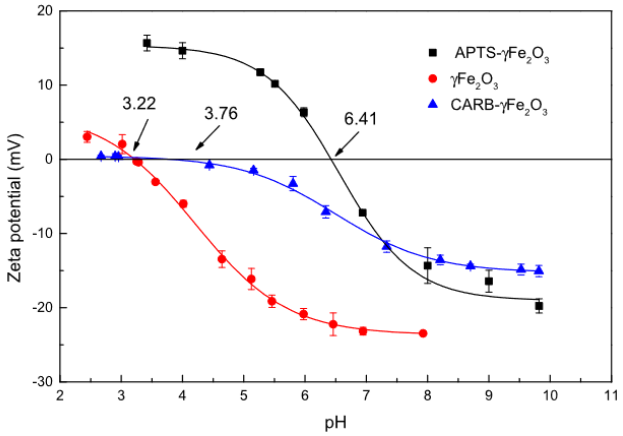

Figure 11: pH dependence of ζ-potential of γFe₂O₃, 3-aminopropyltrimethoxysilane-γFe₂O₃ and carboxylic-γFe₂O₃ samples [27].

The particle properties (e.g., charge density) and the buffer properties (e.g., ionic strength, pH and composition) will influence the zeta-potential. When magnetic particles are suspended in a buffer, their surface or functional groups will be positively or negatively charged depending on the buffer pH (*Figure 11*).

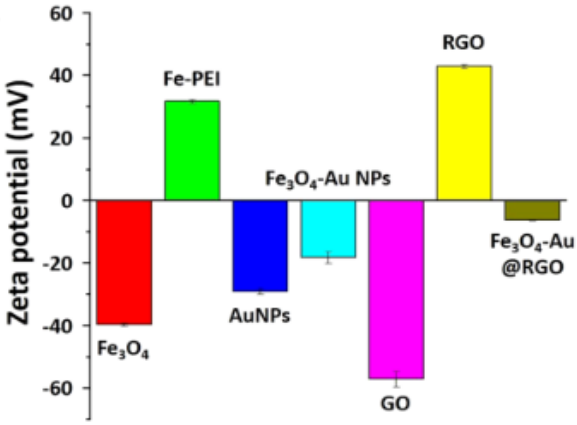

Figure 12: Zeta potential values of Fe₃O₄, Fe₃O₄-polyethylenimine (PEI) NPs, gold nanoparticles (AuNPs), Fe₃O₄-gold NPs, graphene oxide nanosheets (GO), reduced graphene oxide (RGO) and Fe₃O₄-Au@RGO nanocomposites [28].

We can observe from *Figure 12* the zeta potential variation of different nanocomposites after their

surface's modification. For example: the zeta potential at -39.7 mV of Fe_3O_4 with negative surface charge increased to 31.4 mV after immobilizing PEI onto their surface. Then, when AuNPs (zeta potential value of -30.2 mV) were immobilized on the surface of the Fe_3O_4-PEI NPs, they became negatively charged Fe_3O_4-Au NPs (zeta potential of -17.3mV). Moreover, the incorporation of Fe_3O_4-Au NPs onto the surface of reduced graphene oxide (RGO) (zeta potential of 43.4 mV) leaded to negatively charged Fe_3O_4-Au@RGO with a net zeta potential of -8.9 mV [28].

1.2.4 Chemical identification of binding groups on MP's surface

Fourier transform infrared (FTIR) spectroscopy

FTIR is a spectroscopic method widely employed to confirm the chemical group composition on beads 'surface [11, 33].

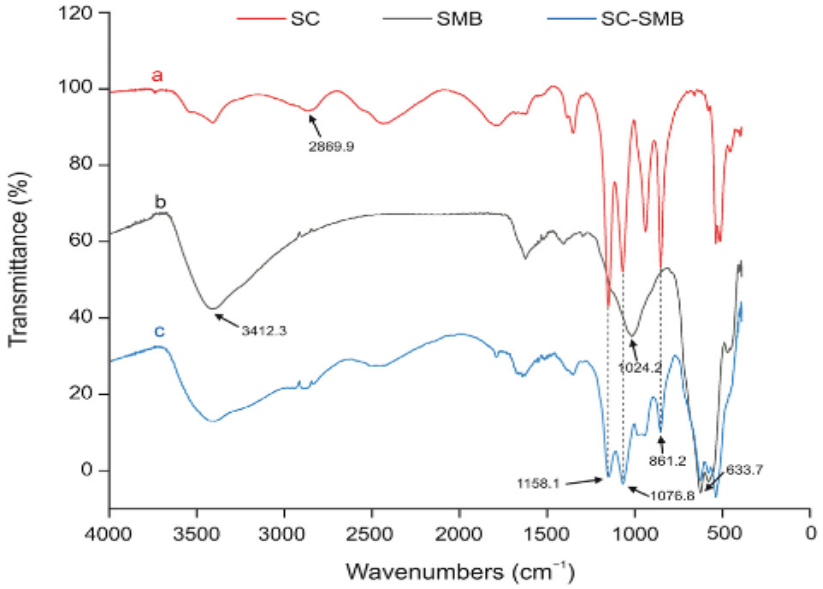

Figure 13: FTIR spectra of the (a) purified His-tagged SC, (b) SMBs, and (c) SC-SMBs [31].

For example, the binding protein on magnetic beads through the Syptag/Spycatcher were monitored by FTIR *(Figure 13).* The SpyCatcher-SpyTag system was developed as a method for protein ligation. It is based on a modified domain from a Streptococcus pyogenes surface protein (SpyCatcher), which recognizes a cognate 13-amino-acid peptide (SpyTag). The spectra proved that the proteins were successfully immobilized on silica-coated magnetic beads functionalized with carboxylic group (SMB) via Spycatcher (SC). Indeed, without any proteins binding on magnetic beads surface, we can observe on the FTIR spectrum of SMB with three peaks 3412.3 cm^{-1}, 1024.2 cm^{-1}, and 633.7 cm^{-1} corresponding to the hydroxyl group of carboxylic acids, the asymmetric stretching of the Si-O-Si chain, and the Fe-O stretching of Fe_3O_4, respectively [31]. In

the FTIR spectrum of the purified His-tagged SC, peak 1 (2869.9 cm^{-1}) correspond to a symmetric C-H stretching of a methyl group from hydrophobic amino acids, such as alanine, valine, leucine, and isoleucine. Peaks found at 1076.8 cm^{-1} and 1158.1 cm^{-1} are related to the C-O stretching vibrations of serine (primary alcohol) and threonine (secondary alcohol), respectively. The peak observed at 861.2 cm^{-1} is related to the disubstituted benzene rings from tyrosine. The peaks at 1076.8 cm^{-1} (threonine), 1158.1 cm^{-1} (serine), 861.2 cm^{-1} (tyrosine) and 633.7 cm^{-1} (Fe-O) were also observed in the FTIR spectrum of SC-SMBs, indicating that SC proteins were successfully immobilized onto the surface of SMBs.

However, FTIR required a long and complicated sample preparation. The solid sample must be mixed with potassium bromide and submitted to a high pressure to make a thin film layer.

Overall, we can see from many works in the literature that MPs characterization relied on several orthogonal methods.

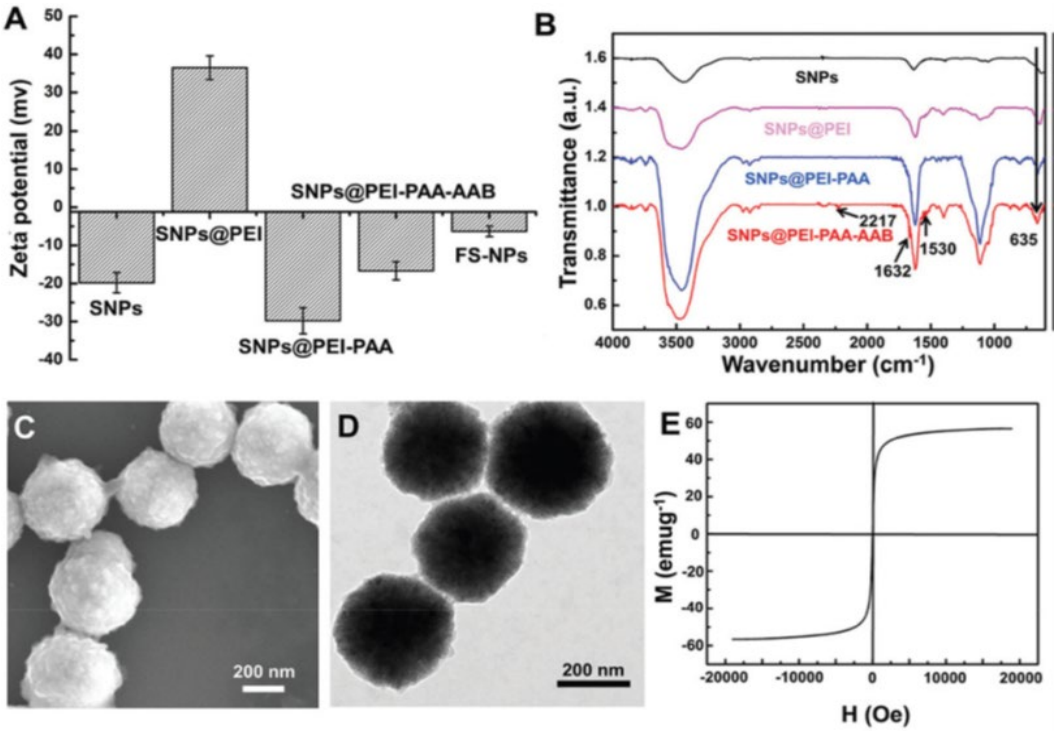

Figure 14: Characterization of the MNPs/nanoparticles: (A) zeta potential of superparamagnetic nanoparticles (SNPs), SNPs-PEI, SNPs-PEI-PAA, SNPs-PEI-PAA-(4-aminoazobenzene) (AAB), and functionalized superparamagnetic-NPs (FS-NPs). (B) FTIR spectra of SNPs, SNPs-PEI, SNPs-PEI-PAA, and SNPs-PEI-PAA-AAB. The SEM image (C), TEM image (D) and magnetic hysteresis (E) of immunoaffinitive MNPs [37].

The interaction of MPs with the (bio)molecules regarding density, orientation, affinity cannot be measured by employing these presented techniques. In this context, capillary electrophoresis is a good choice. It provides the interaction information of MPs and allows the integration of many treatment steps inside the capillary (e.g., preconcentration, extraction, labeling).

1.2.5 Charge, size and interaction between MPs and (bio)molecules

Capillary electrophoresis (CE)

CE is a key technique to characterize the MPs. Chapter 2 of the thesis is dedicated for the working principles of CE as well as its numerous applications for MPs characterization.

1.3 BIOMEDICAL APPLICATIONS OF MAGNETIC BEADS

In the last decades, magnetic micro and nanoparticles have gained important research interest in several fields such as protein separation, cell tracking, immunoassay, imaging, and drug delivery, etc. The miniaturized analytical systems (e.g., lab-on-chip) employing these particles were also developed with many interesting applications. This **1.3** parts will present the following applications of MNPs in biomedical: imaging and diagnostics *(Figure 15)*.

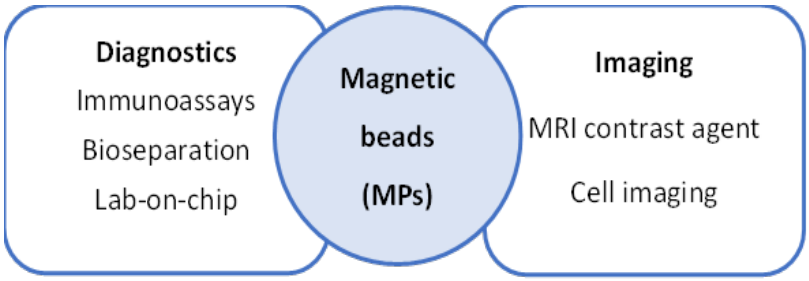

Figure 15: Schema of MPs applications in biomedical.

1.3.1 Magnetic particles as a solid support

Magnetic particles are also widely used in biomedical diagnosis. Once biofunctionalized, they can selectively extract biomolecules or biomarkers in complex media such as blood. They could also be exploited as carriers for biomolecules in microsystems (e.g., microfluidics, lab-on-chips).

1.3.1.1 Bioseparation

Magnetic particles are employed as a separation carrier under an external magnetic field. They allow extraction of biological targets such as proteins/peptides, cells, or exosome from biofluids. This bioseparation based on MPs is described in *Figure 16* [6].

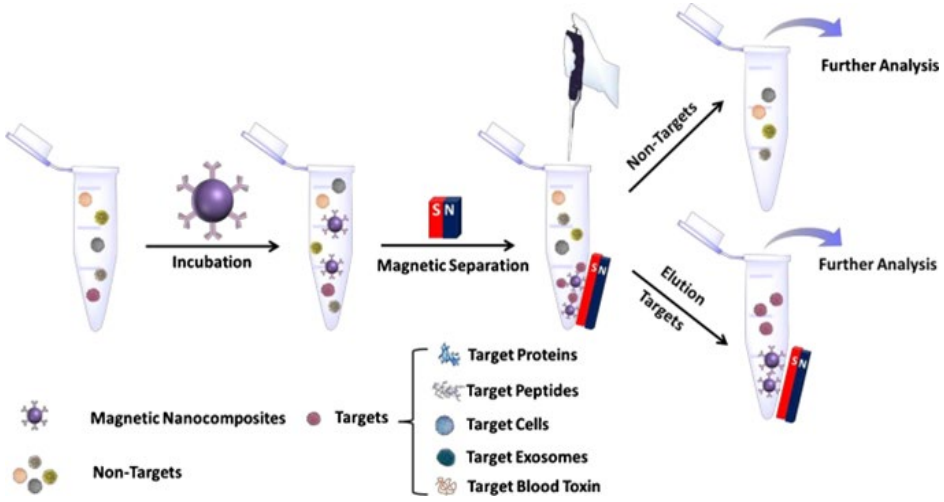

Figure 16: Schematic illustration of the bioseparation process based on magnetic particles [6].

Proteins separation from biosamples could be selective or nonselective. It depends on the interaction of proteins with the surface biofunctionalization.

Nonselective separation

For the nonselective approach, proteins separation is achieved through their adsorption on MP's surfaces. For instance, proteins such as lysozyme or cytochrome C (cyt C) were extracted from cell lysate by adsorption on nanosphere Fe_3O_4 (diameter 7.8 nm) coated by poly methyl methacrylate (PMMA) (total diameter from 10 nm – 90 nm) [38]. The cyt C (0.5 mg/L) enrichment was obtained through hydrophobic interactions. After enrichment (MP's concentration 5 mg/ mL), the S/N detection on MALDI-TOF-MS increased 68 folds.

Proteins adsorption was evaluated on Fe_3O_4/carboxymethylated chitosan (Fe_3O_4/CMCS)

nanoclusters (diameter 500 nm). An in depth evaluation of the material coating (Fe^{3+}) and environment (pH, ionic strength) influence on proteins adsorption was performed with four models proteins: lysozyme (LYZ), bovine hemoglobin (BHB), apo-transferrin (TRT) and bovine serum albumin (BSA) [39]. As the influence of Fe^{3+} on the interactions between proteins and other molecules was highlighted in previous studies [40, 41].

This study showed that the adsorption amount of four proteins is similar on the two types of MPs (Fe_3O_4/CMCS and Fe_3O_4/CMCS-Fe^{3+}) (*Figure 17*). The addition of Fe^{3+} to the coating layer had no influence on the protein's adsorption on MPs. Additionally, the amount of adsorbed BHB and LYZ is higher on both MPs compared to BSA and TRT showing a selective capture of these two proteins (BHB and LYZ) on the two types of MPs.

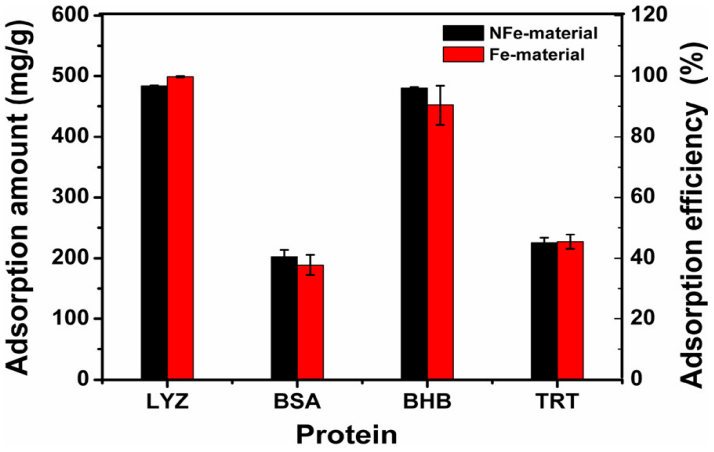

Figure 17: LYZ, BSA, BHB and TRT adsorption amounts of the Fe_3O_4/CMCS nanoclusters [39].

However, conformation changes were observed on adsorbed proteins. Further studies showed that the best results regarding conformational changes were obtained with PBS buffer at pH 7.

Selective separation by ligands-functionalized MPs.

Relying on ligand-functionalized MPs, this approach allows specific extractions of single proteins, cells or exosomes from a complex sample, which can be essential for diagnosis. For this purpose, ligands/bioreceptors such as antibodies or aptamers that are able to selectively and sensitively capture the biomolecule targets (e.g., proteins, cells, exosomes) are immobilized onto MPs surfaces. For example, selective separation relying on MNPs (Fe_3O_4) grafted with antibodies was tested. These MNPs chemically functionalized by β-cyclodextrine-polyethylen glycol (β CD-PEG 2000) and terminated by a carboxylic group (COOH) (hydrodynamic diameter 391 nm). Antibodies against CD63 were therefore grafted via N-Hydroxysuccinimide (NHS)/3-ethyl-carbodiimide

hydrochloride (EDC) activation. The complexe of MNPs-anti CD63 demonstrated their ability to extract exosomes from pre-cleared cell-culture supernatant (cell-lines MCF-7 and 4T1). A capture efficiency of 80% was obtained while the release efficiency of exosomes was 86.5%. The isolation efficiency obtained was 8 times better than conventional ultracentrifugation, and twice than polyethylene glycol-based precipitation, and commercial kits [37].

MPs able to capture glycoproteins were also developed. Indeed, glycoproteins play major roles in cellular functions and are considered as potential biomarkers for different diseases such as cancer and cardiovascular diseases. Therefore, numerous studies focused on the improvement of their analysis and detection. For example, ethylenediamine tetraacetic acid (EDTA)-MNPs (diameter 15 nm) were developed to immobilized concanavalin A through a Cu^{2+} bridge (Con A-MNPs) to enrich the glycoproteins. These MNPs were able to specifically separate a glycoprotein, ovalbumin from a non-glycoprotein (lysozyme) in a standard mixture composed by a ratio of 1: 600 (ovalbumin/ non-glycoproteins). Furthermore, Con A-MNPs showed their ability to capture selectively three glycoproteins (ovotransferrine, ovalbumin and ovoinhibitor) from a 500-fold diluted real egg white sample (total amount of 430 µg of three glycoproteins captured by 6 mg of Con A-MNPs) [42].

1.3.1.2 Immunoassay

Immunoassays is a test that measures the concentration of analytes such as proteins, peptides, etc. in a biological sample through the use of antibodies which are immobilized on a solid support such as microplate [43], column [44], capillary [45], beads [46]. A second antibody is added, binding also to the antigen and generates a measurable signal provided by enzymes digestion, radioisotopes, fluorescent markers, or chemiluminescent labels [47]. Thanks to extremely high surface-to-volume ratio, MPs raise the sensitivity by increasing the grafting surface of antibodies and distribute homogenously them throughout the whole volume of the reaction medium, leading to a faster and better capture performance [48]. The complexes between the particles and antibodies are formed by covalent or non-covalent immobilization. Generally, in immunoassay, MPs can be used as (i) a solid support for the formation of the immune complex or (ii) a detection label measured by different detectors (*Figure 18*).

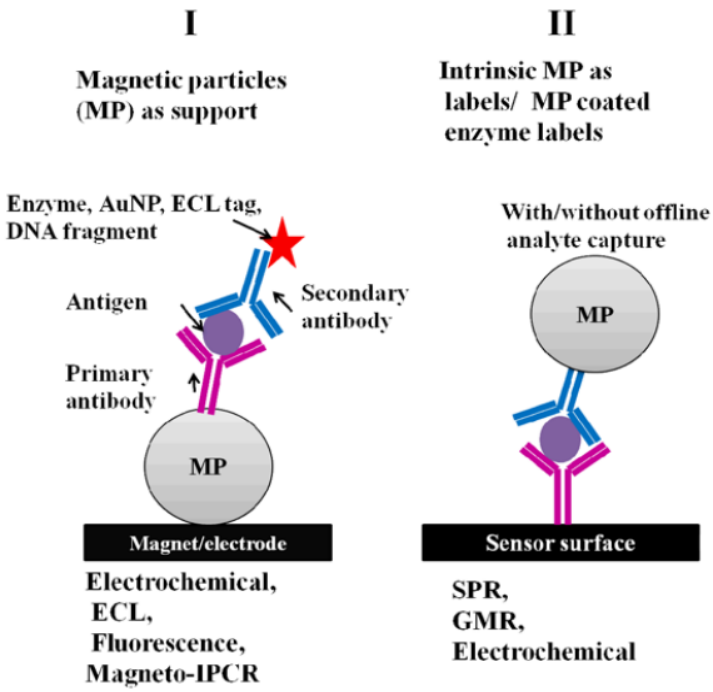

Figure 18: Schematic representation of the use of MPs as (I) solid phase support or (II) the detection labels [49].

Regarding solid phase application, MPs support has been recently applied for immunoassay to detect SARS-CoV-2 antibody in serum [50]. This method was proved to be rapid (duration of the whole process 15 minutes), simple (without sample pretreatment), and inexpensive. Recombinant 6xHis-tagged SARS-CoV-2 nucleocapsid protein was immobilized on the surface of Ni^{2+} magnetic beads prior the incubation with blood of Covid-19 patients. The complex was then detected by blue color intensity when adding anti-human IgG-HPR conjugate and its substrate. A better sensitivity of 97% and reproducibility were recorded (CV 2-3%), compared to classical immunoassay method without MPs support (90% and CV 8-9%, respectively).

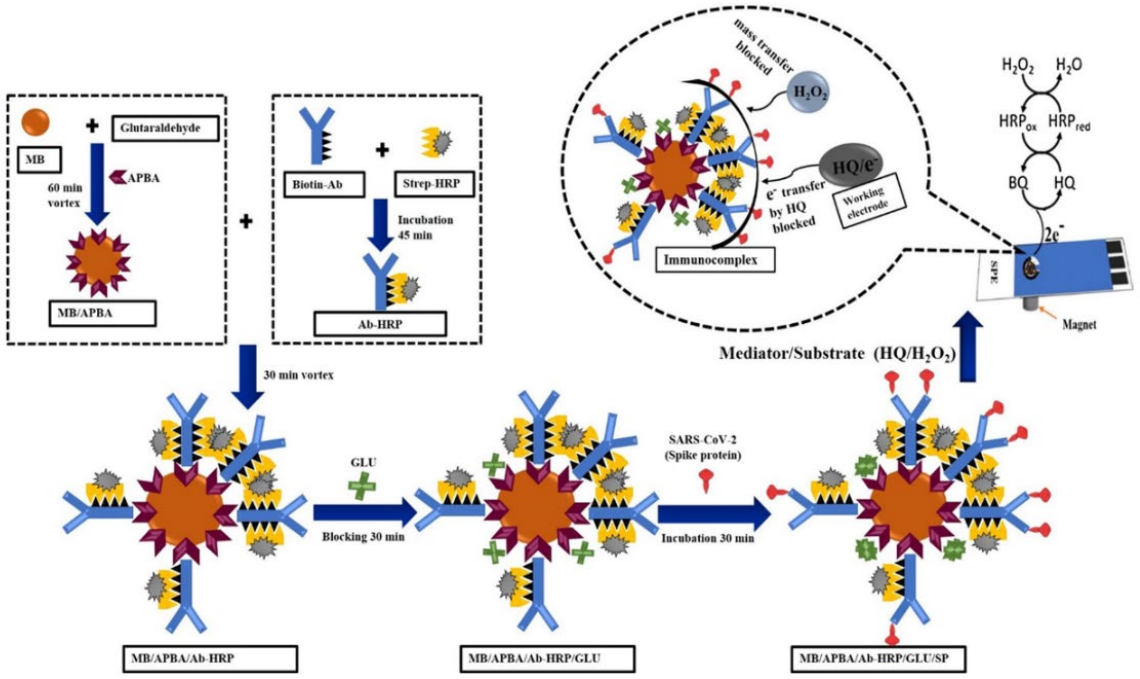

Figure 19: Schematic illustration for spike protein Covid-19 detection using the MNPs-based electrochemical immunoassay [51].

Other studies relying on the improvement of immunoassay for Covid-19 diagnosis thanks to MPs have been reported in the other studies [51, 52] (*Figure 19*).

Moreover, the use of antibody against carcinoembryonic antigen immobilized on Fe_3O_4 nanoparticles (diameter of 51.3 nm) in PBS for the immunoassay of carcinoembryonic antigen was also developed [53]. The method is more sensitive with a limit of detection at 0.21 ng/mL, compared to commercial kits (0.5 ng/mL), was successfully applied on clinical tests. The diagnosis of colorectal cancer from 54 serum samples (24 healthy people and 30 colorectal cancer patients) was conducted. While the control group had value range from 0.6 ng/mL to 1.5 ng/mL, the values of patients were from 6.0 ng/mL to 20 ng/mL.

1.3.1.3 Lab-on-chip

Development of miniaturized devices has attracted attention, since it can combine several integrated steps for biomolecules: extraction, analysis, and detection in an automated device (e.g., lab-on-a-chip (LOC)). The miniaturization technology allowing device portability, hold a great potential for point-of-care testing [54]. LOC could provide many advantages such as automation, high sensitivity, high throughput, small sample volume and reagent-consuming, and multiplexing. Microsystems are therefore promising tools in the field of diagnosis.

MPs have demonstrated their ability to improve analytical steps when integrated in miniaturized

devices. Because of their magnetism property and micro/nanosize, they can be easily manipulated under an external magnetic field for capture and transportation of the target molecules in the micro/nanochannel. Additionally, MPs' biofunctionalization with different bioreceptors (e.g., antibody, aptamers, etc.) renders them ideal for the specific capture of biomarkers of interest in lab on-chip. This is why they have been widely used for the context of diagnosis.

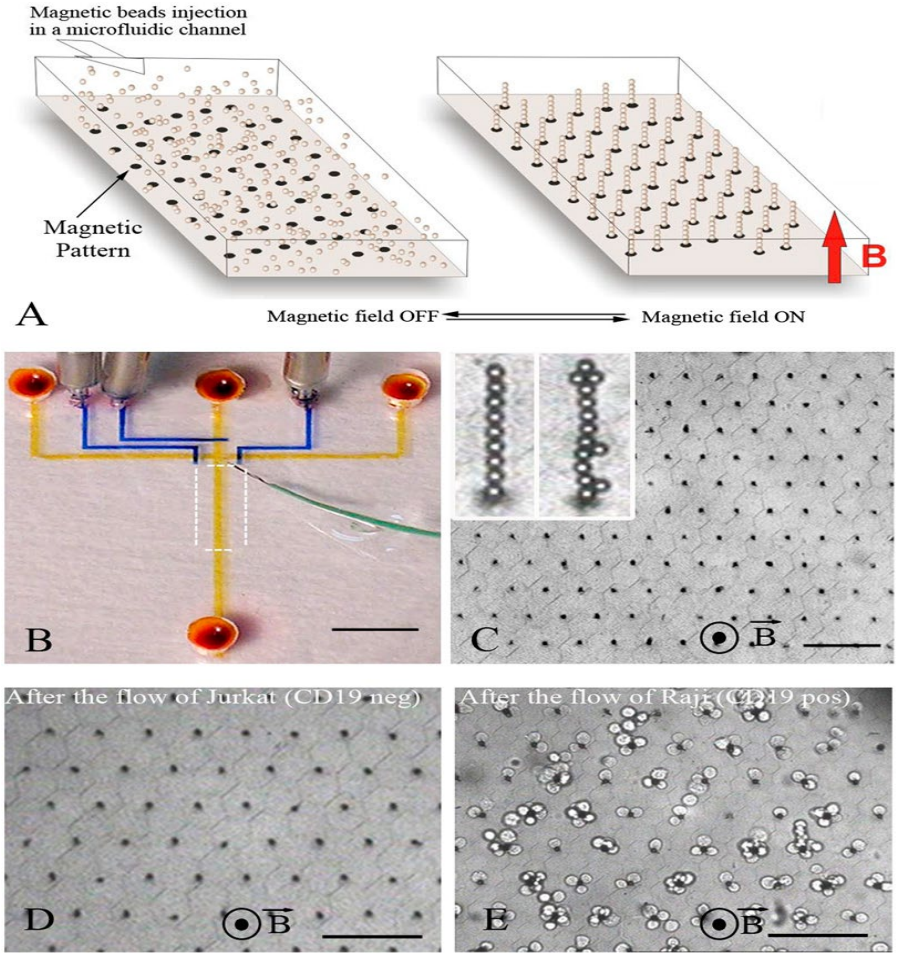

Figure 20: Principle and practical implementation of the Ephesia system [55].

Magnetic beads packed in a microfluidic device were first investigated. Biofunctionalized MPs were introduced in a microchannel and packed under an external magnetic field, produced by a permanent magnet [56]. The sample could be therefore percolated through the packed magnetic beads grafted with bioreceptors such as enzymes or antibodies [57, 58]. However, in this design, the MP's aggregation and clogging could occur, leading thereby to a decrease of the capture or digestion efficiency [59]. To prevent these phenomenons, different strategies have been proposed. Among them, chips based on columns of biofunctionalized MPs in a microfluidic channel, such as "Ephesia". These columns made of self-assembled magnetic beads, bearing antibodies anti-CD19,

showed that they were able to capture B-cells (*Figure 20)* [55].

This Ephesia chips were also recently employed to capture and characterize the circulating tumor cells (CTC), HER2 positive, and identify their HER2-HER3 status, considered as a predictive biomarker [60].

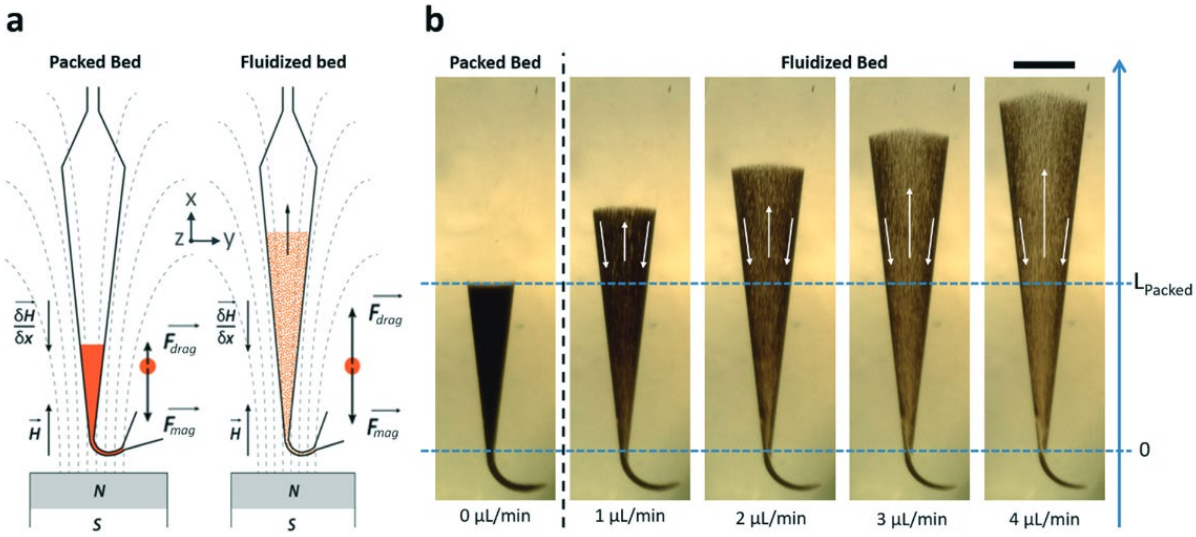

Figure 21: Schematic illustrations of the microfluidic fluidized bed for two working regimes: at low imposed pressure, particles are organized in a packed bed. Fluidization occurs when the pressure is sufficient to induce a fluid flow associated with drag forces [61].

Another approach relying on microfluidic magnetic fluidized bed was proposed [61]. Briefly, the fluidized bed results on the balance between magnetic forces (generated by permanent magnet) on one side and hydrodynamic forces exerted by incoming liquid flow on the other side, leading thereby to a circulating movement of the particles (*Figure 21*). Channel geometry, magnet position and pressure/flow rate conditions were optimized to maximize sample/particle interaction. Compared to packed beds, fluidized beds provide higher mixing efficiency, and decrease beads plugging in the microdevice.

This concept was successfully applied to extract amyloid beta peptides detection [62], bacteria quantification [63], and DNA analysis [64].

In the last example, microfluidic chip where magnetic beads are immobilized on the floor of the device, called magnetically actuatable surface attached posts (ASAPs) or “BeadPak,”.

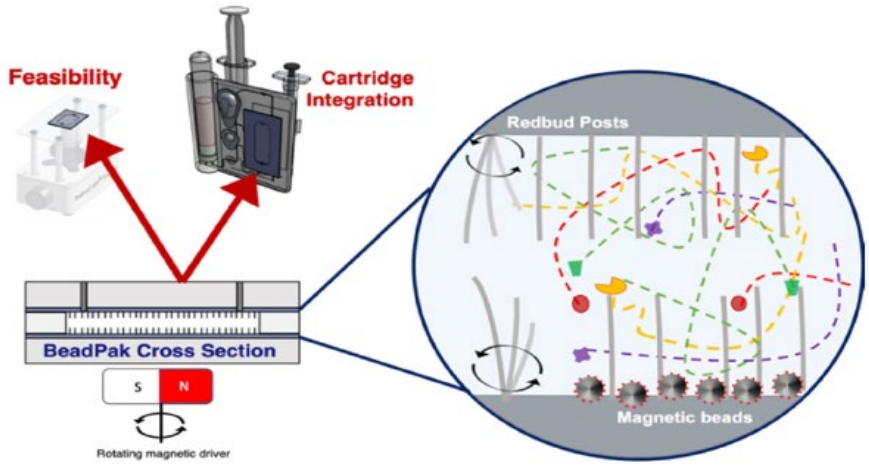

Figure 22: Schematic depiction of the BeadPak system [65].

The ASAPs enhanced the analyte's mixing and transport by using cilia array (moving hair-like structures) to generate directed or chaotic fluid flow under magnetic field, leading to the higher interaction between sample and MPs (*Figure 22*) [65]. This immobilization on the floor of the device prevents the MPs loss that may occur in fluidized bed. BeadPak was successfully applied for the capture of nucleosomes (histone/DNA complex), used for early cancer detection [65].

In conclusion, magnetic micro/nano particles have a wide range of applications in diagnostic fields. Regarding bioseparation and immunoassay based on MPs support, the cited examples showed better sensitivity and selectivity compared to traditional methods. It is also revealed that the integration of MPs to microchip design highlighted many advantages of MPs using for biomolecules' extraction, analysis and detection. However, the strategies of MPs' transportation and mixing with analytes in miniaturized devices are not widely performed, leading the modest biomolecules extraction and detection. Besides magneto- immune enrichment, there are diverse established preconcentration methods for biomolecules. Among them, the electrokinetic preconcentration technique in CE are widely used and showed high performance (will be discussed in chapter 2). Taking into account that the MPs can be characterized by CE and transported in capillary, the combination of two strategies (magneto and electrokinetic preconcentration) will be developed with the aim to achieve better enrichment factors and sensitivity detection.

1.3.2 Magnetic particles as an contrast agent in imaging

Magnetic particles were recently proposed as advanced contrast agents for magnetic resonance imaging (MRI) [66, 67].

Magnetic resonance imaging (MRI) is well-known as non-invasive and high resolution for

diagnosis. The MP contrast agents allow the discrimination of healthy and malignant tissues thanks to different distribution of contrast agent in sample, leading to dark signal on image. Many iron oxide particles were developed to replace the gadolinium, Fe and Au, employed individually or combined to other metals. This is related to their high biocompatibility, high contrast, and targeting potential [68, 69]. Uniform-sized iron oxide nanocubes with an edge length of 22 nm, was successfully employed in mice, to perform *in vivo* MRI of tumors after their intravenous injection [70]. Their passive targeting at the tumor site has been demonstrated by MRI. Ferumoxytol, iron oxide nanoparticle, coated by carboxydextran, (mean hydrodynamic diameter 30 nm) also proved their ability to detect tumor-associated macrophages (TAM) in a mouse model of mammary carcinogenesis. The best contrast achieved 1 hour after using Ferumoxytol (*Figure 23*) [71].

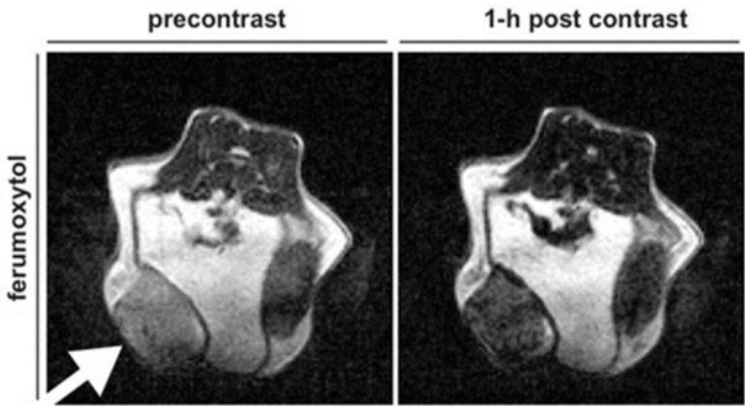

Figure 23: MRI images of TAM in mouse before and 1 hour after using Ferumoxytol contrast [71].

Ferumoxide (diameter 60-80 nm) and Ferumoxstran (diameter 17-20 nm) were approved by Food and Drugs Administration (FDA) for liver tumor imaging on patients [72, 73]. The smaller one has longer blood half-life (more than 100 minutes) because they can avoid the massive uptake by liver and spleen while that of the larger one has less than 30 minutes.

MPs were employed to perform at cellular level. The ability of innate immune cells to phagocytate iron oxide nanoparticles has been demonstrated: (i) *in vitro* with macrophage, microglia, and neutrophils, (ii) *in vivo* in mouse model of experimental autoimmune encephalomyelitis (EAE), mimicking multiple sclerosis. Therefore, the molecular imaging of innate immune responses can be served as an imaging biomarker in autoimmune-mediated neuroinflammation, with potential clinical applications in many inflammatory diseases [74].

Additionally, glucosamine-modified polyacrylic acid-coated ultra-small iron oxide particle

(diameter 40 nm) was tested as a mesenchymal stem cell label for tracking applications by MRI. Results obtained showed that these MPs enhanced the cellular uptake and exhibited a higher biocompatibility, thus, they could be considered as promising labeling agent for cells tracking application in animal models of ischemia [75].

References of chapter 1

1. Low, L.E., et al., *Stimuli-controllable iron oxide nanoparticle assemblies: Design, manipulation and bio-applications*. Journal of Controlled Release, 2022. **345**: p. 231-274.
2. Ruffert, C., *Magnetic Bead-Magic Bullet*. Micromachines (Basel), 2016. **7**(2).
3. Galogahi, F.M., et al., *Core-shell microparticles: Generation approaches and applications.* Journal of Science: Advanced Materials and Devices, 2020. **5**(4): p. 417-435.
4. Hasan, S., *A Review on Nanoparticles: Their Synthesis and Types*. 2015. **4**: p. 1-3.
5. Stueber, D.D., et al., *Magnetic Nanoparticles in Biology and Medicine: Past, Present, and Future*. Trends. Pharmaceutics, 2021. **13**(7): p. 943.
6. Yang, Q., et al., *Design of Functional Magnetic Nanocomposites for Bioseparation*. Colloids and Surfaces B: Biointerfaces, 2020. **191**: p. 111014.
7. Anu Mary Ealia, S. and M.P. Saravanakumar, *A review on the classification, characterisation, synthesis of nanoparticles and their application*. IOP Conference Series: Materials Science and Engineering, 2017. **263**: p. 032019.
8. Anwar, S., *A Brief Review on Nanoparticles: Types of Platforms, Biological Synthesis and Applications*. Research & Reviews Journal of Material Sciences, 2018. **06**.
9. Reddy, L.H., et al., *Magnetic Nanoparticles: Design and Characterization, Toxicity and Biocompatibility, Pharmaceutical and Biomedical Applications*. Chemical Reviews, 2012. **112**(11): p. 5818-5878.
10. Zhang, K. and X.Y. Wu, *Temperature and pH-responsive polymeric composite membranes for controlled delivery of proteins and peptides*. Biomaterials, 2004. **25**(22): p. 5281-5291.
11. Wang, F.-Q., et al., *pH-sensitive magnetic alginate-chitosan beads for albendazole delivery*. Pharmaceutical Development and Technology, 2011. **16**(3): p. 228-236.
12. Geißler, D., et al., *Analyzing the surface of functional nanomaterials—how to quantify the total and derivatizable number of functional groups and ligands*. Microchimica Acta, 2021. **188**(10): p. 321.
13. Jeong, S., et al., *Highly robust and optimized conjugation of antibodies to nanoparticles using quantitatively validated protocols*. Nanoscale, 2017. **9**(7): p. 2548-2555.
14. Bouzas-Ramos, D., et al., *Controlling Ligand Surface Density on Streptavidin-Magnetic Particles by a Simple, Rapid, and Reliable Chemiluminescent Test*. Bioconjugate Chemistry, 2018. **29**(8): p. 2646-2653.
15. Shen, M., et al., *Restricted Proteolysis and LC-MS/MS To Evaluate the Orientation of Surface-Immobilized Antibodies*. Analytical Chemistry, 2019. **91**(7): p. 4913-4919.
16. Eivazzadeh-Keihan, R., et al., *Functionalized magnetic nanoparticles for the separation and purification of proteins and peptides*. TrAC Trends in Analytical Chemistry, 2021. **141**: p. 116291.
17. Zhang, Y., et al., *Uniform Magnetic Core/Shell Microspheres Functionalized with Ni2+–Iminodiacetic Acid for One Step Purification and Immobilization of His-Tagged Enzymes*. ACS Applied Materials & Interfaces, 2013. **5**(7): p. 2626-2633.
18. Kim, B.-S., et al., *Magnetomicelles: Composite Nanostructures from Magnetic Nanoparticles and Cross-Linked Amphiphilic Block Copolymers.* Nano Letters, 2005. **5**(10): p. 1987-1991.
19. Kim, G., et al., *Noble Polymeric Surface Conjugated with Zwitterionic Moieties and Antibodies for the Isolation of Exosomes from Human Serum*. Bioconjugate Chemistry, 2012. **23**(10): p. 2114-2120.
20. Moroz, E.M., *X-Ray diffraction structure diagnostics of nanomaterials*. Russian Chemical Reviews, 2011. **80**(4): p. 293-312.
21. Sharma, A., et al., *XANES, EXAFS and photocatalytic investigations on copper oxide nanoparticles and nanocomposites*. RSC Advances, 2015. **5**(28): p. 21762-21771.

22. Lim, J., et al., *Characterization of magnetic nanoparticle by dynamic light scattering*. Nanoscale research letters, 2013. **8**(1): p. 381-381.
23. Gonzales, M. and K.M. Krishnan, *Phase transfer of highly monodisperse iron oxide nanocrystals with Pluronic F127 for biomedical applications*. Journal of Magnetism and Magnetic Materials, 2007. **311**(1): p. 59-62.
24. Yeap, S.P., et al., *Colloidal Stability and Magnetophoresis of Gold-Coated Iron Oxide Nanorods in Biological Media*. The Journal of Physical Chemistry C, 2012. **116**(42): p. 22561-22569.
25. Filipe, V., A. Hawe, and W. Jiskoot, *Critical evaluation of Nanoparticle Tracking Analysis (NTA) by NanoSight for the measurement of nanoparticles and protein aggregates*. Pharm Res, 2010. **27**(5): p. 796-810.
26. Soo, C.Y., et al., *Nanoparticle tracking analysis monitors microvesicle and exosome secretion from immune cells*. Immunology, 2012. **136**(2): p. 192-7.
27. Rodriguez, A.F.R., et al., *Synthesis, characterization and applications of maghemite beads functionalized with rabbit antibodies*. Nanotechnology, 2018. **29**(36): p. 365701.
28. Yang, M.-C., et al., *Reduced graphene oxide nanosheets decorated with core-shell of Fe3O4-Au nanoparticles for rapid SERS detection and hyperthermia treatment of bacteria*. Spectrochimica Acta Part A: Molecular and Biomolecular Spectroscopy, 2022. **281**: p. 121578.
29. Adolphi, N.L., et al., *Characterization of magnetite nanoparticles for SQUID-relaxometry and magnetic needle biopsy*. J Magn Magn Mater, 2009. **321**(10): p. 1459-1464.
30. Guillaume, A., *SQUIDs for the characterization of magnetic nanoparticles*. SQUIDs fuer die Charakterisierung magnetischer Nanoteilchen. 2015, Germany: Mensch und Buch.
31. Yi, Y., et al., *A preparation strategy for protein-oriented immobilized silica magnetic beads with Spy chemistry for ligand fishing*. Journal of Pharmaceutical Analysis, 2022. **12**(3): p. 415-423.
32. Li, J., et al., *Graphene-Coated Iron Nitride Streptavidin Magnetic Beads: Preparation and Application in SARS-CoV-2 Enrichment*. Magnetochemistry, 2022. **8**(4): p. 41.
33. Chammem, H., et al., *Functionalised magnetic beads on gold surface for C-reactive protein detection*. International Journal of Nanotechnology, 2015. **12**(8-9): p. 552-561.
34. Gleichmann, N., *SEM vs TEM*. Technology networks Analysis and Separation, 2020.
35. Chapman, J.N. and M.R. Scheinfein, *Transmission electron microscopies of magnetic microstructures*. Journal of Magnetism and Magnetic Materials, 1999. **200**(1): p. 729-740.
36. Shnoudeh, A.J., et al., *Chapter 15 - Synthesis, Characterization, and Applications of Metal Nanoparticles*, in Biomaterials and Bionanotechnology, R.K. Tekade, Editor. 2019, Academic Press. p. 527-612.
37. Cai, S., et al., *Immuno-modified superparamagnetic nanoparticles via host–guest interactions for high-purity capture and mild release of exosomes*. Nanoscale, 2018. **10**(29): p. 14280-14289.
38. Lan, F., et al., *Superparamagnetic Fe3O4/PMMA composite nanospheres as a nanoplatform for multimodal protein separation*. RSC Advances, 2013. **3**(5): p. 1557-1563.
39. Yang, Q., et al., *Conformational changes of adsorbed and free proteins on magnetic nanoclusters*. Colloids and Surfaces B: Biointerfaces, 2018. **170**: p. 664-672.
40. Li, D., et al., *The effect of Cu2+ or Fe3+ on the noncovalent binding of rutin with bovine serum albumin by spectroscopic analysis*. Spectrochimica Acta Part A: Molecular and Biomolecular Spectroscopy, 2011. **78**(1): p. 74-79.
41. Li, D., et al., *Characterization of the baicalein–bovine serum albumin complex without or with Cu2+or Fe3+ by spectroscopic approaches*. European Journal of Medicinal Chemistry, 2011. **46**(2): p. 588-599.
42. Dong, L., et al., *Preparation of Concanavalin A-Chelating Magnetic Nanoparticles for Selective Enrichment of Glycoproteins*. Analytical Chemistry, 2015. **87**(13): p. 6849-6853.

43. Mehta, P.D., et al., *A Sensitive and Cost-Effective Chemiluminescence ELISA for Measurement of Amyloid-β 1-42 Peptide in Human Plasma*. Journal of Alzheimer's disease : JAD, 2020. **78**(3): p. 1237-1244.
44. Mahara, A. and T. Yamaoka, *Antibody-immobilized column for quick cell separation based on cell rolling*. Biotechnol Prog, 2010. **26**(2): p. 441-7.
45. Cole, L.J. and R.T. Kennedy, *Selective preconcentration for capillary zone electrophoresis using protein G immunoaffinity capillary chromatography*. ELECTROPHORESIS, 1995. **16**(1): p. 549-556.
46. Eissa, M.M., et al., *Reactive magnetic poly(divinylbenzene-co-glycidyl methacrylate) colloidal particles for specific antigen detection using microcontact printing technique*. Acta Biomaterialia, 2013. **9**(3): p. 5573-5582.
47. Urusov, A.E., et al., *Application of Magnetic Nanoparticles in Immunoassay*. Nanotechnologies in Russia, 2017. **12**(9): p. 471-479.
48. Urusov, A.E., et al., *Rapid immunoenzyme assay of aflatoxin B1 using magnetic nanoparticles*. Sensors (Basel, Switzerland), 2014. **14**(11): p. 21843-21857.
49. Mani, V., B.V. Chikkaveeraiah, and J.F. Rusling, *Magnetic particles in ultrasensitive biomarker protein measurements for cancer detection and monitoring*. Expert Opinion on Medical Diagnostics, 2011. **5**(5): p. 381-391.
50. Huergo, L.F., et al., *Magnetic Bead-Based Immunoassay Allows Rapid, Inexpensive, and Quantitative Detection of Human SARS-CoV-2 Antibodies*. ACS Sensors, 2021. **6**(3): p. 703-708.
51. Malla, P., et al., *Voltammetric biosensor for coronavirus spike protein using magnetic bead and screen-printed electrode for point-of-care diagnostics*. Microchimica Acta, 2022. **189**(4): p. 168.
52. Ha, Y. and I. Kim, *Recent Developments in Innovative Magnetic Nanoparticles-Based Immunoassays: From Improvement of Conventional Immunoassays to Diagnosis of COVID-19*. BioChip Journal, 2022.
53. Yang, C.-C., et al., *Development of antibody functionalized magnetic nanoparticles for the immunoassay of carcinoembryonic antigen: a feasibility study for clinical use*. Journal of Nanobiotechnology, 2014. **12**(1): p. 44.
54. Yager, P., et al., *Microfluidic diagnostic technologies for global public health*. Nature, 2006. **442**(7101): p. 412-418.
55. Saliba, A.-E., et al., *Microfluidic sorting and multimodal typing of cancer cells in self-assembled magnetic arrays*. Proceedings of the National Academy of Sciences, 2010. **107**(33): p. 14524-14529.
56. Svobodova, Z., et al., *Development of a magnetic immunosorbent for on-chip preconcentration of amyloid β isoforms: Representatives of Alzheimer's disease biomarkers*. Biomicrofluidics, 2012. **6**(2): p. 24126-2412612.
57. Slovakova, M., et al., *Use of self-assembled magnetic beads for on-chip protein digestion*. Lab on a Chip, 2005. **5**(9): p. 935-942.
58. Le Nel, A., et al., *Controlled proteolysis of normal and pathological prion protein in a microfluidic chip*. Lab Chip, 2008. **8**(2): p. 294-301.
59. van Reenen, A., et al., *Integrated lab-on-chip biosensing systems based on magnetic particle actuation – a comprehensive review*. Lab on a Chip, 2014. **14**(12): p. 1966-1986.
60. Tulukcuoglu Guneri, E., et al., *Deciphering HER2-HER3 Dimerization at the Single CTC Level: A Microfluidic Approach*. Cancers, 2022. **14**(8): p. 1890.
61. Pereiro, I., et al., *Magnetic fluidized bed for solid phase extraction in microfluidic systems*. Lab on a Chip, 2017. **17**(9): p. 1603-1615.
62. Mai, T.D., et al., *Magneto-immunocapture with on-bead fluorescent labeling of amyloid beta*

peptides: towards a microfluidized-bed-based operation. Analyst, 2015. **140**: p. 5891-5900.
63. Pereiro, I., et al., *A new microfluidic approach for the one-step capture, amplification and label-free quantification of bacteria from raw samples*. Chemical Science, 2017. **8**(2): p. 1329-1336.
64. Hernández-Neuta, I., et al., *Microfluidic magnetic fluidized bed for DNA analysis in continuous flow mode*. Biosensors and Bioelectronics, 2018. **102**: p. 531-539.
65. Kanies, O.S., et al., *A modular microfluidic device that uses magnetically actuatable microposts for enhanced magnetic bead-based workflows*. Lab on a Chip, 2023. **23**(2): p. 330-340.
66. Gleich, B. and J. Weizenecker, *Tomographic imaging using the nonlinear response of magnetic particles*. Nature, 2005. **435**(7046): p. 1214-1217.
67. Zhou, X.Y., et al., *Magnetic particle imaging for radiation-free, sensitive and high-contrast vascular imaging and cell tracking*. Curr Opin Chem Biol, 2018. **45**: p. 131-138.
68. Caspani, S., et al., *Magnetic Nanomaterials as Contrast Agents for MRI*. Materials (Basel, Switzerland), 2020. **13**(11): p. 2586.
69. Langsjoen, J., et al., *A comparison of ferumoxytol with gadolinium as contrast agents for the diagnostic magnetic resonance imaging of osteomyelitis*. Magn Reson Imaging, 2020. **71**: p. 45-54.
70. Lee, N., et al., *Water-dispersible ferrimagnetic iron oxide nanocubes with extremely high r_2 relaxivity for highly sensitive in vivo MRI of tumors*. Nano Lett, 2012. **12**(6): p. 3127-31.
71. Daldrup-Link, H.E., et al., *MRI of tumor-associated macrophages with clinically applicable iron oxide nanoparticles*. Clin Cancer Res, 2011. 17(17): p. 5695-704.
72. Reddy, L.H. and P. Couvreur, *Nanotechnology for therapy and imaging of liver diseases*. Journal of Hepatology, 2011. **55**(6): p. 1461-1466.
73. Reimer, P. and B. Tombach, *Hepatic MRI with SPIO: detection and characterization of focal liver lesions*. Eur Radiol, 1998. **8**(7): p. 1198-204.
74. Kirschbaum, K., et al., *In vivo nanoparticle imaging of innate immune cells can serve as a marker of disease severity in a model of multiple sclerosis*. Proceedings of the National Academy of Sciences, 2016. **113**(46): p. 13227-13232.
75. Guldris, N., et al., *Magnetite Nanoparticles for Stem Cell Labeling with High Efficiency and Long-Term in Vivo Tracking*. Bioconjugate Chemistry, 2017. **28**(2): p. 362-370.

Chapter 2: CAPILLARY ELECTROPHORESIS AND THE ASSOCIATING PRECONCENTRATION METHODS FOR BIOMOLECULE ANALYSIS AND MAGNETIC PARTICLE CHARACTERIZATION

CE is a powerful method for separation and characterization of biomolecules (e.g.,, proteins [1], peptides [2], glycans [3], DNA [4]) and magnetic bead analysis [5] thanks to its high separation resolution, and small sample volume consumption (in the nL - µL ranges). When using CE for separation of biomolecules in biofluids for diagnostic purposes in particular, very often their concentrations are at trace levels. High detection sensitivity is therefore required. Different detection strategies for CE, relying mostly on fluorescent, UV, contactless conductivity (C4D) and mass spectrometry (MS) detection, were proposed to allow tracing target molecules down to nM ranges [6]. However small optical pathlength and small loaded volumes are always the inherent problems preventing sensitive detection of target molecules in CE analysis. In a related context, several strategies were studied for sample preconcentration and well proved their indispensability in biomolecule analysis [7]. Forefront sample treatment and preconcentration, which can be conducted on-line or off-line, allow obtaining enriched and purified analytes and eliminating the sample matrix prior to their CE separation. This chapter will present in detail the principles of CE together with some associating preconcentration methods, with particular attention to CE analysis of DNA, amyloid beta (Aβ) peptides and characterization of magnetic particles (MPs).

2.1 FUNDAMENTALS OF CE

2.1.1 Working principle of CE

CE is a separation technique based on the different mobilities of ions under an electrical field [8]. The simple setup of a CE instrument is illustrated in *Figure 24*. All CE steps are carried out inside a narrow channel (typically 25-75 µm internal diameter). The capillary is normally made from fused silica covered with a polyimide coating outside.

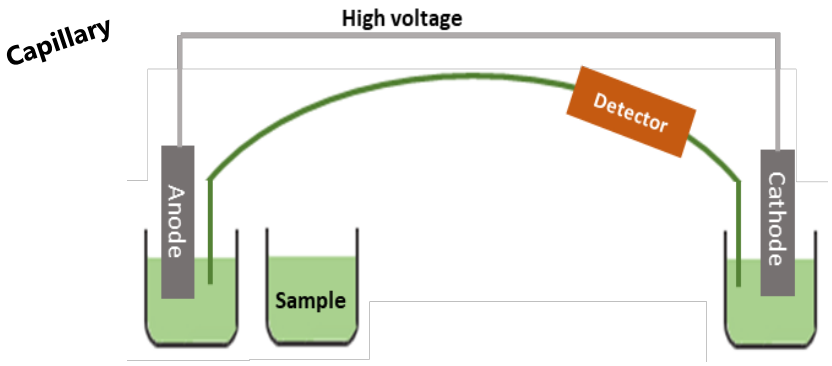

Figure 24: The typical setup of a capillary electrophoresis system.

Each side of the capillary, together with an electrode, is dipped in a vial containing the background electrolyte (BGE, normally, a solution of buffering salt). During the injection step, the BGE vial at one side is replaced with a sample vial. In the simplest mode of CE, called 'capillary zone electrophoresis' (CZE), the capillary is first fulfilled with the BGE, the sample solution is then injected accounting for 1-3% of the total capillary's volume. Upon application of a high voltage, the charged molecules are separated according to their electrophoretic mobilities and the electroosmotic flow (refer to the next chapter for further details). The role of BGE is to provide constant conditions (e.g., pH, ionic strength (IS), conductivity) for the analyte ions during the separation. Only under constant conditions, the target molecule can be identified by its migration time in CZE [9].

The electric current, generated by the movement of ions in the BGE under an electrical field, should be kept as low as possible during a CE run in order to minimize heating gradient inside the capillary, called Joule heating [10]. Indeed, the Joule heating effect limits the separation and resolution. The thermal gradient loads to the higher temperature in the center of capillary than at the wall which could be risky for heating sensible biomolecules. While the viscosity at the center decreases, the velocity of analyte in the center will go up, generating the deformation in analyte plug, increasing the peak tailing and broadening. To avoid/minimize Joule heating, normally the use of capillaries having small internal diameters (ID of 25-50 µm) is preferable since they offer high surface over volume ratio, leading to faster heat dissipation [11]. An increase in IS of the BGE generally results in current increase and therefore Joule heating generation [12]. To dissipate the heat generated during a CE run, the CE instrument is normally equipped with a cooling system using air or liquid, which thermostats the capillary. While liquid cooling is reported more efficient, under typical conditions of less than 5 to 7 W/m power generation, air cooling is sufficient [13].

So far, four modes of detection are commercially available for CE, including UV, fluorescent (laser-induced fluorescence (LIF) and LED-induced fluorescent (LEDIF)) detection, conductively coupled contactless conductivity detection (C4D), and mass spectrometry (MS). Each detection type requires different criteria of BGE compositions for its best performance. *Table 2* summarizes the BGE normally used for each detection mode. The UV and LIF detectors detect the analyte directly in the capillary via an optical window created on capillary by eliminating the coating. With UV detection, the absorbance of the analytes is measured with the light that passes through the optical window at the predefined wavelength in the UV range [6]. With LIF and LEDIF detection modes, the sample is excited with a laser source or a LED source, and the fluorescence emitted by the analyte in the sample is subsequently measured by a photodetector [14]. In C4D, no optical window is required as the electrodes are positioned outside and along the capillary to form a series of capacitors and resistors. By applying an alternative voltage at a high frequency (typically more than 300 kHz), the resistance of the solution changes when the ions pass through the electrodes, leading to a change of the resulted alternative current [15]. The signal in C4D is then dependent on the difference between the conductivity of the target analytes and that of the BGE. With the off-capillary MS detection, the mass over charge (m/z) values of ions from target analytes are achieved after their ionization upon exiting the end of capillary after CE separation [6].

Table 2: The typical BGEs used for each detection mode.

Detection mode for CE	**Typical BGE composition**	**Advantages**	**Limitations**	**References**
UV detection	Compounds with no or little UV absorption. Typically small inorganic ions such as borate, phosphate, etc.	Simple, no need for forefront derivatization	Creation of an optical window required, risk of capillary breaking. Low sensitivity (typically 1 µM LOD). High electric current (thus Joule heating) when using BGEs at high IS for CE.	[6, 16]

Fluorescent detection	Compounds normally used for CE-UV. Other organic compounds can be also used, such as citrate, 2-Amino-2-hydroxymethyl -propane-1,3-diol (Tris), etc.	High sensitivity (down to sub nM ranges) and high selectivity (thanks to fluorescent tagging).	Creation of an optical window required, risk of capillary breaking. Forefront labelling step requirement. Joule heating at high IS buffer (similar to the problem encountered with BGE for CE-UV).	[14, 17, 18]
C4D	Compounds have low specific conductivities. BGEs are normally composed of organic weakly charge molecules, such as Tris, histidine, etc.	Simple, and straightforward. No need for optical window. No derivatization needed. Can be used for detection of non or poor UV absorbing analytes. BGE has low conductivity, generating low electric currents to minimize Joule heating.	Bulk detection with no selectivity (thus CE separation is required). Low sensitivity (typically 1 µM LOD)	[19, 20]
MS	BGE contains no inorganic salts. Use volatile	High sensitivity and selectivity. Structural information provided.	Complicated Expensive instrumentation. Unstable currents and	[21-23]

	small compounds such as formic acid, ammonium hydroxide, acetic acid, etc.		failure of CE-MS coupling frequently encountered.	

2.1.2 Electrophoretic mobility

The electrophoretic mobility μep ($cm^2.V^{-1}.s^{-1}$), reflecting the displacement of a charged species under the electrical field, measures the influence of the electric field (E) on the speed (v) of a charged particle. It is constant and specific to each compound and the electrolyte. The electrophoretic mobility of a charged species is dependent on its hydrodynamic radius Rh, its charge q, and the buffer's viscosity η [24], defined as:

$$ep = \frac{q}{6\pi \times Rh \times \eta} \quad (1)$$

Accordingly, the electrophoretic mobilities are higher for more charged and smaller-sized species. While the negative or positive ion with its own charge q is attracted towards the electrode of polarity opposite to its charge, a neutral species, for which q is zero, has no electrophoretic mobility, and thus velocity of zero. The velocity ν ($cm.s^{-1}$) of a charged species indeed depends on the electrophoretic mobility of the species and the electric field E ($V.cm^{-1}$) [25], and can be calculated according to equation (2)

$$v = \mu ep \; x \; E \quad (2)$$

2.1.3 Electroosmotic flow

2.1.3.1 Principles of EOF

The fused silica capillary used in CE contains silanol groups (Si-OH) on its internal wall's surface. The inner wall of capillary is normally negatively charged due to the ionization of surface to form SiO^- groups when pH of the BGE filled inside the capillary is superior to 3 [13]. A double layer of

cations from the BGE is then created to balance the negative charge of the capillary's internal surface. It leads to formation of the Stern layer binding to the inner capillary wall and a diffuse layer. As a result, a surface potential between the double layer is generated, called the zeta potential (ζ), which is described as:

$$\zeta = \frac{\delta . \sigma}{\varepsilon_r . \varepsilon_0} \quad \text{with} \quad \delta = \sqrt{\frac{\varepsilon_r . \varepsilon_0 . R . T}{2 . I . F^2}} \tag{3}$$

With:

δ: thickness of the double layer

σ: density of surface charges of the capillary

ε_r: dielectric constant of the electrolyte

ε_o: permittivity of the vacuum

R: ideal gas constant

T: temperature (K)

I: ionic strength of the electrolyte

F: Faraday constant

Upon application of an electrical field, the cations forming the double-layers are attracted toward the cathode. Their movement drags a bulk solution in the capillary also toward the cathode, called EOF. The EOF can be described according to equation below:

$$v_{eo} = \mu_{eo} . E = -\frac{\varepsilon_r . \varepsilon_0 . \zeta}{\eta} . E \tag{4}$$

With:

ε_r: dielectric constant of the electrolyte

ε_o: permittivity of the vacuum

η: the buffer's viscosity

ζ: zeta potential

E: electrical field (V)

In practice, μeo is calculated following the equation (5), by measuring the migration time of a neutral molecule (e.g., dimethyl sulfoxide (DMSO)).

$$\mu eo = \frac{l \times L}{E \times tDMSO} \quad (5)$$

With:

L, l: total length and effective length (the length from the injection end of the capillary to the detector) of the capillary (cm), respectively.

E: electrical field (V)

tDMSO: migration time of DMSO (s)

It is revealed that the µeo value obtained with a fused silica capillary increases rapidly in the pH from 4 to 8 where the silanol sites begin to dissociate and starts to level off at pH higher than 8 where silanols are almost fully dissociated [26, 27].

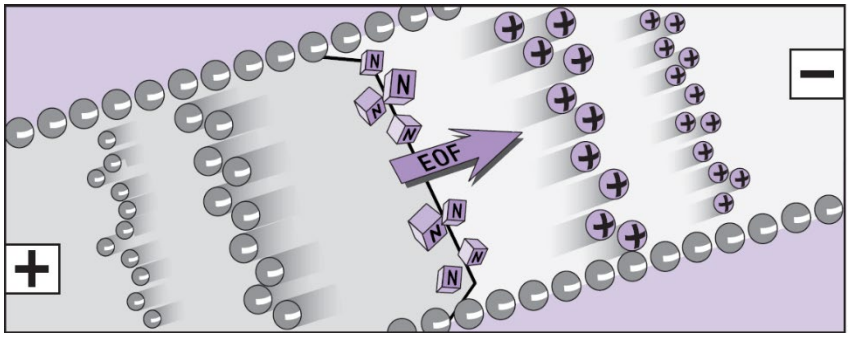

Figure 25: The separation of negative, positive, and neutral ions with the presence of EOF inside the capillary [13].

Compared to the parabolic profile of the hydrodynamic flow in chromatography, the displacement of the bulk solution by EOF has a flat profile, therefore the diffusion during separations is limited. The positively charged analytes migrate toward cathode in the same direction as EOF, while the negatively charged ones migrate electrophoretically against the EOF direction (*Figure 25)*.

As a consequent, the apparent migration of an ion inside the capillary under an electrical field is due to its electrophoretic mobility and the electroosmotic mobility (µeo). The apparent mobility µapp ($cm^2.V^{-1}.s^{-1}$) of an ion is accordingly calculated with the following the equation (6)

$$\mu app = \mu eo + \mu ep = \frac{l \times L}{E \times t} \quad (6)$$

With:

L, l: total length and effective length (the length from the injection end of the capillary to the detector) of capillary (cm), respectively.

E: electrical field (V)

t: migration time (s)

A strong EOF can accelerate much the migration of cationic analytes because both electrophoretic migration and electroosmotic flow are in the same direction. When the EOF is too strong, the analytes can be pushed out by EOF before being separated, resulting in poor separation resolution in this case. Regarding the anionic compounds, which migrate electrophoretically towards the anode, if their μep are stronger than EOF (see equation above), their apparent migration direction is against EOF towards the anode. Reversely, they are pushed gradually by EOF toward the cathode. Note that when the capillary internal surface is modified, for example due to adsorption of analytes on the fused silica capillary wall, the EOF is changed and/or fluctuates, resulting in unsatisfied repeatability and/or separation efficiency [28]. In many cases, suppression of EOF is preferable to allow better performance in CE separation. Different strategies to suppress EOF based on the effective factors shown in equation (4) are accordingly described below.

2.1.3.2 Strategies to suppress EOF

Commonly used strategies to suppress EOF relying on these parameters are summarized in Table 3.

Table 3: Some established methods to suppress EOF.

Parameters	Effect	Advantages	Considerations	References
pH of the BGE	Decrease EOF at acidic pH Increase EOF at basic pH.	Simple and effective way to modulate EOF up to 1x 10^{-3} (cm^2/V.s).	Possible denaturation of proteins, peptides at acidic pH.	[26]
Ionic strength of	Decrease EOF at high IS or high salt	EOF modulation in wide range of pH	High current, Joule heating when the conductivity of the	[29-33]

the BGE	concentration.	EOF suppression to 0.47 x 10^{-5} (cm^2/V.s) at pH 4.5.	BGE increases too much.	
Viscosity of the BGE	Decrease EOF at high viscosity.	Wide range of pH application EOF suppression to 10 x 10^{-5} (cm^2/V.s) at pH up to 10.5.	Hard to find the BGE with suitable viscosity and compatible with CE. More difficult to remove BGE from the capillary after analysis.	[34-36]
Coating capillary	Decrease EOF by covering the negative charge of capillary wall.	The best effective EOF suppression is so far 0.1 x 10^{-5} (cm^2/V.s) at acidic pH. Dynamic coating: cost-effective, easy to removal by washing after analysis and regeneration. Permanent coating: stability, no need to add additives in buffer to maintain the coating layer, MS compatibility.	*Dynamic coating:* Unwanted interaction between analytes and coating reagents in the BGE. *Permanent coating:* Limited lifetime Laborious protocol for preparation of some coatings.	[37-44]

The most commonly used strategies to suppress EOF include modification of the pH and/or IS of the BGE and capillary coating. Numerous studies reported the use of capillary coating for reduction of analyte adsorption and EOF suppression [45]. The coating strategies are classified into two

categories: dynamic and permanent coating. The coating layer can reverse the capillary inner surface charge from negative to positive, leading to reversion of EOF direction, or cover the negative charge of capillary's wall with a neutral layer, therefore suppressing the EOF [38]. For dynamic coating strategies, the additives are added into the BGE, and create a temporary coating on the capillary inner surface during the CE separation [39]. Some commonly used additives for dynamic coating include sodium dodecyl sulfate, cetyltrimethylammonium bromide (CTAB), and polymers such as polyethylene oxide (PEO), polyvinyl alcohol (PVA), and dextran [28, 41, 42]. For the permanent coating, the coating layer irreversibly attaches to the capillary's wall by hydrophobic, electrostatic force, hydrogen bonding [43] and/or covalent bonding by modifying the silanol surface [38]. The coating strategies can suppress the EOF down to 0.1-0.5 x 10^{-5} ($cm^2.V^{-1}.s^{-1}$) [37, 44]. Recently, coating strategies using nanoparticles (NPs), especially polymer NPs have drawn much attention since they have many advantages *(Figure 26)*. These particles form stable suspensions in water and in BGE. Thanks to their variety of functional surface groups and high surface-to-volume ratio, they may provide diverse chemical groups and charges (negative, positive and neutral one) as coating materials and display high adhesion to the fused silica capillary surface due to electrostatic as well as nonspecific interactions [46].

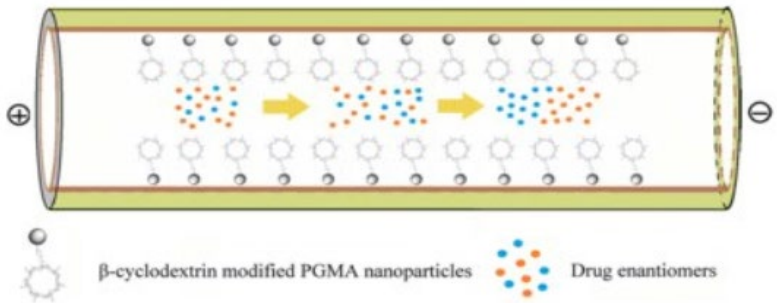

Figure 26: Schematic presentation of capillary coated by poly(glycidyl methacrylate) (PGMA) nanoparticles functionalized with β-cyclodextrin [47].

In the second strategy using high IS of the BGE to suppress EOF [27, 31], the high quantity of ions inside the capillary results in compression of the double layer on the capillary inner wall, and thus decrease of the zeta potential, leading to EOF suppression *(Figure 27)*. µeo can be decreased down to 0.47 x 10^{-5} ($cm^2.V^{-1}.s^{-1}$) by employing BGE IS up to 150 mM [33].

Regarding the strategy to use viscosity of the BGE to suppress EOF, glycerol-water with the ratio of 30: 70 (v/v) was often used to suppress effectively EOF in bare silica capillaries in a wide range of pH application (from 3 to 10) [34-36]. This glycerol-water mixture results in a lower dielectric constant of the medium and thus lower zeta potential. The lowest µeo obtained was 10 x 10^{-5}

($cm^2.V^{-1}.s^{-1}$) at pH 10.5. Furthermore, this strategy using glycerol-water is compatible with subsequent MS. Other viscous gels such as PEO or acrylamide-based hydrogel were also used at the anodic end of the capillary to stop the electroosmotic pumping effect which allows to obtain a zero net-flow during CE separation [48, 49].

The dependence of μeo on electrical fields and temperature was reported elsewhere in the 1990s [29, 50, 51]. While the electrical field induced an additional charge on the inner capillary surface, which in turn effects the ζ potential, and therefore μeo; a high temperature affects EOF indirectly through the temperature-induced change of the BGE viscosity. Nevertheless, these strategies are not widely used in studies nowadays.

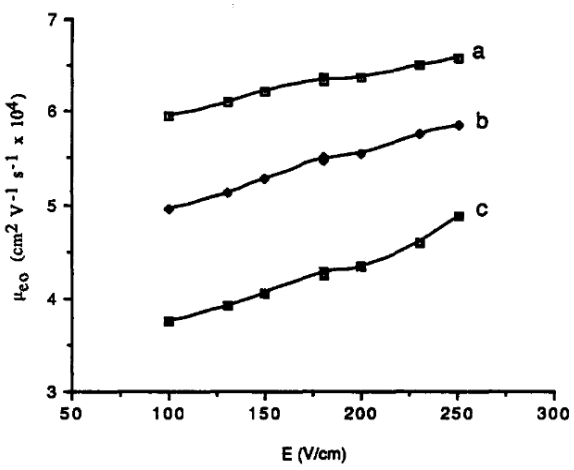

Figure 27: Influence of the buffer concentration and electric field strength on the EOF in a 50 μm capillary. Na2HPO4 concentrations in the BGE: a = 0.01 M; b = 0.02 M, c = 0.05 M [51].

2.2 Some selected forefront electrokinetic preconcentration techniques in CE

To overcome the limitation of low detection sensitivity when working with CE, several preconcentration approaches have been investigated [52]. This chapter will present three particular modes of electrokinetic preconcentrations that have been frequently used for CE and are directly linked to the experimental scope of this thesis, including field-amplified sample stacking (FASS)/field-amplified sample injection (FASI), large volume sample stacking (LVSS), and isotachophoresis (ITP).

2.2.1 Field-amplified sample stacking (FASS) and field-amplified sample injection (FASI)

Since 1979, Mikkers et al reported for the first time the sharper peak obtained when the analyte was diluted in water instead of BGE [53]. This phenomenon, named FASS, can be explained that

when an ion migrates from a low-conductivity medium (e.g., water) into a BGE at higher conductivity, it will slow down dramatically at the boundary of the two solutions and stack into a narrow band (*Figure 28*) [7].

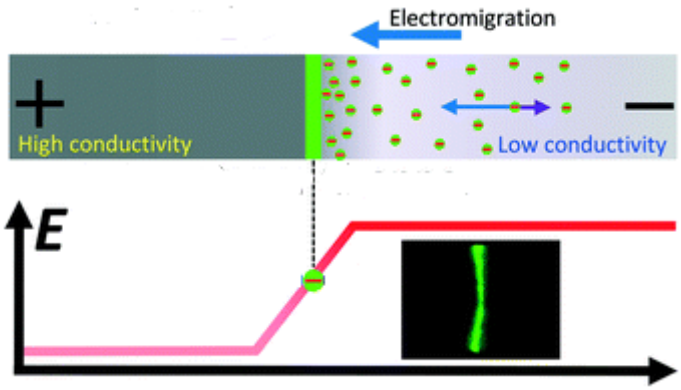

Figure 28: The working principle of field-amplified sample stacking [54].

Indeed, as the analyte's velocity is directly proportional to field strength, the ion will accelerate when it goes from low resistance (high conductivity) to high resistance (low conductivity) and vice versa. FASS is supposed to be the simplest electrokinetic preconcentration method and normally occurred concurrently with other modes of preconcentration/separation in CE when working with analytes prepared in another medium other than the BGE.

Nevertheless, there are some considerations when using FASS. First, low conductivity buffer cannot be reached for all biomolecule samples. Second, if the sample plug is long, the gradient in electric field needed for stacking causes a gradient of electroosmotic velocity that generates a laminar flow inside the capillary. The laminar flow will broaden the sharp stacking peak and at the same time decrease the capillary length for separation, therefore reducing the resolution. Hence, the maximum sample injection volume is limited to about 3–5% of the capillary volume, resulting in modest enrichment factors [55, 56].

The working principle of FASI is similar to that of FASS. The only differences between them are from the injection step. With FASS, sample injection is done via pressure application, whereas in FASI, the injection is carried out via application of an electrical field while the capillary end is dipped in the sample vial [56]. Positive or negative voltage is applied depending on the charge of analytes. As little sample matrix is coinjected by electrokinetic injection, the injection time can be longer and this technique can provide exceptionally high preconcentration factors (up to 1000 times) [57]. Nevertheless, FASI can be applied for only fast migrating analytes and the injection

sample volume is hardly defined since it is not proportional to the injection time [58]. Moreover, the ions with high mobility will be favorably introduced to capillary and stacked at injection point compared to slow ones, leading to stacking bias [59].

2.2.2 Large volume sample stacking (LVSS)

In the 1990s, the LVSS was designed by Chien and Burgi to overcome the small injection volume in FASS which limits the sensitivity of CE. Similarly to FASS, the sample is prepared in a low conductivity buffer while the capillary is filled with a high conductivity BGE. The sample is hydrodynamically introduced to more than 5% of capillary length. To stack the long sample plug without decrease the separation resolution, it is necessary to remove the sample matrix after stacking. The LVSS technique allows removing sample matrix out of capillary during the stacking process [60]. When most of sample matrix is removed, the current increases as the low conductivity sample zone is replaced by the higher one of BGE, reaching 90-95% of BGE's current [61].

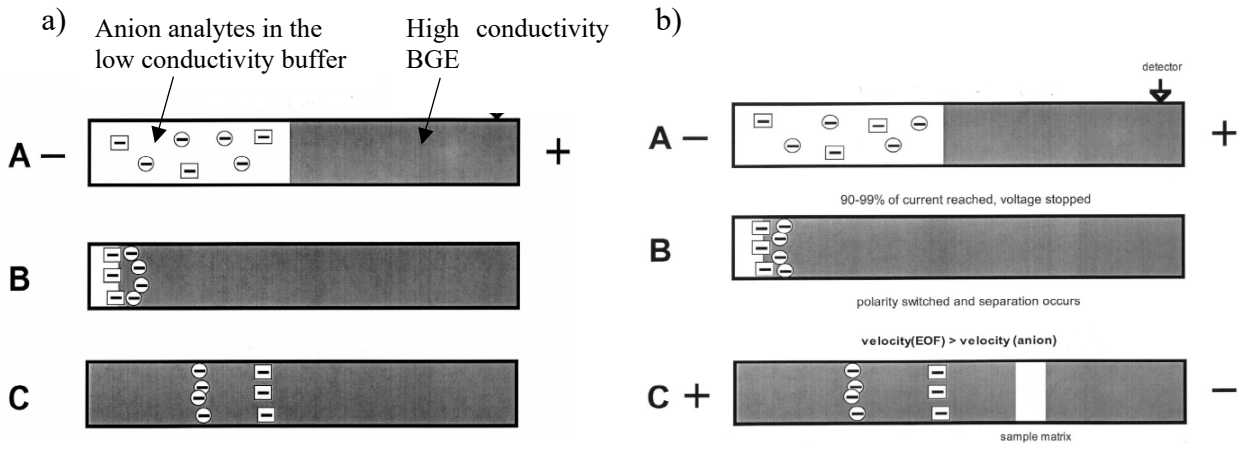

Figure 29: The preconcentration step of large volume sample stacking: a) with electroosmotic pump; b) with polarity switching [59].

For sample removal purpose, the voltage is applied to push the sample matrix out at the injection end thanks to EOF and the sample will be stacked at the boundary of sample/BGE. Since the velocity of anions is lower than EOF when the capillary is filled with a low conductivity matrix, the direction of electrical field is as described in (*Figure 29*, step A). As the BGE penetrates more and more into capillary, the EOF will decrease gradually before reaching the stable value. Then, for anion separation, there are two strategies. The separation is taken by the electrophoretic mobilities of anions if they are higher than EOF when the capillary is filled with BGE, well known as LVSS with electroosmotic pump (LVSEP) (*Figure 29a*). Contrary, the polarity must be switched if the EOF is significantly higher than the electrophoretic mobilities of anions. The later strategy is

named LVSS with polarity switching (*Figure 29b*) [59]. The fundamental of this method is that the electrophoretic mobilities of the analytes must be opposite to that of the EOF. Hence, for cation stacking by LVSS, capillary coating or an additive should be used to reverse the direction of EOF. Note that large amount of other sample components can be also concentrated in LVSS, which may degrade the separation and mask the interested analyte.

2.2.3 Isotachophoresis (ITP)

ITP is an electrokinetic preconcentration method based on a discontinuous electrolyte system.

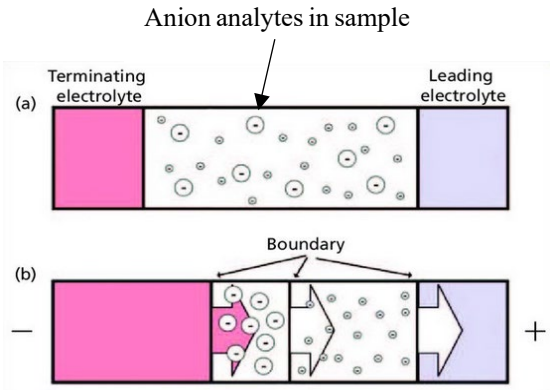

Figure 30: Illustration of ITP conditions (a) initial conditions and (b) ITP separation and preconcentration [62].

The analyte migrates between a leading electrolyte (LE) and a terminating one (TE), with the migration order according to their effective mobilities (e.g., LE co-ion having the highest mobility, followed by the mobility of the analyte and then TE co-ion having the lowest one) (*Figure 30*). The ITP has two interesting features: (i) the self-sharpening effect and (ii) electrophoretic memory effect. For the self-sharpening effect, the velocity of an ion in each ITP zone is at a steady-state. The electrical field is self-adjusting to maintain its constant velocity. Following the equation (2) (part II.1.2), the lowest field across the zone having highest mobility of ions. If an ion diffuses into a neighboring zone, its velocity changes and it immediately returns to its own zone. Consequently, the dispersion is minimized by keeping their sharp boundaries between the zones and therefore the resolution is optimized. For electrophoretic memory effect, when one zone is replaced by another with different compositions, the concentrations of ions adjust in a defined way and usually remain in the same order of magnitude. When an analyte electromigrates from a zone having a low ions concentration into another having a higher one, its concentration is accordingly adjusted to a new higher value. This property of ITP is used as the preconcentration step [63, 64].

2.3 CE OF SOME TARGET BIOMOLECULES AND MAGNETIC NANO PARTICLES (MNPS)

CE is one important method for separation and characterization of biomolecules [65] and nanoparticles [66]. As the categories of biomolecules and nanoparticles are very large, we keep our focus on those that are directly related to the work done in the context of this thesis, including nucleic acids, amyloid beta peptides (used as biomarkers for molecular diagnosis of Alzheimer's disease) and MNPs.

2.3.1 CE of DNA analysis

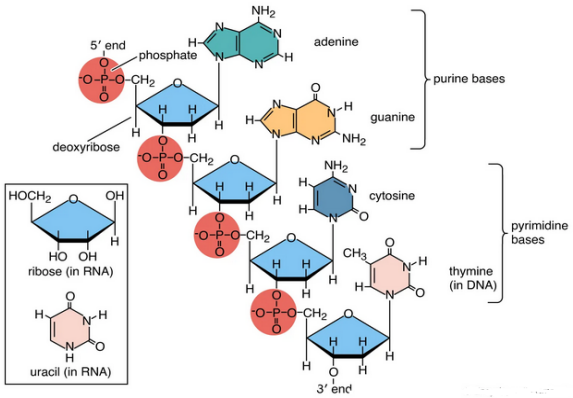

Figure 31: Polydeoxyribosenucleotide structure of a DNA strand (Encyclopedia Britannica, Inc).

For DNA analysis (see *Figure 31* for the typical structure of a DNA), CE was developed as an alternative method for standard slab gel electrophoresis to offer many advantages such as higher sensitivity and resolution, faster operation, and faster data treatment [67, 68]. A variant of CE, capillary gel electrophoresis (CGE), was commonly used to separate the single-strand (ssDNA) or double-strand (dsDNA) fragments with different lengths from several base pairs to hundred base pairs, as well as evaluate the purity and modification of oligonucleotides and PCR products [68, 69]. CGE employs a gel in the BGE as a molecule sieve to separate the molecules by size. When they go through the sieve net, the larger molecules are hindered more than the small ones. This method allows baseline separation of DNA fragments thanks to the polymer sieve [13]. An ideal matrix for DNA analysis with CGE should have high hydrophilicity, high concentration, low viscosity to loading and replacement and stability [70, 71]. The linear polyacrylamide (LPA) and hydroxyethyl cellulose (HEC) are two gel candidates for DNA, able to extend and strengthen a robust entanglement thanks to their higher hydrophilicity than other polymers [72, 73].

For DNA detection after CE separation, UV detection is normally used at the wavelength of

260/280 nm [74]. LIF detection is also a commonly used method to improve the sensitivity of DNA detection. In this case, DNA staining is needed. Intercalating dyes, notably ethyl bromide, propidium iodine, mono and bis-intercalating cyanine (e.g., SYBR Green, YOYO-1), are normally used for this purpose [75]. Other fluorophores such rhodamine derivatives are also used for DNA labeling prior to their LIF detection. These compounds can be added to the BGE [76]. They can also covalently attach to the DNAs to render them fluorescent prior to their electrophoretic separation [77]. Other DNA staining molecules were also proposed as an alternative to the toxic ethyl bromide, notably GelGreen, and SYBR safe [72]. A summary of different CE approaches for DNA analysis and characterization can be found in the *Table 4* and commonly used electrokinetic preconcentration methods in *Table 5*.

Table 4: Commonly used CE modes to for separation of DNAs.

CE mode	Compound	Buffer used	Remarks/Refs
CGE-LIF	100bp DNA ladder.	30 mM Tris, 9.5 mM H_3PO_4, 2 mM EDTA, 4.5% HEC and fluorescent dye (Gelgreen or YOPRO-1), pH 7.3.	For Gelgreen: LOD: 6.4 pg/µL LOQ: 21.2 pg/µL Resolution < 2.1 bp for fragments 18-100 bp DNA [72].
CGE-UV and CGE-LIF	50bp and 100bp DNA.	Tris-phosphate-EDTA buffer (TBE) containing 2-hydroxyethyl cellulose (HEC) at pH 7.3. Rinse capillary by 1% PVA before sample injection.	LOD and resolution not mentioned [78].
CGE-LIF	DNA fragments <70 bp.	TBE buffet at pH 6.5 containing LPA 2-8%.	Resolution: 1.62 or 5 bp LOD not mentioned [73].
CGE-LIF	131, 151, 170 and	20 mM Tris, 10 mM phosphoric acid,	LOD: 125 pM [79].

	194 bp dsDNA.	2 mM EDTA, and 4.5% HEC at pH 7.3.	
CGE-LIF	ΦX174-Hae III digest DNA (11 fragments: 72, 118, 194, 234, 271, 281, 310, 603, 872, 1078 and 1353 bp).	TBE buffer at pH 7 containing PVP 6%.	LOD: 0.1 ng/μL Resolution not mentioned [80].
CGE-LIF	DNA standard sample FX174 DNA–Hae III digest.	TBE buffer at pH 8.3 (89 mM boric acid, 89 mM Tris, and 2.0 mM EDTA) and 3mg/mL added ethyl bromide dye. Copolymer gel F127 ($PEO_{99}PPO_{69}PEO_{99}$) in TBE and 1-butanol.	LOD and resolution not mentioned [81].
CGE-LIF	DNA extracted from cells.	TBE buffer containing 1mM/L YO-PRO-1 and 1.2% HEC (w/v), pH 8.3. Capillary coated by LPA.	LOD and resolution not mentioned [82].
CGE-LIF	8.27 to 48.5 kbp DNA and λ-DNA 0.12 to 23.1 kbp.	10 mM Glycine-citrate buffer at pH 7. Capillary coated by gold-NPs immobilized with PEO.	Resolution is 10.1 for 2027 bp and 564 bp [83].
CGE-LIF	DNA ladder	2, 5% PVP: HEC (5: 95) solution is diluted in 100 mM TAPS pH 8.0 and 7.1 M urea, pH 8.4.	Resolution: 1.3 bp for fragments 139–160 bp and 4.6 bp for fragments > 400

			bp [84].

Table 5: Commonly used methods for electrokinetic preconcentration of DNAs.

CE mode	Compound	Buffer used	Remarks/Refs
ITP-LIF	Standard: Salmon sperm DNA fragments 200 bp and 2000bp Sample: DNA from a crude yeast cell lysate.	LE: 160 mM creatinine, 40 mM oxalic acid, 0.5% HPMC, and 0.25% Triton X-100 in water. TE: 10 mM TAPS and 10 mM Tris base.	Enrichment factor: 34 folds for standard and 12 folds for samples [76].
ITP-LIF	DNA 200bp from blood.	LE: 375 mM Tris and 250 mM HCl at pH 7.8. TE: 25 mM Tris and 25 mM serine at pH of 8.7.	Enrichment factor 100 folds [77].
ITP-LIF	DNA 200bp from blood.	LE: 250 mM HCl and 375 mM Tris at pH 7.8. TE: 25mM serine and 25mM Tris at pH 8.7.	Enrichment factor not mentioned [85].
ITP-LIF	Salmon sperm DNA.	LE: 0.01% Tween 20 in 40 mM MES and 20 mM NaOH at pH 6.0. TE: 0.01% Tween 20 and 500 nM SYTO 64 in 36 mM 6-aminocaproic acid and 18 mM HCl at pH 4.4.	Enrichment factor not mentioned [86].
ITP-LIF	ssDNA and an RNA ladder.	LE: 30 mM HCl, 60 mM Tris, 1% PVP, 4 M urea, and 2.5% HEC.	Enrichment factor not mentioned [87].

		TE: 30 mM HEPES, 60 mM Tris, 10 mM aspartic acid, and 1% PVP.	
ITP-LIF	Scaffolded DNA origami.	LE: 15 mM HCl and 30 mM imidazole, pH 7.0. TE: 20 mM HEPES and 35 mM imidazole pH 7.0.	Enrichment factor 150-folds [88].
ITP-LIF	DNA and cDNA.	LE 1: 250 mM HCl, 500 mM Tris, 5 mM $MgCl_2$, 0.1% PVP, 10% formamide, and 0.01% Tween20. LE 2: 250 mM HCl, 500 mM Tris, and 25% Pluronic F-127. TE : 5 mM HEPES, 50 mM Bis–tris, 1% PVP.	Enrichment factor 30-folds [89].
ITP-FLD	PNA probes-DNA complexes.	LE: 200 mM HCl, 400 mM Bis, and 1% PVP TE: 10 mM MES and 20 mM bistris	Enrichment factor 2-folds [90].
Microchip CGE-LVSEP	φX174/HaeIII digest.	0.5–2.0% (Hydroxypropyl)methyl cellulos and 0–3.0% D-mannitol dissolved in 0.5–1 TBE buffer (pH 8.0–8.3). PVA-coated channel.	Enrichment factor 74 to 108-folds [91].
CGE-UV-LVSS	ϕ174 RF DNA-HaeIII digest or the mixture of pBR 322/HaeIII, pBR328/BglI, and pBR	2.5% PEO + 400 mM TB buffer, pH 10.0	Enrichment factor 400 -folds [92].

	328/HinfI digests.		

2.3.2 CE of MNPs

A summary of the CE approaches and their variants in the microchip format for characterizing and electrokinetic preconcentrating MPs is presented in *Table 6* and *Table 7*. CZE is one of the powerful techniques to characterize MNPs as well as to monitor their interaction with the (bio)molecules. UV detection (normally at 200 nm or 254 nm) was commonly used for characterization of MNPs' size and surface charge [93]. LIF detection was used sometimes for engineered MNPs conjugated with fluorescence group [94]. The inductively coupled plasma-MS (ICP-MS), was also used in CE to provide additional information about the interaction between MNPs and biomolecules [95, 96].

Table 6: The CE modes to characterize the MNPs.

CE mode	MNPs composition and size	Buffer used	Remarks/References
CZE-UV	Bare (7-13 nm) and MNPs (10 nm) functionalized with carboxylic group.	10 mM Tris-nitrate containing 20 mM of tetramethylammonium hydroxide at pH 9.	Characterization of surface chemistry and separation 2 groups of MNPs in 10 minutes [93].
CZE-UV	MNPs functionalized with carboxylic group (75 nm).	10 mM borate/NaOH pH 9.5.	Studying the stacking effect on NPs. MNPs' mobility and double layer thickness decrease due to the increase of IS buffer [97].
CZE-ICP-MS	MNPs functionalized with carboxylic group (7 nm).	25 mM phosphate buffer at pH 7.4.	Study of interactions between carboxylated MPs and polymyxin B from 0-250 M/L [96].
CZE-UV	MNPs 20-30 nm	Na_2SO_4 –NaOH (pH 10.8) and Na_2SO_4–Na3	Studying the electrophoretic mobility and aggregation of

		citrate (pH 7.1).	MNPs in different buffer and pH [98].
CZE-UV	MNPs functionalized with NH_2/PEG	Capillary coating with didodecyldimethyl-ammonium bromide 165.9 mM Tris/100 mM HCl buffer at pH 8	Characterization of charge-based of bifunctional MNPs, the dependence of electrophoretic mobility on charge and amino group density [99].
CZE-LIF	MNPs functionalized with carboxylic or aminopropyltrimeth-oxysilane groups (hydrodynamic radius 163-194 nm)	100 mM sodium borate buffer at pH 9.2.	Characterization of conjugation efficiency of antibodies and proteins to MNPs [94].
CZE-ICP-MS	Polymer MNPs functionalized with different terminal groups (carboxyl and amino).	20 mM ammonium bicarbonate at pH 7.4.	The study of MNPs interactions with proteins and their changes under analysis conditions (e.g., pH, buffer, etc.) [95].
CZE-UV	MNPs 6-10 nm	Capillary coated with hydroxypropylcellulose or hexadimethrine bromide or didodecyldimethylamm-onium bromide 10.5 mM β-alanine buffer +10 mM HCl at pH 2.9.	Characterization of size-dependence of MNPs on electrophoretic mobility and analysis conditions [100].
CZE-UV	Polyacrylic acid	10 mM borate buffer at	Characterization of the

	coated MNPs 8-10 nm.	pH 8.3.	interaction between MNPs and proteins [101].
CZE-UV	MNPs functionalized with carboxylic group 100 nm.	Sodium borate buffer pH 9.2 at different ionic strengths.	Studying the surface charge and electrophoretic mobility of MNPs under analysis conditions [102].
CZE-LIF	Fluorescent MNPs functionalized with poly(hexadecyl cyanoacrylate); PLA; PLA-b-PGE (163 nm; 105 nm; 110 nm, respectively).	80 mM phosphate buffer pH 7.4.	Monitoring of NP interaction with Aβ1-42 monomers [103].
CE-LIF	Fluorescent aptamer MNPs (hydrodynamic radius 79.1 ± 4.2 nm).	100 mM MOPS buffer pH 7.3.	Quantitative study of lysozyme-binding aptamer conjugated to fluorescent MNPs. Binding site number, constant and affinity are also studied [104].

Table 7: Electrokinetic preconcentration techniques for CE characterisation of MNPs.

Analytes	**Techniques**	**Preconcentration Effect (LOD/LOQ)**	**References**
MNPs 75 nm	CE-UV-FASS	76	[97]
MNPs 75 nm	CE-UV-FASI	860	[105]
MNPs 80 nm	CE-UV-Dynamic pH junction	12	[106]

2.3.3 CE of amyloid beta peptide

Alzheimer's disease (AD) is a progressive neurologic disorder. It is the most common state of

dementia (60-70% cases), which is a continuous decline in memorizing, thinking, behavioral and social skills that affects a person's ability to live independently. AD affects 50 million patients worldwide in 2019 and will reach 139 million by the year 2050. AD could be a huge burden for medical service and social budget, costing about 2,8 trillion dollars in 2030 (World Alzheimer report 2021). Increasing age is the greatest known risk for AD since the majority of patients are 65 years old and over. The AD progresses over years, even decades, in silence before having a symptom when the loss of memory is irreversible and interferes deeply with the patient's daily life. There is so far no definitive cure for AD. However, there are some medicaments validated by Food and Drug Administration (FDA) in AD treatment, divided into two categories: (i) drugs that may change disease progression in AD patient, and (ii) drugs that may temporarily mitigate some symptoms of the disease. For the former class, aducanumab (Aduhelm) and lecanemab (Leqembi) are the first two drugs accepted recently by FDA. They are the anti-amyloid antibody, able to remove amyloid from the brain, reducing the cognitive and functional decline in AD patients. It is indicated for people with mild cognitive impairment (MCI) or mild state of AD who also have evidence of a buildup of amyloid plaques in the brain [107]. For second class, the drugs in the acetylcholine esterase inhibitor group such as galantamine, donepezil, and rivastigmine are administrated for long time. These inhibitor drugs block the normal break down in AD patients, leading to the increase of acetylcholine's concentration in the space between synapses, in order to have only modest effect on dementia symptoms [108].

The cause of the disease is supposed to be linked to the formation of abnormal structure called plaque and tangles, which is suspected to damage the neurons and killing neural cells. It is related to a proteolytic process of the amyloid precursor protein (APP) which leads to the formation of different isoforms of amyloid beta (Aβ) peptides. The fragments Aβ1-42 and Aβ1-40 have respectively 42 and 40 amino acid-length and possess high tendency (especially Aβ1-42) to aggregate to form oligomers, then fibrils and finally senile plaques, leading to reduction of cerebral clearance. This accumulation activates the neurotoxic signaling pathways, leading to neuron death [109, 110].

So far, the drug development for AD treatment encounters several challenges, including (i) ineffectiveness treatment due to late detection since the neuron damage is irreversible; (ii) difficulty in monitoring treatment process since the amyloid beta peptides and tau protein (another AD biomarker) exist more in cerebrospinal fluid (CSF) than in blood, leading to the difficulty in sample collection and (iii) lack of sensitive and selective methods for discrimination of AD from other

dementia due to very low abundance of biomarkers. Hence, novel analytical strategies for early AD diagnosis, partially based on Aβ peptide analysis, are always of utmost need in order to obtain the effective clinical AD assay and treatment. Among different analytical strategies developed for this purpose, CE is a promising one for Aβ peptide separation and detection. There are many CE strategies developed over 15 years to trace Aβ peptides in biofluids, which are presented in the following review.

Review: Recent Electrokinetic and Microfluidic Strategies for Detection of Amyloid Beta Peptide Biomarkers: Towards Molecular Diagnosis of Alzheimer's Disease

REVIEW

Recent electrokinetic and microfluidic strategies for detection of amyloid beta peptide biomarkers: towards molecular diagnosis of Alzheimer's disease

Ngoc Van Thanh Nguyen[1], Myriam Taverna[1,2], Claire Smadja[1*] and Thanh Duc Mai[1*]

[1] *Université Paris-Saclay, CNRS, Institut Galien Paris-Saclay, 92296, Châtenay-Malabry, France.*

[2] *Institut Universitaire de France*

Correspondence: E-mail: thanh-duc.mai@u-psud.fr;

claire.smadja@u-psud.fr

Keywords: Alzheimer's disease; diagnosis; amyloid beta peptide; microscale electrophoresis; immuno-preconcentration on magnetic beads; microfluidics

Abstract

Among all neurodegenerative diseases, Alzheimer's Disease (AD) is the most prevalent worldwide, with a huge burden to society and no efficient AD treatment so far. Continued efforts have been being made towards early and powerful diagnosis of AD, in the hope for a successful set of clinical trials and subsequently AD curative treatment. Towards this aim, detection and quantification of amyloid beta (Aβ) peptides in cerebrospinal fluid (CSF) and other biofluids, which are established and validated biomarkers for AD, have drawn attention of the scientific community and industry over almost two decades. In this work, an overview on our major contributions over 15 years to develop different electrokinetic and microfluidic strategies for Aβ peptides detection and quantification is reported. Accordingly, discussions and viewpoints on instrumental and methodological developments for microscale electrophoresis, microfluidic designs and immuno-enrichment / assays on magnetic beads in microchannels for tracing Aβ peptides in CSF are given in this review.

1. Introduction

Neurodegenerative diseases (ND), whether it is Alzheimer's Disease (AD), Amyotrophic Lateral Sclerosis (ALS), Parkinson's Disease or FrontoTemporal Dementia (FTD), are creating huge burden to the society and economy worldwide, affecting 150 million people and inducing a cost expected to reach 2 trillion USDs by 2030 [1]. Of all types, AD is the most prevalent one that affected more than 50 million of patients worldwide in 2018 and reaching 150 million by 2050 [1]. Unfortunately, there is so far no curative treatment of ND in general and AD in particular, which prevalence is expected to increase with the aging of the population. Most of these diseases are characterized by a slow degeneration progression and start several years or decades before the first symptoms appear. Despite the massive investment in AD drugs, there have been more setbacks and failures than treatment success. To have a chance of success, clinical trials of AD will need to be conducted early in the disease process, i.e. in prodromal or preclinical disease stages when damages are not too spread and are still reversible. Early and powerful diagnosis of AD is therefore primordial before any hope for efficient AD treatment can be set.

For molecular diagnosis of AD and monitoring of AD evolution, the 42-amino-acid long amyloid β (Aβ 1−42) peptide in cerebrospinal fluid (CSF) has been used as an established biomarker as its concentration is decreased in the CSF of AD patients [2-4]. Its quantification in CSF is nevertheless only one hallmark used in the molecular diagnosis of AD, and tendency is emerging to use combinations of various Aβ isoforms (notably Aβ 1−42 / Aβ 1−40) to improve the differential diagnostic power between AD and healthy subjects or to discriminate better AD from other NDs [5, 6]. The structures and some characteristics of some target Aβ isoforms for AD diagnostic purpose are presented in Fig. 1.

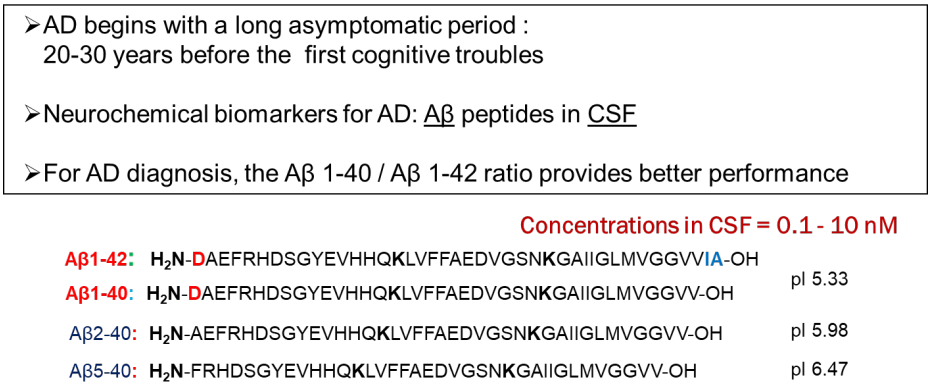

Fig.1. Some key information on AD and structures of some target Aβ peptides

These Aβ isoforms, composed of a more hydrophilic N-terminal domain (1–16) and a hydrophobic C-terminal domain, are cleaved from the amyloid precursor protein (APP) by β- and γ-secretases, with the predominant ones containing 40 and 42 residues (named Aβ 1-40 and Aβ 1-42, respectively)[7,8]. An Aβ concentration of < 500 pg/mL (0.1 nM) is indicative that this accumulates in the brain and does not circulate in the CSF, rendering determination of its level in CSF relevant for prediction of the severity and progression at early or preclinical stages of AD [9]. Aβ peptides are also present in blood. This gives potential for plasma Aβ detection as a simple and minimally invasive way for early diagnosis of AD [10]. The plasma level of Aβ 1-42 (~20 pg/mL) is considerably lower than that in CSF [11]. At the present stage, AD molecular diagnosis has nevertheless not reached the expected specificity and sensitivity (< 90 %) [12]. Towards better sensitivity and selectivity for Aβ detection (in CSF and plasma), serving for reliable early AD diagnosis, continued efforts have been made to develop novel analytical strategies and improve the existing ones. Over 15 years, we have developed several analytical strategies, focusing mostly on electrokinetic and microfluidic approaches for improvement of Aβ peptide detection and quantification. Herein, we review our efforts and achievements for this purpose, towards advancement of AD molecular diagnosis.

2. A glance at the developments for Aβ peptides analysis detection

In the years from 2001 to 2020, there have been 225 publications covering this topic, based on a search on the Web of Science with the keywords “Alzheimer’s disease” and “amyloid beta peptides analysis” or “Aβ 1-42 detection” for the titles. The attention paid by the research community grew rapidly in the period of 2001-2005, reaching a maximum in 2004, and then stayed stable year by year onwards. This can be attributed to achievement and recognition of immunoassays as a popular and efficient method for Aβ peptides quantification, and translation of scientific outcomes for this purpose into industrial products (i.e. commercial enzyme-linked immunosorbent assay (ELISA) kits for Aβ peptides detection). Among the methods for tracing Aβ peptides in CSF [7,13-15], immunoassays, notably ELISA [2,16,17], single molecule array (SiMoA) [18,19] and multi-analyte profiling assay (Luminex xMAP) [20] have been up to now the most practiced ones in clinical routine. Some considerations (if not drawbacks) for conventional immunoassays should be nevertheless considered (see [21,22]), notably a lack of antibodies specific to all Aβ peptides of interest (other than those specific to the well-studied Aβ 1-40 and 1-42), and cross reactions of different truncated Aβ peptides with the antibodies employed. As improved sensitivity and selectivity are required for detection and quantification of Aβ peptides, continued efforts have been made to improve the

performance of existing methods or seek for innovative approaches, aiming at faster, more precise, non-invasive and earlier prediction (e.g. blood diagnosis) of AD likelihood. There are at least three StartUps that were founded in recent years to propose state-of-the-art technologies to detect Alzheimer's patients up to 20 years before the irreversible symptoms [23-25]. In recent communications, different groups presented their advances in tracing Aβ peptides in either conventional CSF or blood / plasma matrices. Agnello et al. for instance provided the evidence for diagnostic accuracy of CSF biomarkers for AD using the recently released chemiluminescence enzyme immunoassay [26]. Other authors introduced in the last two years different electrochemical sensors and mass spectrometry (MS) platforms for ultrasensitive monitoring of Aβ peptides [27-31]. Our group maintains an active role in this domain with the recent development towards albuminome biomarker identification for AD, relying on efficient extraction of intact human serum albumin (HSA)-Aβ peptide complexes from serum [32]. All these efforts, whether they come from scientific communities or industries / StartUps, target improvement of AD molecular diagnosis, rendering the patient's journey less complex, less time-consuming and less expensive. Also towards this aim, the international Federation of Clinical Chemistry and Laboratory Medicine (IFCC) has recently facilitated the standardization of CSF Aβ 1–42 measurements by ELISA and homogenization of results obtained from different clinical and research groups [33]. This relies mostly on the introduction of the certified reference material (CRM), which is a well-characterized standard to validate the calibrators (i.e. Aβ 1–42 standard) for ELISA kits [34]. Sharing the same objective, our group has recently proposed a novel type of Aβ 1–42 standard based on chemical modification of the native Aβ 1–42 to avoid / minimize aggregation of this peptide during sample treatment and analysis, while still preserving its intact immunoaffinity features for efficient and no-bias ELISA measurements (patent pending) [35].

3. Microscale electrophoresis for separation and quantification of Aβ peptides

3.1. Capillary electrophoresis

One of our major contributions to this domain is the development of electrokinetic approaches for preconcentration, separation and detection of Aβ peptides, aiming at providing a chemical (eventually antibody-free) alternative to conventional immunoassays. Both formats of microscale electrophoresis (i.e. capillary electrophoresis CE and microchip electrophoresis MCE) were targeted (see table 1).

Table 1: Typical electrophoretic and microfluidic strategies for separation and detection of Aβ peptides

Analytical strategy	Approach	Sample treatment	Aβ peptides	Detection limit	Applications
Strategy 1: Microscale electrophoresis	CE-UV [36]	-	Aβ 1-42, 1-40, 1-39, 1-38, and 1-37	1 µM	Monitoring of the aggregation process of Aβ 1-42 [37-39] [40]
	CE-LIF [41]	-	Aβ 1-42, 1-40, 1-39, 1-38, and 1-37	1 nM	Monitoring of the interaction between nanoparticles and the Aβ peptides [42-46]
	CE-LIF [41]	Immunoprecipitation and off-line labelling	Aβ1-42/ Aβ1-38	0.1 nM	Discrimination between AD patients and healthy persons [41]
	CE-LIF [47]	Immuno-enrichment - on-bead fluorescent labelling - thermal elution	Aβ1-42, Aβ1-40, Aβ1-38	0.1 nM	Discrimination between AD patients and healthy persons [47]
	ITP-UV [48]	-	Aβ1-40	700 nM	-
	Multiple-ITP-UV [49]	-	Aβ1-40	50 nM	-
	ITP-MS [50]	Off-line fluorescent labelling of peptides	Aβ1-40, Aβ1-42, Aβ1-38	0.1 nM	Discrimination between AD patients and healthy persons [50]
	Multiple LVSEP-LIF [51]	Off-line fluorescent labelling of peptides	Aβ 1-42, 1-40, 1-38, 2-40, and 5-40	0.05 nM	Discrimination between AD patients and healthy persons [51]
	MCE-UV [52]	-	Aβ 1-37, Aβ 1-38, Aβ 1-39, Aβ 1-40, and Aβ 1-42	µM range	-
	MCE-UV [53]	-	Aβ 1-38, Aβ 1-40, and Aβ 1- 42	µM range	-
Strategy 2: Microfluidic and biosensor systems	Biosensors [54, 55]	Sandwich immunoassay	Aβ 1- 42	0.5 µM	Proof of concept
	Immuno-enrichment on magnetic beads prior to CE-UV [60]	-	Aβ 1- 42 and Aβ 1- 40	sub µM range	-
	Immuno-enrichment on magnetic beads and fluorescent labelling prior to CE-LIF [41, 52, 61-63] [47]	-	Aβ 1-38, Aβ 1-40, and Aβ 1- 42	sub nM ranges	Discrimination between AD patients and healthy persons [41, 52, 61-63] [47]
	Immunoassay in microfluidic droplets [57]	Single-step immunoassay using functionalized magnetic beads	Aβ 1-40 and Aβ 1- 42	0.5 nM	-
	Microfluidic fluidized bed [47]	On-bead immuno-capture and fluorescent labelling of peptides	Aβ 1-38, Aβ 1-40, and Aβ 1- 42	-	Proof of concept
	Magneto-CE [59]	Immuno-capture and chemical elution of labelled peptides inside a CE microchannel	Aβ 1- 42	10 nM	Proof of concept

CE is a separation method based on different migrations of molecules (charged analytes in most of the cases) under a high electric field. The electrophoresis process is conducted in a narrow and long fused silica capillary (typically 50 - 75 µm and 30-100 cm for inner diameter and total length, respectively), which is filled with a background electrolyte buffer (BGE). The positive features of CE, notably high separation resolution, little sample and reagent consumption, setup flexibility and possibility for miniaturization, make it an efficient technique for biomolecule separation and detection generally, and for quantification of peptides in biofluids in particular. The first CE method for separation and ultraviolet (UV) detection of Aβ peptides was communicated in 2008 [36]. Five peptides (Aβ 1-42, 1-40 ,1-39,1-38, and 1-37) could be baseline separated in a single run within 30 min. Interestingly, the Aβ 2-40 and Aβ 5-40 that were not possible to quantify with classical immunoassays due to the lack of specific antibodies could be separated and detected with CE-UV [36]. The CE-UV method was then employed to monitor the aggregation process of Aβ 1-42, in order to gain more understanding of the AD provoking mechanism and serve for anti-Alzheimer's drug discovery [37-39]. This work was later complemented with the results on time-dependent Aβ 1–42 oligomerization pattern by electrospray differential mobility analysis (ES-DMA) [40]. The detection limit achieved with CE-UV was in the range of 1 µM, which was nevertheless not enough to trace these peptides in CSF samples as their expected concentrations are in sub nM ranges. To overcome this challenge, laser induced fluorescence (LIF) detection with a fluorescent labelling strategy was then developed for CE of Aβ to significantly improve the detection sensibility [41]. The labelling principle and typical electropherograms for CE-LIF of labelled Aβ peptides are shown in Fig. 2.

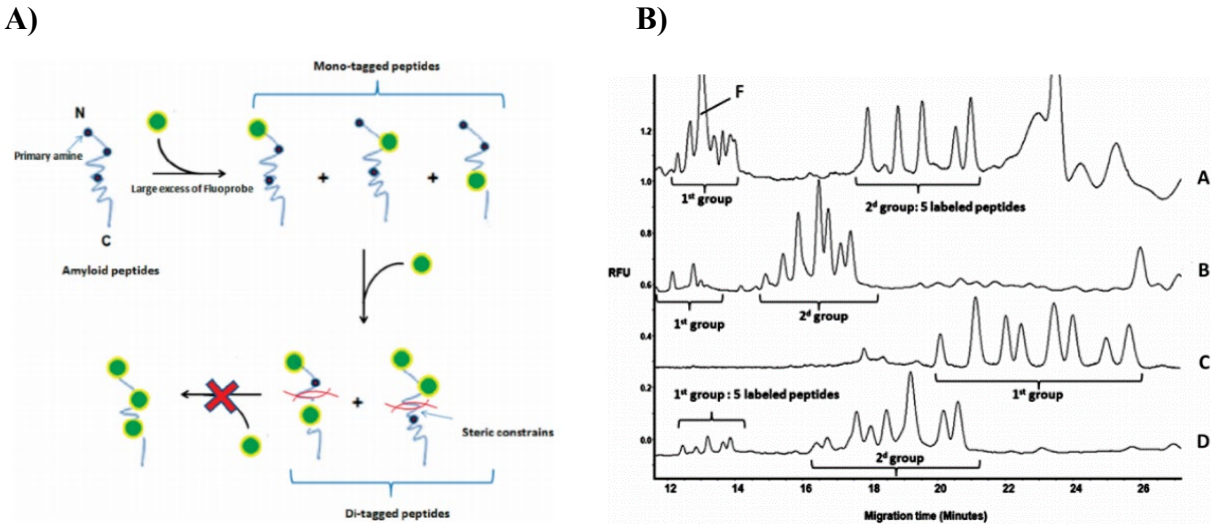

Fig. 2. **A)** Proposed model of the derivatization reaction of the five amyloid peptides with the Fluoprobe 488; **B)** CZE-LIF profile of the five amyloid peptides derivatized with Fluoprobe 488 (A) or Alexa fluor (B), FAM-X-SE (C), and 5-FITC (D) as the tagging agents. F is a peak from the fluorophore. The peptide concentration was 100 nM except for the Fluoprobe derivatization (50 nM). Brackets indicate regions corresponding to the migration of tagged Aβ peptides. CE conditions; BGE: borate buffer pH 9; IS 40 mM with 3.25 mM of DAB, Detection: LIF (λ exc 488 nm). Reprinted from [41] with permission. Copyright (2011) ASC.

Five fluorescently tagged Aβ peptides could be separated and detected down to 1 nM, approaching their concentrations in CSF. The significant difference in Aβ1-42/ Aβ1-38 ratio between healthy people and AD patients was also reported [41]. The CE-LIF method was then applied to monitor the interaction between nanoparticles and the Aβ peptides, aiming at designing functional nanomedicines for AD treatment [42-46].

Immuno-capture is an enrichment technique in which the target analytes (i.e. antigens) are captured and enriched onto a solid support (typically magnetic beads in our case) functionalized with specific antibodies. This approach is often used for preconcentration of biomolecules (such as proteins and peptides) and at the same time removal of biofluid's matrices. The trapping of the analytes of interest is realized via the antigen-antibody interaction. As the marriage of immuno-capture and CE can inherit the separation power (selectivity) of CE and at the same time the excellent extraction / preconcentration feature of immunocapture (see Fig. 3A for the logic behind), the hybrid mode of immuno-CE has been developed to further improve the detection limits. Accordingly, a novel preconcentration protocol prior to CE-LIF was developed, allowing immune-enrichment of Aβ peptides on functionalized magnetic beads (see more in the following section), followed by on-

beads Aβ fluorescent labelling and thermal elution [47]. Enrichment factors better than 100 were achieved in this case, which in turn rendered detection of Aβ1-42, Aβ1-40 and Aβ1-38 in CSF possible (Fig. 3B).

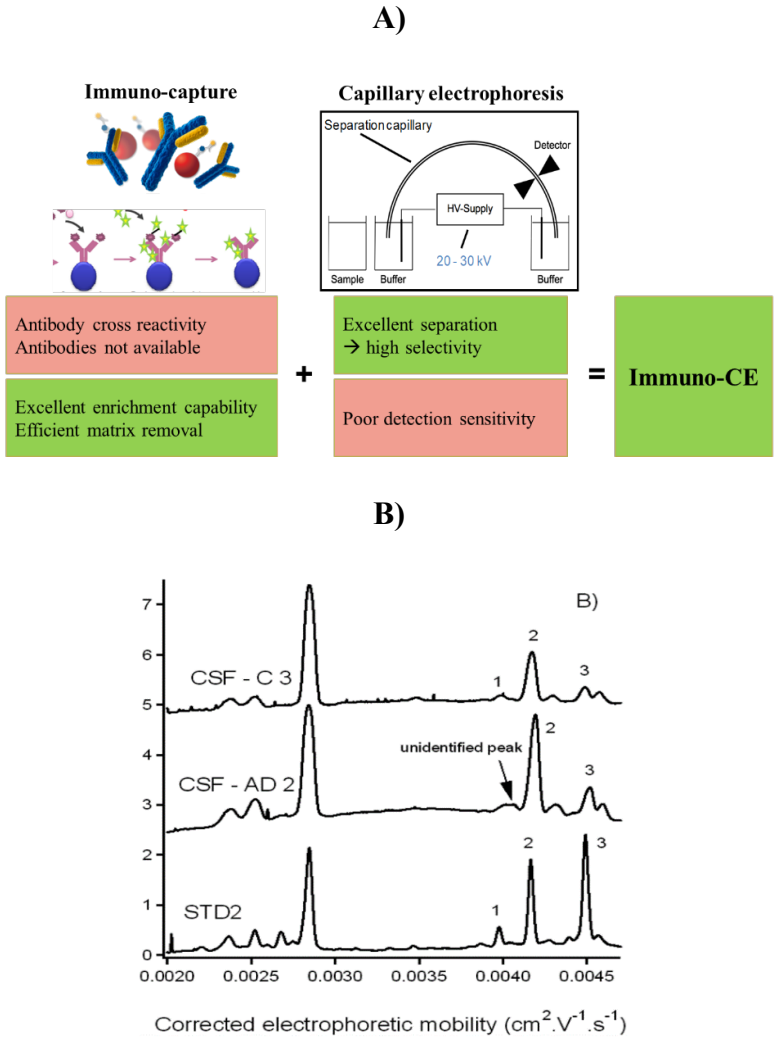

Fig. 3. **A)** Principle of the immune-CE for Aβ peptide detection. **B)** CE-LIF electropherograms of CSF samples after magnetic immune-precipitation using the antibody 6E10 (enrichment factor of 100) and on-beads fluorescent labelling. Thermal elution conditions: 95 °C for 5 min in the presence of borate buffer (pH 10.5, IS 40 mM). CE conditions as in Fig. 1. Sample treatment with pre-filtering of CSF samples using 3 K Dalton filters. Peak identification: (1) Aβ 1-42, (2) Aβ 1-40, (3) Aβ 1-38. CSF – AD stands for CSF samples from AD patients; CSF – C stands for CSF samples from cognitive normal people used as controls; STD 1: standard solution of Aβ 1-42 (0.2 nM), Aβ 1-40 (0.2 nM) and Aβ 1-38 (0.2 nM); STD 2: standard solution of Aβ 1-42 (2 nM), Aβ 1-40 (8 nM) and Aβ 1-38 (8 nM). The indicated concentrations in the brackets were those of the standards before immune-enrichment. Both standards and CSF samples were subjected to the same immunocapture–label–elution procedure. Reprinted from [47] with permission. Copyright (2015) RSC.

In parallel to the advancements in immune-capture coupled to CE of Aβ peptides, efforts were also made to develop antibody-free on-line electrokinetic preconcentration approaches for improvement of Aβ peptides detection. Capillary isotachophoresis (ITP), a technique which uses two different buffer solutions (i.e. a leading electrolyte LE and a terminating one TE) to sandwich the sample plug in between, was the first to be used for stacking Aβ peptides in a sharp peak [48]. Under electroosmotic-flow (EOF) suppression conditions (i.e. elimination of the bulk liquid motion normally occurred under application of a high voltage over a silica capillary possessing negative surface charges), the target Aβ peptides were trapped between two anions, OH- in TE and CH3COO- in LE, during their electrophoretic migrations to the detector. This stacking method allowed to quantify Aβ1-40 down to 700 nM just with UV detection [48]. To further improve the detection limit, a multiple-electrokinetic preconcentration concept was developed [49]. In this novel technique, a sample containing Aβ1-40 was repeatedly injected and stacked by ITP for preconcentration for several cycles, allowing for the first time quantification limit down to 50 nM with UV detection [49]. ITP was then coupled with MS to preconcentrate a mixture of Aβ 1-40, Aβ 1-42, Aβ 1-38 [50]. Separation of these peptides in this case was implemented by MS via their different mass-to-charge ratios. The significant difference in Aβ 1–42/Aβ 1–40 ratio between AD patients and healthy volunteers was demonstrated [50]. Inspired from the 'multi-preconcentration concept', we then went further with the development of a new mode named 'multiple cycles of large volume sample stacking with electro-osmotic pump' (M-LVSEP) [51]. In this method (see Fig. 4A for working principle), an Aβ peptide mixture was injected into the whole CE capillary and was swept back to the capillary inlet by the bulk liquid flow (EOF) for preconcentration. This process was repeated several times, allowing unlimited sample volumes to be injected and analyte enrichment prior to CE-LIF separation of 5 Aβ peptides (see Fig. 4B). The quantification limit for the Aβ peptides down to 0.05 nM (with a preconcentration factor up to 800) was for the first time possible without any recourse to antibody-based enrichment. The discrimination between AD patients and healthy persons using this method gave equivalent accuracy compared to the conventional ELISA method [51].

A)

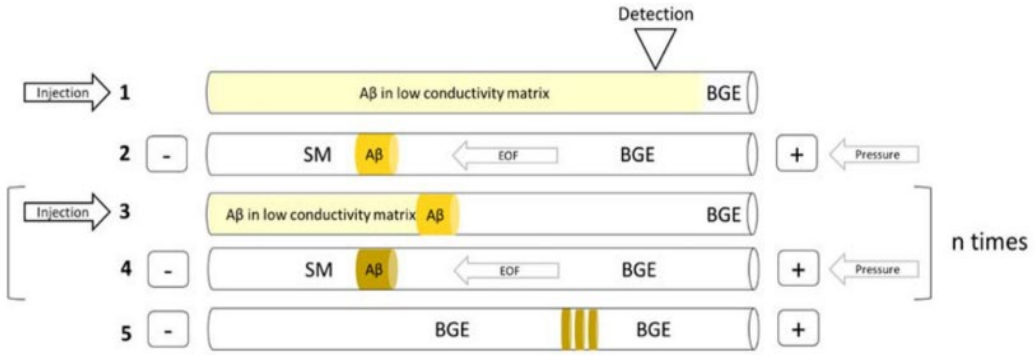

B)

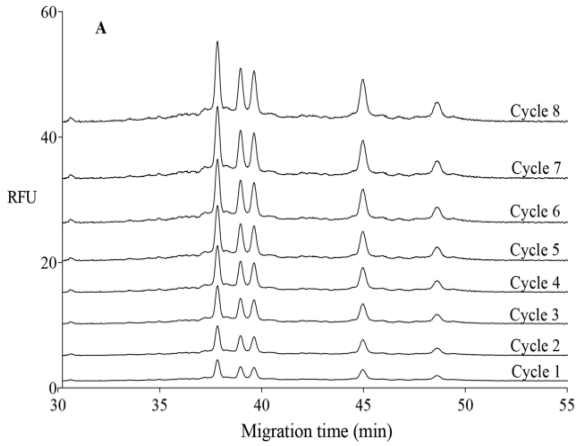

Fig. 4. **A)** Principle of the multiple LVSEP protocol. (1) First hydrodynamic injection of the sample. (2) LVSEP process by exploiting conductivity differences between sample and the separation buffer and under an electro-osmotic flow (EOF). (3) Second hydrodynamic injection. (4) Second process of LVSEP. (5) Separation and detection of the peptides in the absence of EOF (due to the sample matrix removal). Steps 3 and 4 can be repeated several times (cycles) for further preconcentration of analytes newly injected at each cycle. **B)** multiple LVSEP of the 5 fluorescently labelled peptides (5 nM) for different number of cycles from 1 to 8. For the first injection, the capillary is totally filled with the sample. For the subsequent cycles, 40% of sample is injected. Between each injection, the voltage was set at −30 kV with an additional pressure of 700 Pa for 180 s. Reprinted from [51] with permission. Copyright (2018) RSC.

3.2. Microchip electrophoresis

The development of point-of-care (POC) testing (or bedside testing) has gained much attention as this allows realization of medical diagnostic tests at the time and place of patient care, without sending off samples away. By avoiding the long waiting period (hours to days) to learn the results,

POC may offer better, easier treatment monitoring during therapeutic clinical tests. Efforts were therefore focused on MCE and microfluidics towards this goal for AD diagnosis. The MCE separation principle is similar to that in CE, in which a sample is injected into the separation channel of typically less than 10 cm long prior to application of a high voltage (1000 - 3000 V) to trigger electrokinetic separation of target analytes. The sample introduction in MCE is normally implemented via the electrokinetic mode (i.e. application of a lower voltage), rather than hydrodynamic injection (using pressure or vacuum) as frequently used in CE. The presence of two perpendicular channels (separation and injection channels) on the microchip leads to a cross section by which the injected sample volume can be precisely tuned. In the microchip format, the microchannel used for separation is much shorter than that in CE (typically 60 cm), which in turn requires careful optimization of various parameters (notably microchip material and design, channel coating, injection amount and voltage pattern) in order to reach satisfactory separation and detection performance. The first work on MCE of Aβ peptides was carried out by Mohamadi et al. in 2010 [52]. They employed a microchip made from polydimethylsiloxane (PDMS) with the channel cross section of 100 µm (width) x 50 µm (depth) and an alkaline buffer containing 2% methylcellulose for EOF suppression to perform separation of Aβ 1-37, Aβ 1-38, Aβ 1-39, Aβ 1-40, and Aβ 1- 42. This proof-of-concept work at that moment still required improvement in terms of resolution and sensitivity before this approach could be used routinely for detection of Aβ peptides in CSF. To provide new clues toward this direction, Mesbah et al. then improved the MCE separation of Aβ 1-38, Aβ 1-40, and Aβ 1- 42, using a glass microchip with a narrower separation channel (50 µm wide and 20 µm deep) and a new surface coating strategy with poly(dimethylacrylamide-co-allyl glycidyl ether) [53]. Compared to the CE configuration, this MCE system allowed 6-fold faster separation of Aβ peptides while keeping excellent repeatability, recovery and resolution for simultaneous quantification.

4. Magneto-immuno-capture of Aβ peptides in microfluidic and biosensor systems

4.1. Magneto-immuno-capture-based sample treatment

Another important contribution of our group is the development and application of immuno-capture / precipitation of Aβ peptides onto solid supports (typically magnetic beads, called magneto-immuno-capture) functionalized with anti-Aβ antibodies via the antigen-antibody reaction mechanism (see Fig. 5 for the typical working principles and table 1 for a summary of the developed approaches). This contribution, which belongs to the afore-mentioned strategy of immuno-CE,

focuses mainly on microfluidic sample treatment modules and protocols. These were then often used as the forefront of CE/MCE systems. Note, that while different solid-phase supports (such as silicon surface chemically silanized with carboxylatedalkyltrichlorosilane [54,55]) can be employed for immune-capture/precipitation of biomolecules, particular interest is given to functionalized magnetic particles as they offer much higher throughput and ease of bead manipulation through an external magnetic field [56]. Different antibody grafting strategies (using magnetic beads functionalized with various chemical groups such as carboxylate, immunoglobulin G, tosylate etc.) as well as bead washing protocols were developed to maximize the quantity of captured Aβ peptides and at the same time minimize unwanted non-specific adsorption of interferants, notably proteins, from the biofluids [47,57-59]. Various operations then were carried out with the captured Aβ peptides for different detection modes. They could be eluted from magnetic beads into a smaller eluent volume for preconcentration, prior to either direct CE-UV detection [60] or off-line fluorescent labelling of Aβ peptides for CE/MCE-LIF analysis [41,52,61-63]. Preconcentration factors better than 170-fold were achieved, with more than 90% of the peptides captured and 80% of them eluted. Alternatively, on-bead labeling of immobilized Aβ peptides prior to thermal elution at 95 °C to release them from magnetic beads could be realised for a similar purpose [47].

A)

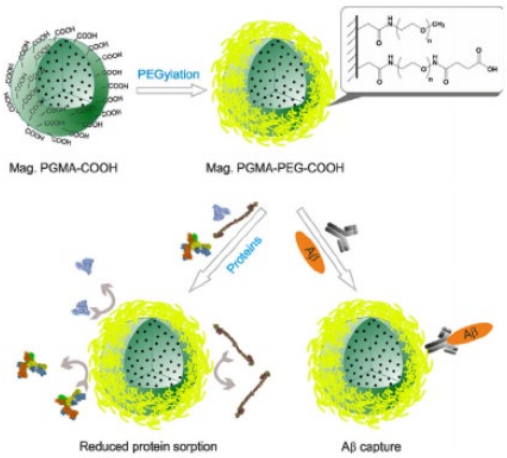

B)

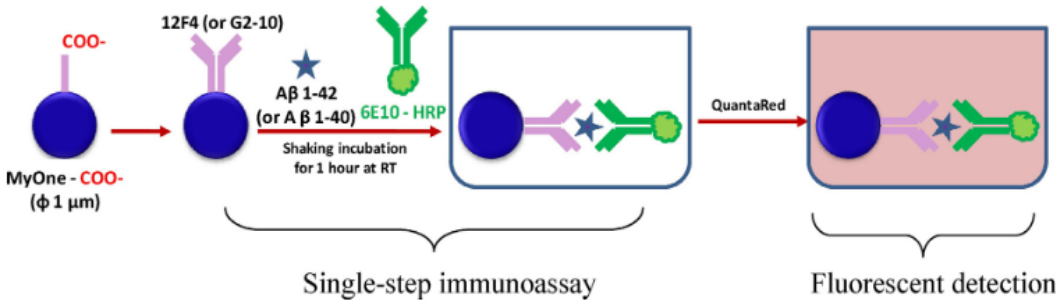

Fig. 5. **A)** Schematic representation of PEGylation of a magnetic PGMA microsphere for immune-capture of Aβ peptides and suppression of non-specific sorption. Reprinted from [58] with permission. Copyright (2014) Wiley. **B)** Protocol of magnetic beads-based immunoassays of Aβ 1–40 and Aβ 1–42. Reprinted from [57] with permission. Copyright (2018) Elsevier.

4.2. Magneto-immunoassays and in-capillary immuno-capture of Aβ peptides

The magneto-immuno-capture could also be employed to develop a single-step immunoassay in microfluidic droplets, in which the magnetic beads grafted with capture antibodies, the sample containing target Aβ 1-40 and Aβ 1-42, as well as the detection antibodies were mixed and allowed to react in a nanometric droplet [57]. By using a train of droplets encapsulated in oil (see Fig. 6A for this microfluidic setup), each step was implemented in a specific droplet and high throughput analyses of Aβ peptides were made possible. A sequence of 8 assays performed in less than 1 h

could be achieved with such microfluidic setup, compared to a duration of 2 h per assay in conventional batch mode. Using only 200 nL of sample for each analysis, the Aβ 1-42 and Aβ 1-40 peptides can be detected down to 0.5 - 1 nM, which is quite close to the expected range of 0.1 nM for Aβ 1-42 in CSF samples (see Fig. 6B for typical detection signals). In most of the cases, magnetic beads are captured and separated using permanent magnets. This was the case for our pioneering studies on batchwise and on-chip magneto-immuno-capture of Aβ peptides [41,52,60-63]. A low degree of automation and / or problem of bead cluster aggregation were the limitations of such setup. Different strategies were therefore developed to overcome these challenges. First, a microfluidic fluidized bed was designed to allow continuous recirculation of magnetic beads under a flow stream containing target analytes in a microchip for interaction improvement, thanks to the counterbalancing between magnetic and hydrodynamic forces [64]. This technology, inspired from the fluidized bed reactor (FBR) used to carry out a variety of multiphase biochemical reactions, was applied to implement all three steps (i.e. immune-capture, fluorescent labelling and elution of enriched labelled Aβ peptides) in the same microchamber in which functionalized magnetic microparticles continuously re-circulate. To allow a high throughput via automation, the permanent magnets were replaced recently with the magnetic tweezer technology developed by Viovy et al. [65]. These tweezers, composed of a metallic tip surrounded by a copper coil, can generate a magnetic field upon application of an electric current through the coil (see Fig. 6A). These were applied for immunoassays of Aβ 1-42 and Aβ 1-40 in droplets, allowing the transfer of magnetic carriers between different matrices (i.e. droplets) with a high purification rate and a low supernatant carryover, thus opening the possibility to implement multi-steps protocols in the same microfluidic system [57]. With this technology, we could also precisely control the capture, release and circulation of magnetic beads inside a CE capillary thanks to the tweezers situated at both ends of the capillary (see Fig. 7). The CE separation channel was accordingly converted into a reactor for immune-enrichment of Aβ 1-42 on circulating beads, which was found to offer a superior capture performance than the bead cluster approach using permanent magnets [59]. This novel concept and instrument could help eliminate the incompatibility of working dimensions in different steps (as all steps were realized in a single CE capillary) and allow automation of the whole protocol. It should be noted that the forms of Aβ peptides can influence drastically the separation and detection performance regardless of the employed analytical approaches. For this reason, different strategies were implemented to ensure the monomeric form of Aβ peptides used in all aforementioned developments. These include i) verification of the quality of the Aβ peptide batch with different analytical methods (e.g. CE-UV [38], thioflavin-T fluorescence assay [39]) before use, ii) chemical

modification of Aβ peptides to prevent aggregation [35] and iii) establishment of a standard protocol for preparation and storage of Aβ peptides stock aliquots [38].

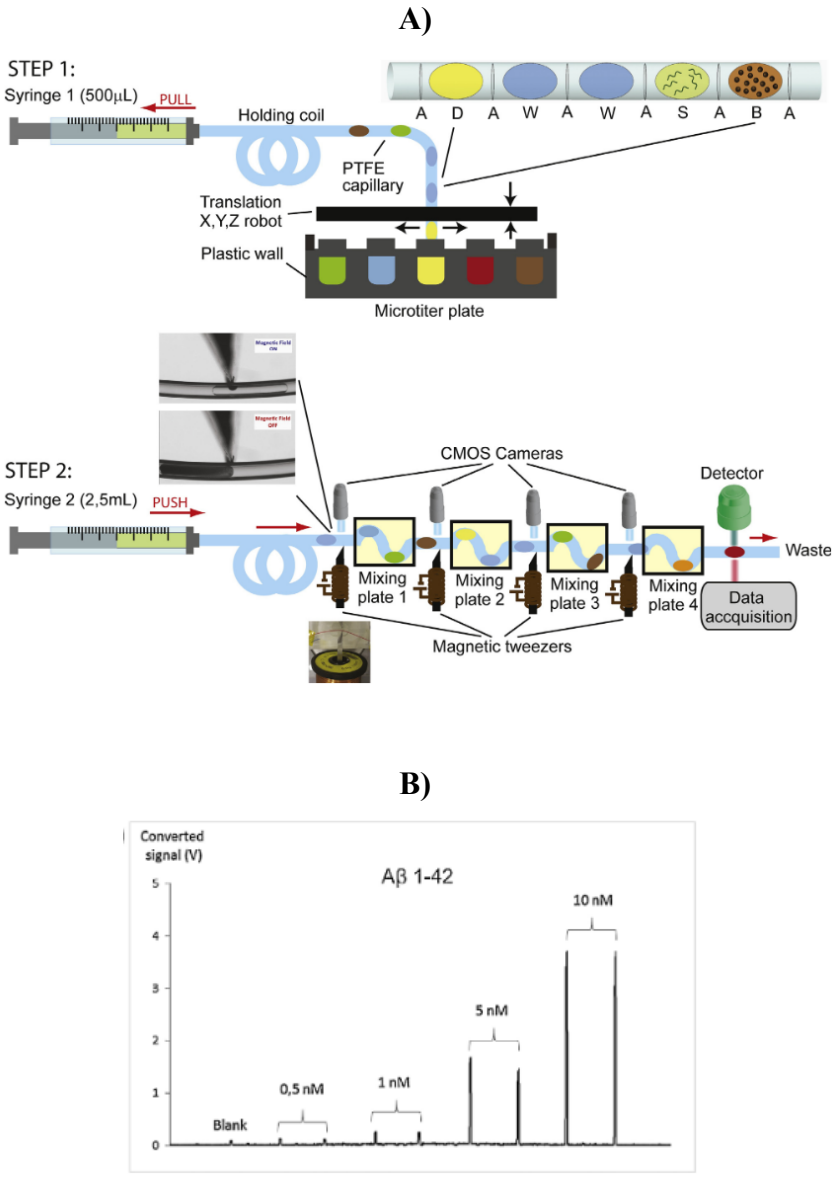

Fig. 6. **A)** Schematic drawing of the microfluidic droplet setup using magnetic tweezers for magnetic beads manipulation. D: detection droplet; W: washing droplet; S: sample droplet; B: magnetic bead droplet; A: air bubble. Droplets are separated by oil. **B)** Fluorescent signals for Aβ 1-42 on passage of detection droplets through the fluorescent detector. Reprinted from [57] with permission. Copyright (2018) Elsevier.

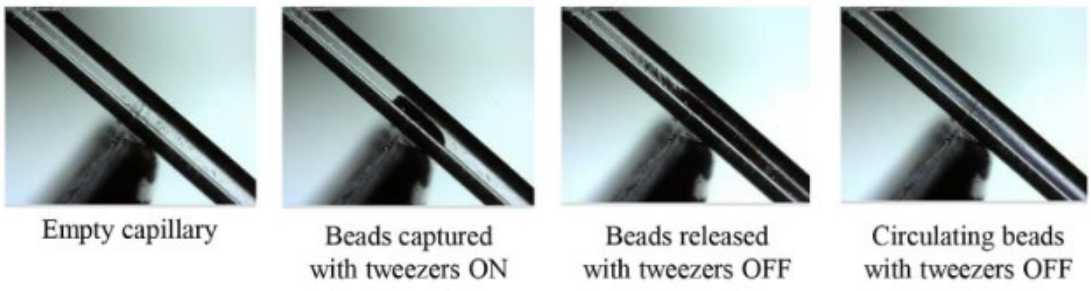

Fig. 7. Photos of bead capture and release inside a transparent capillary (75mm ID and 375mm OD) with the activation/deactivation of magnetic tweezers. Reprinted from [59] with permission. Copyright (2019) Elsevier.

5. Conclusion remarks and perspectives

Among continued efforts for improvement of Aβ peptide detection, our major contributions focus on electrokinetic approaches and / or magneto-immuno-capture. Equivalent detection performance has been achieved compared to the conventional ELISA method. Our approaches hold a high potential for miniaturization, automation and integration, towards a high-throughput and miniature solution / device conception for AD diagnosis. Technology readiness improvement and clinical tests with a large cohort of AD / control samples are still needed to validate the utility and applicability of our proposed technologies / methods. Hope is of course given that more precise and earlier prediction of AD will be possible with these analytical advances, in which our group has contributed very actively in the last decade. More research is also needed to overcome the actual challenges encountered with Aβ peptide separation and quantification, notably i) the aggregation of Aβ 1-42 during sample storage, treatment and analysis, as well as ii) large deviation of the results obtained from different laboratories using different analytical strategies (MS, immunoassays or separation techniques). These result mismatches need to be solved before the diagnostic power of Aβ peptide analysis could be fully exploited. To further improve the selectivity and sensitivity for AD prediction, efforts need to be spent as well to trace an extended spectrum of Aβ peptides in biofluids, focusing on other truncated ones beyond the well-studied Aβ 1-42 and Aβ 1-40. Continuous development of novel analytical strategies and / or improvement of actual methods' performance are therefore always required in order to reach this achievement.

Acknowledgement

The authors thank the 'bourse d'excellence de l'ambassade de France' for PhD scholarship of

N.V.T. Nguyen. This work has been financially supported by the Institut Universitaire de France (for M. Taverna, senior member) and the Agence Nationale de la Recherche (ANR, France, the grant no. ANR-18-CE29-0005-01).

The authors have declared no conflict of interest.

References of REVIEW

1. https://www.alz.co.uk/research/WorldAlzheimerReport2018.pdf 2018.
2. C. E. Teunissen, M. Otto, S. Engelborghs, S. K. Herukka, S. Lehmann, P. Lewczuk, A. Lleo, A. Perret-Liaudet, H. Tumani, M. R. Turner, M. M. Verbeek, J. Wiltfang, H. Zetterberg, L. Parnetti, K. Blennow, Alzheimers Res. Ther. 2018, 10, 8 30 10.1186/s13195-018-0359-x.
3. B. Olsson, R. Lautner, U. Andreasson, A. Ohrfelt, E. Portelius, M. Bjerke, M. Holtta, C. Rosen, C. Olsson, G. Strobel, E. Wu, K. Dakin, M. Petzold, K. Blennow, H. Zetterberg, Lancet Neurol. 2016, 15, 673-84 10.1016/S1474-4422(16)00070-3.
4. C. Somers, J. Goossens, S. Engelborghs, M. Bjerke, Biomark. Med. 2017, 11, 169-178 10.2217/bmm-2016-0276.
5. K. Blennow, H. Zetterberg, J. Alzheimer's Dis. 2018, 62, 1125-1140 10.3233/jad-170773.
6. D. R. Galasko, L. M. Shaw, Nat. Rev. Neurol. 2017, 13, 131-132 10.1038/nrneurol.2017.11.
7. Y. Zhou, L. Liu, Y. Hao, M. Xu, Chem. Asian J. 2016, 11, 805-817 10.1002/asia.201501355.
8. D. J. Hayne, S. Lim, P. S. Donnelly, Chem. Soc. Rev. 2014, 43, 6701-6715 10.1039/c4cs00026a.
9. I. W. Hamley, Chem. Rev. 2012, 112, 5147-5192 10.1021/cr3000994.
10. H. M. Vanderstichele, C. E. Teunissen, E. Vanmechelen, Neuro. Ther. 2019, 8, S129-S145 10.1007/s40120-019-00166-3.
11. M. Pesaresi, C. Lovati, P. Bertora, E. Mailland, D. Galimberti, E. Scarpini, P. Quadri, G. Forloni, C. Mariani, Neurobiol. Aging 2006, 27, 904-905 https://doi.org/10.1016/j.neurobiolaging.2006.03.004.
12. M. J. Savage, J. Kalinina, A. Wolfe, K. Tugusheva, R. Korn, T. Cash-Mason, J. W. Maxwell, N. G. Hatcher, S. J. Haugabook, G. X. Wu, B. J. Howell, J. J. Renger, P. J. Shughrue, A. McCampbell, J. Neurosci. 2014, 34, 2884-2897 10.1523/jneurosci.1675-13.2014.
13. J. Schuster, S. A. Funke, J. Alzheimers Dis. 2016, 53, 53-67 10.3233/jad-151029.
14. S. S. Hwang, H. Chan, M. Sorci, J. van Deventer, D. Wittrup, G. Belfort, D. Walt, Anal. Biochem. 2019, 566, 40-45 10.1016/j.ab.2018.09.011.
15. B. Veerabhadrappa, C. Delaby, C. Hirtz, J. Vialaret, D. Alcolea, A. Lleo, J. Fortea, M. S. Santosh, S. Choubey, S. Lehmann, Crit. Rev. Cl. Lab. Sci. 2020, 57, 99-113 10.1080/10408363.2019.1678011.
16. J.-H. Kang, M. Korecka, J. B. Toledo, J. Q. Trojanowski, L. M. Shaw, Clin. Chem. 2013, 59, 903-916 10.1373/clinchem.2013.202937.
17. S. Lista, H. Zetterberg, B. Dubois, K. Blennow, H. Hampel, J. Neurol. 2014, 261, 1234-1243 10.1007/s00415-014-7366-z.
18. L. Song, D. R. Lachno, D. Hanlon, A. Shepro, A. Jeromin, D. Gemani, J. A. Talbot, M. M. Racke, J. L. Dage, R. A. Dean, Alzheimer's Res. Ther. 2016, 8, 58 58, 10.1186/s13195-016-0225-7.
19. D. H. Wilson, D. M. Rissin, C. W. Kan, D. R. Fournier, T. Piech, T. G. Campbell, R. E. Meyer, M. W. Fishburn, C. Cabrera, P. P. Patel, E. Frew, Y. Chen, L. Chang, E. P. Ferrell, V. von Einem, W. McGuigan, M. Reinhardt, H. Sayer, C. Vielsack, D. C. Duffy, J. Lab. Autom. 2016, 21, 533-547 10.1177/2211068215589580.
20. J.-H. Kang, H. Vanderstichele, J. Q. Trojanowski, L. M. Shaw, Methods 2012, 56, 484-493 10.1016/j.ymeth.2012.03.023.
21. N. Le Bastard, P. P. De Deyn, S. Engelborghs, Clin. Chem. 2015, 61, 734.
22. N. Mattsson, U. Andreasson, S. Persson, M. C. Carrillo, S. Collins, S. Chalbot, N. Cutler, D. Dufour-Rainfray, A. M. Fagan, N. H. H. Heegaard, G.-Y. R. Hsiung, B. Hyman, K. Iqbal, D. R. Lachno, A. Lleo, P. Lewczuk, J. L. Molinuevo, P. Parchi, A. Regeniter, R. Rissman, H. Rosenmann, G. Sancesario, J. Schroeder, L. M. Shaw, C. E. Teunissen, J. Q. Trojanowski, H.

Vanderstichele, M. Vandijck, M. M. Verbeek, H. Zetterberg, K. Blennow, S. A. Kaeser, Alzheimer's & dementia : the journal of the Alzheimer's Association 2013, 9, 251-261.
23. AgenT, https://www.agent-biotech.com/#contact 2018.
24. Alzohis, https://www.alzohis.com/en/ 2016.
25. WinterlightLabs, https://winterlightlabs.com/about 2015.
26. L. Agnello, T. Piccoli, M. Vidali, L. Cuffaro, B. Lo Sasso, G. Iacolino, V. R. Giglio, F. Lupo, P. Alongi, G. Bivona, M. Ciaccio, Scand. J. Clin. Lab. Invest. 2020, 80, https://doi.org/10.1080/00365513.2020.1740939 10.1080/00365513.2020.1740939.
27. S. Ding, Y. Xu, Q. Liu, H. Gu, A. Zhu, G. Shi, Analyst 2020, 145, 2331-2338 10.1039/c9an02285f.
28. Y. Kutovyi, H. Hlukhova, N. Boichuk, M. Menger, A. Offenhaeusser, S. Vitusevich, Biosens. Bioelectron. 2020, 154, 10.1016/j.bios.2020.112053.
29. Y.-J. Lu, A. Purwidyantri, H.-L. Liu, L.-W. Wang, C.-Y. Shih, D. G. Pijanowska, C.-M. Yang, Ieee Sens. J. 2020, 20, 6248-6255 10.1109/jsen.2020.2976561.
30. H. Qin, X. Gao, X. Yang, W. Cao, S. Liu, Biosens. Bioelectron. 2019, 141, 10.1016/j.bios.2019.111438.
31. G. Grasso, Mass Spectrom. Rev. 2019, 38, 34-48 10.1002/mas.21566.
32. E. Rossi, T. Tran, C. Hirtz, S. Lehmann, M. Taverna, Talanta 2020, 121002 10.1016/j.talanta.2020.121002.
33. J. Kuhlmann, U. Andreasson, J. Pannee, M. Bjerke, E. Portelius, A. Leinenbach, T. Bittner, M. Korecka, R. G. Jenkins, H. Vanderstichele, E. Stoops, P. Lewczuk, L. M. Shaw, I. Zegers, H. Schimmel, H. Zetterberg, K. Blennow, Clin. Chim. Acta 2017, 467, 27-33 https://doi.org/10.1016/j.cca.2016.05.014.
34. C. E. A.-i. CSF, https://crm.jrc.ec.europa.eu/p/ERM-DA482-IFCC/CSF-amyloid-s1-42-peptide-As1-42-Alzheimer-s-EUROIMMUN-beta-amyloid-IBL-Amyloid-beta-INNOTEST-s-AMYLOID-1-42-Lumipulse-V-PLEX-As-Peptide-Panel-1-Roche-Elecsys-s-amyloid-1-42-cerebrospinal-fluid/ERM-DA482-IFCC-Amyloid-42-in-CSF/ERM-DA482_IFCC 2017.
35. M. Taverna, C. Crosnier De Lassichere, T. D. Mai, M. Otto, Demande de brevet n°1904400 déposée le 25 avril 2019 par CNRS 2019.
36. R. Verpillot, M. Otto, H. Klafki, M. Taverna, J. Chromatogr. A 2008, 1214, 157-164 10.1016/j.chroma.2008.10.051.
37. S. Pellegrino, N. Tonali, E. Erba, J. Kaffy, M. Taverna, A. Contini, M. Taylor, D. Allsop, M. L. Gelmi, S. Ongeri, Chemical Science 2017, 8, 1295-1302 10.1039/C6SC03176E.
38. D. Brinet, J. Kaffy, F. Oukacine, S. Glumm, S. Ongeri, M. Taverna, Electrophoresis 2014, 35, 3302-3309.
39. J. Kaffy, D. Brinet, J.-L. Soulier, L. Khemtémourian, O. Lequin, M. Taverna, B. Crousse, S. Ongeri, Eur. J. Med. Chem. 2014, 86C, 752-758 10.1016/j.ejmech.2014.09.031.
40. D. Brinet, F. Gaie-Levrel, V. Delatour, J. Kaffy, S. Ongeri, M. Taverna, Talanta 2017, 165, 84-91 10.1016/j.talanta.2016.12.011.
41. R. Verpillot, H. Esselmann, M. R. Mohamadi, H. Klafki, F. Poirier, S. Lehnert, M. Otto, J. Wiltfang, V. J.L, M. Taverna, Anal. Chem. 2011, 83, 1696-1703.
42. D. Brambilla, R. Verpillot, M. Taverna, L. De Kimpe, B. Le Droumaguet, J. Nicolas, M. Canovi, M. Gobbi, F. Mantegazza, M. Salmona, V. Nicolas, W. Scheper, P. Couvreur, K. Andrieux, Anal. Chem. 2010, 82, 10083-10089 10.1021/ac102045x.
43. D. Brambilla, R. Verpillot, B. Le Droumaguet, J. Nicolas, M. Taverna, J. Kóňa, B. Lettiero, S. Hashemi, L. De Kimpe, M. Canovi, M. Gobbi, N. Valérie, W. Scheper, S. Moghimi, I. Tvaroška, P. Couvreur, K. Andrieux, ACS nano 2012, 6, 5897-908 10.1021/nn300489k.

44. B. Le Droumaguet, H. Souguir, D. Brambilla, R. Verpillot, J. Nicolas, M. Taverna, P. Couvreur, K. Andrieux, International journal of pharmaceutics 2011, 416, 453-60 10.1016/j.ijpharm.2011.01.015.
45. D. Brambilla, H. Souguir, J. Nicolas, N. Mackiewicz, R. Verpillot, B. Le Droumaguet, M. Taverna, P. Couvreur, K. Andrieux, J. Biotech. 2011, 156, 338-40 10.1016/j.jbiotec.2011.07.020.
46. D. Brambilla, R. Verpillot, L. De Kimpe, M. Taverna, B. Le Droumaguet, J. Nicolas, M. Canovi, M. Gobbi, M. Salmona, N. Valérie, W. Scheper, P. Couvreur, K. Andrieux, J. Controlled. Release 2010, 148, e112-3 10.1016/j.jconrel.2010.07.084.
47. T. D. Mai, I. Pereiro, M. Hiraoui, J.-L. Viovy, S. Descroix, M. Taverna, C. Smadja, Analyst 2015, 140, 5891-5900.
48. F. Oukacine, M. Taverna, Anal. Chem. 2014, 86, 3317-3322 10.1021/ac403337j.
49. T. D. Mai, F. Oukacine, M. Taverna, J. Chromatogr. A 2016, 1453, 116-23 10.1016/j.chroma.2016.05.048.
50. C. Crosnier de Lassichere, T. Mai, M. Taverna, J. Chromatogr. A 2019, 1601, 10.1016/j.chroma.2019.05.006.
51. C. Crosnier de Lassichère, T. D. Mai, M. Otto, M. Taverna, Anal. Chem. 2018, 90, 2555-2563 10.1021/acs.analchem.7b03843.
52. M. R. Mohamadi, Z. Svobodova, R. Verpillot, H. Esselmann, J. Wiltfang, M. Otto, M. Taverna, Z. Bilkova, J.-L. Viovy, Anal. Chem. 2010, 82, 7611-7617 10.1021/ac101337n.
53. K. Mesbah, R. Verpillot, M. Chiari, A. Pallandre, M. Taverna, Analyst 2014, 139, 6547-55.
54. M. Ammar, C. Smadja, L. G. T. Phuong, M. Azzouz, J. Vignerond, A. Etcheberry, M. Taverna, E. Dufour-Gergam, Biosens. Bioelectron. 2013, 40, 329-335 10.1016/j.bios.2012.07.072.
55. M. Ammar, C. Smadja, G. L, D. Tandjigora, J. Vigneron, A. Etcheberry, M. Taverna, E. Dufour-Gergam, Langmuir 2014, 30, 10.1021/la500695y.
56. M. Serra, D. Ferraro, I. Pereiro, J. L. Viovy, S. Descroix, Lab on a Chip 2017, 17, 3979-3999 10.1039/c7lc00582b.
57. T. D. Mai, D. Ferraro, N. Aboud, R. Renault, M. Serra, N. T. Tran, J.-L. Viovy, C. Smadja, S. Descroix, M. Taverna, Sens. Actuators B 2018, 255, 2126-2135.
58. D. Horák, H. Hlídková, M. Hiraoui, M. Taverna, V. Proks, E. Mázl Chánová, C. Smadja, Z. Kucerová, Macromolecular bioscience 2014, 14, 10.1002/mabi.201400249.
59. T. D. Mai, P. C. Hauser, S. Descroix, C. Crosnier de Lassichère, M. Taverna, C. Smadja, Anal. Chim. Acta 2019, 1062, 156-164.
60. Z. Svobodova, M. R. Mohamadi, B. Jankovicova, H. Esselmann, R. Verpillot, M. Otto, M. Taverna, J. Wiltfang, J.-L. Viovy, Z. Bilkova, Biomicrofluidics 2012, 6, 024126 024126, 10.1063/1.4722588.
61. M. R. Mohamadi, R. Verpillot, M. Taverna, M. Otto, J.-L. Viovy, Methods Mol. Biol. (Clifton, N.J.) 2012, 869, 173-84 10.1007/978-1-61779-821-4_14.
62. R. Mohamadi, R. Verpillot, M. Taverna, M. Otto, J.-L. Viovy, in, 2019, pp. 327-340.
63. R. Mohamadi, Z. Svobodova, Z. Bílková, M. Otto, M. Taverna, S. Descroix, J.-L. Viovy, Biomicrofluidics 2015, 9, 054117 10.1063/1.4931394.
64. I. Pereiro, A. Bendali, S. Tabnaoui, L. Alexandre, J. Srbova, Z. Bilkova, S. Deegan, L. Joshi, J. L. Viovy, L. Malaquin, B. Dupuy, S. Descroix, Chem. Sci. 2017, 8, 1329-1336 10.1039/c6sc03880h.
65. D. Ferraro, J. Champ, B. Teste, M. Serra, L. Malaquin, J. L. Viovy, P. de Cremoux, S. Descroix, Sci. Rep. 2016, 6, 25540 10.1038/srep25540.

References of chapter 2

1. Toseland, C.P., *Fluorescent labeling and modification of proteins.* Journal of chemical biology, 2013. **6**(3): p. 85-95.
2. Kasicka, V., *Recent developments in capillary and microchip electroseparations of peptides (2011-2013).* Electrophoresis, 2014. **35**(1): p. 69-95.
3. Hu, Y., et al., *Analysis of compositional monosaccharides in fungus polysaccharides by capillary zone electrophoresis.* Carbohydr Polym, 2014. **102**: p. 481-8.
4. Smith, A. and R.J. Nelson, *Capillary electrophoresis of DNA.* Curr Protoc Nucleic Acid Chem, 2003. **Chapter 10**: p. Unit 10.9.
5. Vanifatova, N.G., et al., *Size separation of silica nanospheres by means of capillary zone electrophoresis.* Talanta, 2003. **59**(2): p. 345-353.
6. Tůma, P. and F. Opekar, *Detectors in Capillary Electrophoresis*, in *Analytical Separation Science*. 2015. p. 607-628.
7. Almeda, S., L. Arce, and M. Valcarcel, *The More and Less Common Approaches to Enhancing Sensitivity in Capillary Electrophoresis.* Current Analytical Chemistry, 2010. **6**(2): p. 126-143.
8. Kuhn, R. and S. Hoffstetter-Kuhn, *Basic Principles*, in *Capillary Electrophoresis: Principles and Practice*, R. Kuhn and S. Hoffstetter-Kuhn, Editors. 1993, Springer Berlin Heidelberg: Berlin, Heidelberg. p. 5-36.
9. Kok, W., *The Background Electrolyte*, in *Capillary Electrophoresis: Instrumentation and Operation*, W. Kok, Editor. 2000, Vieweg+Teubner Verlag: Wiesbaden. p. 36-43.
10. Xuan, X. and D. Li, *Analytical study of Joule heating effects on electrokinetic transportation in capillary electrophoresis.* Journal of Chromatography A, 2005. **1064**(2): p. 227-237.
11. Xiangchun, X. and L. Dongqing, *Joule heating effects on peak broadening in capillary zone electrophoresis.* Journal of Micromechanics and Microengineering, 2004. **14**(8): p. 1171.
12. Divan, K., *IMPROVED SEPARATION AND DETECTION OF INORGANIC IONS BY CAPILLARY ELECTROPHORESIS*, in *Progress in Ion Exchange*, A. Dyer, M.J. Hudson, and P.A. Williams, Editors. 1997, Woodhead Publishing. p. 176-186.
13. DN., H., *High Performance Capillary Electrophoresis : An Introduction : A Primer.* Agilent Technologies. 2000.
14. Brambilla, D., et al., *New Method Based on Capillary Electrophoresis with Laser-Induced Fluorescence Detection (CE-LIF) to Monitor Interaction between Nanoparticles and the Amyloid-beta Peptide.* Anal. Chem., 2010. **82**(24): p. 10083-10089.
15. Mai, T.D. and P.C. Hauser, *Contactless conductivity detection for electrophoretic microseparation techniques.* The Chemical Record, 2012. **12**(1): p. 106-113.
16. Verpillot, R., et al., *Simultaneous analysis by capillary electrophoresis of five amyloid peptides as potential biomarkers of Alzheimer's disease.* J Chromatogr A, 2008. **1214**(1-2): p. 157-64.
17. Michels, D.A., M. Parker, and O. Salas-Solano, *Quantitative impurity analysis of monoclonal antibody size heterogeneity by CE-LIF: example of development and validation through a quality-by-design framework.* Electrophoresis, 2012. **33**(5): p. 815-26.
18. Morani, M., M. Taverna, and T.D. Mai, *A fresh look into background electrolyte selection for capillary electrophoresis-laser induced fluorescence of peptides and proteins.* Electrophoresis, 2019. **40**(18-19): p. 2618-2624.
19. Mai, T.D. and P.C. Hauser, *Pressure-assisted capillary electrophoresis for cation separations using a sequential injection analysis manifold and contactless conductivity detection.* Talanta, 2011. **84**(5): p. 1228-1233.

20. Le, T.B., et al., *Low-cost and versatile analytical tool with purpose-made capillary electrophoresis coupled to contactless conductivity detection: Application to antibiotics quality control in Vietnam.* Electrophoresis, 2020. **41**(23): p. 1980-1990.
21. Bergström, S.K., et al., *A simplified multidimensional approach for analysis of complex biological samples: on-line LC-CE-MS.* Analyst, 2006. **131**(7): p. 791-798.
22. Huhn, C., et al., *Relevance and use of capillary coatings in capillary electrophoresis-mass spectrometry.* Anal Bioanal Chem, 2010. **396**(1): p. 297-314.
23. Qu, H., T. Mudalige, and S. Linder, *Capillary electrophoresis coupled with inductively coupled mass spectrometry as an alternative to cloud point extraction based methods for rapid quantification of silver ions and surface coated silver nanoparticles.* Journal of Chromatography A, 2015. **1429**.
24. Stalcup, A.M., *CHAPTER 8 - Chiral separations by capillary electrophoresis*, in *Chiral Analysis*, K.W. Busch and M.A. Busch, Editors. 2006, Elsevier: Amsterdam. p. 241-275.
25. Charcosset, C., *Electrophoretic Mobility*, in *Encyclopedia of Membranes*, E. Drioli and L. Giorno, Editors. 2016, Springer Berlin Heidelberg: Berlin, Heidelberg. p. 658-659.
26. Hayes, M.A., I. Kheterpal, and A.G. Ewing, *Effects of buffer pH on electroosmotic flow control by an applied radial voltage for capillary zone electrophoresis.* Analytical Chemistry, 1993. **65**(1): p. 27-31.
27. Pietrzyk, D.J., S. Chen, and B. Chanthawat, *Enhanced capillary zone electrophoretic separation of dinitrophenyl-amino acid derivatives through control of electroosmotic flow by the buffer cation.* Journal of Chromatography A, 1997. **775**(1): p. 327-338.
28. Znaleziona, J., et al., *Dynamic Coating Agents in CE.* Chromatographia, 2008. **67**(1): p. 5-12.
29. Reijenga, J.C., et al., *Buffer capacity, ionic strength and heat dissipation in capillary electrophoresis.* Journal of Chromatography A, 1996. **744**(1): p. 147-153.
30. Corradini, D. and L. Sprecacenere, *Dependence of the electroosmotic flow in bare fused-silica capillaries from pH, ionic strength and composition of electrolyte solutions tailored for protein capillary zone electrophoresis.* Chromatographia, 2003. **58**(9-10): p. 587-596.
31. Ding, W., M.J. Thornton, and J.S. Fritz, *Capillary electrophoresis of anions at high salt concentrations.* Electrophoresis, 1998. **19**(12): p. 2133-9.
32. Bushey, M.M. and J.W. Jorgenson, *Capillary electrophoresis of proteins in buffers containing high concentrations of zwitterionic salts.* Journal of Chromatography A, 1989. **480**: p. 301-310.
33. Liénard--Mayor, T., et al., *High sensitivity capillary electrophoresis with fluorescent detection for glycan mapping.* Journal of Chromatography A, 2021. **1657**: p. 462593.
34. Busnel, J.M., et al., *Evaluation of capillary isoelectric focusing in glycerol-water media with a view to hydrophobic protein applications.* Electrophoresis, 2005. **26**(17): p. 3369-3379.
35. Mokaddem, M., P. Gareil, and A. Varenne, *Online CIEF-ESI-MS in glycerol-water media with a view to hydrophobic protein applications.* Electrophoresis, 2009. **30**(23): p. 4040-8.
36. Lecoeur, M., P. Gareil, and A. Varenne, *Separation and quantitation of milk whey proteins of close isoelectric points by on-line capillary isoelectric focusing--electrospray ionization mass spectrometry in glycerol-water media.* J Chromatogr A, 2010. **1217**(46): p. 7293-301.
37. Beneito-Cambra, M., et al., *Stability and effectiveness of linear polyacrylamide capillary coating to suppress EOF in acidic media in the presence of surfactants, ionic liquids and organic modifiers.* Talanta, 2016. **150**: p. 546-52.
38. Sola, L. and M. Chiari, *Modulation of electroosmotic flow in capillary electrophoresis using functional polymer coatings.* Journal of Chromatography A, 2012. **1270**: p. 324-329.
39. Righetti, P.G., et al., *The state of the art of dynamic coatings.* ELECTROPHORESIS, 2001. **22**(4): p. 603-611.

40. Melanson, J.E., N.E. Baryla, and C.A. Lucy, *Dynamic capillary coatings for electroosmotic flow control in capillary electrophoresis.* TrAC Trends in Analytical Chemistry, 2001. **20**(6): p. 365-374.
41. Giordano, B.C., et al., *Dynamically-coated capillaries allow for capillary electrophoretic resolution of transferrin sialoforms via direct analysis of human serum.* J Chromatogr B Biomed Sci Appl, 2000. **742**(1): p. 79-89.
42. Lanz, C., et al., *Evaluation and optimization of capillary zone electrophoresis with different dynamic capillary coatings for the determination of carbohydrate-deficient transferrin in human serum.* J Chromatogr A, 2002. **979**(1-2): p. 43-57.
43. Robb, C.S., *Applications of Physically Adsorbed Polymer Coatings in Capillary Electrophoresis.* Journal of Liquid Chromatography & Related Technologies, 2007. **30**(5-7): p. 729-759.
44. Mai, T.D., F. d'Orlye, and A. Varenne, *A Comprehensive Study of Silanization and Co-Condensation for Straightforward Single-Step Covalent Neutral Capillary Coating.* Chromatographia, 2015. **78**(11-12): p. 775-783.
45. Hajba, L. and A. Guttman, *Recent advances in column coatings for capillary electrophoresis of proteins.* Trac-Trend Anal. Chem., 2017. **90**: p. 38-44.
46. Kartsova, L.A., D.V. Makeeva, and V.A. Davankov, *Nano-sized polymer and polymer-coated particles in electrokinetic separations.* TrAC Trend Anal. Chem., 2019. **120**: p. 115656.
47. Sun, X., et al., *Enantioseparation of propranolol, amlodipine and metoprolol by electrochromatography using an open tubular capillary modified with β-cyclodextrin and poly(glycidyl methacrylate) nanoparticles.* Microchimica Acta, 2019. **186**(2): p. 128.
48. Oukacine, F. and M. Taverna, *Suppression of apparent fluid flow in capillary isotachophoresis without recourse to capillary coating.* Anal Chem, 2014. **86**(7): p. 3317-22.
49. A. Wuethrich, P. R. Haddad, and P. Quirino, *Zero net-flow in capillary electrophoresis using acrylamide based hydrogel.* Analyst, 2014. **139**: p. 3722-3726.
50. Bello, M.S., L. Capelli, and P.G. Righetti, *Dependence of the electroosmotic mobility on the applied electric field and its reproducibility in capillary electrophoresis.* J Chromatogr A, 1994. **684**(2): p. 311-22.
51. Rasmussen, H.T. and H.M. McNair, *Influence of buffer concentration, capillary internal diameter and forced convection on resolution in capillary zone electrophoresis.* Journal of Chromatography A, 1990. **516**(1): p. 223-231.
52. Osbourn, D.M., D.J. Weiss, and C.E. Lunte, *On-line preconcentration methods for capillary electrophoresis.* Electrophoresis, 2000. **21**(14): p. 2768-79.
53. Mikkers, F.E.P., F.M. Everaerts, and T.P.E.M. Verheggen, *High-performance zone electrophoresis.* Journal of Chromatography A, 1979. **169**: p. 11-20.
54. Ma, B., et al., *Highly efficient sample stacking by enhanced field amplification on a simple paper device.* Lab on a Chip, 2016. **16**(18): p. 3460-3465.
55. Bharadwaj, R. and J.G. Santiago, *Dynamics of field-amplified sample stacking.* Journal of Fluid Mechanics, 2005. **543**: p. 57-92.
56. Chien, R.-L. and D.S. Burgi, *Field amplified sample injection in high-performance capillary electrophoresis.* Journal of Chromatography A, 1991. **559**(1): p. 141-152.
57. Zhang, C.X. and W. Thormann, *Head-Column Field-Amplified Sample Stacking in Binary System Capillary Electrophoresis: A Robust Approach Providing over 1000-Fold Sensitivity Enhancement.* Anal Chem, 1996. **68**(15): p. 2523-32.
58. Simpson, S., J.P. Quirino, and S. Terabe, *On-line sample preconcentration in capillary electrophoresis. Fundamentals and applications.* Journal of chromatography. A, 2008. **1184 1-2**: p. 504-41.

59. Quirino, J.P. and S. Terabe, *Sample stacking of cationic and anionic analytes in capillary electrophoresis.* Journal of Chromatography A, 2000. **902**(1): p. 119-135.
60. Chien, R.L. and D.S. Burgi, *Sample stacking of an extremely large injection volume in high-performance capillary electrophoresis.* Analytical Chemistry, 1992. **64**(9): p. 1046-1050.
61. Breadmore, M.C., et al., *Recent advances in enhancing the sensitivity of electrophoresis and electrochromatography in capillaries and microchips (2016–2018).* ELECTROPHORESIS, 2019. **40**(1): p. 17-39.
62. Sänger, M.C.B.C., *In-Capillary Sample Concentration in CE - "This is my analyte, how do I stack?".* Lc Gc North America 2014. **32**: p. 174-186.
63. Malá, Z. and P. Gebauer, *Analytical isotachophoresis 1967–2022: From standard analytical technique to universal on-line concentration tool.* TrAC Trends in Analytical Chemistry, 2023. **158**: p. 116837.
64. Breadmore, M.C., et al., *Recent advances in enhancing the sensitivity of electrophoresis and electrochromatography in capillaries and microchips (2012-2014).* Electrophoresis, 2015. **36**(1): p. 36-61.
65. Volpi, N. and F. Maccari, *Capillary Electrophoresis of Biomolecules: Methods and Protocols*. 2013.
66. Trapiella-Alfonso, L., et al., *Electromigration separation methodologies for the characterization of nanoparticles and the evaluation of their behaviour in biological systems.* TrAC Trends in Analytical Chemistry, 2016. **84**: p. 121-130.
67. Swerdlow, H. and R. Gesteland, *Capillary gel electrophoresis for rapid, high resolution DNA sequencing.* Nucleic Acids Res, 1990. **18**(6): p. 1415-9.
68. Durney, B.C., C.L. Crihfield, and L.A. Holland, *Capillary electrophoresis applied to DNA: determining and harnessing sequence and structure to advance bioanalyses (2009-2014).* Anal Bioanal Chem, 2015. **407**(23): p. 6923-38.
69. Datinská, V., et al., *Recent progress in nucleic acids isotachophoresis.* J Sep Sci, 2018. **41**(1): p. 236-247.
70. Albarghouthi, M.N. and A.E. Barron, *Polymeric matrices for DNA sequencing by capillary electrophoresis.* Electrophoresis, 2000. **21**(18): p. 4096-111.
71. Kleemiss, M.H., M. Gilges, and G. Schomburg, *Capillary electrophoresis of DNA restriction fragments with solutions of entangled polymers.* Electrophoresis, 1993. **14**(5-6): p. 515-22.
72. Valdés, A., V. García-Cañas, and A. Cifuentes, *CGE-laser induced fluorescence of double-stranded DNA fragments using GelGreen dye.* Electrophoresis, 2013. **34**(11): p. 1555-62.
73. Jia, Z.-P., et al., *CE of Small DNA Fragments Using Linear Polyacrylamide Matrices.* Chromatographia, 2009. **70**(7): p. 1127.
74. Zinellu, A., et al., *Evaluation of Global Genomic DNA Methylation in Human Whole Blood by Capillary Electrophoresis UV Detection.* Journal of Analytical Methods in Chemistry, 2017. **2017**: p. 4065892.
75. Biebricher, A.S., et al., *The impact of DNA intercalators on DNA and DNA-processing enzymes elucidated through force-dependent binding kinetics.* Nature Communications, 2015. **6**(1): p. 7304.
76. Duša, F., D. Moravcová, and K. Šlais, *DNA purification and concentration by isotachophoresis in nonwoven fabric strip.* Anal Chim Acta, 2020. **1117**: p. 41-47.
77. Marshall, L.A., et al., *An injection molded microchip for nucleic acid purification from 25 microliter samples using isotachophoresis.* J Chromatogr A, 2014. **1331**: p. 139-42.

78. García-Cañas, V., R. González, and A. Cifuentes, *Highly reproducible capillary gel electrophoresis (CGE) of DNA fragments using uncoated columns. Detection of genetically modified maize by PCR-cGE.* Journal of Separation Science, 2002. **25**(9): p. 577-583.
79. García-Cañas, V., M. Mondello, and A. Cifuentes, *Simultaneous detection of genetically modified organisms by multiplex ligation-dependent genome amplification and capillary gel electrophoresis with laser-induced fluorescence.* ELECTROPHORESIS, 2010. **31**(13): p. 2249-2259.
80. Cheng, Y.-Q., et al., *An automated capillary electrophoresis system for high-speed separation of DNA fragments based on a short capillary.* ELECTROPHORESIS, 2010. **31**(19): p. 3184-3191.
81. Wan, F., et al., *Nanostructured copolymer gels for dsDNA separation by CE.* ELECTROPHORESIS, 2008. **29**(23): p. 4704-4713.
82. Liu, B.-F., et al., *Pharmaceutical-Induced Cell Apoptosis Characterized by Capillary Zone Electrophoresis.* Analytical Biochemistry, 2001. **297**(1): p. 10-14.
83. Huang, M.-F., et al., *Separation of Long Double-Stranded DNA by Nanoparticle-Filled Capillary Electrophoresis.* Analytical Chemistry, 2004. **76**(1): p. 192-196.
84. Hurth, C., et al., *Direct loading of polymer matrices in plastic microchips for rapid DNA analysis: A comparative study.* ELECTROPHORESIS, 2012. **33**(16): p. 2604-2611.
85. Sullivan, B.P., et al., *Nucleic acid sample preparation from whole blood in a paper microfluidic device using isotachophoresis.* J Chromatogr B Analyt Technol Biomed Life Sci, 2021. **1163**: p. 122494.
86. Qu, Y., L.A. Marshall, and J.G. Santiago, *Simultaneous purification and fractionation of nucleic acids and proteins from complex samples using bidirectional isotachophoresis.* Anal Chem, 2014. **86**(15): p. 7264-8.
87. Eid, C., S.S. Branda, and R.J. Meagher, *A rapidly-prototyped microfluidic device for size-based nucleic acid fractionation using isotachophoresis.* Analyst, 2017. **142**(12): p. 2094-2099.
88. Mei, Q., et al., *On-chip isotachophoresis separation of functional DNA origami capture nanoarrays from cell lysate.* Nano Research, 2013. **6**(10): p. 712-719.
89. Han, C.M., E. Katilius, and J.G. Santiago, *Increasing hybridization rate and sensitivity of DNA microarrays using isotachophoresis.* Lab on a Chip, 2014. **14**(16): p. 2958-2967.
90. Ostromohov, N., O. Schwartz, and M. Bercovici, *Focused upon Hybridization: Rapid and High Sensitivity Detection of DNA Using Isotachophoresis and Peptide Nucleic Acid Probes.* Analytical Chemistry, 2015. **87**(18): p. 9459-9466.
91. Kitagawa, F., et al., *On-line coupling of sample preconcentration by LVSEP with gel electrophoretic separation on T-channel chips.* Electrophoresis, 2017. **38**(2): p. 380-386.
92. Huang, C.-C., et al., *Maximization of injection volumes for DNA analysis in capillary electrophoresis.* ELECTROPHORESIS, 2001. **22**(20): p. 4328-4332.
93. Alves, M.N., et al., *Separation of superparamagnetic magnetite nanoparticles by capillary zone electrophoresis using non-complexing and complexing electrolyte anions and tetramethylammonium as dispersing additive.* ELECTROPHORESIS, 2018. **39**(12): p. 1429-1436.
94. Wang, F.-H., et al., *Determination of Conjugation Efficiency of Antibodies and Proteins to the Superparamagnetic Iron Oxide Nanoparticles by Capillary Electrophoresis with Laser-Induced Fluorescence Detection.* Journal of Nanoparticle Research, 2003. **5**(1): p. 137-146.
95. Kruszewska, J., et al., *A CE-ICP-MS/MS method for the determination of superparamagnetic iron oxide nanoparticles under simulated physiological conditions.* Analytical and Bioanalytical Chemistry, 2020. **412**(29): p. 8145-8153.

96. Baron, D., et al., *Study of interactions between carboxylated core shell magnetic nanoparticles and polymyxin B by capillary electrophoresis with inductively coupled plasma mass spectrometry.* J. Chromatogr. A, 2020. **1609**.
97. Baron, D., et al., *Online stacking of carboxylated magnetite core–shell nanoparticles in capillary electrophoresis.* Journal of Separation Science, 2017. **40**(11): p. 2482-2487.
98. Vanifatova, N.G., et al., *Investigation of iron oxide nanoparticles by capillary zone electrophoresis.* Talanta, 2005. **66**(3): p. 605-610.
99. d'Orlye, F., et al., *Charge-based characterization of nanometric cationic bifunctional maghemite/silica core/shell particles by capillary zone electrophoresis.* Electrophoresis, 2009. **30**(14): p. 2572-2582.
100. d'Orlye, F., A. Varenne, and P. Gareil, *Size-based characterization of nanometric cationic maghemite particles using capillary zone electrophoresis.* Electrophoresis, 2008. **29**(18): p. 3768-3778.
101. Li, N., et al., *Probing Nanoparticle−Protein Interaction by Capillary Electrophoresis.* Analytical Chemistry, 2010. **82**(17): p. 7460-7466.
102. Ibrahim, A., et al., *Determination of effective charge of small ions, polyelectrolytes and nanoparticles by capillary electrophoresis.* Journal of Chromatography A, 2012. **1247**: p. 154-164.
103. Brambilla, D., et al., *PEGylated Nanoparticles Bind to and Alter Amyloid-Beta Peptide Conformation: Toward Engineering of Functional Nanomedicines for Alzheimer's Disease.* Acs Nano, 2012. **6**(7): p. 5897-5908.
104. Girardot, M., et al., *Aptamer-conjugated nanoparticles: Preservation of targeting functionality demonstrated by microchip electrophoresis in frontal mode.* Analytical Biochemistry, 2013. **435**(2): p. 150-152.
105. Baron, D., C. Cacho, and J. Petr, *Electrokinetic preconcentration of magnetite core - carboxylic shell nanoparticles by capillary electrophoresis.* J. Chromatogr. A, 2017. **1499**: p. 217-221.
106. Cacho, C., et al., *Study of behavior of carboxylic magnetite core shell nanoparticles on a pH boundary.* Journal of Chromatography A, 2014. **1364**: p. 59-63.
107. Beshir, S.A., et al., *Aducanumab Therapy to Treat Alzheimer's Disease: A Narrative Review.* International journal of Alzheimer's disease, 2022. **2022**: p. 9343514-9343514.
108. Marucci, G., et al., *Efficacy of acetylcholinesterase inhibitors in Alzheimer's disease.* Neuropharmacology, 2021. **190**: p. 108352.
109. Selkoe, D.J. and J. Hardy, *The amyloid hypothesis of Alzheimer's disease at 25 years.* EMBO molecular medicine, 2016. **8**(6): p. 595-608.
110. De-Paula, V.J., et al., *Alzheimer's disease.* Subcell Biochem, 2012. **65**: p. 329-52.

OBJECTIVES

Understanding the importance of MP's characterization (see chapter 1 of my thesis), the first part of my work focuses on the development of novel techniques to characterize the interaction between these particles with (bio)molecules. In the second part, the attention was put on the combination of CE and MPs for development of novel approaches for sample treatment and bioanalysis.

In this regard, the scope of my PhD project is to develop three analytical approaches for:

- Studying the interaction between magnetic beads with antibodies (for antibody immobilization for magneto-immunoassays) using size exclusion chromatography coupled to fluorescence detector (SEC-FLD).
- Improving the detection sensitivity of CE-LIF of MNPs by developing a new EOF-assisted preconcentration method based on large weakly charged electrolytes in uncoated silica capillary, serving for enrichment and interaction characterization of MNPs.
- Developing a new approach of 2-stage online preconcentration in CE, with magneto extraction on circulating magnetic beads inside the capillary and electrokinetic enrichment for purification and detection of DNA.

Three axes of the thesis are resumed in the *Figure 32*.

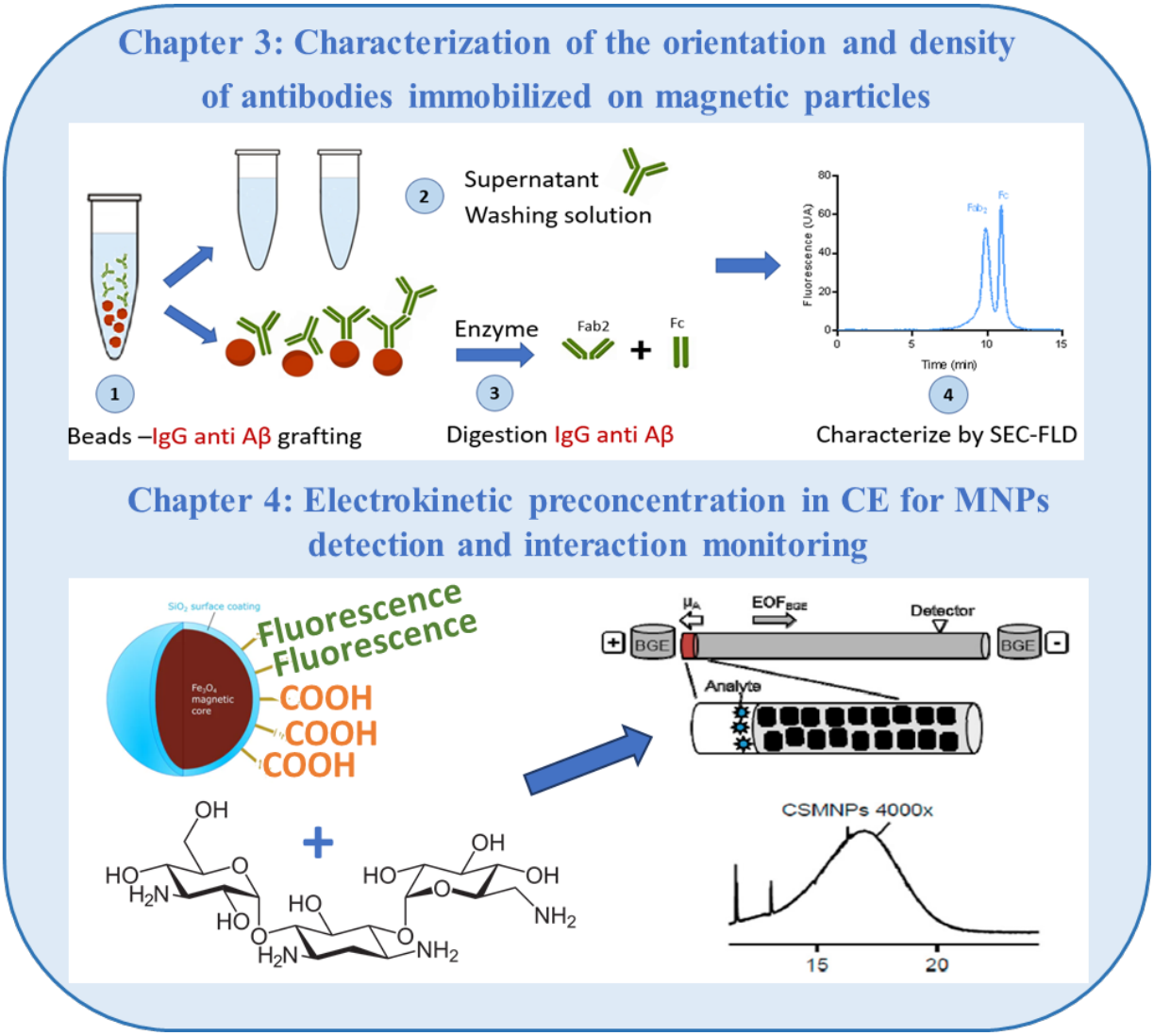

Figure 32: Schematic representation of the thesis work

EXPERIMENTAL PART

Chapter 3: CHARACTERIZATION OF ANTIBODY'S ORIENTATION AND DENSITY IMMOBILIZED ON MPS

As presented in chapter 1, magnetic beads are widely employed as an efficient solid-support for magneto-(immuno)-enrichment or magneto-(immuno)-extraction thanks to their high surface-to-volume ratio, high throughput and ease of manipulation via an external magnetic field [1]. Nevertheless, the performance of magneto-immuno-capture depends on the density and orientation of the grafted antibodies since they affect the efficient and selective capture of the target analyte(s). To obtain the best performance, many conventional methods were studied to characterize the antibodies immobilized on beads such as spectrophotometric and biophysical ones [2]. In this chapter, the development of an enzymatic strategy combined with Size Exclusion Chromatography (SEC) is reported, allowing to simultaneously characterize the orientation and density of antibodies immobilized on beads. Immunoglobulin G degradation enzyme FabRICATOR Z, a cysteine protease was employed to digest antibody IgG_{2a} mouse anti-Aβ 1-42 (clone NAB228) into $F(ab)_2$ and Fc. By determining the quantity of these digested fragments, the density and orientation of immobilized antibodies on beads could be indirectly determined. Based on the obtained results, Tosyl-activated and protein G beads were chosen for further immuno-enrichment studies on Aβ 1-42 peptide, a validated biomarker for molecular diagnosis of Alzheimer's disease, thanks to their significantly higher performance than carboxylic beads.

3.1 SEC-FLD PRINCIPLES

3.1.1 Principles of SEC

Size exclusion chromatography, also known as gel filtration or gel permeation chromatography, separates the macromolecules based on their hydrodynamic sizes [3]. In the column of SEC, the porous particles play the role as the stationary phase. Their surface is modified to avoid the interaction with target analyte(s). The particle and pore sizes determine the sizes of compounds that are to be separated. As a sample travels through a column, small species in the sample can enter into most of the pores and larger ones may enter only in a few or none of the pores, resulting in a separation based on size or molar mass. Hence, the larger components are eluted first from the column (*Figure 33*).

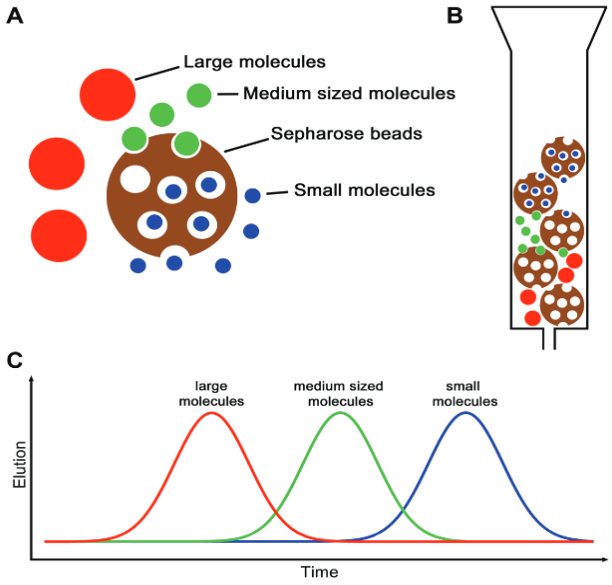

Figure 33: Illustration of the SEC working principle. (A) The porous particles and analyte molecules in different size; (B) SEC column and (C) SEC chromatogram describing the time-dependent elution of different molecule sizes [4].

The total volume V0 of the mobile phase in the column can be divided into two parts: the interstitial volume Vi (interstitial porosity) and pore volume Vp (particle porosity) [3]. Vi represents the volume of the mobile phase required to transport a large molecule while V0 is determined by Vi +Vp corresponding to the volume necessary to elute a small molecule. The elution volume Ve are therefore between Vi and V0 and are described as as follow:

$$Ve = Vi \times K_D + Vp \qquad (7)$$

Where K_D is the thermodynamic retention factor. If the Ve/V0 exceeds 1, the molecules are not only eluted correspond to the size exclusion mechanism but also to physicochemical interactions with the stationary phase (typically hydrophobic and electrostatic interactions, as illustrated in *Figure 34* [5]).

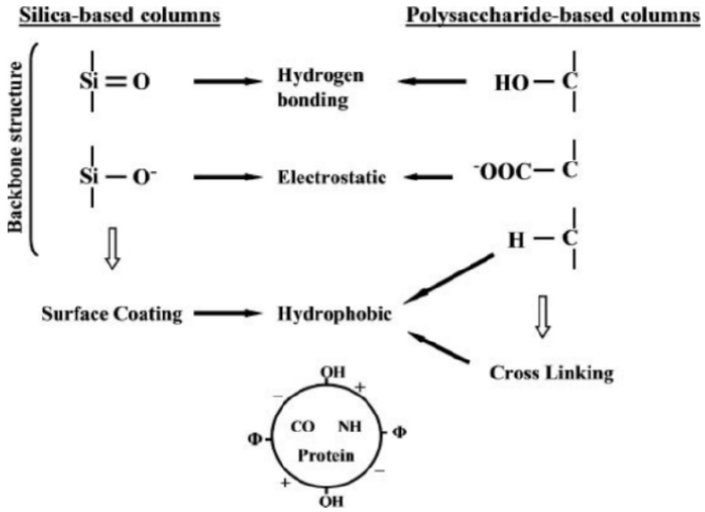

Figure 34: The interaction of analyte molecules with the stationary phase in SEC [5].

Beside of size separation, SEC is also used to characterize the molecular weight of biomolecules, such as peptides/proteins [6, 7], nucleic acid [8], or polymer [9] by calibrating the size-exclusion column with compounds with known molecular weights and having similar structures to those of the desired analytes [10].

There are some considerations when using SEC. First, the technique does require substantial differences in molecular weight to create significant shifts in retention [10]. The second issue is the possible adsorption of analyte on the stationary phase due to the secondary undesirable interaction. The retention time of the analyte is therefore modified, leading to possible conformation change as aggregate and asymmetry peak [10]. Electrostatic interactions can result in faster elution if there is electrostatic repulsion which prevents the analyte from diffusing into the pore, or reversely, longer time retention due to high electrostatic interaction. To prevent these phenomena, the optimization step of the mobile phase and the selection of stationary phase are essential.

3.1.2 Detectors couple to SEC

SEC can be coupled with many modes of detection to provide further information rather than size and molecule weight. Beside the coupling to three predominant detectors UV, LIF, and MS, SEC can also be hyphenated to Multi Angle Light Scattering (MALS). A MALS detector measures the amount of light scattered by particles in solution relative to the angle of the incident light. The advantages and considerations of these detectors when using for SEC of proteins are summarized in *Table 8.*

Table 8: Summarized advantages and considerations of detectors coupled to SEC for protein analysis.

Detectors	Advantages	Considerations	References
UV	Multi-wavelength detection for more information; simple, rapid. Amide peptide bond: 214 and 220 nm Aromatic amino acid: 280 nm	Low sensitivity and selectivity. Only information about estimated molecule weight and concentration.	[11, 12]
FLD	Based on intrinsic amino acids (e.g., tryptophan, tyrosine, etc.). λexcited 280 nm; λemitted 350-370 nm High sensitivity and selectivity, simple, rapid.	Only information about estimated molecule weight and concentration.	[6, 13-15]
MALS	Diverse information: size, form, aggregate, polydispersity, concentration, molecule weight, thanks to the combination with other detection modules: refractometer, UV and viscometer. Independence of molecular weight measurement on elution time.	Complicated calibration and manipulation.	[16-19]
MS	Diverse informations: size, molecule weight, conformation, charge, protein-ligand affinity.	Expensive, complicated Volatile mobile phase requirement	[20-23]

3.2 IMMUNO-CAPTURE OF BIOMOLECULES ON FUNCTIONALIZED MAGNETIC BEADS: FROM CHARACTERIZATION TO APPLICATION FOR A BIOMARKER OF ALZHEIMER'S DISEASE (PAPER 1)

Immuno-capture of biomolecules on functionalized magnetic beads: from characterization to application for a biomarker of Alzheimer's disease

Ngoc Van Thanh Nguyen[1], Claire Smadja[1*], Myriam Taverna[1,2], Frédéric Halgand[3], Thanh Duc Mai [1*]

[1] *Université Paris-Saclay, CNRS, Institut Galien Paris-Saclay, 91400, Orsay, France.*

[2] *Institut Universitaire de France (IUF)*

[3] *Université Paris Saclay-CNRS, Laboratoire de Chimie Physique, Orsay, France*

Correspondence: E-mail: claire.smadja@u-psud.fr; Fax: +33-1-46-83-55-51

thanh-duc.mai@u-psud.fr

Keywords: magnetic beads, density and orientation, antibody anti-amyloid beta, size exclusion chromatography, enzyme digestion, IdeZ.

Abstract

It is reported herein a new approach to study the orientation and density of mouse antibody grafting on magnetic beads, serving for immunoassays and immuno-extraction of biomolecules. This approach is based on selective enzymatic digestion of target grafted antibodies at a specific site below the hinge position to provide $F(ab)_2$ and Fc fragments, followed by separation and determination of these fragments with size exclusion chromatography (SEC) coupled with fluorescence detection (FLD). The developed method was applied for evaluation of immunoglobulin (IgG_{2a}) grafting capacity on three different biofunctionalized magnetic beads (i.e., Tosyl-activated, carboxylic, protein G). Tosyl-activated and protein G beads at different optimal grafting IgG: bead ratios (i.e.,110 µg: 1000 µg and 240 µg: 1000 µg, respectively) exhibited superior grafting capacity than carboxylic counterparts. Under the optimized conditions, more than 70 % of antibodies were grafted on tosyl-activated and protein G beads in the right orientation. This approach was then demonstrated with different commercially available antibodies specific to amyloid-beta peptide 1-42 (Aβ 1-42) for magneto-immunoassays of this peptide that is an established biomarker for molecular diagnosis of Alzheimer's disease.

1. Introduction

Immuno-enrichment and immunoassays, relying on the capture of target peptides and proteins via specific antibodies for their subsequent preconcentration and detection, are the gold techniques used in bioanalysis. Among all solid supports for such purpose, magnetic beads have gained great attention thanks to the ease of manipulation via an external magnetic field and a variety of functionalities (commercially) available for magnetic particles [1, 2]. The performance of immunocapture on magnetic beads nevertheless depends significantly on density and orientation of the grafted antibodies in order to allow their efficient and selective interaction with target molecules as well as avoid / minimize non-specific adsorption. Control and characterization of on-beads immobilized antibodies are therefore of utmost importance to achieve the best immunocapture performance. Different characterization strategies have been developed for such purpose, notably spectrophotometric and biophysical ones [3]. Recently Oliverio et al. reported an indirect method for quantification of protein on the surface of nanoparticles (NPs) based on hydrolysis of free amine groups by HCl 6M at 110°C, followed by a spectrophotometric quantification of primary amines in solution [4]. Our group recently proposed a new simple and rapid analytical approach to evaluate human antibody orientation and density on magnetic beads applied for immunocapture of a biomarker of inflammation (TNF-α) [5]. This approach relies on the cleavage by IdeS, a highly specific protease for human immunoglobulin G (hIgG), of immobilized antibodies, followed by quantification of the $F(ab)_2$ and Fc fragments via size exclusion chromatography (SEC)-coupled to fluorescent detection (FLD). This approach using IdeS nevertheless is not adapted to mouse IgG, which represents the majority of antibodies commercially available for bioanalysis. Indeed, in the context of molecular diagnosis of Alzheimer's disease (AD), which is the most prevalent neurodegenerative disease worldwide causing a huge burden to the society and having no efficient AD treatment so far [6], mouse antibodies have been most widely used for immunoassays of amyloid (Aβ) beta peptides (notably Aβ 1-42 and Aβ 1-40 which are established biomarkers for AD). No human antibodies specific to these compounds have been available so far.

From this rationality, we report in this study the development of an analytical approach to simultaneously characterize the density and orientation of grafted mouse antibody on magnetic beads. This approach relies on selective enzymatic digestion of immobilized mouse antibodies at one specific site below the hinge region using Immunoglobulin G degrading enzymes (FabRICATOR Z) IdeZ to give $F(ab)_2$ and Fc fragments from mouse antibodies, followed by

separation and determination of these fragments with SEC-FLD. Compared to the previous work [5], optimization of the SEC-FLD method was made to allow separation of the $F(ab)_2$ and Fc fragments from residual antibodies and the enzyme, allowing non bias determination of the digestion efficiency via the $F(ab)_2$ / Fc ratios. The developed approach was applied for three functionalized magnetic beads (i.e., Tosyl-activated, carboxylic, Pierce Protein G) grafting with immunoglobulin (IgG_{2a}) from mouse. Following the antibody-grafting optimizations that can be monitored with our method, the activity of grafted antibodies was confirmed via on-bead immunoassays of amyloid beta 1-42 peptide (Aβ 1-42) that is an established biomarker for AD molecular. The work was extended to three antibodies specific to different epitopes of Aβ 1-42 (i.e., NAB228 for N-terminal, 12F4 for C-terminal, and 4G8 for 17-24 epitopes), serving for evaluation of the performance of bead-based immunoassays of Aβ 1-42.

2. Experimental

2.1. Chemicals, reagents and samples

2-(Cyclohexylamino)ethanesulfonic acid (CHES), Tris(hydroxymethyl)aminomethane (TRIS), sodium dodecyl sulphate (SDS), sodium hydroxide (NaOH), potassium hydroxide (KCl), acid boric (H3BO3), sodium dihydrophosphat (NaH2PO4), disodium hydrophosphat (Na2HPO4), Tween 20, ammonium sulfate ((NH4)2SO4), EDC (N-(3-Dimethylaminopropyl)-N′-ethylcarbodiimide hydrochloride), S-NHS (N-Hydroxysulfosuccinimide sodium salt), mouse IgG_{2a} (2 mg/ml) (mIgG), phosphate buffer saline 10X (PBS), Tris buffer saline 10X (TBS), ammonium hydroxide (NH4OH), human IgG from whole serum (hIgG at 10 mg/ml), as well as different anti-Alzheimer antibodies (1 mg/ml), including NAB228 and 6E10-HRP were all provided by Sigma Aldrich (St. Louis, MO, United States). Other antibodies 12F4-HRP, 12F4, and 4G8 were obtained from Biolegend (San Diego, California, United State). HPLC grade isopropanol (IPA), methanol and acetonitrile were purchased from VWR (Pennsylvania, US). Immunoglobulin G degrading enzymes (FabRICATOR enzyme Ides) and (FabRICATOR Z enzyme Idez) were obtained from Genovis (Lund, Sweden). Amyloid beta peptide Aβ 1-42 was purchased from Eurogentec (Seraing, Belgium). FP-488 NHS ester solution was purchased from Interchim (Montluçon, France). Pierce Protein G (ProG), Tosyl-activated (Ts) and Carboxylated (COOH) magnetic beads, QuantaRed Enhanced Chemifluorescent HRP kit were provided by Thermo Fisher (Massachusetts, United States). All buffers were prepared with deionized water and were filtered through a 0.22 µm membranes (Pall Corporation, New York, USA) prior to use.

2.2. Apparatus and Material

Deionized water used in all experiments was purified using a Direct-Q3 UV purification system (Millipore, Milford, MA, USA). Conductivity and pH values of buffer solutions and samples were measured by a Seven Compact pH meter (Mettler Toledo, Schwerzenbach, Switzerland). SEC-FLD experiments were carried out using a 1260 Agilent UPLC, and a 1260 fluorescent detector (λexcitation: 280 nm, λemission: 345 nm) (Agilent Technologies, Santa Clara, CA, USA). Two columns, including Agilent AdvanceBio SEC (2.7µm particle size, 130 Å pore size, i.d 7.8 , length 300 mm) and BioSEC-3 (3µm particle size, 300 Å pore size, i.d 4,6 mm, length 300 mm) were employed for SEC-FLD at temperature of 25°C. Fluorescence detection with the excitation and emission wavelengths of 530 nm and 582 nm respectively were carried out with a FP-750 Spectrofluorometer from Jasco (Lisses, France) using a 40 µL quartz cuvette (Starna Scientific, Essex, England).

2.3. Methods

2.3.1. Antibody digestion in solution

IdeS FabRICATOR S enzyme 5000 U and IdeZ FabRICATOR Z enzyme 2000 U were dissolved in 100 µL and 50 µL miliQ water, respectively, then aliquoted to 2 µL and stored at -20°C. For IgG digestion, 2 µL IdeS enzyme (100UI) was mixed with 50 µL of 100 mM phosphate buffer (pH 7.0) whereas 2 µL IdeZ enzyme (80UI) was added to 50 µL of 10mM phosphate buffer and 10 mM sodium chloride (pH 6.5). hIgG and 6E10 were diluted in PBS to 50 µL at concentration of 0,1 mg/ml and then digested with IdeS at 37°C on a thermo-mixer at 650 rounds per minute (rpm) for 90 minutes. NAB228 and 6E10 (0,1 mg/ml) were prepared and digested with IdeZ under the same conditions for 120 minutes.

2.3.2. Antibody grafting on magnetic beads

Protein G magnetic bead

50 µL of ProG magnetic beads (10 mg/mL) was added to 2 mL LoBind Eppendorf vials and gently vortexed with 500 µL of Tris solution containing 0.05 % v/v of Tween 20. The supernatant was removed, and the beads were washed one more time with 1 mL of Tris- Tween 20 (0.05%). A magnet was employed to retain magnetic beads during removal or addition of a suspension solution. After removal of the supernatant, a predefined volume (0-5-15-22,5-45-60-75-90 µL) of NAB228

at 2 mg/mL was subsequently added to beads. The Tris- Tween 20 (0.05%) solution was then added to 500 µL. The mixtures were then incubated at 25°C, 650 rpm for 1 hour on a Thermomixer. The protocol was also carried out with 100 µL ProG (10 mg/mL) and 4 batches of NAB228 (0-10-55-120 µL at 2 mg/mL). After incubation, the supernatants were collected. The beads were then washed twice with 500 µL of Tris-Tween 20 (0.05%) solution. The washing solutions were collected for subsequent analyses.

Tosyl-activated magnetic bead

10 µL of Dynabeads MyOne Tosylactivated (100 mg/mL) was added to 2mL LoBind Eppendorf vials and washed with 500µL of 0.1 M sodium borate buffer (pH 9.5) using a Thermomixer for 15 min C at 25°C and 650 rpm. Pre-defined volumes (0-10-55-90-120 µL) of NAB228 solution (2 mg/mL) were added to beads. 60 µL of 3M ammonium sulphate buffer (pH 9.5) and 20 µL of 0.1M sodium borate buffer were then added. The mixtures were then incubated at 37°C on a Thermomixer (650 rpm) for 16h. The supernatants were collected with the help of a magnet. The beads were washed twice with 500 µL of PBS- Tween 20 (0.05%) and once with 500 µL of PBS. The washing solutions were also collected for subsequent analyses by SEC-FLD.

Carboxylated magnetic bead

100 µL of a Dynabeads MyOne carboxylic acid suspension (10 mg / mL) were rinsed twice with 1 mL PBS after removing the suspending solution. 500 µL of EDC solution (10 mg / mL inPBS) and 500 µL of S-NHS solution (10 mg / mL in PBS 1X) were then added into the
washed beads, followed by the addition of NAB228 2 mg/ml (10 µL or 55 µL). The mixture was incubated for 3 hours under 650 rpm at room temperature (RT). The supernatant was collected. The antibody-bound magnetic beads were subsequently washed twice with 1 mL of PBS, followed by an incubation at RT with 1mL of 50 mM Tris-HCl (pH 7.4) for 15 min in order to quench the non-reacted activated carboxylic acid groups. The antibody-bound magnetic beads were then washed 3 times with 1 mL of PBS - 0.1 % Tween-20. A magnet was employed to retain magnetic beads during removal or addition of a suspension solution.

2.3.3. Digestion of NAB228 grafted on magnetic beads by IdeZ

100 µL of enzyme Idez (3 UI) was used for 1 µg NAB228. The enzyme solutions were added directly to grafted and washed magnetic beads and incubated for 3h at 37°C on a Thermomixer at 650 rpm. Further optimization of the enzymatic digestion procedure can be referred to section 3.1.

2.3.4. SEC-FLD conditions

The SEC-FLD analyses of digested samples were conducted on two Agilent columns: BioSEC-3 (3µm particle size, 300 Å, i.d 4,6 mm, length 300 mm) and AdvanceBio SEC (2.7µm particle size, 130 Å pore size, i.d 7.8, length 300 mm). Both columns were equilibrated with the mobile phase for 5 column volumes prior to analysis; and flushed with a mixture of miliQ water (80%) and MeOH (20%) for 15 column volumes after each analysis. The flow rate was fixed at 0,3 ml/min for both columns. For each analysis, 2 µL of sample was injected, and analyzed with the phosphate buffer 50 mM that contains 10 % IPA and 150 mM KCl (pH 6,8).
Calibration curves were made using native NAB228 prepared in different matrices and under different conditions that were used for on-bead antibody grafting protocols. The calibration curve served for the study on Tosyl-activated beads was made with NAB228 (at six concentrations from 0,05 to 0.3 mg/ml) diluted in ammonium sulphate 3 M and sodium borate buffer 0,1 M at pH 9.5 and incubated on Thermomixer at 37°C during 16h. The one used for the study on proG beads was done with NAB228 (6 concentration points) prepared in Tris-Tween 20 (0.05%) and incubated at 25°C for 1h on Thermomixer. The non-grafted condition was used as the reference with six concentrations of native mouse IgG2a prepared in PBS. Three SEC-FLD analyses were implemented for each concentration. The respective calibration curve for each bead type was used to determine the non-grafted NAB228 amount in supernatant and washing solutions. The successfully grafted NAB228 was estimated from the difference between the initial antibody concentration and the recovered ones in the supernatant and washing solutions.

2.3.5. Immunoassay of Aβ 1-42 peptide

A volume of 50 µL Aβ 1-42 was incubated with 200 µg magnetic beads coated with the desired antibodies (12F4, 4G8 or NAB228) and 5 µL 6E10- HRP or 12F4- HRP antibodies at concentration of 0.04 µg/ml in PBS 1X on a mixer at RT for 1 hour. The beads were then washed 3 times (10 min each time on a mixer) with 400 µL PBS 1X/ 0.1 % BSA (m/v)/ 0.1 % Tween- 20 (v/v). Then, 100 µL QuantaRed solution was added to the washed beads. The incubation was carried out over 7 min on shaking, followed by addition of 10 µL QuantaRed Stop solution. The colour intensity of

the achieved solution was measured with the excitation and emission wavelengths of 530 nm and 582 nm, respectively.

2.3.6. MS measurements of Aβ 1-42 peptide

Five lots of Aβ 1-42 peptide stock solution at 2 mg/ml are prepared by balancing and dissolving in corresponding volume of DMSO. The Eppendorfs are vortex gently by hand. Then, the stock solutions are diluted in NH4OH 0.16% to obtain the samples at a concentration of 5 µM. These samples are injected directly into MS to verify the quality of Aβ 1-42.

3. Results and Discussion

3.1. Enzymatic digestion of grafted antibodies and analysis of released fragments

Our approach (see Fig.1) to characterize the performance of on-bead antibody grafting relies on the selective enzymatic digestion of the grafted antibody below the hinge position to release F(ab)2 and Fc fragments. The analysis of the remaining antibody as well as these released fragments, which are typical for an antibody, can then provide insight in the density and the orientation of the grafted antibodies thanks to the ratio of $F(ab)_2$'s signal to Fc one.

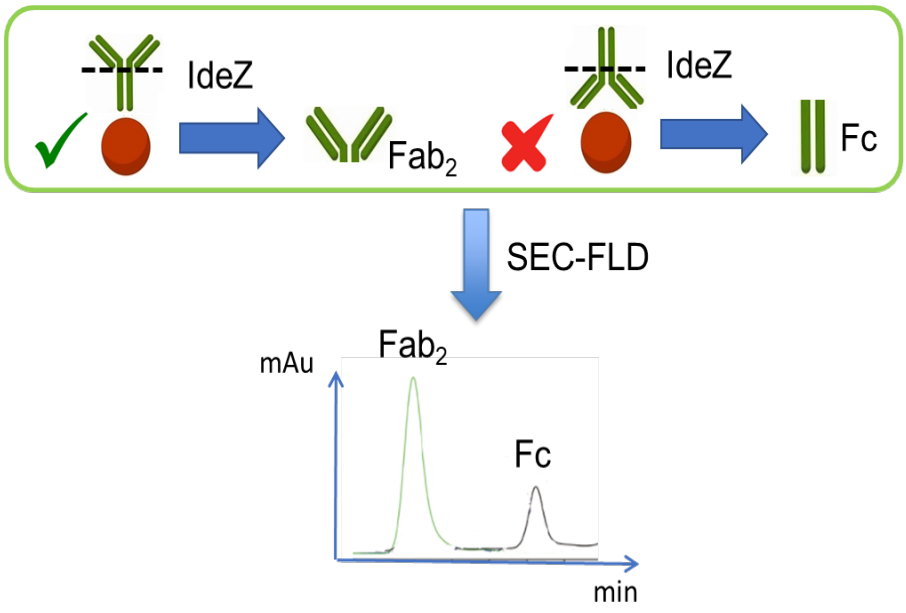

Fig. 1. Proposed strategy for characterization of density and orientation of antibodies grafted on magnetic beads.

Unlike chemically mediated or trypsin-based methods, our approach is softer and more selective, and can provide both information on antibody density and orientation. The challenges here were to find an appropriate enzyme that works on the target mouse antibodies and develop the subsequent separation strategy for determination of the resulting fragments.

In our case, SEC which is frequently used for separation of proteins and peptides was chosen for analysis of $F(ab)_2$ and Fc fragments. The obtained $F(ab)_2$ and Fc fragments and residue IgG possess respective molecular weights of about 100, 50 and 150 kDa. Phase mobile optimization was first carried out to separate these target fragments from the residual antibodies in the solution (Fig. 2). Among two salts commonly used in SEC buffers, KCl offered more symmetric and less tailing peaks than NaCl. Indeed, KCl was found stronger than NaCl in suppression of the secondary interaction between target molecules and the stationary phase, probably due to the larger size and higher interactivity of K+ cation [7]. It was observed from Fig 2 C-D vs Fig. 2 A-B that the column of a smaller pore size (130 Å) provides better resolution for separation of F(ab)2 and Fc.

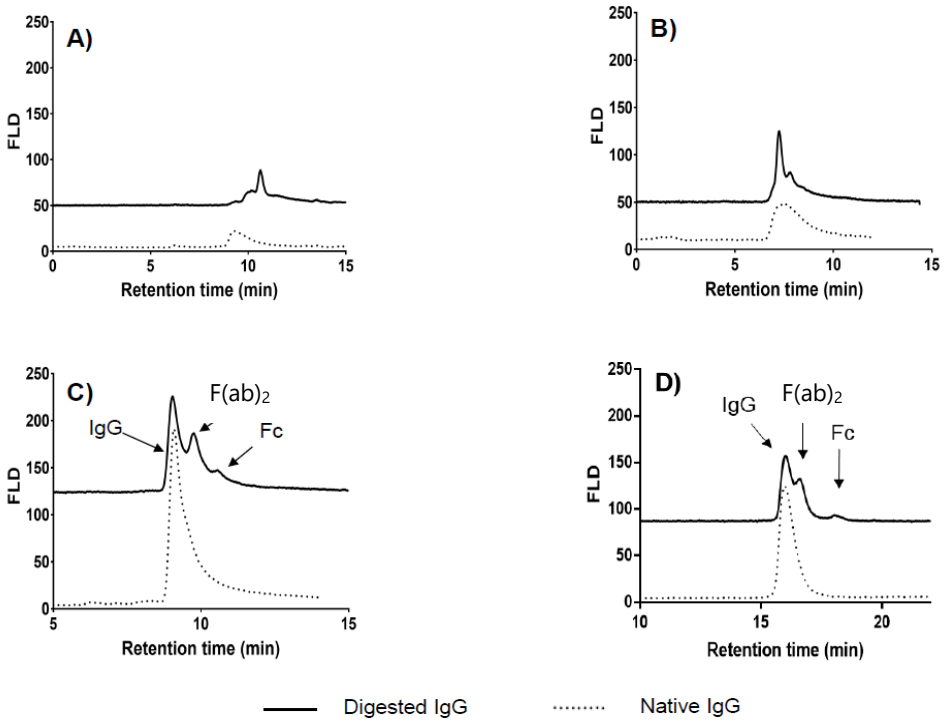

Fig. 2. Analysis of IdeZ-digested NAB228 by SEC-FLD using a column having dimensions of 4.6 x 300mm, particle size of 3µm; pore size of 300 Å and the phosphate buffer containing A) 150 mM NaCl C) 150 mM KCl or a column having dimensions of 7.8 x 300mm, particle size of 2.7µm, pore size of 130 Å and the phosphate buffer containing B) 150 mM NaCl and D) 150 mM KCl.

Moreover, thanks to these optimized conditions, the peak of IdeZ enzyme was well separated from the Fc fragment (see Figs. 3 and 4), which was not the case in the previous work using IdeS [5]. This would help avoid the bias in quantification of the digested fragments.

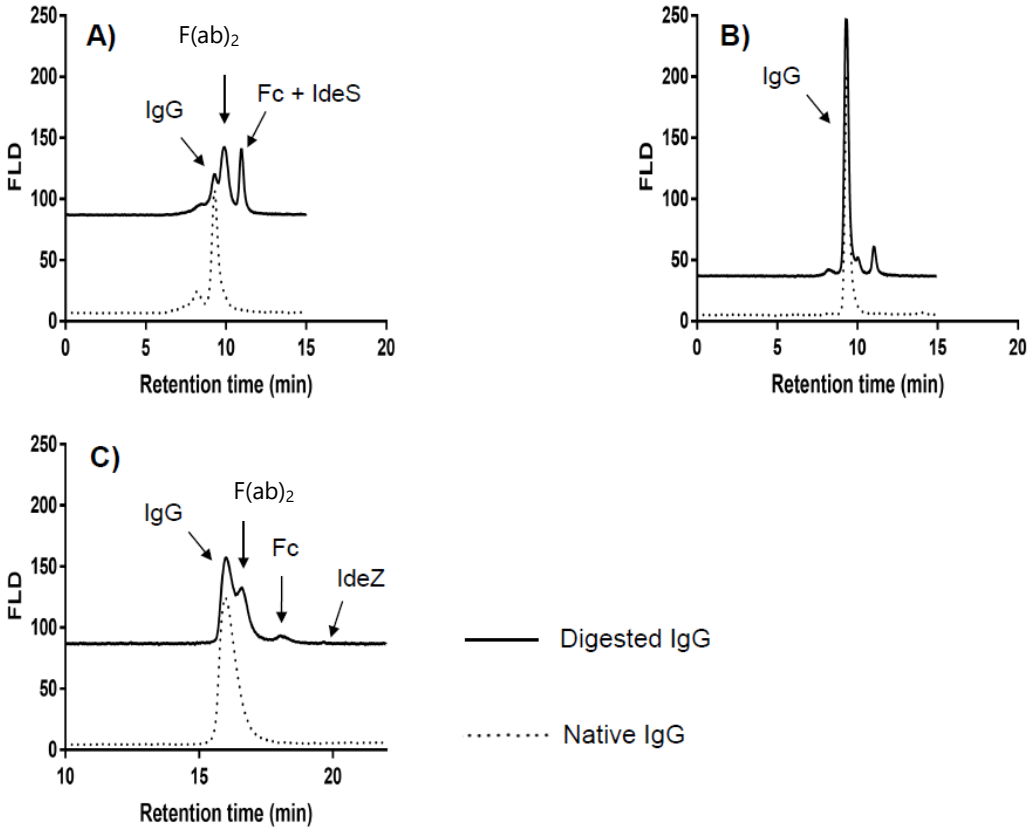

Fig. 3. Digestion of 0,1 mg/ml antibodies in PBS: A) human IgG by IdeS; B) Mouse IgG1 (6E10) by IdeS; C) Mouse IgG2a (NAB228) by IdeZ. SEC-FLD conditions: column having dimensions of 7.8 x 300mm, particle size of 2.7µm, pore size of 130Å and the phosphate buffer containing 150 mM KCl.

The optimized SEC-FLD conditions were then used to monitor the IgG digestion optimization. FabRICATOR IdeS, which was found to offer fast reaction on hIgG, and was found to work well in our previous work on hIgG [5] was tested as the reference. By comparing the peak of IgG before and after digestion in Figs. 3A-B, one can see that almost 80% of hIgG was digested with IdeS without optimization, whereas only 10% of mouse IgG1 could be digested under the same conditions. Indeed, IdeS can digest only on antibodies having CPPCPAPELLG/GPSVF sequence at hinge position that are typical for human, rabbit and sheep IgG. This enzyme nevertheless is less

favorable for mouse IgG, which represents the majority of antibodies commercially available for bioanalysis and is the most widely used one for immunoassays of Aβ peptides. To overcoming this problem, FabRICATOR Z IdeZ was selected for mouse IgG. This kind of enzyme shows its specificity on mouse IgG_{2a} or IgG_3, having CPAPNLLG/ GPSVF sequence at the hinge site. As can be seen in Fig 3C, more than 60% of NAB228 antibody (mouse IgG_{2a} type) was digested in the first trial, which provided encouraging results. IdeZ enzyme was therefore chosen for further optimization of mouse IgG_{2a} digestion. A two-level-three-factors (3^2) ½ fraction experiment was designed to optimize the digestion protocol using Minitab statistical software 17. The three factors covered (i) enzyme unit for 1µg IgG digestion (1 - 3 UI), (ii) incubation time (2 to 4 hour) and (iii) temperature (low 30°C and high 44°C). The response to be evaluated was the digestion efficiency estimated via $F(ab)_2$: Fc peak-area-ratio. A Pareto chart was used to determine the optimal conditions for complete digestion of IgG while using the lowest enzyme unit as possible. Among the investigated factors, the one with the highest impact was found for the added enzyme unit. As can be seen from Fig. 4, with 3 U of enzyme IdeZ for 1 µg IgG (in an incubation over 3 hours at RT), a quasi-complete digestion (98%) of IgG in solution, calculated according to peak areas of initial IgG and residual one after digestion, could be achieved. Compared to the digestion performance obtained with the commercial protocol for IdeZ (see Figs. 2 C-D where there was much residual IgG after the digestion), that achieved with our optimized conditions is superior with almost no trace of IgG left (Fig. 4).

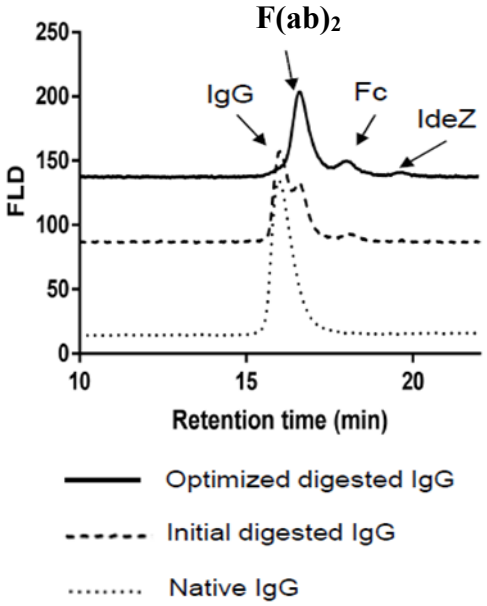

Fig. 4. Digestion of NAB228 antibodies (0.1 mg/ml IgG2a) in PBS by IdeZ under different digestion conditions. SEC-FLD conditions as in Fig. 3.

3.2. Optimization of the density and orientation of antibodies grafted on magnetic beads

The optimized digestion conditions (i.e., incubation with 3 UI IdeZ over 3h at 37°C) and the optimized SEC-FLD ones (i.e., column of 130 Å pore-size, phosphate buffer containing 150 mM KCl) were employed to release and determine the F(ab)2 and Fc fragments from on-bead grafted NAB228 antibody (mouse IgG). Quantification of grafted NAB228 was made with following the formula (1), respectively:

$$m_{grafted} = m_{initial} - (m_{supernatant} + m_{washing}) \qquad (1)$$

where

minitial, mgrafted, msupernatnant and mwashing are the initial quantity of antibodies, the quantity of antibodies grafted on 1000 µg beads, and those of remaining antibodies in the supernatant and washing solutions, respectively.

The peak ratios for $F(ab)_2$/Fc fragments released from NAB228 antibodies grafted on Tosyl-activated, ProG and carboxylated magnetic beads were determined and compared (Fig. 5).

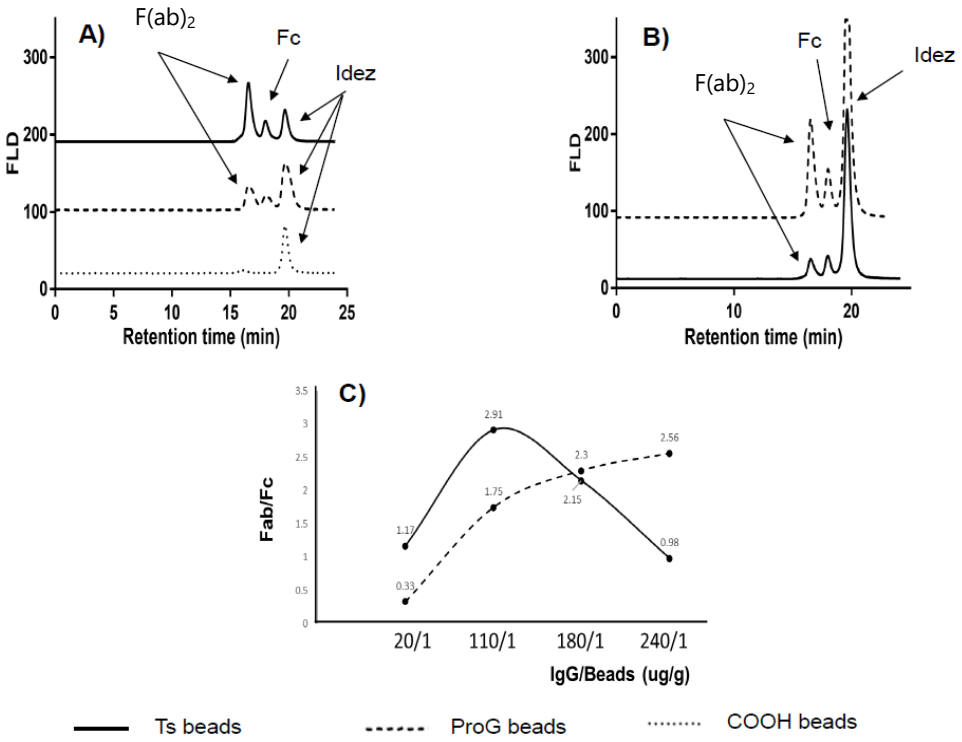

Fig. 5. Digestion of NAB228 antibodies grafted on different magnetic beads (i.e., carboxylated, tosylactivated, protein G using IgG / beads (µg / mg) ratio of A) 110: 1; B) 240:1. C) Dependence of $F(ab)_2$: Fc peak ratios on IgG quantity for on-bead grafting. SEC-FLD conditions as in Fig. 3

With the same quantity of antibodies available for grafting, proG and tosyl-activated beads allowed higher amount of grafted NAB228, whereas very little trace of grafted antibodies could be found with carboxylated ones. As shown in Fig 5A and B, proG and tosyl-activated beads would require different initial antibody amount to achieve the best $F(ab)_2$ / Fc ratio. The best grafted antibody density and orientation was achieved with 110 µg antibodies per 1 mg bead for tosyl-activated beads (at $F(ab)_2$ / Fc of 2.9), whereas for proG beads the best $F(ab)_2$ / Fc ratio of 2.5 was achieved at a higher quantity of 240 µg antibodies per 1 mg beads (Fig. 5C). This can be explained by the fact that tosyl-activated beads with a covalent group (H3CC6H4SO2) has more affinity to Fc fragment. Note that further addition of antibodies led to less grafting performance on tosyl-activated beads (Fig. 5C), probably due the abundant presence of PBS used for antibody suspension, which is the blocking solution and not favorable for tosylated groups on magnetic beads, according to the instructions in the commercial protocol. In the case of proG, at low IgG quantity (< 50 µg), the non-covalent linkage is more effective towards $F(ab)_2$, leading to less-oriented antibody grafting (with decreased $F(ab)_2$ / Fc peak ratio). At higher IgG quantity, the tendency was reversed, leading to an improved in $F(ab)_2$ / Fc peak ratio for ProG beads. This important observation indicates that different magnetic beads would require different antibody quantities to reach the maximum density and best orientation. Under our best grafting conditions, 74.4 % of antibodies grafted on tosyl-activated beads were at the right orientation, calculated from the ($F(ab)_2$ / (Fc + $F(ab)_2$) peak ratio. This was 71.9 % for the case of ProG beads. The grafting orientation under our conditions was equivalent to the best one obtained in the previous work (73.8 % for ProG beads and 31.3 % for tosyl-activated ones, respectively) [5]. Using the formula (1), the maximum grafted quantity of NAB228 antibodies on ProG and tosyl-activated beads were estimated to be 43 µg and 35 µg per 1000 µg beads, respectively. Note that different conditions (i.e., the matrices, the temperatures and incubation times) were used for grafting antibodies on different beads. To avoid the bias in quantification of grafted antibodies, different calibration curves were made for different bead types, using NAB228 prepared in respective grafting matrices (see Fig. S1 in the supporting information ESI).

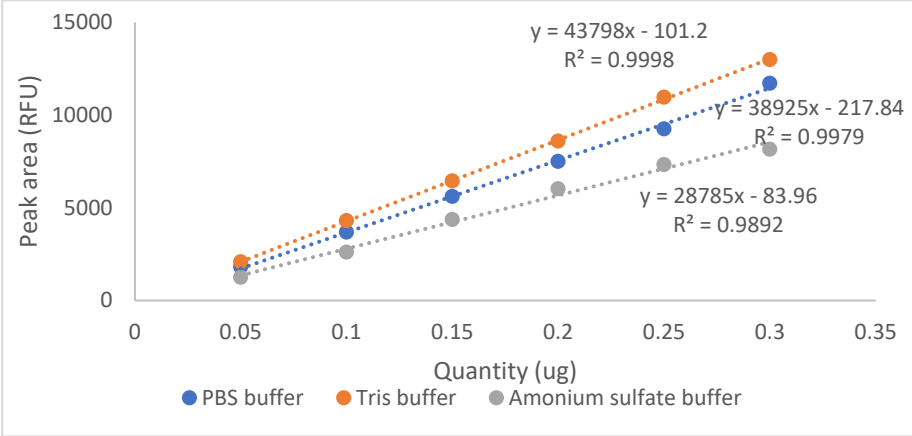

Fig.S1. The calibration curve of NAB228 under different grafting conditions .
Conditions 1: PBS buffer
Condition 2: Tris-Tween 20 (0.05%) buffer and incubated at 25°C for 1h on Thermomixer
Condition 3: Ammonium sulphate 3 M and sodium borate buffer 0,1 M at pH 9.5 and incubated on Thermomixer at 37 °C during 16h

Note also that the peak of IdeZ were observed together with those of $F(ab)_2$ and Fc fragments after the digestion (Fig. 5). The peaks of IdeZ in the supernatants after incubation with different beads were lower than that of IdeZ in the initial one, which was due to some absorption of IdeZ on to ProG and tosyl-activated beads during the incubation for digestion of grafted IgG, as demonstrated in Fig. S2 in the ESI. The peak of residual IdeZ could induce some interference to the peaks of target F(ab)2 and Fc, and therefore confirm again the need to have an improved SEC-FLD method in our case to separated IdeZ from the target fragments.

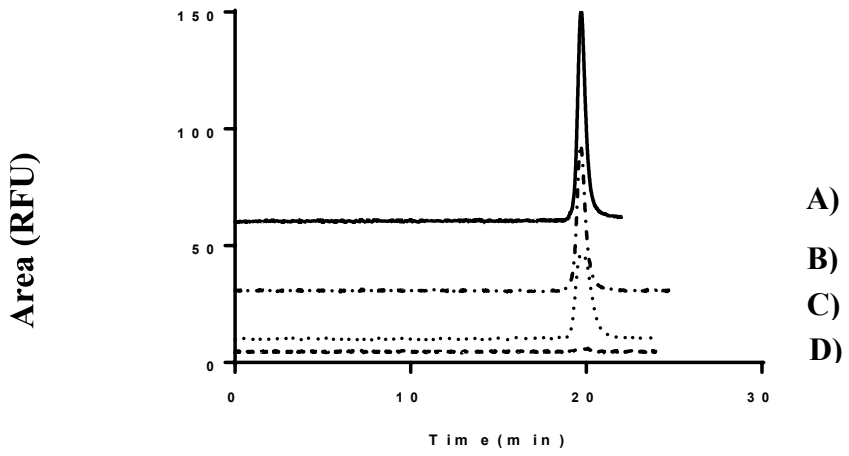

Fig.S2. Chromatograms of (A) initial solution of IdeZ enzyme at 80UI and the supernatant of Idez enzyme after incubation 3 hours at 37°C on a Thermomixer at 650 rpm with magnetic beads functionalized with B) carboxylic group; C) Protein G; D) Tosyl-activated.

3.3. Immunoassays of Aβ 1-42 on functionalized magnetic beads

To validate the aforementioned optimization, the tosyl-activated and proG beads grafted with NAB228 (an anti Aβ 1-42 antibody specific at N-terminal of this peptide) at their optimal concentrations were employed to carry out immunoassays of Aβ 1-42 (Fig. 6).

A)

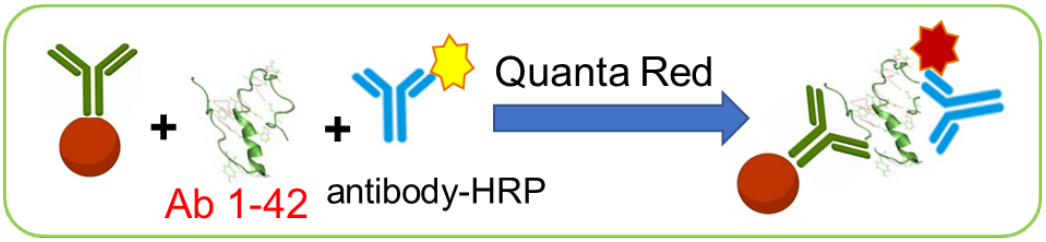

B)

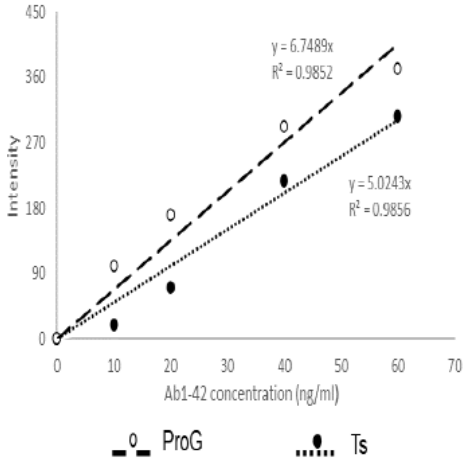

Fig. 6. A) Schematic of the immunocapture of Aβ 1-42 on different magnetic beads grafted with NAB288. Detection was carried out using ELISA with 12F4 HRP as the detection antibody. See section 2.3 for ELISA protocol. B) Calibration curves for Aβ 1-42 made with NAB288 grafted on ProG and Tosylactivated beads.

Since Aβ 1-42 peptide is prone to aggregation [6], the good quality of each batch was first confirmed with MS (see Fig. S3 in the ESI). Aβ 1-42 solutions were prepared freshly from the confirmed batch just before each immunoassay series. Detection in this case was made with another anti Aβ 1-42 antibody specific at C-terminal of this peptide, which is bound with HRP to trigger

subsequently the enzymatic reaction with Quanta Red substrate (Fig. 6A). NAB228 grafted on ProG showed higher signals than those obtained with tosyl-activated beads (Fig. 6B). Further results on the immunoassays of Aβ 1-42 can be seen in Fig. S4 in the ESI. This observation was in good accordance with the results indicating that more antibodies were grafted on ProG beads than on tosyl-activated ones, with equivalent antibody grafting orientation (see section 3.2 above).

A)

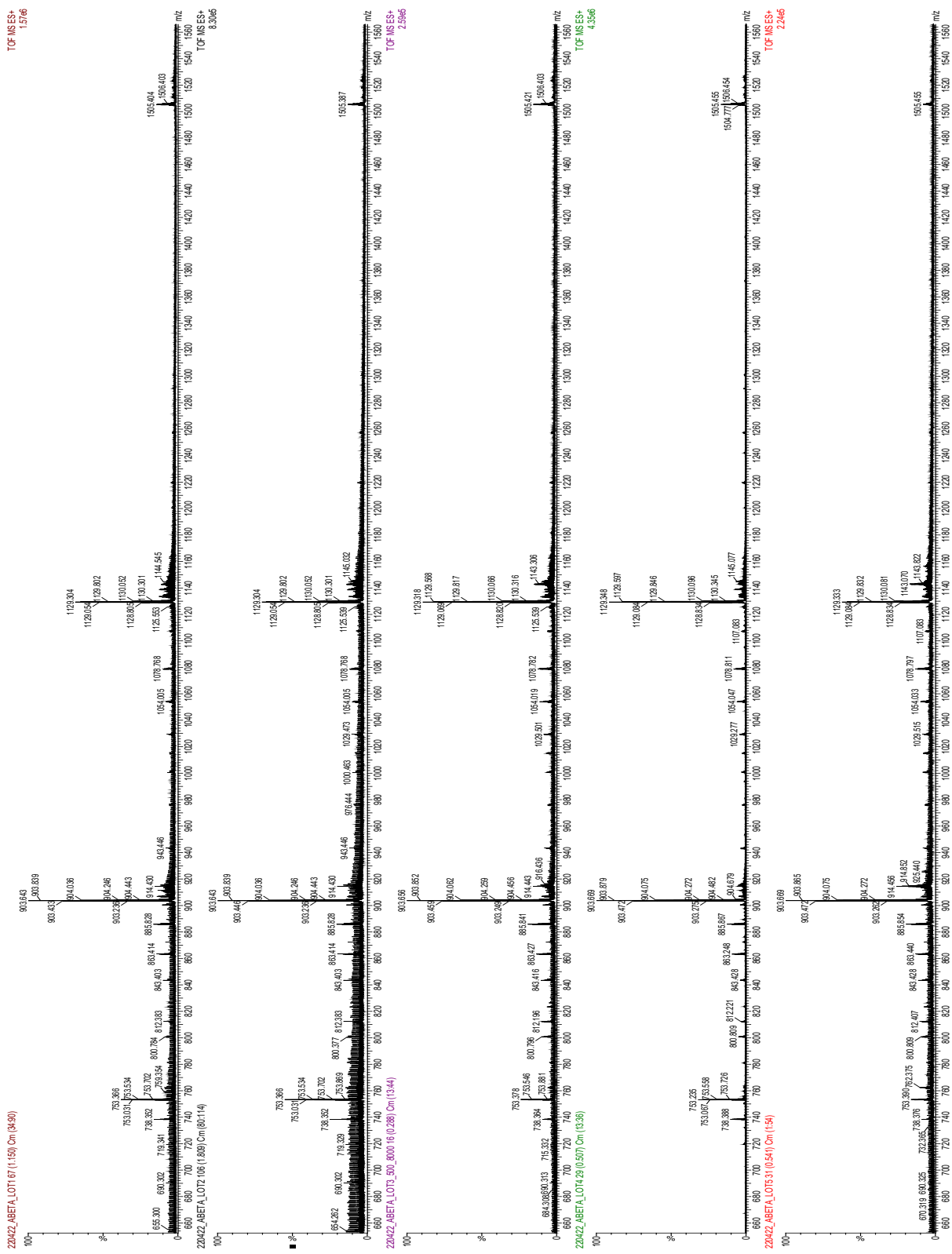
220422_ABETA_LOT1 67 (1.150) Cm (34:90)
TOF MS ES+
1.57e6
220422_ABETA_LOT2 106 (1.809) Cm (80:114)
TOF MS ES+
8.30e5
220422_ABETA_LOT3_500_8000 16 (0.288) Cm (13:44)
TOF MS ES+
2.59e5
220422_ABETA_LOT4 29 (0.507) Cm (13:36)
TOF MS ES+
4.35e6
220422_ABETA_LOT5 31 (0.541) Cm (1:54)
TOF MS ES+
2.24e5
m/z

B)

	m/z				
lot	CS 3	CS 4	CS 5	CS 6	Mwav
1	1505,4	1129,3	903,6	753,36	
MW 1	4513,2	4513,2	4513	4514,16	4513,39
2	1505,4	1129,3	903,6	753,36	
MW 2	4513,2	4513,2	4513	4514,16	4513,39
3	1505,4	1129,3	903,6	753,36	
MW3	4513,2	4513,2	4513	4514,16	4513,39
4	1505,4	1129,3	903,6	753,36	
MW4	4513,2	4513,2	4513	4514,16	4513,39
5	1505,4	1129,3	903,6	753,36	
MW5	4513,2	4513,2	4513	4514,16	4513,39

Fig. S3. A) Mass spectrometry of five lots of Aβ 1-42 5μM dilluted in NH_4OH 0.16%, injected directly to MS. B) Determination of molecular weigth of Aβ 1-42 based on m/z of these ionized fragments.

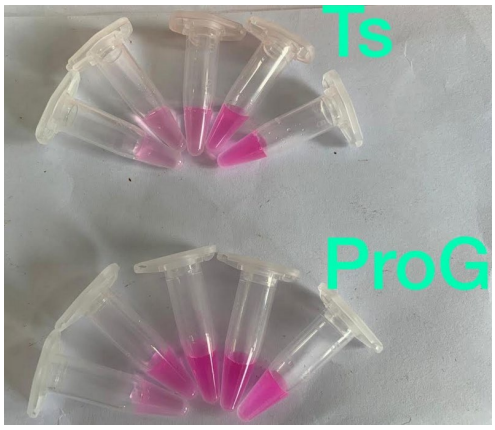

Fig. S4. The picture of the supernatant of Aβ 1-42 peptide, captured by NAB228 immobilized on Tosyl-activated and Protein G magnetic beads and 12F4-HRP as a secondary antibody for 1 hour prior to the ddition of QuantaRed solution and the incubation for 7 minutes. The intensity of fluorescence was measured by FP-750 Spectrofluoromete with the excitation and emission wavelengths of 530 nm and 582 nm respectively.

Employing the antibody / bead ratios optimized for NAB228, the test on immunocapture of Aβ 1-42 was also extended to other antibodies specific to this peptide, i.e., 12F4 specific to N-terminal and 4G8 specific to 17-24 epitopes (Fig. S5 in the ESI). An antibody specific to N-terminal of Aβ 1-42 (6E10-HRP) was employed in this case for detection of the captured peptide. Among three capture antibodies, NAB228 exhibited the best on-bead capture performance, regardless of the bead

type used (tosyl-activated or ProG). The signals obtained with 12F4 and 4G8 were relatively low for both types of beads. The limit of detection was 10 mg/ml for NAB228 and 20 mg/ml for other antibodies. This implies that for each antibody, re-optimization of the antibody : bead ratio would be needed. And the optimal ratio achieved for 1 specific antibody (NAB228 in our case) cannot be generic to other ones. This remark is important, because so far one tends to follow the same antibody : bead ratio according to the established grafting protocol for different antibodies, which may lead to non-optimal immunocapture performance.

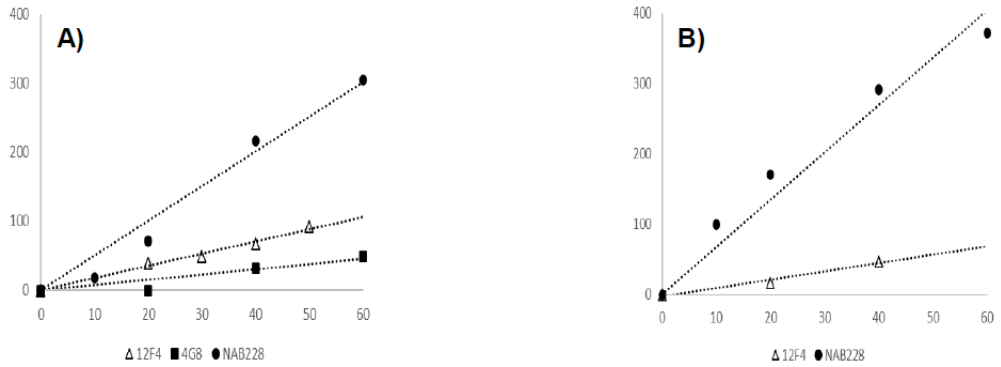

Fig. S5. Performance of Aβ 1-42 immunocapture on magnetic beads grafted with different antibodies (NAB228, 12F4 and 4G8) specific to Aβ 1-42. A) Immunocapture with tosyl-activated beads; B) Immunocapture with ProG beads.

4. Conclusions

We developed successfully an enzyme-based approach for evaluation at same time the density and orientation of mouse IgG_{2a} immobilized on three different magnetic beads. Using this approach to follow the optimization of antibody grafting conditions, more than 70 % of antibodies could be grafted on tosyl-activated and protein G beads in the right orientation. The developed method was applied for monitoring the density and orientation of anti- Aβ 1-42 antibodies on different magnetic bead supports, serving for immunoassays of this amyloid-beta peptide. The antibody NAB228 grafted on ProG beads exhibited the best performance. The strategy using IdeZ enzyme to check the density and orientation of mouse antibodies on magnetic beads provides us a powerful tool for optimization and improvement of the performance of immunocapture and immunoassays of target biomolecules on magnetic beads. Other applications targeting different biomarkers using this enzyme-based method are envisaged to further demonstrate the significance of our work.

Acknowledgement

This work has been financially supported by the ‘bourse d’excellence de l’ambassade de France’ (for PhD scholarship of N.V.T. Nguyen).

References of PAPER 1

[1] C. Comanescu, Magnetic Nanoparticles: Current Advances in Nanomedicine, Drug Delivery and MRI, Chemistry-Switzerland, 4 (2022) 872-930.
[2] C. Susy Piovesana and Anna Laura, Magnetic Materials for the Selective Analysis of Peptide and Protein Biomarkers, Curr. Med. Chem., 24 (2017) 438-453.
[3] B. Moreira-Alvarez, L. Cid-Barrio, H.S. Ferreira, J.M. Costa-Fernández, J. Encinar, Integrated analytical platforms for the comprehensive characterization of bioconjugated inorganic nanomaterials aiming at biological applications, Journal of Analytical Atomic Spectrometry, 35 (2020) 1518-1529.
[4] R. Oliverio, B. Liberelle, F. Murschel, A. Garcia-Ac, X. Banquy, G. De Crescenzo, Versatile and High-Throughput Strategy for the Quantification of Proteins Bound to Nanoparticles, ACS Applied Nano Materials, 3 (2020) 10497-10507.
[5] E. Laborie, V. Le-Minh, T.D. Mai, M. Ammar, M. Taverna, C. Smadja, Analytical methods of antibody surface coverage and orientation on bio-functionalized magnetic beads: application to immunocapture of TNF-α, Anal. Bioanal. Chem., 413 (2021) 6425-6434.
[6] N. Van Thanh Nguyen, M. Taverna, C. Smadja, T.D. Mai, Recent Electrokinetic and Microfluidic Strategies for Detection of Amyloid Beta Peptide Biomarkers: Towards Molecular Diagnosis of Alzheimer's Disease, Chem. Record, 21 (2021) 149-161.
[7] B.L. Duivelshof, S. Fekete, D. Guillarme, V. D'Atri, A generic workflow for the characterization of therapeutic monoclonal antibodies—application to daratumumab, Anal. Bioanal. Chem., 411 (2019) 4615-4627.

Electronic supplementary data

Immuno-capture of biomolecules on functionalized magnetic beads: from characterization to application for a biomarker of Alzheimer's disease

Ngoc Van Thanh Nguyen[1], Claire Smadja[1*], Myriam Taverna[1,2], Frédéric Halgand[3], Thanh Duc Mai [1*]

[1] *Université Paris-Saclay, CNRS, Institut Galien Paris-Saclay, 91400, Orsay, France.*

[2] *Institut Universitaire de France (IUF)*

[3] *Université Paris Saclay-CNRS, Laboratoire de Chimie Physique, Orsay, France*

Correspondence: E-mail: claire.smadja@u-psud.fr; Fax: +33-1-46-83-55-51

thanh-duc.mai@u-psud.fr

Keywords: magnetic beads, density and orientation, antibody anti-amyloid beta, size exclusion chromatography, enzyme digestion, IdeZ.

Fig.S1. The calibration curve of NAB228 under different grafting conditions .

Conditions 1: PBS buffer

Condition 2: Tris-Tween 20 (0.05%) buffer and incubated at 25°C for 1h on Thermomixer

Condition 3: Ammonium sulphate 3 M and sodium borate buffer 0,1 M at pH 9.5 and incubated on Thermomixer at 37°C during 16h

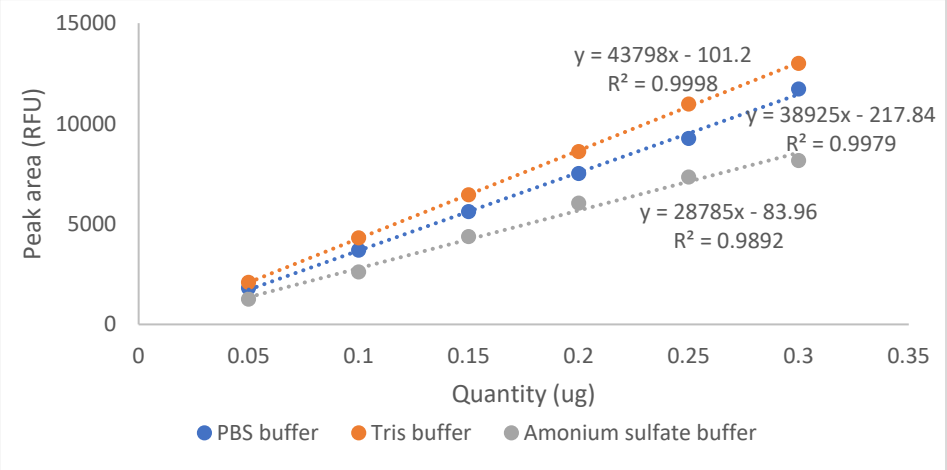

Fig.S2. Chromatograms of (A) initial solution of IdeZ enzyme at 80UI and the supernatant of Idez enzyme after incubation 3 hours at 37°C on a Thermomixer at 650 rpm with magnetic beads functionalized with B) carboxylic group; C) Protein G; D) Tosyl-activated.

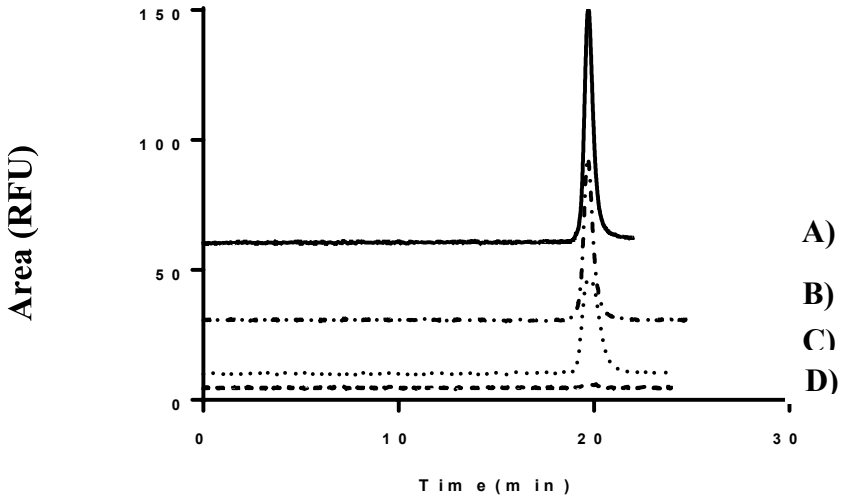

Fig. S3. A) Mass spectrometry of five lots of Aβ 1-42 5µM dilluted in NH_4OH 0.16%, injected directly to MS. B) Determination of molecular weigth of Aβ 1-42 based on m/z of these ionized fragments.

A)

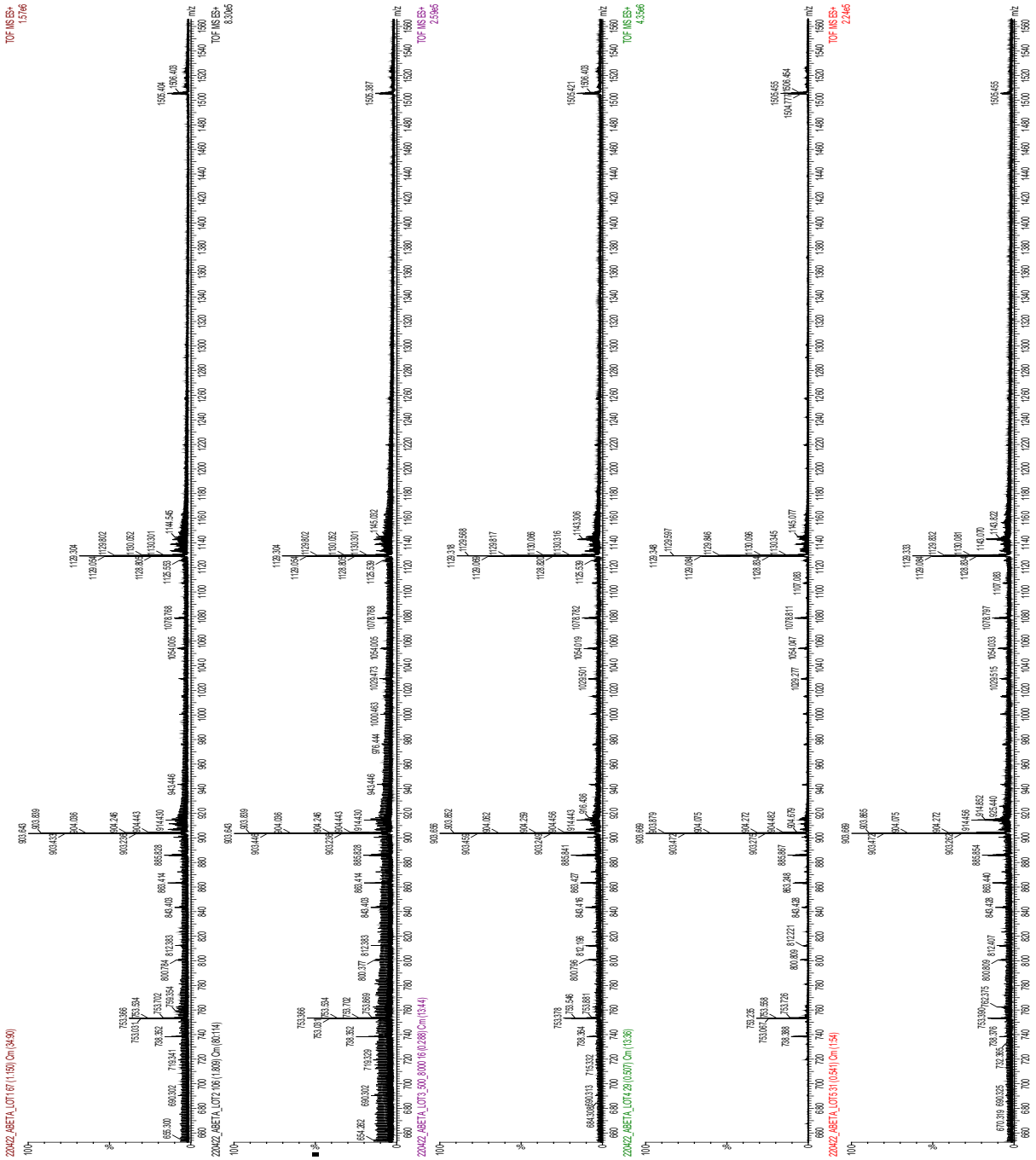

B)

	m/z				
lot	CS 3	CS 4	CS 5	CS 6	Mwav
1	1505,4	1129,3	903,6	753,36	
MW 1	4513,2	4513,2	4513	4514,16	4513,39
2	1505,4	1129,3	903,6	753,36	
MW 2	4513,2	4513,2	4513	4514,16	4513,39
3	1505,4	1129,3	903,6	753,36	
MW3	4513,2	4513,2	4513	4514,16	4513,39
4	1505,4	1129,3	903,6	753,36	
MW4	4513,2	4513,2	4513	4514,16	4513,39
5	1505,4	1129,3	903,6	753,36	
MW5	4513,2	4513,2	4513	4514,16	4513,39

Fig. S4. The picture of the supernatant of Aβ 1-42 peptide, captured by NAB228 immobilized on Tosyl-activated and Protein G magnetic beads and 12F4-HRP as a secondary antibody for 1 hour prior to the ddition of QuantaRed solution and the incubation for 7 minutes. The intensity of fluorescence was measured by FP-750 Spectrofluoromete with the excitation and emission wavelengths of 530 nm and 582 nm respectively.

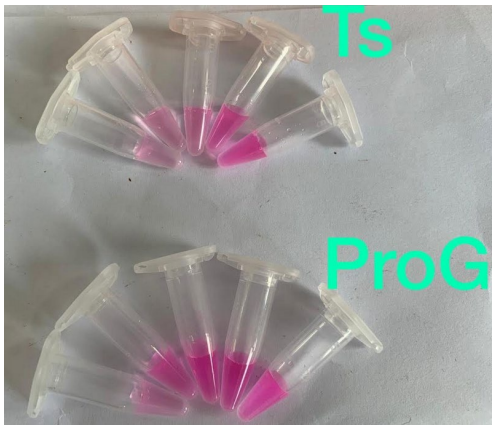

Fig. S5. Performance of Aβ 1-42 immunocapture on magnetic beads grafted with different antibodies (NAB228, 12F4 and 4G8) specific to Aβ 1-42. A) Immunocapture with tosyl-activated beads; B) Immunocapture with ProG beads

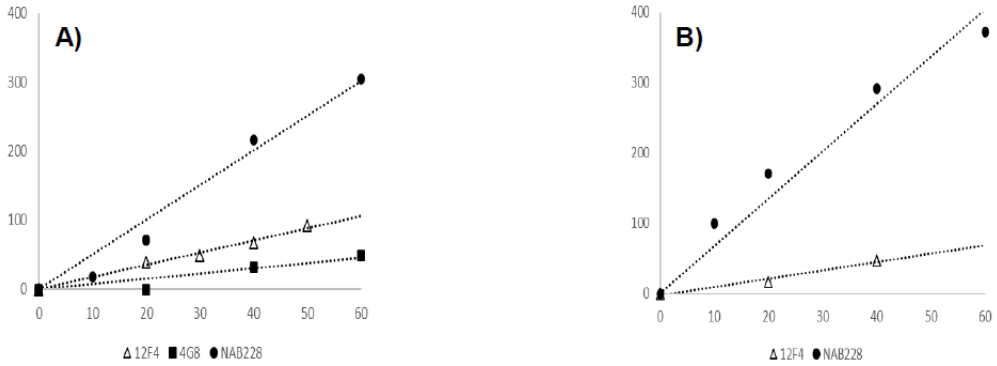

Fig. S6. Chromatograms of A) Diferent density of NAB228 immobilized on 1000 µg ProG beads and B) Different density of NAB228 immobilized on 1000 µg Ts beads (µg/µg). Conditions are described in Fig. S1.

A)

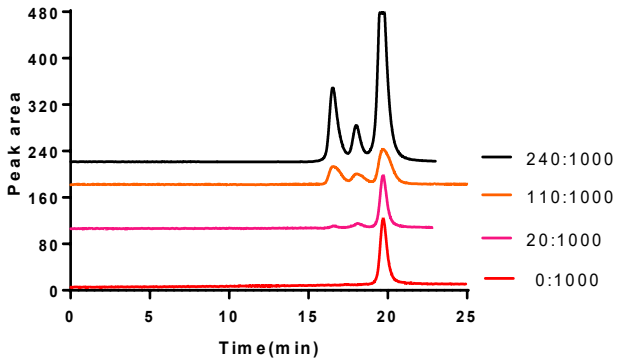

B)

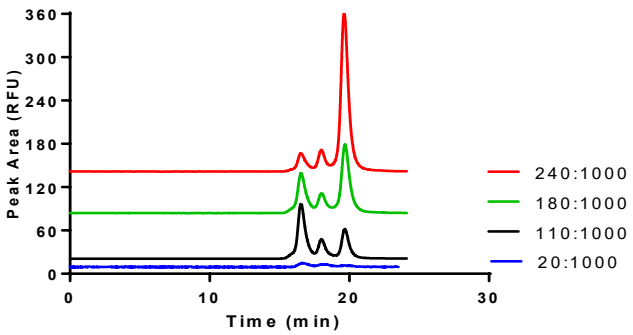

3.3 CONCLUSIONS

We successfully developed an enzymatic strategy combined with the SEC-FLD method for characterizing anti-Aβ antibody immobilized on three types of magnetic beads regarding their density and orientation. The beads grafted with antibodies were employed for immunoassays of this amyloid-beta peptide. Protein G beads showed the most effective in grafting with NAB228 antibody. This opens the perspective for targeting more biomolecules by using magneto-(immune)-extraction and enzyme-based methods.

References of chapter 3

1. Serra, M., et al., *The power of solid supports in multiphase and droplet-based microfluidics: towards clinical applications.* Lab on a Chip, 2017. **17**(23): p. 3979-3999.
2. Moreira-Alvarez, B., et al., *Integrated analytical platforms for the comprehensive characterization of bioconjugated inorganic nanomaterials aiming at biological applications.* Journal of Analytical Atomic Spectrometry, 2020. **35**: p. 1518-1529.
3. Barth, H.G., *The Early Development of Size-Exclusion Chromatography: A Historical Perspective.* LCGC North America, 2013. **31**(7): p. 550–558.
4. Ludwig, N., et al., *Isolation and Analysis of Tumor-Derived Exosomes.* Current Protocols in Immunology, 2019. **127**(1): p. e91.
5. Arakawa, T., et al., *The critical role of mobile phase composition in size exclusion chromatography of protein pharmaceuticals.* J Pharm Sci, 2010. **99**(4): p. 1674-92.
6. Laborie, E., et al., *Analytical methods of antibody surface coverage and orientation on bio-functionalized magnetic beads: application to immunocapture of TNF-α.* Analytical and Bioanalytical Chemistry, 2021. **413**: p. 1-10.
7. Hong, P., S. Koza, and E.S. Bouvier, *Size-Exclusion Chromatography for the Analysis of Protein Biotherapeutics and their Aggregates.* J Liq Chromatogr Relat Technol, 2012. **35**(20): p. 2923-2950.
8. Folta-Stogniew, E., *Characterization of Protein-Nucleic Acid Complexes by Size-Exclusion Chromatography Coupled with Light Scattering, Absorbance, and Refractive Index Detectors.* Methods Mol Biol, 2021. **2263**: p. 381-395.
9. Lederer, A. and J. Brandt, *Chapter 2 - Multidetector size exclusion chromatography of polymers*, in *Molecular Characterization of Polymers*, M.I. Malik, J. Mays, and M.R. Shah, Editors. 2021, Elsevier. p. 61-96.
10. Hage, D.S., *1 - Chromatography*, in *Principles and Applications of Clinical Mass Spectrometry*, N. Rifai, A.R. Horvath, and C.T. Wittwer, Editors. 2018, Elsevier. p. 1-32.
11. Ziegler, A. and J. Zaia, *Size-exclusion chromatography of heparin oligosaccharides at high and low pressure.* J Chromatogr B Analyt Technol Biomed Life Sci, 2006. **837**(1-2): p. 76-86.
12. Qian, J., et al., *Development of a high performance size exclusion chromatography method to determine the stability of Human Serum Albumin in a lyophilized formulation of Interferon alfa-2b.* J Chromatogr A, 2008. **1194**(1): p. 48-56.
13. Diress, A., et al., *Study of aggregation, denaturation and reduction of interferon alpha-2 products by size-exclusion high-performance liquid chromatography with fluorescence detection and biological assays.* J Chromatogr A, 2010. **1217**(19): p. 3297-306.
14. Anurag S. Rathore, S.M., Vivek Halan, Ira S. Krull, *Fluorescence-Detection Size-Exclusion Chromatography — An Analytical Technique with Multiple Applications.* LCGC Europe, 2014. **28**(2): p. 118-121.
15. Gunturi, S.R., I. Ghobrial, and B. Sharma, *Development of a sensitive size exclusion HPLC method with fluorescence detection for the quantitation of recombinant human erythropoietin (r-HuEPO) aggregates.* J Pharm Biomed Anal, 2007. **43**(1): p. 213-21.
16. Some, D., et al., *Characterization of Proteins by Size-Exclusion Chromatography Coupled to Multi-Angle Light Scattering (SEC-MALS).* J Vis Exp, 2019(148).
17. Challener, C.A., *Analyzing Proteins Using SEC, MALS, and UHPLC.* BioPharm International, July 1, 2014. **27**(7).
18. Wen, J., T. Arakawa, and J.S. Philo, *Size-exclusion chromatography with on-line light-scattering, absorbance, and refractive index detectors for studying proteins and their interactions.* Anal Biochem, 1996. **240**(2): p. 155-66.
19. Sahin, E. and C.J. Roberts, *Size-exclusion chromatography with multi-angle light scattering for elucidating protein aggregation mechanisms.* Methods Mol Biol, 2012. **899**: p. 403-23.
20. Le-Minh, V., et al., *Conformation assessment of therapeutic monoclonal antibodies by SEC-MS: Unravelling analytical biases for application to quality control.* Journal of Pharmaceutical and Biomedical Analysis, 2020. **185**: p. 113252.

21. Ren, C., et al., *Quantitative Determination of Protein–Ligand Affinity by Size Exclusion Chromatography Directly Coupled to High-Resolution Native Mass Spectrometry.* Analytical Chemistry, 2019. **91**(1): p. 903-911.
22. Goyon, A., et al., *Characterization of 30 therapeutic antibodies and related products by size exclusion chromatography: Feasibility assessment for future mass spectrometry hyphenation.* Journal of Chromatography B, 2017. **1065-1066**: p. 35-43.
23. Haberger, M., et al., *Rapid characterization of biotherapeutic proteins by size-exclusion chromatography coupled to native mass spectrometry.* MAbs, 2016. **8**(2): p. 331-9.

Chapter 4: ELECTROKINETIC PRECONCENTRATION IN CE FOR MNPS DETECTION AND INTERACTION MONITORING

As already mentioned in chapter 2, EOF suppression is in many cases needed to improve the CE preconcentration and separation performance. In this chapter, I present the development of a new method for EOF modulation and suppression for CE-LIF, relying on the use of BGEs composed of large weakly charged compounds. As these species are slowly migrating ones, we could increase their ionic strengths (IS, and thus concentrations) to a very high level to suppress EOF without introducing too much current as encountered with conventional inorganic buffers for CE. An online preconcentration approach, relying on the modulation and suppression of EOF via IS increase, was then developed. The first application of this approach was for i) detection of fluorescent MNPs (30 nm diameter) functionalized with carboxylic groups, which were synthesized by our partner from the group of Physico-chimie des Electrolytes et Nanosystemes Interfaciaux (PHENIX, Sorbonne University), and ii) monitoring their interaction with aminoglycoside antibiotics, serving for drug delivery purpose. The work was also extended for Aβ 1-42 preconcentration.

4.1 ELECTROOSMOTIC FLOW MODULATION FOR IMPROVED ELECTROKINETIC PRECONCENTRATION: APPLICATION TO CAPILLARY ELECTROPHORESIS OF FLUORESCENT MAGNETIC NANOPARTICLES (PAPER 2)

Electroosmotic flow modulation for improved electrokinetic preconcentration : application to capillary electrophoresis of fluorescent magnetic nanoparticles

Ngoc Van Thanh Nguyen[1], Claire Smadja[1]*, Myriam Taverna[1,2], Sirine El Mousli[3], Emilie Secret[3], Jean-Michel Siaugue[3], Lac Thuy Huu Nguyen[4] and Thanh Duc Mai [1]*

[1] *Université Paris-Saclay, CNRS, Institut Galien Paris-Saclay, 92296, Châtenay-Malabry, France*

[2] *Institut Universitaire de France (IUF)*

[3] *Sorbonne Université, CNRS, Physico-chimie des Électrolytes et Nanosystèmes Interfaciaux, PHENIX, F-75005 Paris, France*

[4] *Faculty of Pharmacy - University of Medicine and Pharmacy at Ho Chi Minh City - 41 Dinh Tien Hoang St., Ben Nghe Ward, District 1, Ho Chi Minh City, Vietnam*

Correspondence: E-mail: thanh-duc.mai@u-psud.fr;
claire.smadja@u-psud.fr

Keywords: capillary electrophoresis; fluorescence detection; stacking; preconcentration; EOF suppression and modulation; magnetic nanoparticles

Abstract

It is reported in this study a new approach for modulation and even suppression of the electroosmotic flow (EOF) to achieve better electrokinetic preconcentration in capillary electrophoresis This is based on the augmentation of the buffer's concentrations to very high levels (more than a thousand of mM) without recourse to any dynamic/permanent coating nor viscous gel. The use of large weakly charged molecules as background electrolyte's constituents allows working at extreme concentration ranges without penalty of high electric currents and Joule heating. By this way, the electroosmotic mobility could be modulated over a wide range (2 - 60 × 10^{-5} $cm^2.V^{-1}.s^{-1}$ under alkaline conditions), and suppressed to levels equivalent to those obtained with several neutral coatings. For demonstration, this new approach was applied for sensitive determination of core-shell magnetic nanoparticles (CSMNPs) having high potential for healthcare applications such as imaging agents for diagnostics and controllable cargos for nanomedicine. Different profiles were achieved for purpose-made and commercial magnetic nanoparticles using CE coupled with light-emitting-diode induced fluorescence (LEDIF) detection. Compared to the conventional capillary electrophoresis (CE-UV) method for characterization of magnetic nanoparticles, our proposed approach with fluorescent detection and EOF-assisted preconcentration offers almost 350-fold sensitivity improvement. Furthermore, our scheme can be used for monitoring the interaction between CSMNPs and target pharmaceutical molecules, serving for drug delivery development. A preliminary study with two antibiotics using this approach revealed that kanamycin interacts better with the target nanoparticles than amikacin.

1. Introduction

Nanoparticles are appealing candidates for biomedical and analytical applications (e.g. imaging, drug delivery, sensors, magneto-immunoassays, lab on chip development). Their analysis is essential to obtain information on their size, shape, potential heterogeneity and surface chemistry or functionalization, enabling their practical use for various applications [1, 2]. Capillary electrophoresis (CE) is a well-described technique to characterize nanoparticles and monitor their interaction with target (pharmaceutical and biological) molecules [3]. These CE characterization methods are so far coupled with either UV or MS detection [2, 4]. CE with laser-induced fluorescent (LIF) detection of nanoparticles (other than quantum dots) has never been communicated to the best of our knowledge. As detection sensitivity is always limited with reported CE-UV or CE-MS approaches, some specific modes of on-line preconcentration are often needed prior to electrophoretic separations of nanoparticles [5]. In the case of core–shell magnetic nanoparticles (CSMNPs) that have been exploited in different health-care applications (i.e. multimodal imaging for diagnostics and controllable cargo for drug delivery [6-11]), two approaches for on-line electrokinetic preconcentration prior to their CE-UV separations have been communicated so far. These include field-amplified sample injection [12, 13] and dynamic pH junction [14], allowing preconcentration of sample plugs accounting for less than 30 % of the total capillary volume. Due to the heterogeneous population of nanoparticles in general, and CSMNPs in particular, electrokinetic preconcentration from a more significant sample volume (*i.e.* equivalent to 100 % of the capillary one) is more challenging and has not been explored so far.

Large volume sample stacking (LVSS) with polarity switching is a performing electrokinetic preconcentration mode in CE that exploits the bulk electro-osmotic flow (EOF) to allow stacking of target analytes for enrichment [15-24]. Preconcentration in this case can be realized even from a sample solution filling up to 100 % of the capillary volume. LVSS with polarity switching in fused silica capillaries requires, however, two different EOF magnitudes for sample preconcentration and then separation of stacked analytes. A high EOF is needed to remove sample matrix from the capillary during the stacking of negatively charged analytes whereas a much lower one (even suppressed EOF) is often required to ensure baseline separation of enriched species. This EOF change needed for LVSS with polarity switching can be created through significant buffer's pH variation or the use of neutral capillary coatings [15-24]. To reduce EOF under neutral and alkaline conditions, dynamic and permanent capillary coatings are commonly employed [25, 26]. An alternative to conventional capillary coating methods has been recently developed, exploiting

the potential of nanomaterials as nano-coating layers [27]. EOF can also be suppressed by significantly increasing the electrolyte viscosity [28, 29]. Accordingly, viscous gels (i.e. polyethylene oxide gel and acrylamide-based hydrogel) were employed to block the apparent electro-osmotic (EO) fluid flow [30, 31]. The increase in buffer viscosity to reduce EOF can also be carried out by addition of organic modifiers (glycerol, chemical gels or polymer solutions) to the running buffer [32]. Another option is to increase the electrolyte's ionic strength (IS) to such a high level that sufficiently compresses the thickness of the diffusion double layer [33-39]. Nevertheless, this approach normally comes with high current generation and unwanted Joule heating effect with conventional CE electrolytes containing inorganic ions.

Herein, we report for the first time a CE coupled with light-emitting-diode (LED) induced fluorescence detection approach (CE-LEDIF) for CSMNPs, offering significant improvement of detection sensitivity compared to the previously reported methods using UV or inductively coupled plasma mass spectrometry (ICP-MS) detection [40-43]. This was achieved with a novel way to perform on-line electrokinetic preconcentration of CSMNPs via modulation of the EO mobility (μ_{EO}) in fused silica capillaries without recourse to any coating nor viscous gel. This method for EOF modulation is based on the augmentation of the buffer's concentrations to very high levels (more than a thousand mM) using selected background electrolytes (BGEs) composed of large, weakly charged molecules. The magnitude of EOF could be regulated or suppressed whatever the pH (neutral and alkaline ranges) of the BGE without incurring high electric currents. The coupling of our coating-free electrokinetic preconcentration and CE-LEDIF analysis for sensitive detection of CSMNPs as well as monitoring of their interaction with different target pharmaceutical compounds is presented.

2. Experimental

2.1. Chemicals and reagents

2-(Cyclohexylamino)ethanesulfonic acid (CHES), 3-(Cyclohexylamino)-1-propanesulfonic acid (CAPS), 2-(N-morpholino)ethanesulfonic acid (MES), phosphoric acid, 3-(N-morpholino)propanesulfonic acid (MOPS), Triethanolamine (TEA, ≥98%), Diethanolamine (DEA, ≥98%), Ethanolamine (≥98%), Tris(hydroxymethyl)aminomethane (TRIS), sodium dodecyl sulphate (SDS), sodium hydroxide (NaOH), acid boric (H_3BO_3), sodium dihydrophosphat (NaH_2PO_4), disodium hydrophosphat (Na_2HPO_4), Dimethyl sulfoxide (DMSO

99.9%), amikacin sulfate were all provided by Sigma (St. Louis, MO, United States). Kanamycin sulfate was obtained from Sequoia Research Product Ltd (Pangbourne, UK). Fluorescein isothiocyanate (FITC) was purchased from Beckman (Sciex Separation, Brea, CA). All buffers were prepared with deionized water and were filtered through a 0.22 µm membranes (Pall Corporation, New York, USA) prior to use. Carboxylate-modified nanoparticles, fluorescent (λex ~470 nm; λem ~505 nm), 30 nm in diameter were obtained from Sigma (St. Louis, MO, United States).

2.2. Apparatus and Material

Uncoated capillaries were purchased from Phymep (Paris, France). All experiments were performed using a Beckman Coulter PA 800 plus system (Sciex Separation, Brea, CA) equipped with UV detection and Agilent CE G1600AX Capillary Electrophoresis System (California, USA) coupled with a LED-based fluorescence detector (LEDIF with $\lambda_{excitation}$: 480 nm, $\lambda_{emission}$: 520 nm, Adelis, Labege, France). Data acquisition for UV detection and instrument control were carried out using Karat 9.1 software (Sciex Separation, Brea, CA) whereas fluorescence detection data were recorded by Power Chrome software (eDAQ, Australia). Deionized water used in all experiments was purified using a Direct-Q3 UV purification system (Millipore, Milford, MA, USA). Conductivity and pH values of buffer solutions and samples were measured by a Seven Compact pH meter (Mettler Toledo, Schwerzenbach, Switzerland). Selection of background electrolyte (BGE) and buffer IS calculations were simulated by the computer program PhoeBus (Analis, Suarlée, Belgium).

2.3. Methods

Synthesis and physio-chemical characterization of core-shell MNPs

The Fe_2O_3@SiO_2-COOH core-shell MNPs were synthesized according to reported protocols [9, 44]. Maghemite MNPs (γ-Fe_2O_3, with a mean diameter of 12.3 nm) were prepared following the procedure described by Massart [45]. They were subsequently size-sorted in order to have a narrower size distribution and then coated with citrate anions [46]. The obtained solution (121.2 µL) of citrated maghemite MNPs at an iron concentration of 1.9 mol/L was dispersed in 10 mL of water and 20 mL of ethanol. A coating by a fluorescent silica shell was performed by adding 152.6 µL of tetraethylorthosilicate (TEOS, Merck), 500 µL of a 30% ammonia solution, and 25.4 µL of

aminopropyltriethoxysilane (APTS)-functionalized fluorescein (Sigma-Aldrich) at 18.75 mmol/L. After 2 h of agitation, the surface of the silica shell was functionalized with amino groups and short polyethyleneglycol (PEG) chains by the simultaneous condensation of APTS (V = 27 µL) and a silica PEG-derived compound, 2-(methoxy(polyethyleneoxy)propyl)trimethoxysilane (PEOS, ABCR) (V = 61.8 µL), with an appropriate amount of TEOS (V = 50.8 µL) in order to generate a cross-linked silica shell. The mixture was stirred overnight. The resulting nanoparticles were then rinsed 3 times with a mixture of diethylether/ethanol 15:1 and finally re-dispersed in 5 mL of a 3-morpholinopropane-1-sulfonic acid (MOPS) buffer at 0.1 mol/L and pH = 7.4. These Fe_2O_3@SiO_2-NH2 MNPs were then converted to Fe_2O_3@SiO_2-COOH MNPs via a 45 min reaction of 3 mL of this dispersion of MNPs with 1 mL of a solution of succinic anhydride at 0.5 mol/L in DMSO. Finally, the Fe_2O_3@SiO_2-COOH MNPs were washed with MOPS buffer in PD-10 columns containing Sephadex G-25 (GE Healthcare).

The Fe_2O_3@SiO_2-COOH MNPs were then characterized by transmission electron microscopy (TEM) on a JEOL 1011 instrument, and by dynamic light scattering (DLS) and zetametry with a Zetasizer Nano ZS (Malvern Instruments). The mean physical diameter of the MNPs was measured to be 31.7 ± 4.4 nm (see Figure S1 in the electronic supplementary information ESI). The zeta potential and hydrodynamic diameter of the MNPs in MOPS buffer were measured to be -23 ± 4.4 mV and 32 nm respectively (see Fig. S1 in the ESI) with a polydispersity index of 0.25.

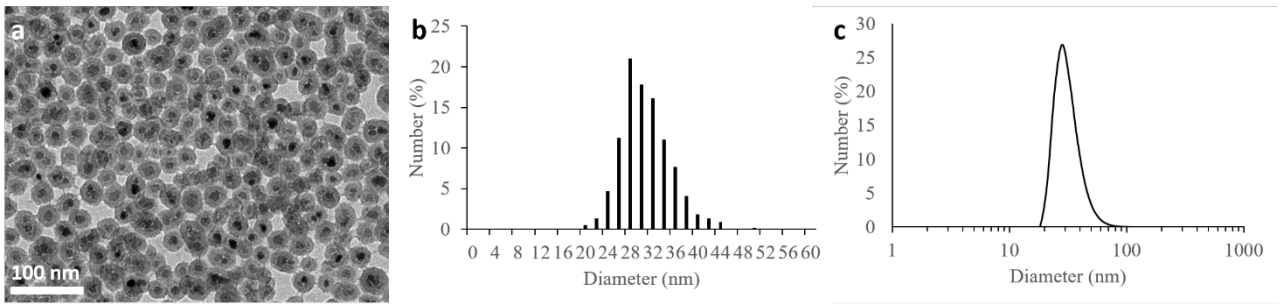

Fig. S1: a) Transmission electron microscopy or the Fe_2O_3@SiO_2-COOH MNPs. b) Physical diameter distribution obtained by TEM image analysis. The average physical diameter of the MNPs is 31.7 ± 4.4 nm. c) Hydrodynamic diameter of the MNPs obtained by dynamic light scattering. The MNPs have a hydrodynamic diameter of 32 nm with a polydispersity index of 0.25.

Measurement of electroosmotic flow (EOF)

EOF was measured using the Beckman Coulter system and the signals were detected with UV detection at 200 nm. The fused silica capillary (I.D. of 50 µm, effective length (L_{eff}) of 10 cm and total length (L_{tot}) of 40 cm) was pre-conditioned with NaOH 1 M for 5 min, DI water for 5 min and BGE for 15 min prior to the first use and post-conditioned with BGE for 3 min after each analysis. The EOF marker, DMSO (1 % in water) was injected for 10 sec at 50 mbar, followed by application of a voltage of 17 kV. All EOF measurements were performed in triplicate. Between analysis, the capillary was rinsed with NaOH 1 M for 3 min, DI water for 2 min and BGE for 5 min.

CE-LEDIF of FITC and core-shell MNPs

These experiments were carried out with the Agilent system coupled with LIF and UV detection. Prior to the first use, the silica capillary (I.D. of 50 µm, L_{eff} of 50 cm for UV detection, L_{eff} of 35 cm for LIF detection and L_{tot} of 60 cm) was flushed with following sequence: NaOH 1 M for 5 min, DI water for 5 min, then BGE for 25 min. Before each analysis, the capillary was flushed with SDS for 5 min, NaOH for 5 min, then DI water for 3 min and BGE for 5 min. FITC or CSMNPs samples were hydrodynamically injected at 50 mbar for 30 s. FITC samples for CE-LEDIF were prepared by dilution of the stock solution FITC (1000 nM) with deionized water whereas CSMNPs samples were prepared by dilution of the stock Fe_2O_3@SiO_2-COOH (whose iron concentration was 0.024 M) with Tris/ CHES (IS 10 mM, pH 8.5). The samples were prepared daily. The separation was performed under 25 kV (normal polarity) at 25ºC. The signal of EOF was recorded by UV detection whereas FITC and MNPs signals were observed by LIF detection. The fluorescent signals (analog signals) were recorded with a data acquisition system and converted into digital ones, which are displayed in the mV scale.

Large volume sample stacking (LVSS) with polarity switching - CZE

For LVSS of FITC or CSMNPs, samples were filled to 100 % of the capillary volume. A voltage of - 25 kV was applied at the injection end (inlet) of the capillary for 5 min. The current was monitored visually during this process. When the current reached the stable value after a stacking duration of 5 min, the polarity of the high voltage was immediately switched to trigger the separation. The separation was conducted for 30 min under 25 kV with normal polarity.

3. Results and Discussion

3.1. EOF-assisted preconcentration in an uncoated fused silica capillary

3.1.1. Suppression and modulation of EO mobility via variation of BGE concentrations

Our coating-free approach to significantly reduce EOF under alkaline conditions in fused silica capillaries is based on the use of BGEs at extremely high concentrations. This approach so far is not trivial with conventional BGEs for CE-UV and CE-LIF, which normally contain inorganic ions for buffering and pH adjustment, due to too high current generation at certain ionic strength (IS) ranges. In our study, various BGEs composed of large weakly charged ions were investigated regarding their ability to prevent Joule heating at high IS values. Among all BGEs simulated with the Phoebus software (table 1), we selected 16 compositions covering the pH range from 5.5 to 9.6 for further experiments on μ_{EO} suppression. For a selected anion and at the predefined IS of 150 mM, the cations that allow to produce the highest simulated concentrations and the lowest simulated currents were chosen. Accordingly, four organic acids, including CAPS, CHES, MOPS and MES were combined with four organic bases (triethanolamine, diethanolamine, ethanolamine and Tris). Working with such BGEs at this IS range (150 mM and more) is considered extreme because the constituent concentrations can go up to a thousand mM or more (see table 1), which are very high compared to those in conventional buffers for CE.

Table 1. Inorganic-species-free BGE compositions at different pH, simulated with Phoebus program

BGE compositions at 150mM	pH	I (µA) at E = 400 V/cm*	Mobility (cm^2/V.s)		Buffer capacity (mmol/l.pH)	Remark
			Cation	Anion		
Triethanolamine 150.6 mM + MES 638.6 mM	5.5	28	0.00001	-0.00007	281	To be tested**
Diethanolamine 150 mM + MES 638.6 mM		58	0.00031		279.7	To be tested
Ethanolamine 150 mM + MES 638.6 mM		71	0.00044		279.6	To be tested
Tris 150.3 mM + MES 638.6 mM		57	0.00030		280.3	To be tested
Triethylamine 150mM +MES 638.7mM		63	0.00036		279.6	
Diethylamine 150mM + MES 638.7mM		70	0.00044		279.6	
Trimethylamine 150mM+ MES 638.7mM		76	0.00049		279.6	
Triethanolamine 181.6 mM + MOPS 194.6 mM	7.2	27	0.00001	-0.00021	139.3	To be tested
Diethanolamine 152.4 mM + MOPS 194.6 mM		57	0.00030		85.2	To be tested
Ethanolamine 150.6 mM + MOPS 194.6 mM		70	0.00044		81.1	To be tested
Tris 165.2 mM + MOPS 194.6 mM		56	0.00027		111.4	To be tested
Triethylamine 150mM +MOPS 194.6mM		62	0.00036		79.9	
Diethylamine 150mM + MOPS 194.6mM		69	0.00044		79.8	
Trimethylamine 150.3mM+ MOPS 194.6mM		75	0.00049		80.4	
Triethanolamine 966,5 mM + CHES 872,7 mM	8.7	18	0.00001	-0.00004	488.9	To be tested
Diethanolamine 225,7 mM + CHES 872,7 mM		51	0.00020		414.1	To be tested
Ethanolamine 168,2 mM + CHES 872,7 mM		64	0.00040		340	To be tested
Tris 582 mM + CHES 817,6 Mm		50	0.00007		551.7	To be tested
Triethylamine 151.1mM +CHES 872.7mM		56	0.00036		306.7	
Diethylamine 150.7mM + CHES 872.7mM		64	0.00043		305.8	
Trimethylamine 150.3+ CHES 872.7mM		69	0.00046		323.2	
Diethanolamine 751.2 mM + CAPS 872.5 mM	9.6	36	0.00007	-0.00001	563.7	To be tested
Ethanolamine 294.9 mM + CAPS 872.5 mM		50	0.00024		464.7	To be tested
Triethylamine 158.69mM +CAPS 872.5mM		43	0.00034		322.4	
Diethylamine 155.3mM + CAPS 872.5mM		52	0.00042		315.7	
Trimethylamine 222.28+ CAPS 872.5mM		58	0.00034		410.8	

* *Electric current simulated for a capillary of 50 µm ID*

** *This simulated BGE was then experimentally tested for EOF suppression with CE-LEDIF. See equation (1) (GBI calculation) for the logic behind the selection of these BGEs to be experimentally tested.*

The capability for EOF suppression of these BGE compositions is reflected by the measured μ_{EO} values (Fig. 1).

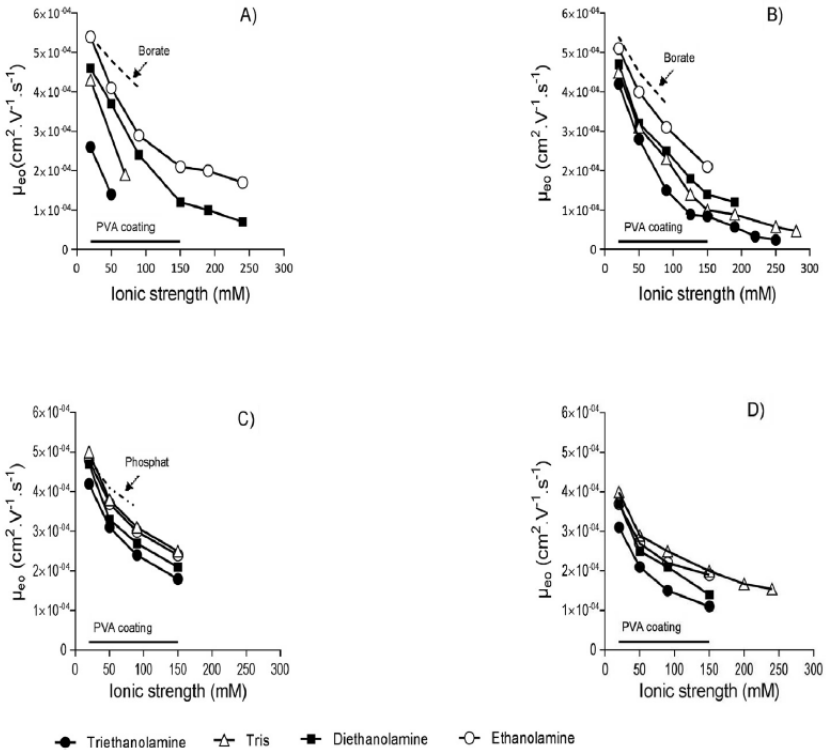

Fig. 1. The measured EOF magnitudes at different pH and IS values. A) pH 9.5-10; B) pH 8.4-8.7; C) pH 7.2-7.4; D) pH 5.5-6.0 Fused silica capillary with ID of 50 µm, L_{eff} of 10 cm, L_{tot} of 40 cm. Sample DMSO 0.1%. Hydrodynamic injection at 50 mbar over 10 s. CE voltage 17kV. See 'Experimental section' and table 1 for preparation of the tested BGEs.

Some µEO measurements were also carried out with the method of Williams and Vigh [47]. The results obtained (table S1 in the ESI) showed similar ranges with no remarkable systematic bias between two different approaches for µEO measurements. We can assume that the deviation linked to the non-thermostated section of the capillary encountered in the short-end injection method for µEO measurement is negligible. Whatever the pH and tested combination, the EOF was found to decrease drastically from more than $40 \cdot 10^{-5}$ $cm^2.V^{-1}.s^{-1}$ (*i.e.* the normal EOF magnitudes observed with conventional BGEs for CE at these pH values) to less than $10 \cdot 10^{-5}$ $cm^2.V^{-1}.s^{-1}$.

Table S1: µEO values for different BGEs measured with conventional method and Williams and Vigh's one

Buffers	EOF short end (cm^2/V/s)	Vigh's method (cm^2/V/s)
Tris- CHES 200 mM pH 8.4	8.90E-05 (RSD 0.94 %)	8.94E-05 (RSD 0.64 %)
DEA- CAPS 200 mM pH 9.5	9.56E-05 (RSD 0.59 %)	8.46E-05 (RSD 0.55 %)

In some cases, EOF dropped down to $2 \cdot 10^{-5}$ ($cm^2.V^{-1}.s^{-1}$), which is a μ_{EO} value achieved with different home-made coatings [48, 49] and is very close to that obtained with a commercial

permanent neutral one (poly-vinyl alcohol (PVA) coating, 0.5 - $1 \cdot 10^{-5}$ $cm^2.V^{-1}.s^{-1}$) [50]. This is the first time very low μ_{EO} values, close to total EOF suppression, have been achieved with such a principle. Furthermore, the desired range of EOF can be easily tuned just by changing the BGE's concentrations. This is on the other hand not trivial with coated capillaries which generally exhibit fixed μ_{EO} values. Capillary regeneration which is sometimes limited by chemical stability of the coatings is now possible with our IS-based approach. Among all tested cations, the most efficient for EOF reduction was triethanolamine, followed by diethanolamine (see Fig. 1). Besides the contribution of extremely high BGE concentrations (to provide elevated IS values), alkylamines as the cationic BGE constituents are known to reduce the EOF, which explains the excellent efficiency in EOF blocking offered by the tested BGEs. Note that the current was measured over the whole capillary, rather than for only the non-thermostated length (10 cm). In both measurements a bias due to the non-cooled capillary section may occur [51]. Nevertheless, we considered this bias negligible, as the surrounding temperature was less than 30°C [52]. In addition, the relatively small currents generated with our BGEs ensured the Joule heating to be reduced, which in turn help minimize the bias due to the non thermostated part of the capillary. The Ohm's law is strictly fulfilled at electrical fields less than 250-300 V/cm for all tested buffers (see Fig. S2 in the ESI). Depending on the composition of the BGEs, the linear relationship between voltage vs. generated current can be maintained up to 400 V/cm in some cases (for instance the BGE composed of TEA-CHES with ionic strength up to 240 mM). The currents measured for all these BGEs, even at their highest IS values, remain inferior to 50 µA under an electrical field of 400 V/cm. This is considered tolerable for a capillary of 50 µm ID [53].

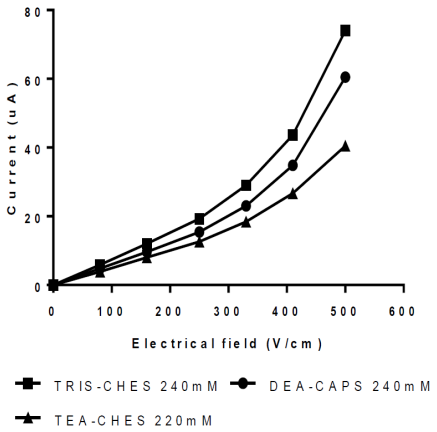

Fig. S2. The electrical field versus current profiles for different tested BGEs at their highest ionic strengths. The currents were measured on applying variable voltages over a 60.2 cm long uncoated fused silica capillary with i.d. of 50 µm.

In our IS-based approach for EOF suppression, the increase in IS of the BGE is not limited by the generated current as in conventional buffers for CE, but rather by the solubility of the least soluble component of the BGE. The highest BGE concentrations (or IS values), and the lowest EOF magnitudes, accordingly, were achieved with diethanolamine/CAPS (250 mM, pH 9.5), Tris/CHES (280 mM, pH 8.7) and triethanolamine/CHES (250 mM, pH 8.5). It is possible that the amine moiety of the tested anions interacts with the silanols and contributes to some certain extend to diminish the EOF. However, we expect this effect to be negligible compared to that provoked by the cationic constituent of the buffer. The total net charge of the tested anions in the working pH ranges is negative, meaning that the positive charge of its amine moiety is outnumbered by the sulfonic acid negative one. The anions have therefore less chance than the cations to approach the inner capillary surface; and the electrostatic interaction between the anions' amine moiety with silanols is expected to be much less favorable.

In our approach for EOF suppression, we considered simultaneously different parameters (*i.e.* BGE's IS, concentrations and generated electric currents) rather than focusing only on the key factor IS as in previous studies [33-39]. It is well known that an increase in the buffer's IS can lead to reduction of the electrical double layer thickness, thus decreasing EO mobility. However, for the same IS, different BGEs provided different EOF magnitudes, as demonstrated clearly in Fig. 1. Accordingly, EOF is not only dependent on the IS of the BGE, but also on its constituents' nature and concentrations which include the cations that can interact with the silanols [54]. Effort was therefore made to establish a theoretical index of a good BGE in terms of EOF reduction capacity, based on the simulated parameters and the measured μ_{EO} values (Fig. 2).

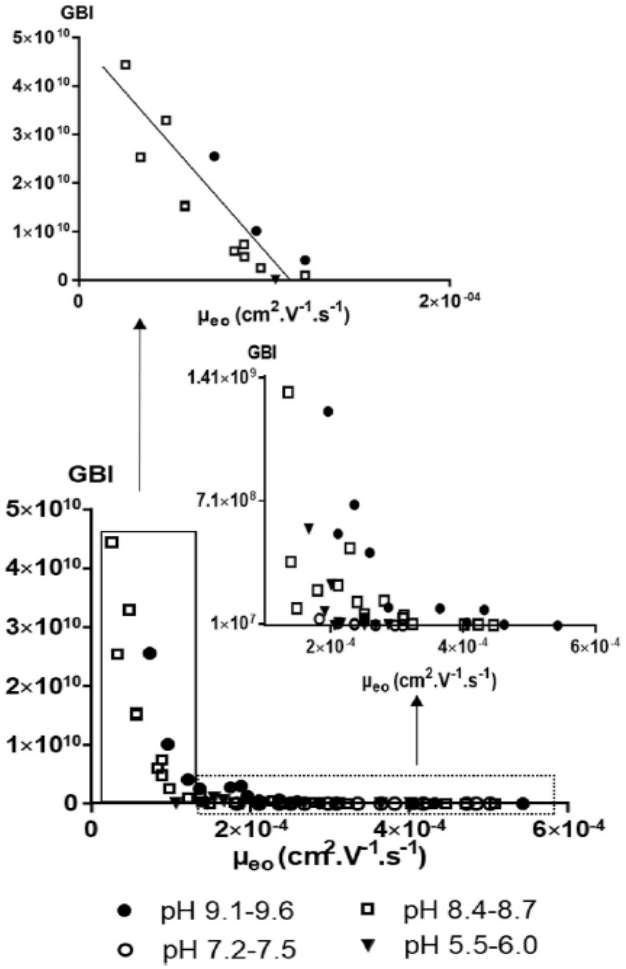

Fig. 2. Correlation between calculated good-buffer-index (GBI) values and the experimentally measured μ_{EO} values for different tested BGE compositions. See 'Experimental section' and table 1 for preparation of the tested BGEs.

A good buffer for EOF suppression should possess an IS and constituents' concentrations as high as possible while generating an electric current (I) as low as possible. The nature and concentration of cations in the BGE significantly contribute to the μ_{EO}. The cation's concentration therefore is expected to play a more pronounced role for EOF suppression. A high buffer capacity is also another factor to consider for a good BGE. Accordingly, we propose a good-buffer index (GBI) as follow:

$$GBI = \frac{IS \times (C_C + C_A) \times C_C \times \beta}{I}$$

with $\boldsymbol{C_A}$, $\boldsymbol{C_C}$ *(mM) as the concentrations of the BGE constituents (e.g. for Tris / CHES BGE,* $C_A = C_{CHES}$ *and* $C_C = C_{Tris}$*);* $\boldsymbol{\beta}$ *(mM/pH) as the buffer capacity; and* $\boldsymbol{I}$ *(μA) as the measured electric current generated by the BGE under a fixed electrical field of 400 V/cm.*

All parameters in the GBI calculation were simulated with PHoeBuS software, except for the current values that were measured experimentally. Note that the generated currents could also be simulated with PhoeBus, with little deviation from the measured values. In this case, the GBI can be fully stimulate-able. To ensure calculation accuracy, different corrections were applied for IS calculation, using Debye-Huckel equation for IS of 1-10 mmol/L, Guntelberg equation for IS of 10-60 mmol/L and Davies equation for IS of 60-500 mmol/L [55].

A clear tendency was observed regardless of the pH tested, where BGEs with low GBI values ($< 2 \times 10^9$) produced medium and high μ_{EO} ($> 20 \times 10^{-5}$ $cm^2 \cdot V^{-1}.s^{-1}$) whereas those with high GBI ($> 5 \times 10^9$) exhibited efficient EOF suppression ($\mu_{EO} < 10 \times 10^{-5}$ $cm^2 \cdot V^{-1}.s^{-1}$). In the GBI range over 2×10^9 (see the insert in the Fig. 2), a good correlation between GBI and μ_{EO} ($r^2 = 0.78$) was achieved, demonstrating the relevance of the proposed model. In case of EOF manipulation for electrokinetic preconcentration or separation of target analytes, users can rely on these GBI (or the tendency shown in Fig. 2) to check the relevant buffers for the expected EOF ranges.

3.1.2. Large volume sample stacking using EOF modulation

We propose here a new way of LVSS, using modulation of μ_{EO} via BGE's IS and concentrations. The principle behind this EOF-assisted enrichment method is illustrated in Fig. 3.

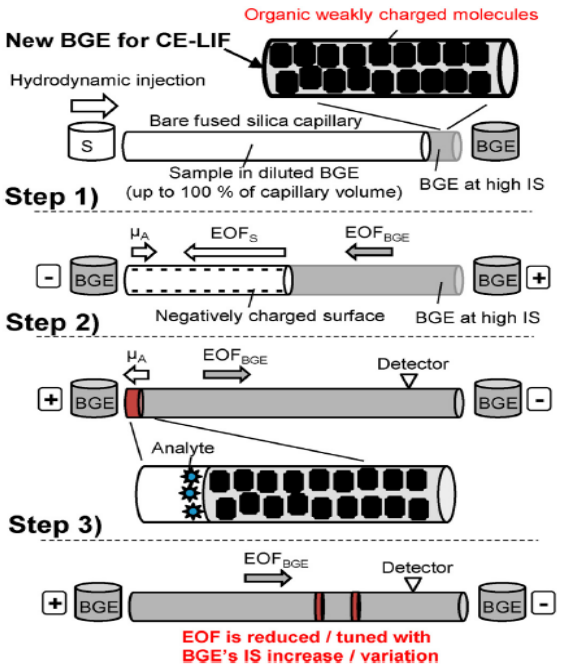

Fig. 3. Principle of LVSS- CE-LEDIF with our new pH-free EOF manipulation approach.

As the EOF is manipulated through IS changes rather than pH, our method allows to select the best pH conditions for the analytes during preconcentration and separation without recourse to any capillary coating. In this case, the low EOF for optimal separation can be generated by playing with different BGE's IS (step 3 in Fig. 3). The use of extremely high BGE concentrations to produce such elevated IS, while not trivial with inorganic ions prone to high current generation, is now feasible thanks to the very low electrophoretic movement of the large weakly charged molecules constituting the BGE. To demonstrate the preconcentration performance of our EOF-assisted method, we showed in Fig. 4 a comparison between our LVSS (sample filling 100 % of the capillary volume) using IS adjustment vs. normal CE (sample filling 7 % capillary volume) of FITC 10 nM. By using a BGE composed of 90 mM DEA /CAPS, an EO mobility of approx. $20 \cdot 10^{-5}$ $cm^2.V^{-1}.s^{-1}$ was obtained for CZE of FITC, whereas a much higher EOF (μ_{EO} of $50 \cdot 10^{-5}$ $cm^2.V^{-1}.s^{-1}$) was necessary during the forefront LVSS step.

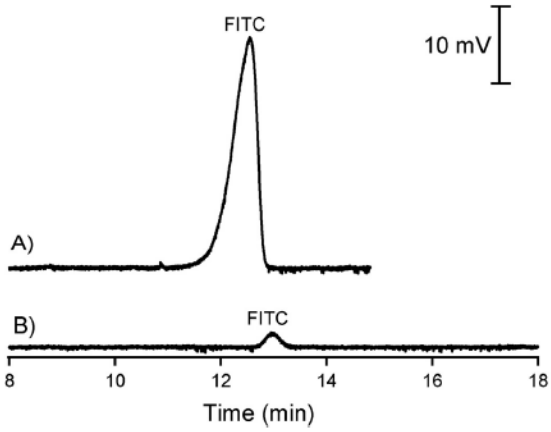

Fig. 4. A) LVSS- CE-LEDIF of 10 nM FITC; B) Normal CE-LEDIF of 10 nM FITC (prepared in deionized water). See section 'Methods' for LVSS and CE-LEDIF protocols.

By comparing the peak height ratios, a 24-fold improvement was achieved. The peak height was used rather than the peak area, as the former reflects better the signal improvement with preconcentration approaches. Indeed, an increase in peak area may be due to peak broadening and velocity decrease rather than stacking effect. The difference in signal improvement factor (24) and injected volume one (14) between LVSS-CE-LEDIF and normal CE-LEDIF of MNPs is due to a certain band broadening observed in CE-LEDIF as the injected volume was quite high (7% of the capillary volume) compared to common ones employed for normal CZE. Some peak broadening and less peak symmetry were observed with LVSS-CE-LEDIF of MNPs. The peak

shape degradation, which comes solely from LVSS due to manual polarity switching required to transit the analytes from the preconcentration stage to the separation one, is nevertheless acceptable considering a stacking of the whole capillary volume. Good calibration linearity (R^2 = 0.9982 for 5 points from 1 to 20 nM) and excellent reproducibilities for peak areas (RSD $\%_{(n=3)}$ = 1.75 %) and migration time (RSD $\%_{(n=3)}$ = 0.25 %) prove satisfied performance of our proposed enrichment method.

3.2. LVSS and CE-LEDIF of CSMNPs

We developed then a new approach based on these preliminary investigations for sensitive detection of CSMNPs, using our coating-free preconcentration strategy coupled with CE-LEDIF. To render fluorescent the carboxylic CSMNPs, a FITC-based fluorophore (fluorescein isothiocyanate-derived 3-aminopropyltriethoxysilane) was encapsulated in their silica shell during the synthesis process without changing their size and surface charge [7, 9]. First, the CE-LEDIF conditions were optimized to separate CSMNPs from the residual fluorophore, using BGE composed of either TEA / MOPS (pH 7.4), DEA / MOPS (pH 7.4), TRIS / MOPS (pH 7.4), TRIS / CHES (pH 8.4) or DEA / CAPS (pH 9.7) (Fig. S3 in the ESI).

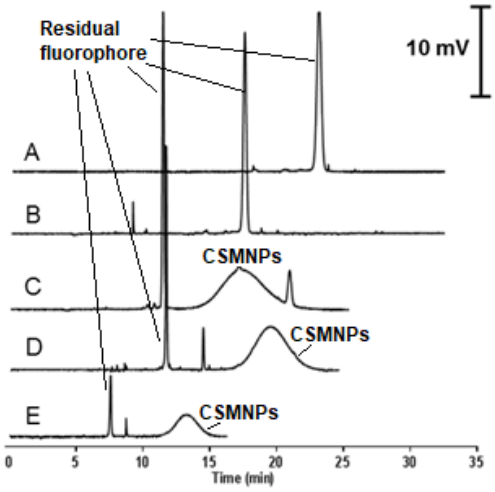

Fig. S3. Optimization of background electrolyte compositions for CE-LIF analysis of core-shell magnetic nanoparticles (CSMNPs). A) TEA / MOPS (pH 7.4), B) DEA / MOPS (pH 7.4), C) TRIS / MOPS (pH 7.4), D) TRIS / CHES (pH 8.4), E) DEA / CAPS (pH 9.7). CE conditions: capillary having ID of 50 µm, total length of 60 cm, effective length of 35 cm; high voltage of 25 kV; sample: CSMNPs in 10-fold diluted BGE; hydrodynamic injection at 50 mbar over 30 s. Fluorescent detection at excitation and emission wavelengths of 480 nm and 520 nm respectively.

As the CSMNPs were found to be stable in buffers having IS of 100 mM [9, 44, 45], this IS was kept constant for all tested BGEs. Indeed, CSMNPs were found stable (with little changes in their sizes) for at least 3 days after dispersion in every tested buffer (see table S2 in the ESI).

Table S2: CSMNPs sizes measured with DLS at different times after dispersion in tested buffers having IS of 100 mM

Buffers	**Size (nm)**	
	Day 1	***Day 4***
TEA- MOPS	41.81	40.31
DEA- MOPS	44.92	46.91
Tris- MOPS	48.21	47.14
Tris- CHES	54.71	61.49
DEA- CAPS	52.32	52.19

With TEA/MOPS and DEA/MOPS buffers (traces A, B in Fig. S3), peaks of MNPs could not be observed due to too long analysis time. The Tris/MOPS buffer (trace C) gave a much broadened peak of MNPs. In the cases of Tris/CHES (trace D) and DEA/CAPS (trace E), the separations between MNPs and residual fluorophore were satisfactory. The peak height was however much smaller when using the DEA/CAPS buffer. The best separation and peak shapes were therefore achieved with the TRIS / CHES BGE at IS of 100 mM. The CE profile of CSMNPs (polydispersity index PDI of 0.25) was then compared with that of the commercial fluorescent latex NPs (average size of 34 nm, PDI of 0.129). Two different peak zones were observed (Fig. S4 in ESI). These two NP types display clear differences in their CE profiles (*i.e.* migration time, peak sharpness) which come from their charge-to-size ratios and PDI differences. As the two types of NPs possess similar sizes (i.e. average diameter of 30 nm), the difference in their migration times may be more dependent on the variation of their surface charge.

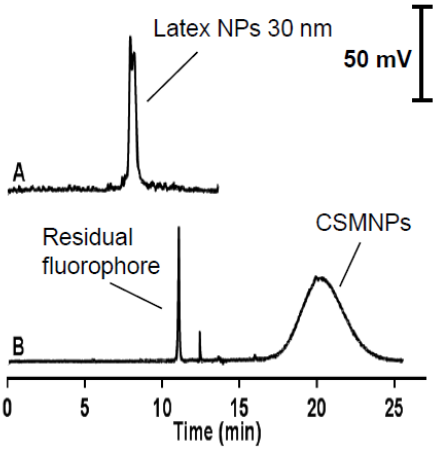

C)

Fig. S4. CE-LIF of the commercial fluorescent latex NPs 30 nm (A) and CSMNPs (B).The nanoparticles were prepared in 10-fold diluted BGE; hydrodynamic injection at 50 mbar over 30 s. BGE composed of Tris / CHES (100 mM, pH 8.4). Fluorescent detection at excitation and emission wavelengths of 480 nm and 520 nm respectively. (C) Size distribution profile of latex NPs 30 nm.

The LVSS was then included as a forefront for CE-LEDIF of CSMNPs. As the inclusion of LVSS preconcentration induced peak sharpness degradation due to manual polarity switching required to transit the analytes from the preconcentration stage to the separation one, a further optimization of the LVSS conditions was needed to ensure a good separation between MNPs and the residual fluorophore. Optimization of the LVSS process was then carried out by varying the IS of TRIS / CHES BGE (from 80 to 140 mM, see table S3 in the ESI for the measured zeta

potentials of MNPs dispersed in these BGEs) at the inlet and outlet ends of the capillary (Fig. S5).

Table S3: zeta potential of MNPs dispersed in different buffers

BGE	Zeta potential (mV)
TEA- MOPS, IS 100 mM – pH 7.2	-9.41
DEA- MOPS, IS 100 mM – pH 7.2	-16.2
Tris- MOPS, IS 100 mM – pH 7.2	-22.3
Tris- CHES, IS 100 mM – pH 8.4	-23.8
Tris- CHES IS 80 mM – pH 8.4	-25.7
Tris- CHES IS 120 mM – pH 8.4	-16.5
Tris- CHES IS 140 mM – pH 8.4	-12.9

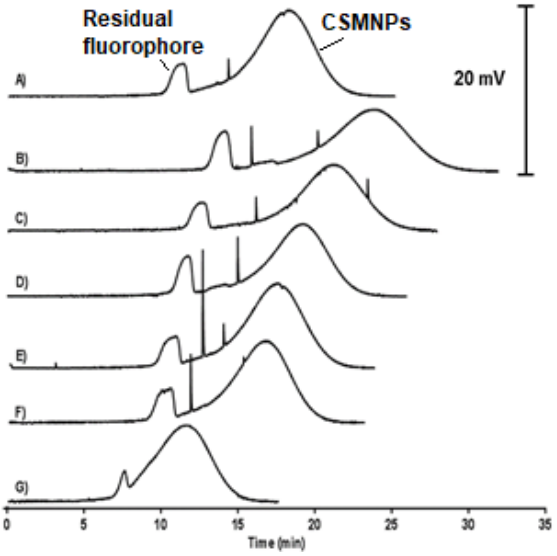

Fig. S5. Optimization of LVSPS for CSMNPs preconcentration. A) Inlet BGE of Tris/CHES 100 mM, outlet BGE of 100 mM; B) Inlet BGE of Tris/CHES 100 mM, outlet BGE of 140 mM; C) Inlet BGE of Tris/CHES 80 mM, outlet BGE of 120 mM; D) Inlet BGE of Tris/CHES 100 mM, outlet BGE of 120 mM; E) Inlet BGE of Tris/CHES 120 mM, outlet BGE of 100 mM; F) Inlet BGE of Tris/CHES 140 mM, outlet BGE of 100 mM; G) Inlet BGE of Tris/CHES 120 mM, outlet BGE of 80 mM. Sample: CSMNPs diluted 4000x in Tris/CHES 10 mM; hydrodynamic injection at 50 mbar over 840s to fill 100 % of the capillary volume. Preconcentration was carried out under -25kV (negative polarity) over 5 min. The polarity of the high voltage was then reversed to trigger CZE separation of the stacked CSMNPs. Fluorescent detection at excitation and emission wavelengths of 480 nm and 520 nm respectively.

The zeta potential of MNPs can vary depending to the IS and compositions of the dispersion buffers. By increasing the IS from 80 to 120 mM using Tris/CHES buffer (pH 8.4), the zeta potential of MNPs increased from -25.7 mV to -12.9 mV. Accordingly, this led to shifting of their electrophoretic mobilities. The variation of MNPs migration time during optimization of the buffer's IS and pH indeed comes from both changes in EOF magnitudes and MNPs' electrophoretic mobilities. Note again, that effort to optimize the CE and LVSS conditions was carried out at IS ranges not far away from 100 mM. Much higher IS (up to 250 mM), while expected to further suppress EOF, would be detrimental to MNPs stability and provoke possible aggregation of nanoparticles. The best performance was achieved with CSMNPs prepared in TRIS / CHES (IS 10 mM, pH 8.4) for preconcentration, and separation under BGE of TRIS / CHES (IS 100 mM, pH 8.4). As can be seen from Fig. S6, the superposition of electropherograms from different runs demonstrated clearly the very good repeatability for LVSS-CZE of CSMNPs under the optimized conditions, with RSD values for migration times of 0.14 % and 2.15 % for the intraday and interday tests, respectively.

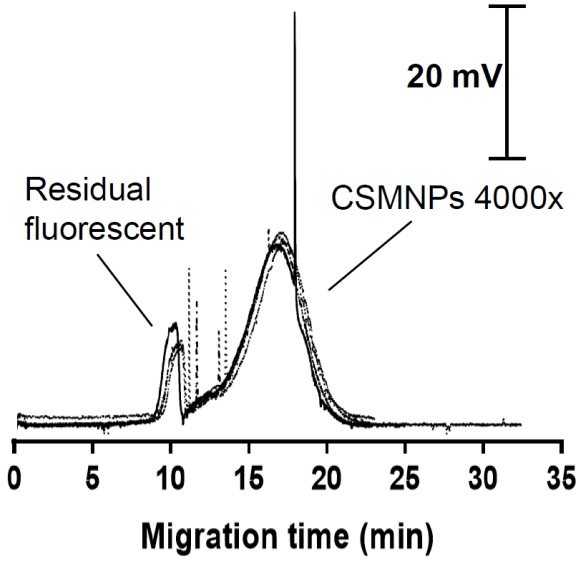

Fig. S6. Repeatability of LVSPS for CSMNPs preconcentration. Inlet BGE of Tris/CHES 100 mM, outlet BGE of 100 mM. Other conditions as in Fig. S5.

Comparison between CE-LEDIF of CSMNPs with and without LVSS (*i.e.* sample filling 100 % vs 7 % of the capillary volume, respectively) was then made (Fig. 5).

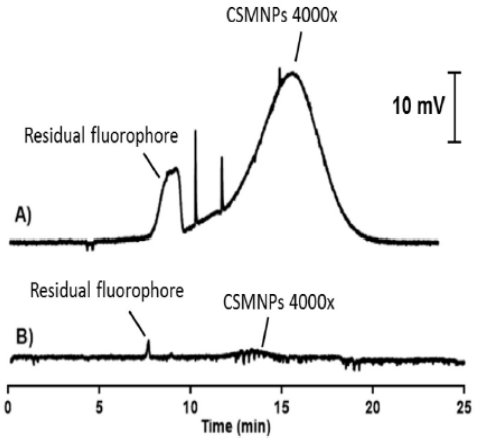

Fig. 5. A) LVSS- CE-LEDIF of CSMNPs (diluted 4000x in Tris/CHES 10 mM); B) CE-LEDIF of CSMNPs (diluted 4000x in Tris/CHES 10 mM). See section 'Methods' for LVSS and CE-LEDIF protocols.

The signal registered for CE-LEDIF of nanoparticles without preconcentration is very small and close to the detection limit level (Fig. 5B) whereas a high peak was achieved with the inclusion of LVSS. Based on peak height ratios, an improvement of detection sensitivity by 20 folds was estimated with the EOF-assisted preconcentration. The CSMNPs peak form with LVSS- CE-LEDIF was a bit more broadened compared to that for normal CE-LEDIF. The heterogenous population of nanoparticles renders the preconcentration of CSMNPs more challenging than that of a single soluble molecule, as it is more difficult to stack all nanoparticles of slightly different electrokinetic mobilities into a very narrow band. Their peak shapes and resolutions nevertheless are satisfactory for further characterization study. Compared to previously reported methods for CSMNPs detection [40, 43], our CE-LEDIF method without LVSS allows an improvement of 3.5 times (compared to CE-MS) and 17 times (compared to CE-UV) respectively for the detection of the CSMNPs' magnetic cores. With the inclusion of the LVSS preconcentration step, a detection limit improvement of 340 was achieved compared to conventional CE-UV for this purpose.

Monitoring interaction between nanoparticles and target drugs is an important step for nanomedicine development and drug delivery [56, 57]. Working with a low quantity of nanoparticles for such study is preferable to avoid problems of cytotoxicity and aggregation. Towards this purpose, the potential of the LVSS- CE-LEDIF method to monitor the interaction between CSMNPs at an extremely low concentration and two antibiotics (kanamycin and amikacin) was tested. In this proof-of-concept study, diluted CSMNPs were mixed with different

antibiotic concentrations and analyzed by LVSS- CE-LEDIF (Fig. 6). As shown in Fig. 6A, the affinity of the positively charged kanamycin to the carboxylic surface of CSMNPs could be confirmed by the clear shift of migration time and change of peak shape in the presence of kanamycin. On the other hand, the peak shape and migration time remained almost unchanged with amikacin, even at a higher concentration (50 µM) (Fig. 6B). These results point out a probable affinity difference of CSMNPs towards these two antibiotics, with much less interaction between amikacin and the target nanoparticles compared to the case of kanamycin. Note that the antibiotics (*i.e.* kanamycin 20 µM or amikacin 50 µM) were included in both samples and buffers in order to maintain the constant presence of antibiotics at all steps. For the first time, the association equilibrium between nanoparticles and target molecules could be maintained during both electrokinetic preconcentration and separation steps, rather than only during the separation process as in other CE works for such purpose.

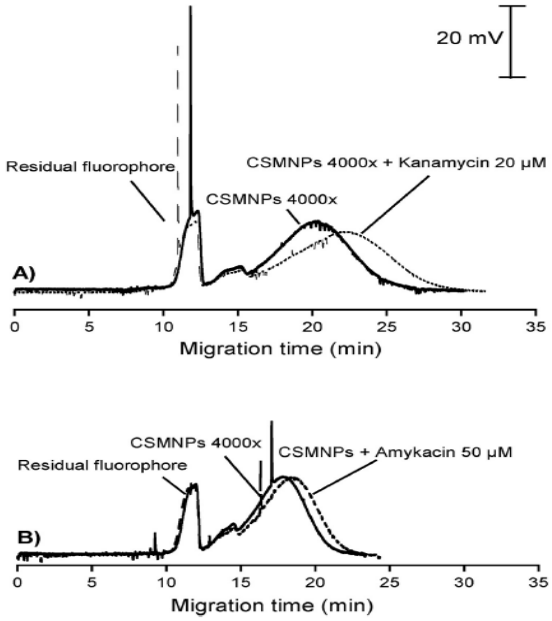

Fig. 6. Electropherograms for LVSS and CE-LEDIF of CSMNPs (diluted 4000x in Tris/CHES 10mM) with / without Kanamycin 20 µM (A) and with / without Amikacin 50 µM (B). Hydrodynamic injection at 50 mbar over 840s to fill 100 % of the capillary volume. Preconcentration was carried out under -25kV (negative polarity) over 5 min. The polarity of the high voltage was then reversed to trigger CZE separation of the stacked CSMNPs in the presence / absence of the tested antibiotics. BGE composed of Tris / CHES (100 mM, pH 8.4) with / without the antibiotics, respectively. Fluorescent detection at excitation and emission wavelengths of 480 nm and 520 nm respectively.

4. Conclusions

We developed a successful combination of electrokinetic preconcentration via EOF modulation under alkaline conditions and CE-LEDIF separation of nanoparticles. For the first time, EOF can be suppressed down to $2 \cdot 10^{-5}$ ($cm^2.V^{-1}.s^{-1}$) in fused-silica capillary without recourse to any capillary coating or gel addition, and can be modulated in a wide range just by changing the BGE's IS. This approach opens the door for different modes of EOF-assisted preconcentration in fused silica capillaries, which have been made possible till now mainly through the use of neutrally coated capillaries. One of its types (i.e. LVSS with polarity switching) was successfully applied to separate and detect CSMNPs, with an improvement of 340 times for detection limit compared to the conventional CE-UV approach. Development of other modes of EOF-assisted preconcentration as well as their exploitations for sensitive and selective determination of biomolecules and nanometric entities with CE-LEDIF are envisaged.

Acknowledgement

This work has been financially supported by the 'bourse d'excellence de l'ambassade de France' (for PhD scholarship of N.V.T. Nguyen). We thank Mr. Ayoub Boulghobra (Université Paris-Saclay) for some preliminary experiments on EOF suppression.

References of PAPER 2

[1] M.N. Alves, M. Miro, M.C. Breadmore, M. Macka, Trends in analytical separations of magnetic (nano)particles, TrAC Trend Anal. Chem., 114 (2019) 89-97.

[2] T.K. Mudalige, H. Qu, D. Van Haute, S.M. Ansar, S.W. Linder, Capillary electrophoresis and asymmetric flow field-flow fractionation for size-based separation of engineered metallic nanoparticles: A critical comparative review, TrAC Trend Anal. Chem., 106 (2018) 202-212.

[3] L. Trapiella-Alfonso, G. Ramírez-García, F. d'Orlyé, A. Varenne, Electromigration separation methodologies for the characterization of nanoparticles and the evaluation of their behaviour in biological systems, TrAC Trend Anal. Chem., 84 (2016) 121-130.

[4] S.S. Aleksenko, M. Matczuk, A.R. Timerbaev, Characterization of interactions of metal-containing nanoparticles with biomolecules by CE: An update (2012-2016), Electrophoresis, 38 (2017) 1661-1668.

[5] S. Dziomba, K. Ciura, M. Dawid, The on-line preconcentration of nanoparticles in electromigration techniques, J. Chromatogr. A, 1606 (2019).

[6] H. Schoneborn, F. Raudzus, E. Secret, N. Otten, A. Michel, J. Fresnais, C. Menager, J.M. Siaugue, H. Zaehres, I.D. Dietzel, R. Heumann, Novel Tools towards Magnetic Guidance of Neurite Growth: (I) Guidance of Magnetic Nanoparticles into Neurite Extensions of Induced Human Neurons and In Vitro Functionalization with RAS Regulating Proteins, J. Funct. Biomater., 10 (2019).

[7] T.D. Mai, F. d'Orlye, C. Menager, A. Varenne, J.M. Siaugue, Red blood cells decorated with functionalized core-shell magnetic nanoparticles: elucidation of the adsorption mechanism, Chem. Comm., 49 (2013) 5393-5395.

[8] M. Laurencin, N. Cam, T. Georgelin, O. Clement, G. Autret, J.M. Siaugue, C. Menager, Human Erythrocytes Covered with Magnetic Core Shell Nanoparticles for Multimodal Imaging, Adv. Healthc. Mater., 2 (2013) 1209-1212.

[9] T. Georgelin, S. Bombard, J.M. Siaugue, V. Cabuil, Nanoparticle-Mediated Delivery of Bleomycin, Angew. Chem. Int., 49 (2010) 8897-8901.

[10] T. Georgelin, V. Maurice, B. Malezieux, J.M. Siaugue, V. Cabuil, Design of multifunctionalized gamma-Fe2O3@SiO2 core-shell nanoparticles for enzymes immobilization, J. Nanoparticle Res., 12 (2010) 675-680.

[11] B. Teste, F. Malloggi, J.M. Siaugue, A. Varenne, F. Kanoufi, S. Descroix, Microchip integrating magnetic nanoparticles for allergy diagnosis, Lab Chip, 11 (2011) 4207-4213.

[12] D. Baron, P. Dolanska, Z. Medrikova, R. Zboril, J. Petr, Online stacking of carboxylated magnetite core-shell nanoparticles in capillary electrophoresis, J. Sep. Sci., 40 (2017) 2482-2487.

[13] D. Baron, C. Cacho, J. Petr, Electrokinetic preconcentration of magnetite core - carboxylic shell nanoparticles by capillary electrophoresis, J. Chromatogr. A, 1499 (2017) 217-221.

[14] C. Cacho, Z. Markova, J. Sevcik, R. Zboril, J. Petr, Study of behavior of carboxylic magnetite core shell nanoparticles on a pH boundary, J. Chromatogr. A, 1364 (2014) 59-63.

[15] R.L. Chien, D.S. Burgi, Sample stacking of an extremely large injection volume in high-performance capillary electrophoresis, Anal. Chem., 64 (1992) 1046-1050.

[16] J.F. Flores-Aguilar, L.C. Medrano, E. Perez-Escalante, J.A. Rodriguez, R.L. Camacho-Mendoza, I.S. Ibarra, Large-volume sample stacking with polarity switching for analysis of azo dyes in water samples by capillary electrophoresis, Int. J. Environ. Anal. Chem., 99 (2019) 1255-1267.

[17] M. Pieckowski, P. Kowalski, T. Baczek, Combination of large volume sample stacking with polarity switching and cyclodextrin electrokinetic chromatography (LVSS-PS-CDEKC) for the determination of selected preservatives in pharmaceuticals, Talanta, 211 (2020).

[18] Y.X. Shao, G.H. Chen, R. Fang, L. Zhang, L.X. Yi, H.L. Meng, Analysis of Six beta-Lactam Residues in Milk and Egg by Micellar Electrokinetic Chromatography with Large-Volume Sample Stacking and Polarity Switching, J. Agric. Food Chem., 64 (2016) 3456-3461.
[19] S.Y. Lee, C.E. Muller, Large-volume sample stacking with polarity switching for monitoring of nucleotide pyrophosphatase/phosphodiesterase 1 (NPP1) reactions by capillary electrophoresis, Electrophoresis, 35 (2014) 855-863.
[20] L.X. Yi, G.H. Chen, R. Fang, L. Zhang, Y.X. Shao, P. Chen, X.X. Tao, On-line preconcentration and determination of six sulfonylurea herbicides in cereals by MEKC with large-volume sample stacking and polarity switching, Electrophoresis, 34 (2013) 1304-1311.
[21] A.V. Herrera-Herrera, L.M. Ravelo-Perez, J. Hernandez-Borges, M.M. Afonso, J.A. Palenzuela, M.A. Rodriguez-Delgado, Oxidized multi-walled carbon nanotubes for the dispersive solid-phase extraction of quinolone antibiotics from water samples using capillary electrophoresis and large volume sample stacking with polarity switching, J. Chromatogr. A, 1218 (2011) 5352-5361.
[22] J. Honegr, J. Safra, M. Polasek, M. Pospisilova, Large-Volume Sample Stacking with Polarity Switching in CE for Determination of Natural Polyphenols in Plant Extracts, Chromatographia, 72 (2010) 885-891.
[23] L. Yu, S.F.Y. Li, Large-volume sample stacking with polarity switching for the analysis of bacteria by capillary electrophoresis with laser-induced fluorescence detection, J. Chromatogr. A, 1161 (2007) 308-313.
[24] C.C. Wang, S.S. Chiou, S.M. Wu, Determination of mercaptopurine and its four metabolites by large-volume sample stacking with polarity switching in capillary electrophoresis, Electrophoresis, 26 (2005) 2637-2642.
[25] L. Sola, Chapter 3 - Column Technology for Capillary Electromigration Methods, in: C.F. Poole (Ed.) Capillary Electromigration Separation Methods, Elsevier2018, pp. 45-68.
[26] L. Hajba, A. Guttman, Recent advances in column coatings for capillary electrophoresis of proteins, Trac-Trend Anal. Chem., 90 (2017) 38-44.
[27] L.A. Kartsova, D.V. Makeeva, V.A. Davankov, Nano-sized polymer and polymer-coated particles in electrokinetic separations, TrAC Trend Anal. Chem., 120 (2019) 115656.
[28] D. Corradini, L. Sprecacenere, Dependence of the electroosmotic flow in bare fused-silica capillaries from pH, ionic strength and composition of electrolyte solutions tailored for protein capillary zone electrophoresis, Chromatographia, 58 (2003) 587-596.
[29] P.C. Hiemenz, Principles of Colloid and Surface Chemistry, Marcel Dekker, New York1986.
[30] F. Oukacine, M. Taverna, Suppression of apparent fluid flow in capillary isotachophoresis without recourse to capillary coating, Analytical chemistry, 86 (2014) 3317-3322.
[31] A. Wuethrich, P.R. Haddad, J.P. Quirino, Zero net-flow in capillary electrophoresis using acrylamide based hydrogel, Analyst, 139 (2014) 3722-3726.
[32] J.M. Busnel, A. Varenne, S. Descroix, G. Peltre, Y. Gohon, P. Gareil, Evaluation of capillary isoelectric focusing in glycerol-water media with a view to hydrophobic protein applications, Electrophoresis, 26 (2005) 3369-3379.
[33] T. Tsuda, K. Nomura, G. Nakagawa, Open-tubular microcapillary liquid chromatography with electro-osmosis flow using a UV detector, J. Chromatogr. A, 248 (1982) 241-247.
[34] B.B. VanOrman, G.G. Liversidge, G.L. McIntire, T.M. Olefirowicz, A.G. Ewing, Effects of buffer composition on electroosmotic flow in capillary electrophoresis, J. Microcolumn Separations, 2 (1990) 176-180.
[35] W.L. Ding, M.J. Thornton, J.S. Fritz, Capillary electrophoresis of anions at high salt concentrations, Electrophoresis, 19 (1998) 2133-2139.

[36] J.C. Reijenga, T. Verheggen, J. Martens, F.M. Everaerts, Buffer capacity, ionic strength and heat dissipation in capillary electrophoresis, J. Chromatogr. A, 744 (1996) 147-153.
[37] D.J. Pietrzyk, S. Chen, B. Chanthawat, Enhanced capillary zone electrophoretic separation of dinitrophenyl-amino acid derivatives through control of electroosmotic flow by the buffer cation, J. Chromatogr. A, 775 (1997) 327-338.
[38] M.M. Bushey, J.W. Jorgenson, CAPILLARY ELECTROPHORESIS OF PROTEINS IN BUFFERS CONTAINING HIGH-CONCENTRATIONS OF ZWITTERIONIC SALTS, J. Chromatogr., 480 (1989) 301-310.
[39] T.V. Popa, C.T. Mant, R.S. Hodges, Ion-interaction CZE: The presence of high concentrations of ion-pairing reagents demonstrates the complex mechanisms involved in peptide separations, Electrophoresis, 28 (2007) 2181-2190.
[40] D. Baron, J. Rozsypal, A. Michel, E. Secret, J.M. Siaugue, T. Pluhacek, J. Petr, Study of interactions between carboxylated core shell magnetic nanoparticles and polymyxin B by capillary electrophoresis with inductively coupled plasma mass spectrometry, J. Chromatogr. A, 1609 (2020).
[41] M. Girardot, F. d'Orlye, A. Varenne, Electrokinetic characterization of superparamagnetic nanoparticle-aptamer conjugates: design of new highly specific probes for miniaturized molecular diagnostics, Anal. Bioanal. Chem., 406 (2014) 1089-1098.
[42] F. d'Orlye, A. Varenne, P. Gareil, Size-based characterization of nanometric cationic maghemite particles using capillary zone electrophoresis, Electrophoresis, 29 (2008) 3768-3778.
[43] F. d'Orlye, A. Varenne, T. Georgelin, J.M. Siaugue, B. Teste, S. Descroix, P. Gareil, Charge-based characterization of nanometric cationic bifunctional maghemite/silica core/shell particles by capillary zone electrophoresis, Electrophoresis, 30 (2009) 2572-2582.
[44] M. Laurencin, T. Georgelin, B. Malezieux, J.M. Siaugue, C. Menager, Interactions Between Giant Unilamellar Vesicles and Charged Core-Shell Magnetic Nanoparticles, Langmuir, 26 (2010) 16025-16030.
[45] R. Massart, Preparation of aqueous magnetic liquids in alkaline and acidic media, Ieee Trans. Magn. , 17 (1981) 1247-1248.
[46] N. Fauconnier, A. Bee, J. Roger, J.N. Pons, Adsorption of gluconic and citric acids on maghemite particles in aqueous medium, in: C. Solans, M.R. Infante, M.J. GarciaCelma (Eds.) Prog. Colloid Polym. Sci.1996, pp. 212-216.
[47] B.A. Williams, C. Vigh, Fast, accurate mobility determination method for capillary electrophoresis, Anal. Chem., 68 (1996) 1174-1180.
[48] K. Mesbah, T.D. Mai, T.G. Jensen, L. Sola, M. Chiari, J.P. Kutter, M. Taverna, A neutral polyacrylate copolymer coating for surface modification of thiol-ene microchannels for improved performance of protein separation by microchip electrophoresis, Microchim. Acta, 183 (2016) 2111-2121.
[49] T.D. Mai, F. d'Orlye, A. Varenne, A Comprehensive Study of Silanization and Co-Condensation for Straightforward Single-Step Covalent Neutral Capillary Coating, Chromatographia, 78 (2015) 775-783.
[50] C.C. de Lassichere, T.D. Mai, M. Otto, M. Taverna, Online Preconcentration in Capillaries by Multiple Large-Volume Sample Stacking: An Alternative to Immunoassays for Quantification of Amyloid Beta Peptides Biomarkers in Cerebrospinal Fluid, Anal. Chem., 90 (2018) 2555-2563.
[51] M.U. Musheev, Y. Filiptsev, S.N. Krylov, Noncooled Capillary Inlet: A Source of Systematic Errors in Capillary-Electrophoresis-Based Affinity Analyses, Anal. Chem., 82 (2010) 8637-8641.
[52] V. Sladkov, Effect of non-thermostated capillary inlet in affinity capillary electrophoresis: Uranyl-selenate system at variable temperatures, J. Chromatogr. A, 1263 (2012) 189-193.

[53] M. Morani, M. Taverna, T.D. Mai, A fresh look into background electrolyte selection for capillary electrophoresis-laser induced fluorescence of peptides and proteins, Electrophoresis, 40 (2019) 2618-2624.
[54] D. Corradini, G. Cannarsa, E. Fabbri, C. Corradini, Effects of alkylamines on electroosmotic flow and protein migration behaviour in capillary electrophoresis
J. Chromatogr. A, 709 (1995) 127-134.
[55] Analis, PhoEBuS software, http://5.189.177.170/~analis/site/objects/media/0/0/5/0/9/0050933_media/media1.pdf, (1996).
[56] Y. Wu, Z. Lu, Y. Li, J. Yang, X. Zhang, Surface Modification of Iron Oxide-Based Magnetic Nanoparticles for Cerebral Theranostics: Application and Prospection, Nanomaterials, 10 (2020) 1441.
[57] K. Li, H. Nejadnik, H.E. Daldrup-Link, Next-generation superparamagnetic iron oxide nanoparticles for cancer theranostics, Drug Discov. Today, 22 (2017) 1421-1429.

Electronic supplementary data

Electroosmotic flow modulation for improved electrokinetic preconcentration : application to capillary electrophoresis of fluorescent magnetic nanoparticles

Ngoc Van Thanh Nguyen[1], Claire Smadja[1]*, Myriam Taverna[1,2], Sirine El Mousli[3], Emilie Secret[3], Jean-Michel Siaugue[3], Lac Thuy Huu Nguyen[4] and Thanh Duc Mai [1]*

[1] *Université Paris-Saclay, CNRS, Institut Galien Paris-Saclay, 92296, Châtenay-Malabry, France*

[2] *Institut Universitaire de France (IUF)*

[3] *Sorbonne Université, CNRS, Physico-chimie des Électrolytes et Nanosystèmes Interfaciaux, PHENIX, F-75005 Paris, France*

[4] *Faculty of Pharmacy - University of Medicine and Pharmacy at Ho Chi Minh City - 41 Dinh Tien Hoang St., Ben Nghe Ward, District 1, Ho Chi Minh City, Vietnam*

Correspondence: E-mail: thanh-duc.mai@u-psud.fr;

claire.smadja@u-psud.fr

Keywords: capillary electrophoresis; fluorescence detection; stacking; preconcentration; EOF suppression and modulation; magnetic nanoparticles

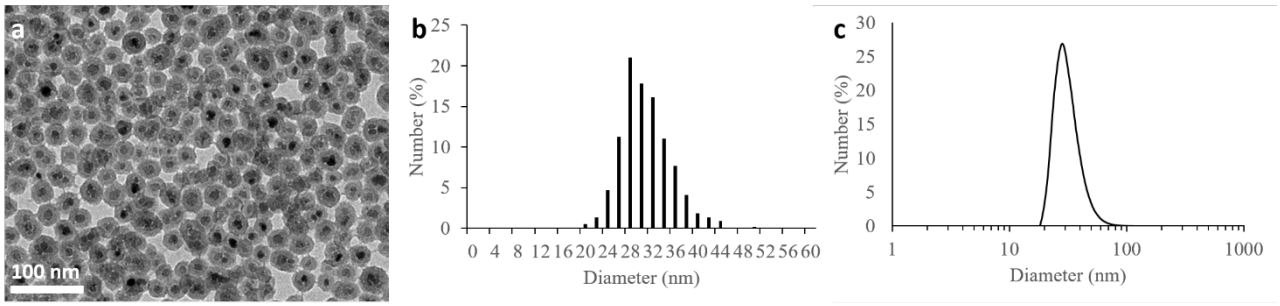

Fig. S1: a) Transmission electron microscopy or the Fe_2O_3@SiO_2-COOH MNPs. b) Physical diameter distribution obtained by TEM image analysis. The average physical diameter of the MNPs is 31.7 ± 4.4 nm. c) Hydrodynamic diameter of the MNPs obtained by dynamic light scattering. The MNPs have a hydrodynamic diameter of 32 nm with a polydispersity index of 0.25.

Fig. S2. The electrical field versus current profiles for different tested BGEs at their highest ionic strengths. The currents were measured on applying variable voltages over a 60.2 cm long uncoated fused silica capillary with i.d. of 50 µm.

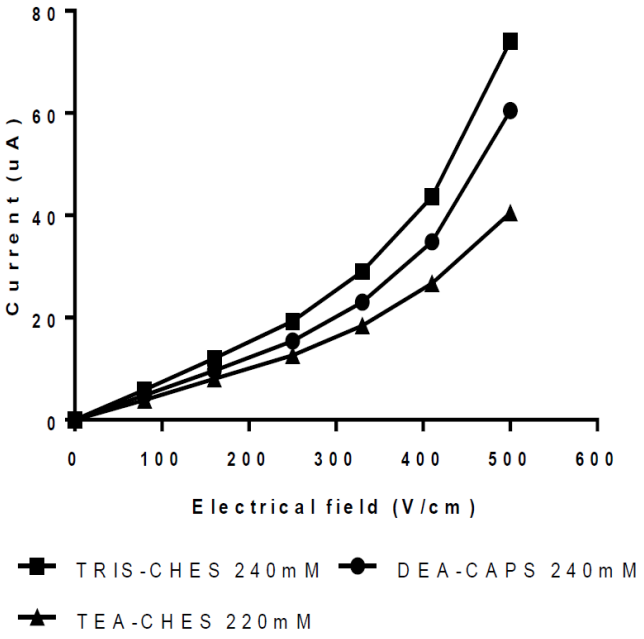

Fig. S3. Optimization of background electrolyte compositions for CE-LIF analysis of core-shell magnetic nanoparticles (CSMNPs). A) TEA / MOPS (pH 7.4), B) DEA / MOPS (pH 7.4), C) TRIS / MOPS (pH 7.4), D) TRIS / CHES (pH 8.4), E) DEA / CAPS (pH 9.7). CE conditions: capillary having ID of 50 µm, total length of 60 cm, effective length of 35 cm; high voltage of 25 kV; sample: CSMNPs in 10-fold diluted BGE; hydrodynamic injection at 50 mbar over 30 s. Fluorescent detection at excitation and emission wavelengths of 480 nm and 520 nm respectively.

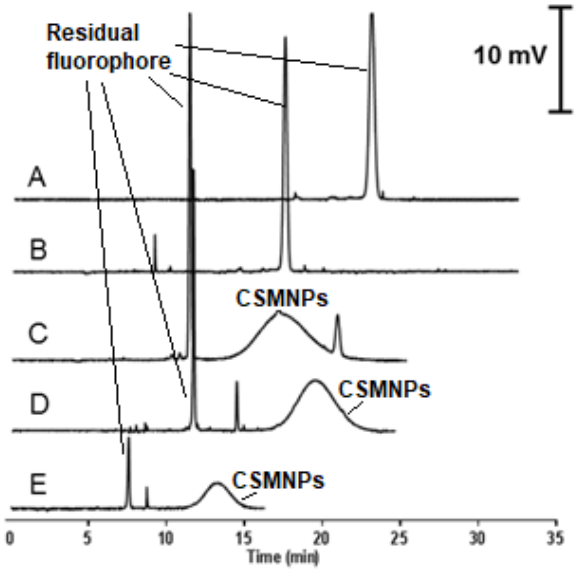

Fig. S4. CE-LIF of the commercial fluorescent latex NPs 30 nm (A) and CSMNPs (B).The nanoparticles were prepared in 10-fold diluted BGE; hydrodynamic injection at 50 mbar over 30 s. BGE composed of Tris / CHES (100 mM, pH 8.4). Fluorescent detection at excitation and emission wavelengths of 480 nm and 520 nm respectively. (C) Size distribution profile of latex NPs 30 nm.

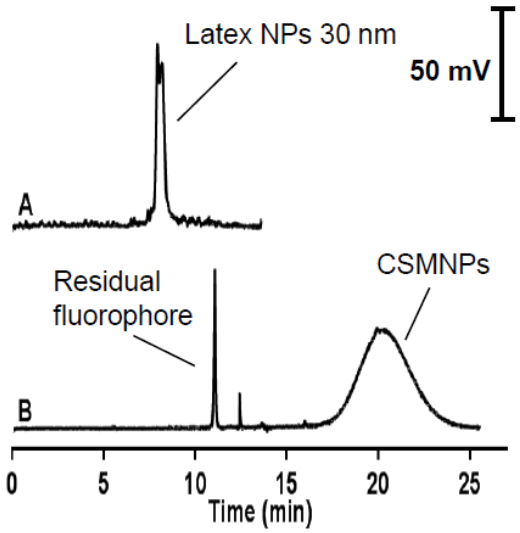

C)

		Size (d.nm...	% Intensity:	St Dev (d.n...
Z-Average (d.nm): 33,89	Peak 1:	36,45	100,0	11,20
PdI: 0,129	Peak 2:	0,000	0,0	0,000
Intercept: 0,969	Peak 3:	0,000	0,0	0,000
Result quality Good				

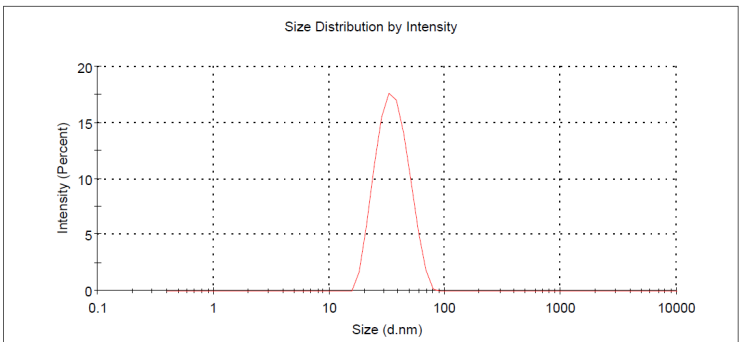

Fig. S5. Optimization of LVSPS for CSMNPs preconcentration. A) Inlet BGE of Tris/CHES 100 mM, outlet BGE of 100 mM; B) Inlet BGE of Tris/CHES 100 mM, outlet BGE of 140 mM; C) Inlet BGE of Tris/CHES 80 mM, outlet BGE of 120 mM; D) Inlet BGE of Tris/CHES 100 mM, outlet BGE of 120 mM; E) Inlet BGE of Tris/CHES 120 mM, outlet BGE of 100 mM; F) Inlet BGE of Tris/CHES 140 mM, outlet BGE of 100 mM; G) Inlet BGE of Tris/CHES 120 mM, outlet BGE of 80 mM. Sample: CSMNPs diluted 4000x in Tris/CHES 10 mM; hydrodynamic injection at 50 mbar over 840s to fill 100 % of the capillary volume. Preconcentration was carried out under -25kV (negative polarity) over 5 min. The polarity of the high voltage was then reversed to trigger CZE separation of the stacked CSMNPs. Fluorescent detection at excitation and emission wavelengths of 480 nm and 520 nm respectively.

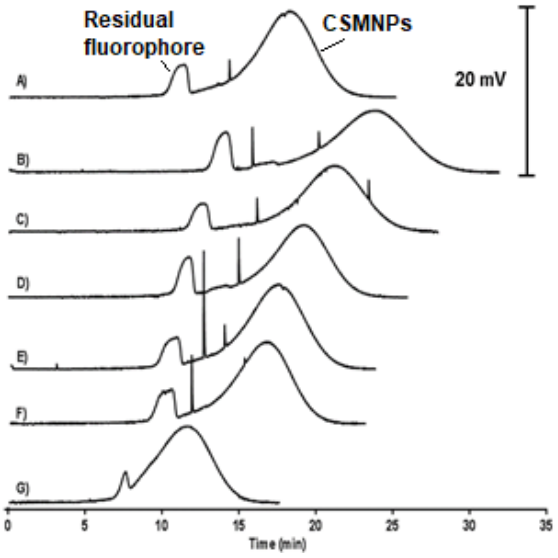

Fig. S6. Repeatability of LVSPS for CSMNPs preconcentration. Inlet BGE of Tris/CHES 100 mM, outlet BGE of 100 mM. Other conditions as in Fig. S5.

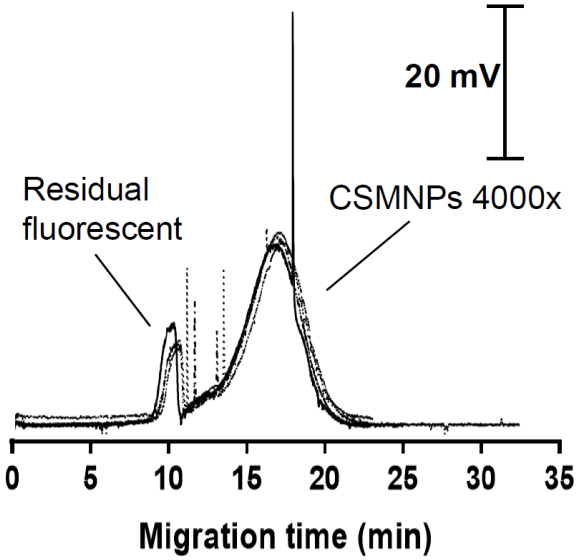

Fig. S7. Chemical structure of antibiotics A) Amikacine and b) Kanamycine

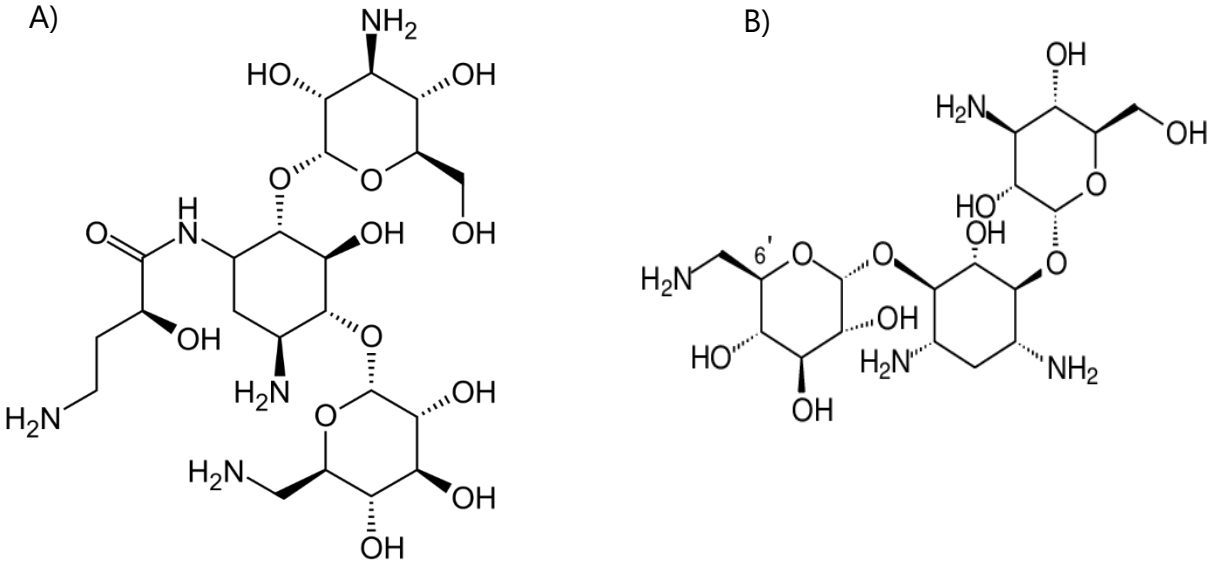

Table S1: µEO values for different BGEs measured with conventional method and Williams and Vigh's one

Buffers	EOF short end ($cm^2/V/s$)	Vigh's method ($cm^2/V/s$)
Tris- CHES 200 mM pH 8.4	8.90E-05 (RSD 0.94 %)	8.94E-05 (RSD 0.64 %)
DEA- CAPS 200 mM pH 9.5	9.56E-05 (RSD 0.59 %)	8.46E-05 (RSD 0.55 %)

Table S2: CSMNPs sizes measured with DLS at different times after dispersion in tested buffers having IS of 100 mM

Buffers	**Size (nm)**	
	Day 1	***Day 4***
TEA- MOPS	41.81	40.31
DEA- MOPS	44.92	46.91
Tris- MOPS	48.21	47.14
Tris- CHES	54.71	61.49
DEA- CAPS	52.32	52.19

Table S3: zeta potential of MNPs dispersed in different buffers

BGE	Zeta potential (mV)
TEA- MOPS, IS 100 mM – pH 7.2	-9.41
DEA- MOPS, IS 100 mM – pH 7.2	-16.2
Tris- MOPS, IS 100 mM – pH 7.2	-22.3
Tris- CHES, IS 100 mM – pH 8.4	-23.8
Tris- CHES IS 80 mM – pH 8.4	-25.7
Tris- CHES IS 120 mM – pH 8.4	-16.5
Tris- CHES IS 140 mM – pH 8.4	-12.9

4.2 EOF-ASSISTED PRECONCENTRATION IN CE-LIF FOR AB 1-42 PEPTIDE

With the aim to extend the application scope of our IS-based electrokinetic preconcentration approach for CE, I also put my effort to apply the LVSS method using BGE composed of large weakly charged molecules for preconcentration and detection of Aβ 1-42 peptide, which is a validated biomarker for molecular diagnosis of AD (see chapter II.3 for more details).

Among the tested BGEs, TRIS-CHES at IS of 90mM at pH of 8.7 was found to provide the best CE-LIF signal of Aβ 1-42 labelled with Fluoprobe 488 NHS ester. In addition, the peptide is stable in basic pH, which explains the choice of the working pH. The electropherograms are showed in *Figure 35*.

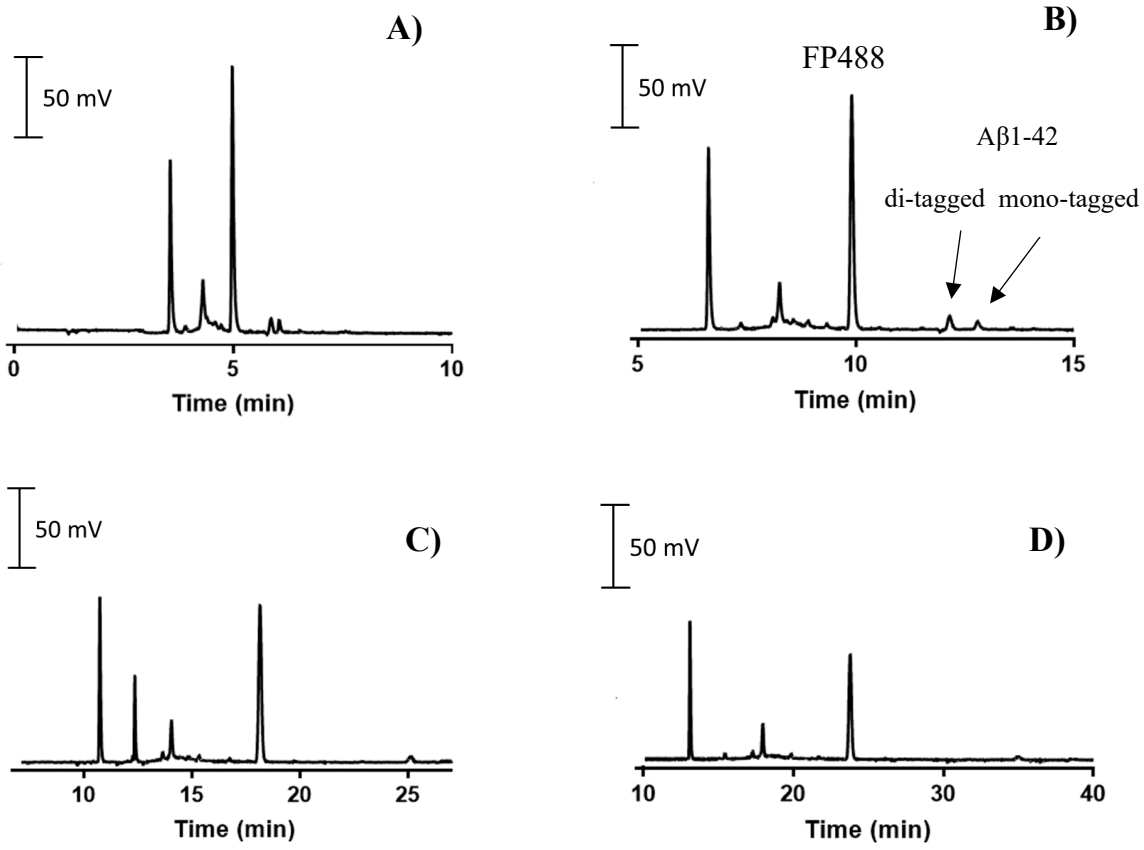

Figure 35: Electropherogram of 20 nM Aβ 1-42, labelled with FP488, diluted in TRIS-CHES 5 mM and separated by normal CE-LIF using TRIS-CHES buffer (pH 8.7) at IS of A) 30 mM; B) 90 mM; C) 120 mM; D) 140 mM. CE conditions: Fused silica capillary (total length 60 cm, effective length 50 cm, inner diameter 50 µm), electrical field 30 kV, injection time 30s under 50 mbar. λexcitation 488 nm and λemission 530 nm.

As can be seen in the *Figure 35* A) and B), there are two small peaks of Aβ 1-42 due to the labelling

on one or two lysine of the peptide, resulting in the peak of di-tagged and mono-tagged. The peak of residual fluorophore, which was not completely removed by filtration after the labeling step, was observed. TRIS-CHES 140 mM was selected for LVSS-CE-LIF of Aβ 1-42 peptide as the BGE at a very high IS was needed for EOF suppression and for significant stacking effect. The electropherogram of Aβ 1-42 peptide at 5 nm and 1 nm after the LVSS preconcentration are illustrated in *Figure 36*.

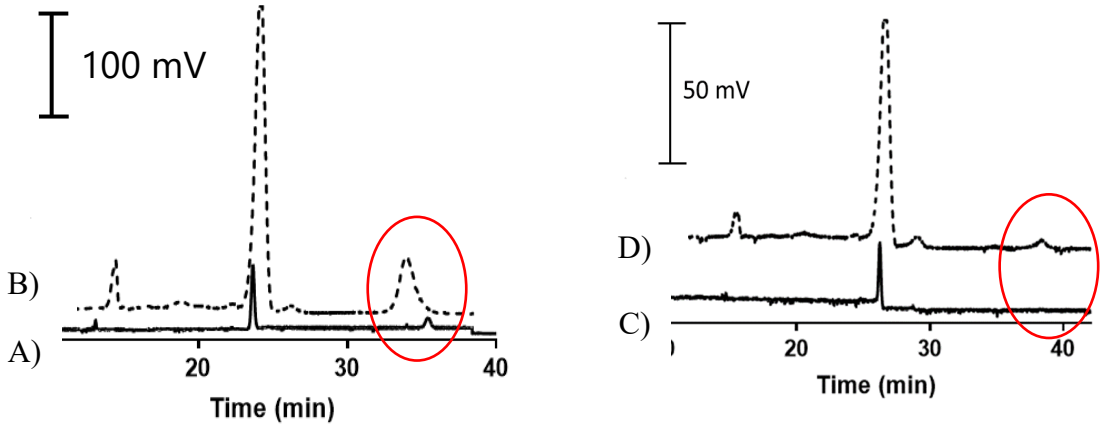

Figure 36: Electropherogram of Aβ 1-42, labelled by FP488, diluted in TRIS-CHES 5 mM and separated in TRIS-CHES 140 mM at pH 8.7 by either normal CE-LIF for Aβ 1-42 (A) 5 nM and (C) 1 nM (with injected sample volume accounting for 100 % of the total capillary volume) or LVSS with polarity switching prior to CE-LIF for Aβ 1-42 B) 5 nM and D) 1 nM. CE conditions were same as described in Figure 35, for electropherograms B and D. Polarity was switched after 5 minutes of LVSS.

The obtained enrichment factor is 18-fold, based on peak area of 5 nM Aβ 1-42. The developed method holds the potential to be used for real samples in biofluids in the next stage of the project, in order to sensitively detect Aβ 1-42, and expand to other Aβ peptides (such as Aβ 1-40 and Aβ 1-38), serving for improvement of molecular diagnosis of AD based on separation and detection of these peptides.

4.3 Conclusion

The electrokinetic preconcentration via EOF modulation was successfully demonstrated for MNPs separation and detection under alkaline conditions in CE-LIF. Compared to normal CE-LIF method, sensitivity improvement by 340 times was achieved. Additionally, EOF can be suppressed down to 2.10^{-5} ($cm^2.V^{-1}.s^{-1}$) in fused-silica capillary without recourse to any capillary coating or

gel addition and can be modulated in a wide range just by changing the BGE's IS. The application of this electrokinetic preconcentration method for Aβ 1-42 peptide determination was also demonstrated. This approach will be for other biomolecules in the next stage phase of the work.

Chapter 5: New on-line operation in CE for DNA extraction, preconcentration and detection

The advantages features of MNPs in sample preconcentration and the extraction, in which the target molecules are captured on bead's surface are presented in chapter 1 and 2. This chapter will present the development of a new dual-stage on-line operation, combining sample extraction on magnetic beads and electrokinetic preconcentration of the extracted analyte prior to its separation with CE-LIF, allowing to avoid laborious off-line sample treatment, contamination from external environment, and mismatch of the working volumes between different steps. Accordingly, a new instrumental setup was developed to precisely manipulate the magnetic beads and realize several sample treatment steps inside the CE capillary. This novel concept and instrument were applied for dsDNA extraction and separation. The work was published on Analytica Chemica Acta.

5.1 On-line dual-stage enrichment via magneto-extraction and electrokinetic preconcentration: a new concept and instrumentation for capillary electrophoresis (PAPER 3)

Highlights:

- In-capillary magneto-extraction and electrokinetic preconcentration of analytes.
- A new microfluidic and electrokinetic setup for on-line dual-stage enrichments
- The new dual-stage enrichment approach and setup for DNA purification and detection.

On-line dual-stage enrichment via magneto-extraction and electrokinetic preconcentration: a new concept and instrumentation for capillary electrophoresis

Ngoc Van Thanh Nguyen[1], Claire Smadja[1*], Myriam Taverna[1,2], Lac Thuy Huu Nguyen [3], Stéphanie Descroix[4], Thanh Duc Mai[1*]

[1] *Université Paris-Saclay, CNRS, Institut Galien Paris-Saclay, 91400, Orsay, France.*

[2] *Institut Universitaire de France (IUF)*

[3] *Faculty of Pharmacy - University of Medicine and Pharmacy at Ho Chi Minh City - 41 Dinh Tien Hoang St., Ben Nghe Ward, District 1, Ho Chi Minh City, Vietnam*

[4] *Laboratoire Physico Chimie Curie, Institut Curie, PSL Research University, CNRS UMR168, 75005, Paris, France*

* Corresponding author

e-mail: thanh-duc.mai@universite-paris-saclay.fr

claire.smadja@universite-paris-saclay.fr

Keywords: Capillary electrophoresis, Magneto-capture, Magnetic beads, DNA; Fluorescent detection; Electrokinetic preconcentration

Abstract

This study reports on the development of a new concept of on-line dual preconcentration stages for capillary electrophoresis (CE), in which two completely different preconcentration approaches can be realized in the same capillary. In the first stage, a dynamic magneto-extraction of target analytes on circulating magnetic beads is implemented within the capillary. In the second one, electrokinetic preconcentration of eluted analytes via large volume sample stacking is carried out to focus them into a nano band, prior to CE separation of enriched analytes. To implement the dual-stage preconcentration operation, a purpose-made instrument was designed, combining electrophoretic and microfluidic modules to allow precise control of the movement of the magnetic beads and analyte's flows. The potential of this new enrichment principle and its associated instrument were demonstrated for CE separation with light-emitting-diode-induced fluorescent (LEDIF) detection of target double-stranded DNA (ds-DNA). The workflow consists of purification and preconcentration of a target DNA fragment (300 bp) on negatively charged magnetic beads, followed by in-capillary elution and fluorescent labelling of the enriched DNA. Large volume sample stacking of the DNA eluent was then triggered to further preconcentrate the labelled DNA before its CE-LEDIF analysis. An enrichment factor of 125 was achieved for the target DNA fragment. With our new approach, dual-stage sample pretreatment and CE separation can now be performed in-capillary without any mismatch of working volumes, nor any waste of pretreated samples.

1. Introduction

When using capillary electrophoresis (CE) for the analysis of biomolecules, sample pretreatment techniques are normally required for matrix removal and preconcentration of target analytes at trace levels in complex matrices [1]. Among different strategies for sample processing, solid-phase enrichment/extraction on magnetic beads, called magneto-extraction, in which target analytes are captured on magnetic particles, attracts much attention in recent years as this strategy offers higher throughput and ease of manipulation through external magnetic fields compared to conventional solid phase extraction [2]. The combination of magneto-extraction and capillary electrophoresis (CE) offers several advantageous features as it combines the high enrichment capability offered by functionalized magnetic beads and the high separation power of CE. So far on-line magneto-extraction and CE have been mostly performed by trapping magnetic particles inside a capillary via permanent magnets [3-8]. Commercial CE instruments can serve for this purpose in some cases. In our recent work using either microfluidic fluidized beds [9], micro/nanometric droplets [10], or a CE capillary [11] as the microreactor, we nevertheless demonstrated that the efficiency of analyte extraction is much improved when using circulating magnetic beads instead of bead cluster, regardless of the microreactor design used.

In a related context, electrokinetic preconcentration strategies, notably large volume sample stacking (LVSS) and isotachophoresis (ITP), have been often used in CE to enhance the detection sensitivity [1, 12, 13]. When using electrokinetic approaches for on-line sample enrichment, samples are normally injected up to 100 % of the capillary volume and the target analytes filled in the whole capillary are then stacked into a nano band at one extremity of the capillary prior to their separation by CE. Among different approaches developed so far, LVSS has been favorably used in many cases using neutrally coated capillaries for the determination of biomolecules and pharmaceutical compounds thanks to the capability of maintaining high separation resolution after the preconcentration step [14-16]. Different strategies have recently been developed to further improve the performance of LVSS, for instance the multiple cycles of LVSS for sensitive detection of beta amyloid peptides [17], combination of LVSS with dynamic pH-junction for determination of urinary nucleosides [18], as well as LVSS under high ionic strengths and with modulation of the electro-osmotic flow (EOF) for separation and detection of magnetic nanoparticles [19] and carbohydrates [20]. When using electrokinetic preconcentration in general, or LVSS in particular, off-line forefront sample treatment (e.g., filtration, solid-phase extraction, dialysis, etc.) is normally required, especially for biofluids, to render the matrix compatible with electrokinetic

preconcentration (i.e., low conductivity) and/or to remove possible interferants that may be co-enriched and overlap the peaks of target analytes. On-line matrix removal and electrokinetic preconcentration prior to CE separation of biomolecules are therefore desirable to allow full automation (thus high throughput) and integration of all steps into the same separation capillary without any problem of working volume mismatch and contamination from the external environment.

We report in this study the development of a new enrichment concept for CE, where dual stages of dynamic magneto-extraction on circulating magnetic beads and electrokinetic preconcentration are performed in the same CE capillary. For this purpose, a new instrumental setup was developed, exploiting new features offered by microfluidics to allow precise back-and-forth manipulation of flows inside the separation capillary. The new concept and instrument were demonstrated for purification and sensitive detection of a target double-stranded DNA (ds-DNA 300bp). Indeed, DNA fragments are often used as starting materials for molecular diagnostic applications, in which sample preparation is of utmost importance to obtain pure target DNA fragments from complex matrices. For CE analysis of DNA fragments, isotachophoresis (ITP) is an electrokinetic preconcentration mode normally used either for DNA purification prior to off-line analysis [21-23] or for on-line DNA enrichment prior to their CE separation [24, 25]. The group of Foret and Datinska have recently introduced a DNA purification method on agarose gel based on a new electrokinetic concept called epitachophoresis [26, 27]. Following this topic, we herein developed a new CE method coupled with light-emitting-diode-induced fluorescence (LEDIF) detection for double-stranded DNA analysis that combines several steps in the same capillary, including purification of the target DNA fragment by dynamic magneto-extraction, fluorescent labeling of extracted DNA with a new fluorophore family, electrokinetic preconcentration of the labeled DNA fragment, prior to its analysis by CE-LEDIF.

2. Experimental

2.1. Chemicals, reagents, and samples

2-(cyclohexylamino)ethanesulfonic acid (CHES), 3-(cyclohexylamino)-1-propanesulfonic acid (CAPS), 3-(N-morpholino)propanesulfonic acid (MOPS), triethanolamine (TEA, ≥98%), diethanolamine (DEA, ≥98%), tris(hydroxymethyl)aminomethane (TRIS), sodium hydroxide (NaOH), Gelgreen 10000X in water were obtained from Sigma (St. Louis, MO, United States).

Ampure XP (pH 8.0- 8.4; Specific gravity 1.127 (water = 1); conductivity 93- 99 (mS/cm)) was purchased from Beckman (Sciex Separation, Brea, CA). The GeneRuler™ Low Range DNA Ladder and DNA NoLimit 300bp at 0.5 µg/ µL were provided by Thermo Fisher (Massachusetts, USA). All buffers were prepared with deionized water and were filtered through a 0.22 µm membranes (Pall Corporation, New York, USA) prior to use.

2.2. Apparatus and Material

Polyimide coated fused silica capillaries of 50 µm id and 375 µm od (TSP050375, Polymicro, CM Scientific, Silsden, UK) or UV transparent coated fused silica capillaries of 50 µm id and 375 µm od (TSH050375, CM Scientific, Silsden, UK) were used for all CE experiments. The off-line methods were developed using a Beckman Coulter MDQ system (Sciex Separation, Brea, CA, USA) equipped with a LEDIF (with $\lambda_{excitation}$: 480 nm, $\lambda_{emission}$: 520 nm, Adelis, Labege, France). Data acquisition for fluorescence detection was carried out with Power Chrome software (eDAQ, Australia). Deionized water used in all experiments was purified using a Direct-Q3 UV purification system (Millipore, Milford, MA, USA). Conductivity and pH values of buffer solutions and samples were measured with a Seven Compact pH meter (Mettler Toledo, Schwerzenbach, Switzerland). Selection of background electrolyte (BGE) and buffer IS calculations were simulated with the computer program PhoeBus (Analis, Suarlée, Belgium). The Minitab statistical software 17 was used to design the two-level-three-factors (3^2) ½ fraction experiments for DNA labelling protocol. Fluorescence spectra were measured with a FP-750 Spectrofluorometer from Jasco (Lisses, France) at the excitation and emission wavelengths of 488 nm and 530 nm, respectively using a 40 µL quartz cuvette (Starna Scientific, Essex, England).

For the purpose-made instrument (see photos in Fig. S1 in the supporting information ESI, and more details in section 3.1 below), all fluid connections were made with 0.02 in. inner diameter (id) and 1/16 in. outer diameter (od) PFA tubing (Upchurch). The electrophoresis module, constructed according to our recent modular design [28], was based on a dual polarity high voltage power supply (HVPS for CZE, Villa Labeco, Slovakia) and the microfluidic manifold (ElectroWell) purchased from Fluigent (Paris, France). Capillary flushing and sample injection were implemented with a pressure and vacuum controller (PushPull, Fluigent) connected to a vacuum pump (MZNT, Vacuubrand, Wertheim, Germany) and a compressed air generator (FLPG, Plus, Fluigent). Fluorescent detection was carried out with a LED induced fluorescence (LEDIF,

Zetalif) detector purchased from Adelis (Toulouse, France). The resulting signal was recorded with a Mini-corder ER180R data acquisition system (eDAQ Europe, Warsaw, Poland) connected to the USB-port of a personal computer. The magnetic tweezers were produced in-house according to the design reported elsewhere [10, 29]. They are composed of a couple of ferromagnetic tips activated by magnetic coils (product No 357-788, RS Components SAS, Beauvais, France). Two cameras for bead observation were purchased from Dino Lite (product no. AM4113ZT, Ludres, France).

A)

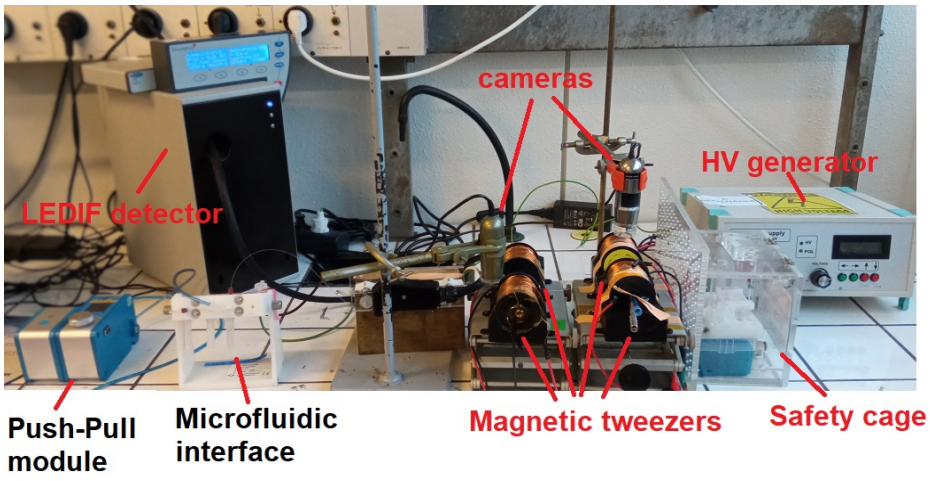

B)

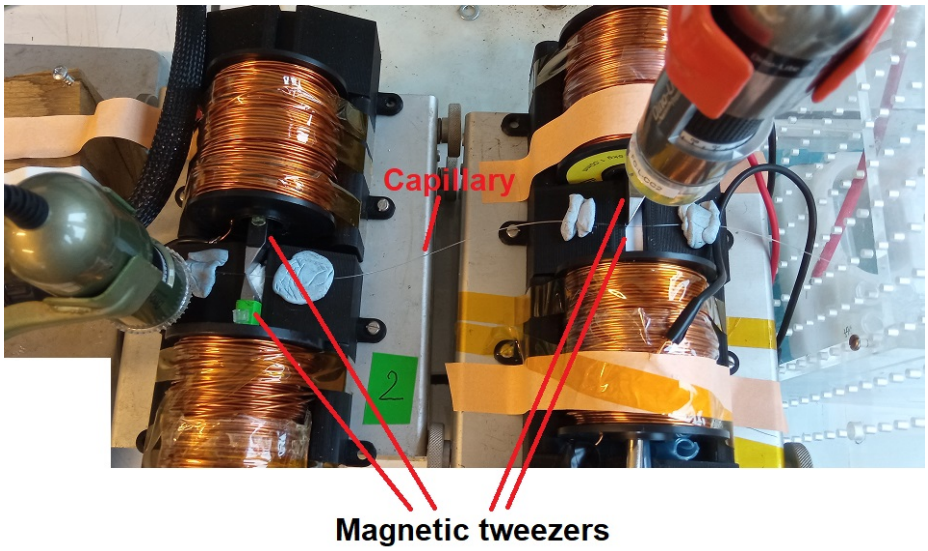

Fig. S1. A) Photo of the purpose-made instrument for on-line dual-layer enrichment for CE-LEDIF analysis. B) Zoom in the setup of four pairs of magnetic tweezers for magnetic bead capture in a 50 µm I.D. capillary

2.3. Methods

Off-line fluorescent labelling of dsDNA for CE-LEDIF

Gelgreen 3X was daily prepared by adding 1 µL Gelgreen 10000X to 3.3 mL deionized water. The dsDNA stock solution at concentration of 10 ng/µL was prepared by diluting 2 µL of the dsDNA ladder or a dsDNA fragment (300bp) at 0.5 µg/µL with 98 µL water. These stock solutions could be stored at 4ºC for one week. The dsDNA solutions at desired concentrations were obtained by diluting the stock dsDNA solution in water. For dsDNA fluorescent labeling, 10 µL of Gelgreen 3X was mixed with 50 µL of the dsDNA solution. This mixture was incubated at 20ºC for 25 minutes on a compact Thermomixter (Eppendorf, Hambourg, Germany) at 300 rpm. Further information on optimization of the dsDNA labelling procedure can be referred to section 3.2.

Purification of dsDNA by Ampure XP

180 µL of dsDNA solution was incubated with 324 µL of Ampure XP at room temperature for 20 minutes on a Thermomixer at 650 rpm. Next, the supernatant was separated from magnetic beads with the help of a magnet. 60 µL of Gelgreen 3X was then added to the magnetic beads and the suspension was incubated at 20ºC for 25 minutes on a Thermomixter at 300 rpm to release and label the target DNA. Finally, the supernatant was collected and transferred to a vial for subsequent analysis.

CE-LEDIF for separation and detection of dsDNA using the MDQ system

Prior to the first use, the silica capillary, with I.D. of 50 µm, effective length (L_{eff}) of 40 cm for LEDIF detection and total length (L_{tot}) of 70 cm, was preconditioned with the following sequence: NaOH 1 M for 5 min, DI water for 5 min, then BGE (composed of diethanolamine / CHES at ionic strength of 40 mM, i.e., diethanolamine concentration of 60 mM and CHES concentration of 233 mM, and pH 8.4) for 30 min. Between each analysis, the capillary was rinsed with NaOH for 5 min, then DI water for 3 min and BGE for 10 min. DNA samples (dsDNA ladder or 300bp fragment) were hydrodynamically injected at 50 mbar for 15 s. The separation was performed under 25 kV at 25ºC. All measurements were performed in triplicate.

Large volume sample stacking (LVSS) with polarity switching using the MDQ system

The DNA sample (dsDNA ladder or 300bp fragment) was filled to 60% of the capillary volume. A high voltage of - 25 kV was applied at the inlet of the capillary for 2.5 min and the current was monitored during this process. When the current reached the stable value, the polarity of the high voltage was immediately switched to trigger the separation. The separation was conducted under 25 kV.

3. Results and Discussion

3.1. Principle of on-line dual-stage enrichment and instrumental conception

The schematic outline of on-line dual-stage enrichment concept is demonstrated in Fig. 1. Functionalized magnetic beads are first injected into the capillary via hydrodynamic injection, and then trapped or released thanks to the magnetic tweezers positioned in proximity of the capillary inlet and outlet. By alternatively switching on/off the two magnetic tweezers and applying a back-and-forth hydrodynamic flow, the magnetic beads can circulate between the two pairs of magnetic tweezers (steps 1 - 2) in order to implement efficient magneto-extraction of target analytes. After their extraction, the target analytes are released by flowing a given volume (smaller than the total capillary volume) of an eluting solution. The elution step takes place in the absence of magnetic field to have access to the whole beads surface (step 3). Subsequently, a high voltage is applied to trigger the preconcentration step (steps 4-5). The online electrokinetic preconcentration via LVSS is required to stack the analytes that are eluted from the magnetic beads into a large elution volume (more than 50 % of the total capillary volume). In principle, CZE separation should be done with an injected sample plug accounting for less than 2 % of the total capillary volume to avoid peak band broadening. However, if such a small plug of eluent is used, this tiny eluent plug that will serve as the sample plug for subsequent CE separation can be easily diluted by the surrounding background electrolyte. Furthermore, the beads cannot circulate in this small volume for efficient analyte elution. To overcome this challenge, we employed a large elution volume to improve the elution efficiency. This comes with the need of the second stage of electrokinetic preconcentration to bring the eluted analytes into a nano band prior to their separation. This is indeed the significance of our on-line dual-stage enrichment approach. The enriched analytes were then separated by CE in the same capillary under a high voltage without any loss of sample (step 6). Note that during the electrokinetic preconcentration and CE separation of eluted analytes, the magnetic tweezers should be turned off to release the magnetic beads in the absence of a hydrodynamic flow (see section 3.3 below for more details). After the CE separation, beads are removed from the capillary by flushing

with BGE while the magnetic tweezers are deactivated (step 7). In principle, the sample can be allowed to flow back and forth with the circulating beads in the capillary to further improve the extraction efficiency. The beads are expected to repeat the circle of 'circulation – packing – recirculation – packing' between two magnetic tweezers. Nevertheless, in this proof-of-concept work, the cycle number in each step of the proposed protocol (7 steps, Fig. 1) was kept minimum to avoid too many uncertainties during the system development and methodology optimization.

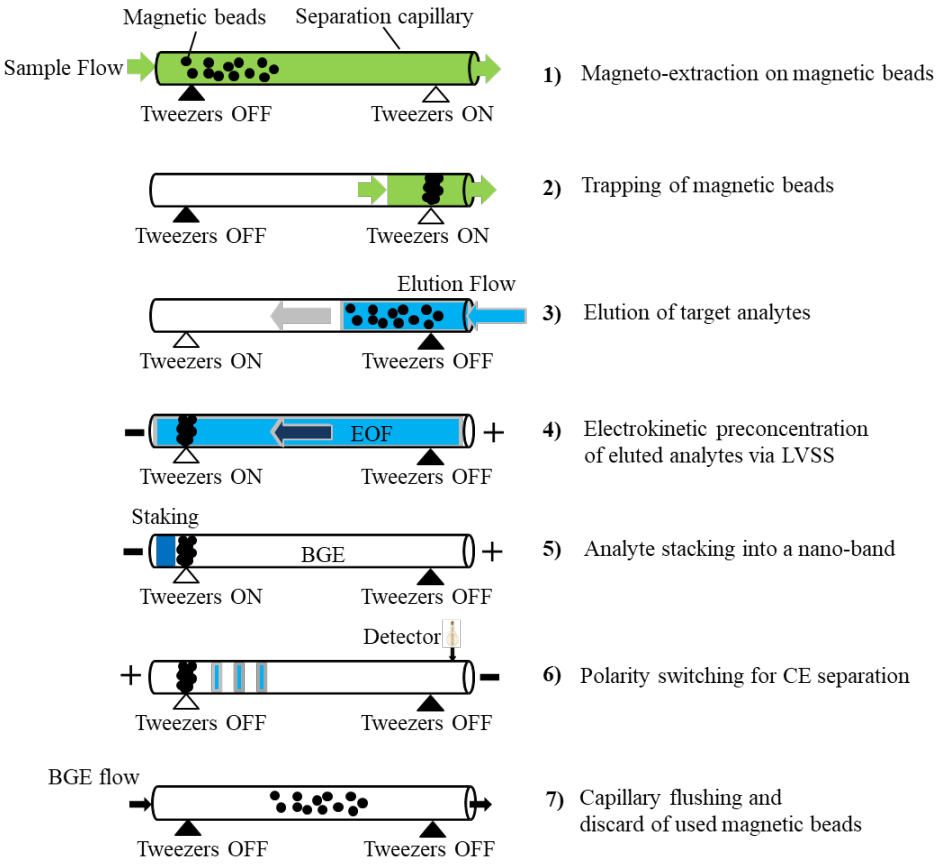

Fig. 1. Proposed principle of on-line dual-stage enrichment for CE, with magneto-extraction on circulating magnetic beads and electrokinetic preconcentration.

Such operations with circulating magnetic beads (rather than with bead clusters using permanent magnets), which allow for the first time two stages of on-line preconcentration via extraction on beads and subsequently electrokinetic preconcentration, cannot be performed so far with any commercial CE instrument, to the best of our knowledge.

We thus designed and built on purpose a CE instrument that hyphenates microfluidic, magnetic and electrophoretic operations. A schematic design of the system and the setup of magnetic tweezers are shown in Fig. 2A and Fig. 2B, respectively.

A)

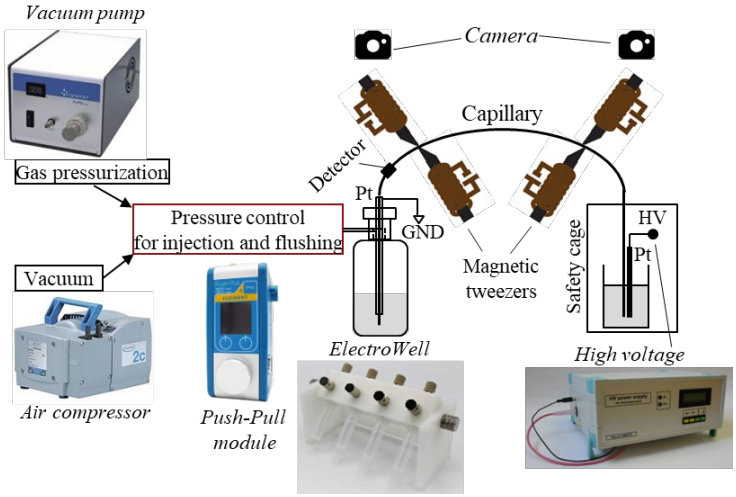

B)

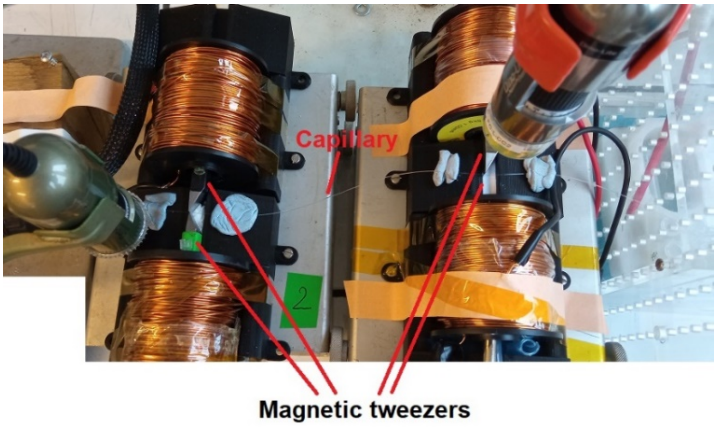

Fig. 2. A) Simplified schematic drawing of the purpose-made instrument. HV: high voltage; GND: electrical ground; Pt: platinum electrodes. B) Photo of the magnetic tweezer setup.

Extensions and modifications have been made to our previous CE designs [11, 28] in order to incorporate advanced features that were not possible in any precedent purpose-made CE instrument. These advanced features include i) precise manipulation of solutions and beads suspension with both vacuum and pressurization, and ii) controllable capture and release of magnetic beads in capillaries of 50 µm I.D. A newly released off-the-shelf push-and-pull module, conventionally used to generate micro- and nano-flows in microfluidics, was employed for CE injection and capillary flushing in our system. The negative and positive pressures required for

back-and-forth flow can be triggered, altered and monitored via a knob and a display integrated on this push-and-pull module (manual mode) or with a computer (automatic mode). Thanks to this new microfluidic setup with the negative and positive pressure controls, the sample can be aspirated back to the capillary for recirculation if required and therefore it is not unintentionally lost out of the capillary outlet. To efficiently trap magnetic beads (Ampure XP beads) inside a 50 µm I.D. capillary, our preliminary tests with a single magnetic tweezer (as in our previous work on the capture of magnetic beads in a 75 µm I.D. capillary [11]) were unsuccessful. Two magnetic tweezers were therefore positioned at each trapping point to generate a higher magnetic field gradient by focusing the magnetic field lines. Accordingly, two pairs of magnetic tweezers were positioned at both sides of the capillary (i.e., one pair at 15 cm from the ground side, and another pair at 14 cm from the first one) to allow magnetic beads to circulate in the capillary zone defined by these magnetic tweezers. To generate sufficient magnetic fields to capture magnetic microbeads inside a 50 µm capillary, big coils were needed, as can be seen in Fig. 2B. In addition, two cameras were required to follow the circulation of magnetic beads. Synchronization of the activation / deactivation of magnetic tweezers, which is needed to capture and release magnetic beads in different in-capillary operations, is another critical point which is not trivial with a commercial CE instrument. For all these reasons, a purpose-made setup was developed and employed. Note that the tweezers were positioned on a straight capillary instead of a coiled one to avoid generation of magnetic fields at different unwanted points (see Fig. 2B). All fluidic controls were carried out from the ground end of the capillary, and the high voltage was insulated in a safety cage. The details of a typical on-line dual-stage enrichment workflow using our purpose-made instrument are given in Table 1. In this protocol, beads are aspired into the capillary from the HV end. This is followed by back-and-forth circulation of magnetic beads in a sample flow. Elution is then carried out with an eluent flow injected from the HV end of the capillary prior to on-line electrokinetic preconcentration and separation of eluted analytes.

Table 1. Typical operation protocol for on-line capture, elution, fluorescent labeling and CE-LEDIF of dsDNA using the purpose-made instrument

Step	**Operation**	**Working vial**	**Pressure (mbar)**	**Dual pairs of tweezers 1**	**Dual pairs of tweezers 2**	**HV**	**Time (min)**
1	Aspiration of magnetic beads	**Ampure XP**	-300	OFF	ON	OFF	1

2	Forward flow of dsDNA standard solution	Mixture of DNA / ampure	-200	OFF	ON	OFF	6
3	Backward flow of dsDNA standard solution	Mixture of DNA / ampure	200	ON	OFF	OFF	10
4	Elution and labeling	Gelgreen	-200	OFF	ON	OFF	6
5	Elution and labeling (Repeat 4 times)	Gelgreen	200	OFF	ON	OFF	6 x 4
			-200	OFF	ON	OFF	
6	Preconcentration	BGE	0	OFF	OFF	ON	2
7	CE separation	BGE	-50	OFF	OFF	ON	25

3.2. Methodological development for purification and CE-LEDIF analysis of the target DNA fragment

dsDNA labeling and CE-LEDIF of labelled DNAs

DNA separation by CE conventionally relies on coated capillaries, as well as intercalating dyes (e.g., ethidium bromide, SYBR green) for fluorescent detection of DNAs [30, 31]. Capillary coating was not desirable in the presence of circulating microparticles according to our preliminary tests, probably due to possible collision of the circulating particles to the capillary wall. In addition, straightforward and fast operations are required in our case because all forefront sample treatment steps prior to CE preconcentration / separation and fluorescent detection of DNA (including DNA purification, elution and fluorescent tagging) are expected to be sequentially performed in-capillary. We therefore put our efforts to develop a new coating-free CE method with a fluorescent tagging protocol for these purposes. This approach to stain dsDNA is based on an alternative dye that was found to be safer, more stable and more sensitive than traditional ones [32]. This dye, named Gelgreen, intercalates in the DNA strands, allowing the detection of the DNA-dye complex at excitation and emission wavelengths of 480 nm and 520 nm, respectively, which can be provided with a LED-based detector. A two-level-three-factors (3^2) ½ fraction experiment was designed to optimize the labelling protocol, including (i) the dye / dsDNA ratio (v/v) (from 0.2 to 2), (ii) the incubation time (15 to 60 minutes) and (iii) the incubation temperature (low 20ºC and high 30ºC). Among the investigated factors, the dye / dsDNA volume ratio was found to provide the highest

impact on the labeling performance. As can be seen in Fig. S2 in the ESI, the fluorescent intensity at a dye / dsDNA volume ratio of 1/5 is superior to that obtained with the ratio of 1/1. The obtained fluorescent signals were found stable for 3- 5 days at room temperature. The incubation time was also optimized, and was found to provide the best performance at 25 min for the chosen dye / dsDNA volume ratio of 1/5. The incubation time was nevertheless found to have less impact than the volume ratio.

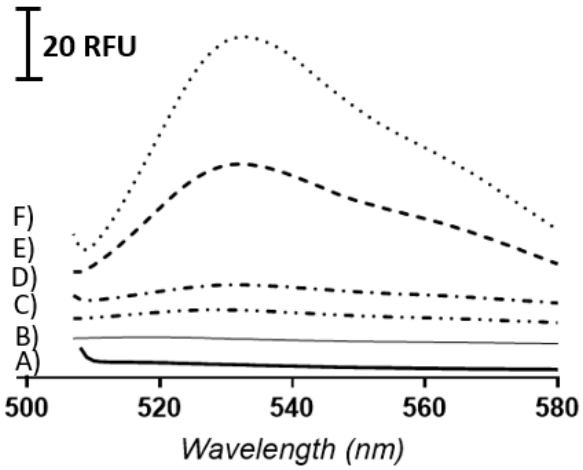

Fig. S2. Fluorescent intensity obtaining by FP-750 Spectrofluorometer for dsDNA ladder labeling conditions using GreenGel in term of different ratio volume V_{gel}: V_{dsDNA} (µl: µl).
A) Gelgreen; B) Ratio volume V_{dye}: V_{dsDNA} (µl: µl) of 2:1; C) Ratio volume V_{dye}: V_{dsDNA} (µl: µl) of 1:1; D) Ratio volume V_{dye}: V_{dsDNA} (µl: µl) of 0.8:1; E) Ratio volume V_{dye}: V_{dsDNA} (µl: µl) of 0.5:1; F) Ratio volume V_{dye}: V_{dsDNA} (µl: µl) of 0.2:1

We next examined the coating-free CE of fluorescently labeled DNAs. From our previous studies [19, 20, 33, 34], BGEs composed of large weakly charged molecules were found to offer high performance (in terms of higher separation resolution and higher signal intensity) for CE-LIF analysis of biomolecules, thanks to the better stacking effect and the possibility to modulate and suppress the electro-osmotic flow (EOF) without recourse to any capillary coating, as well as to minimize unwanted adsorption of biomolecules to the capillary wall. Accordingly, CE separations of DNA were implemented using BGEs at pH 7-9 composed of one organic acid (i.e., CAPS, MOPS or CHES) and one organic base (i.e., Tris, triethanolamine, diethanolamine or ethanolamine). High EOF magnitudes (more than $35x10^{-5}$ $cm^2/V/s$) achieved with the BGE's ionic strength (IS) of 30-50 mM were required in our conditions in order to sweep the negatively charged dsDNA fragments counter their electrophoretic mobilities towards the detector. Among all tested BGEs (see Fig. S3 in the ESI), the one composed of diethanolamine and CHES at ionic strength of

40 mM (pH 8.4) was chosen as the optimal as it offers the highest signal intensity. Note that in this proof-of-concept work, only one target analyte (300 bp DNA fragment) was extract specifically prior to its electrokinetic preconcentration and CE separation, so a high-resolution separation method was not needed. We therefore did not put our effort to develop a high-resolution CE method, as long as the main peak of the target analyte was well observed and quantifiable after the dual-stage preconcentration step.

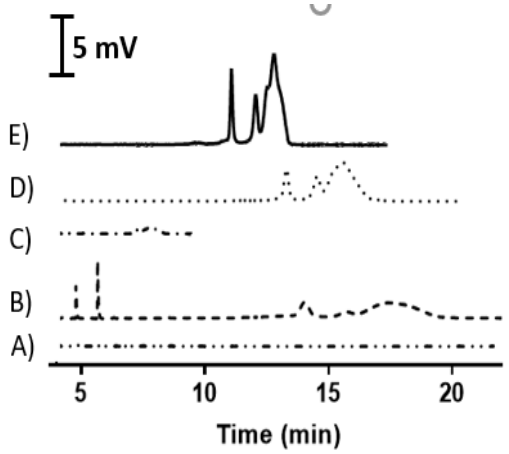

Fig. S3. CE-LEDIF separation of dsDNA ladders using different BGE compositions. CE conditions: uncoated fused silica capillary of 50 µm I.D., 50 cm effective length and 60 cm total length; HV of 25 kV; detection at excitation / emission wavelengths of 480 and 520 nm, respectively. A) Tris-CHES 50 mM pH 8,4; B) Diethanolamin-MOPS 40 mM pH 7.2; C) Diethanolamin-CAPS 50 mM pH 9.2; D) Diethanolamin-CHES 40Mm pH 8.4; E) Triethanolamin-CHES 40mM pH 8.4.

Off-line dsDNA purification and on-line electrokinetic preconcentration of eluted and labelled dsDNA

An off-line DNA purification protocol was then developed to extract selectively a target DNA fragment (300 bp in our study) from a DNA mixture. Here we used the Ampure XP magnetic bead suspension dedicated to the purification and selection of a defined dsDNA size, based on the volume ratio between the Ampure XP suspension and DNA ladder sample (see reference [35] and Fig. S4 in ESI for the working principle). Briefly, DNA precipitation relies on solid-phase reversible immobilization, in which negatively charged magnetic beads can reversibly bind to target DNA under specific concentrations of polyethylene glycol (PEG) and NaCl salt. The size of a target DNA to be captured can be tuned by adjusting the volume ratio of Ampure XP kit (a commercial buffer solution containing magnetic beads, PEG and salt) to DNA solution. For the

extraction of the 300 bp fragment, the volume ratio of 0.9:1 (or 0.9X) was chosen.

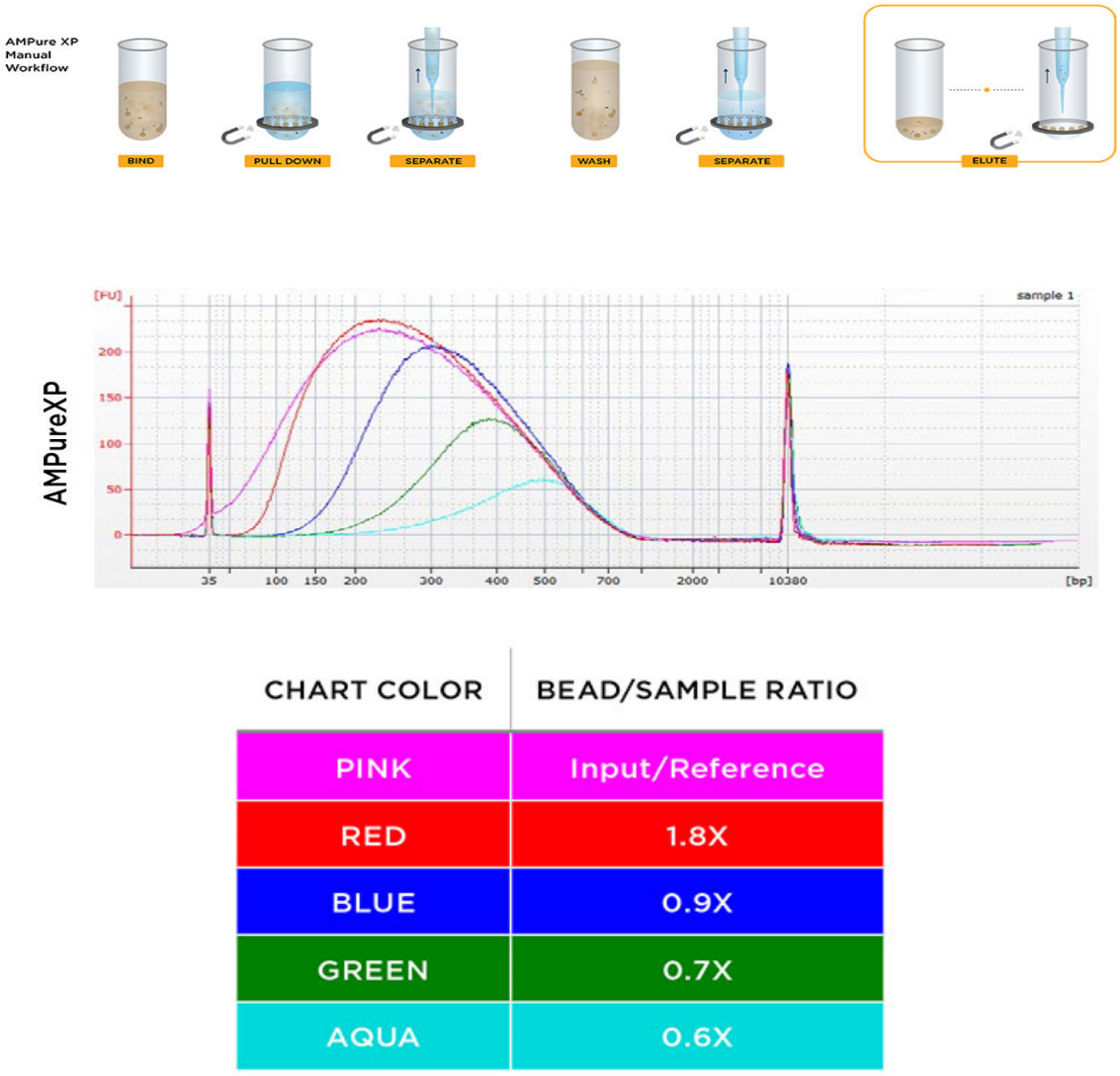

CHART COLOR	BEAD/SAMPLE RATIO
PINK	Input/Reference
RED	1.8X
BLUE	0.9X
GREEN	0.7X
AQUA	0.6X

Fig. S4. Workflow for DNA purification using the Ampure XP beads. For more information, refer to the instructions for use provided by BeckmanCoulter https://www.beckman.fr/reagents/genomic/cleanup-and-size-selection/pcr/performance

The dye solution was then used to elute the DNA fragments previously retained on beads, and at the same time fluorescently label the eluted ones. Fig. 3 shows the electropherograms obtained for CE-LEDIF analysis of a 300 bp dsDNA fragment with and without forefront off-line treatment with Ampure XP. A preconcentration factor of 3 was expected for the former case, based on the ratio between elution volume and that of the sample containing Ampure XP and dsDNA. From Fig. 3, the observed peak intensity was found 3-fold higher when using Ampure XP, demonstrating no significant loss of the target DNA fragment after its capture, elution and fluorescent labeling. Note that the peak of DNA is relatively large, compared to the performance obtained with conventional

capillary gel electrophoresis. In our work (at the proof-of-concept stage), we had to find a compromise between bead circulation, good fluorescent labeling without residual peak and separation resolution. As long as only one DNA peak is concerned, this would not pose any problem of peak identification.

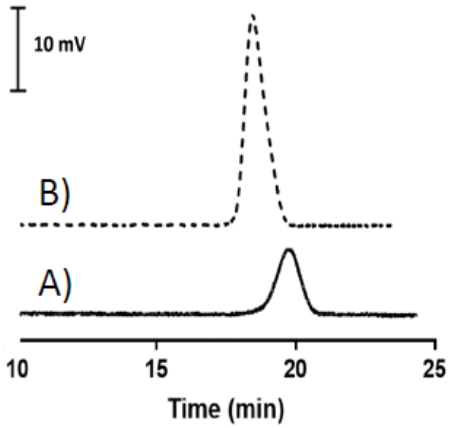

Fig. 3. Separation and detection of labelled 300 bp DNA fragment with CE-LEDIF. A) Electropherogram of DNA 300 bp fragment (1 ng/µL in water) without purification; B) Electropherogram of DNA 300 bp fragment (1 ng/µL in water) purified and enriched with the Ampure XP suspension. CE conditions: BGE: Diethanolamine / CHES at ionic strength of 40 mM and pH 8.4; uncoated fused silica capillary of 50 µm I.D., 40 cm effective length and 70 cm total length; HV of 25 kV; detection at excitation and emission wavelengths of 480 and 520 nm, respectively.

The protocol was then tested with a DNA ladder (100-700 bp), and the electropherogram for the purified and enriched DNA fragment was compared to that from the whole DNA ladder (Fig. 4). The peak for 300 bp fragment was well extracted and 3-fold enriched (based on peak height comparison), confirming the good performance of the method when applying to a DNA standard mixture. A small peak close to the principle one was as well observed (Fig. 4), probably due to the (partial) co-extraction of the 400 bp fragment when using the Ampure XP / DNA ratio of 0.9X.

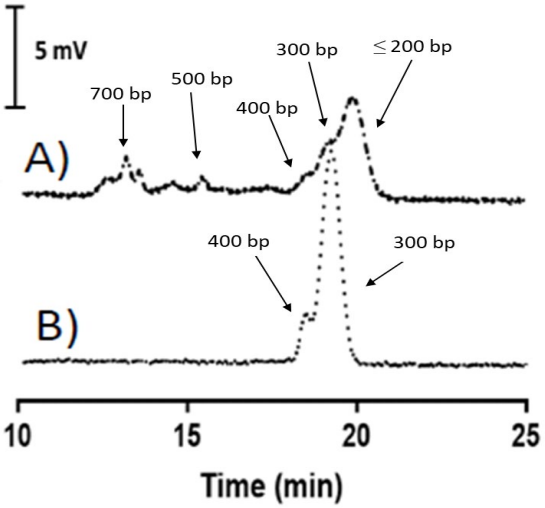

Fig. 4. Separation and detection of labelled dsDNA ladder (100-700 bp) with CE-LEDIF, with and without forefront off-line purification using the Ampure XP suspension. CE conditions as in

The last step of the protocol, i.e., electrokinetic preconcentration of the target eluted and labeled DNA fragment (300 bp) via LVSS with polarity switching, was then investigated. The eluent, obtained after off-line elution of DNA from Ampure XP-beads and fluorescent labeling of DNA, was used as the CE sample. This eluent solution filled up to 60 % of the capillary volume. A voltage of -25 kV was then applied to trigger the electrokinetic preconcentration process. An elevated EOF magnitude is required at this stage to drag the labeled DNA fragment in the capillary towards its inlet, and at the same time allow the BGE to gradually replace the sample matrix inside the capillary. This can be achieved using a sample matrix (the dye in water in our case) with a conductivity much lower than that of the BGE during LVSS preconcentration [19]. The dye in water was considered the most relevant elution solution, as it allows at the same time elution of the captured DNA from beads (thanks to electrostatic repulsion of negatively charged DNA fragments and carboxylic beads in an aqueous medium), fluorescent labeling of the released DNA, and provides a low matrix conductivity which is required for subsequent electrokinetic preconcentration of the labelled DNA fragment. The polarity of the HV was then switched when the BGE replaced the dye matrix in the capillary, in order to implement a transition to CE separation of the enriched and labelled DNA fragment (300 bp). As can be seen in Fig. S5 in ESI, successful preconcentration of the target DNA fragment was achieved for various concentrations. Good calibration curves were achieved in both cases, with the coefficient of determination, R^2, better than 0.991.

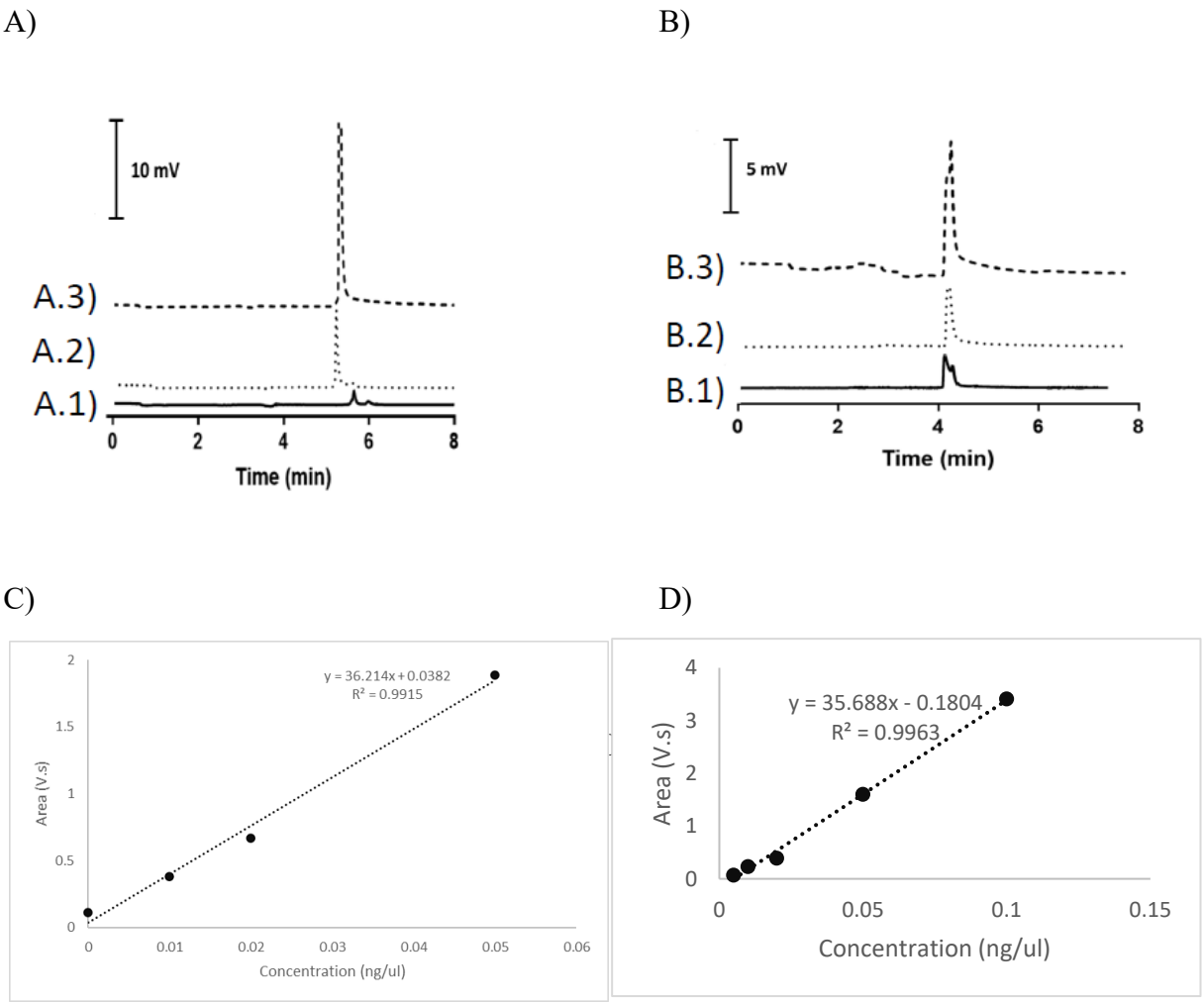

Fig. S5. Electropherograms for electrokinetic preconcentration of DNA eluents using LVSS with polarity switching and CE-LEDIF separation of the enriched DNA fragments. A) The sample containing a 300 bp DNA fragment at different concentrations, purified with Ampure XP at the ratio of 0.9X; A.1) Blank; A.2) 0.01 ng/µL; A.3) 0.05 ng / µL
B) The sample containing DNA ladder (100-700 bp) at different concentrations, purified with Ampure XP at the ratio of 0.9X. BGE: Diethanolamine / CHES at IS of 40 mM and pH 8.4. B.1) Other CE conditions as in Fig. S3.
C) and D) Calibration curves obtained for the tests (A) and (B), respectively.

3.3. On-line dual-stage enrichment and CE-LEDIF analysis of dsDNA

To demonstrate the new on-line dual-stage preconcentration concept, efforts were then made to integrate into a separation capillary all steps that were discretely developed (see section 3.2), using the purpose-made instrumentation. More challenges were identified for in-capillary operations. First, injected magnetic beads from the Ampure XP suspension had to be controlled and monitored in the way that a maximum quantity could be retained by magnetic tweezers without exceeding

their capture capacity that otherwise leads to loss of magnetic beads. Second, the flowrates had to be tuned during recirculation of magnetic beads inside the capillary, in the way that the dragging force induced by the hydrodynamic flow is higher than the gravity of magnetic beads (to avoid sedimentation of beads along the capillary), and at the same time smaller than the magnetic force generated by magnetic tweezers (to allow the beads to be retained at defined points over the capillary). Optimizations of in-capillary operations were therefore implemented in two stages to overcome these hurdles. In the first stage, focus was put on the electrokinetic preconcentration of released and labelled DNA fragment in the presence of magnetic beads and dye inside the capillary. Accordingly, all steps except for the capture of 300 bp DNA fragment on magnetic beads, *i.e.*, steps 2-7 in Fig. 1, were realized on-line, using magnetic beads retaining this DNA fragment (with step 1 carried out off-line) as the starting point. It was found that if magnetic beads were not successfully trapped at the elution step (step 3 in Fig 1), failure of LVSS occurred where several scattered peaks of this DNA fragment were observed (see Fig. S6 in ESI).

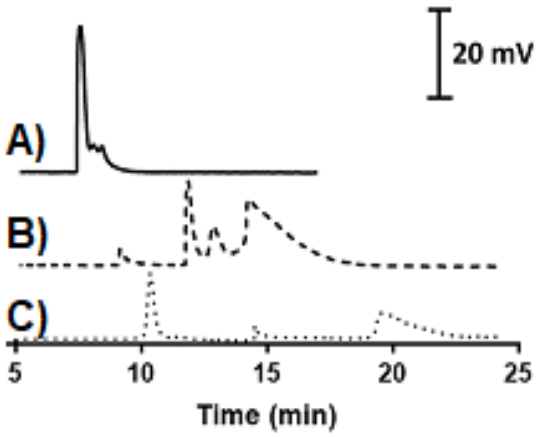

Fig. S6. LVSS of DNAs after in-capillary release from trapped magnetic beads. A) Most of magnetic beads were trapped with dual pairs of magnetic tweezers during the elution step; B) Magnetic beads were partially trapped with dual pairs of magnetic tweezers during the elution step; and C) Magnetic beads were not well retained using only one single pair of magnetic tweezers during elution. Failure of LVSS was more evident with the cases (B) and (C) where with several scattered peaks were observed.

During LVSS of the released DNA fragment under high voltage application (step 4 in Fig. 1), if the magnetic beads were always trapped by magnetic tweezers, they created a barrier inside the capillary, preventing the EOF to flow fluently. The EOF was accumulated to some certain point until the accumulated force can break the cluster of magnetic beads, resulting in failure of LVSS

due to flow perturbation during the electrokinetic preconcentration process (see Fig. S7 in ESI).

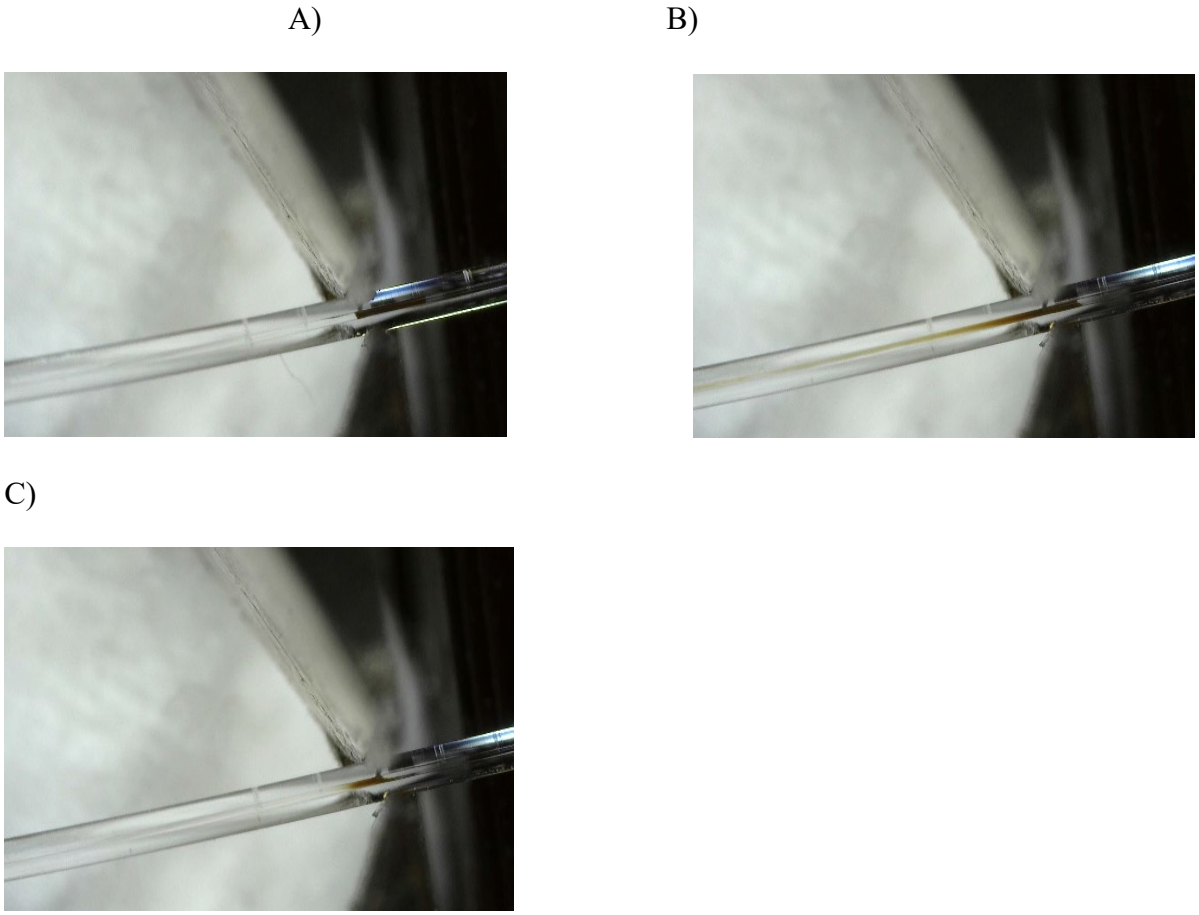

Fig. S7. Behavior of trapped magnetic beads during LVSS of released DNA fragments. A) All beads were trapped at pair of tweezers. B) A back-flow appeared during LVSS, pushed the beads'blog to inlet. C) The blog of beads was broken and the failure of LVSS.

In order to avoid this unwanted phenomenon which mechanism was not elucidated yet, the magnetic tweezers were turned off to release the beads during LVSS. By fully trapping magnetic beads at the elution step (step 3), and releasing them during the LVSS step (step 4), we were able to obtain a single peak of the released, labelled and enriched 300 bp DNA fragment by CE-LEDIF (see Fig. 5). The current was stable at 14-15 µA during the electrokinetic preconcentration and separation operations (steps 5-6), without any problem of current drop or blockage observed. The peak heights and peak areas are well correlated to the DNA concentrations (Fig. 5), proving the successful operation of these steps. A good calibration curve was acquired for 4 different concentrations with the coefficient of determination (R^2) of 0.9904 and the limit of quantification of 2.5 ng/µL. Satisfactory intra-day repeatability was achieved for the peak of DNA at 5 ng/µL, with RSD of 3.3 % for migration times and 3.9 % for peak areas, respectively. As only one single

peak of the target DNA was expected after the dual-stage preconcentration steps, some fluctuation of migration time would be tolerable for the peak identification.

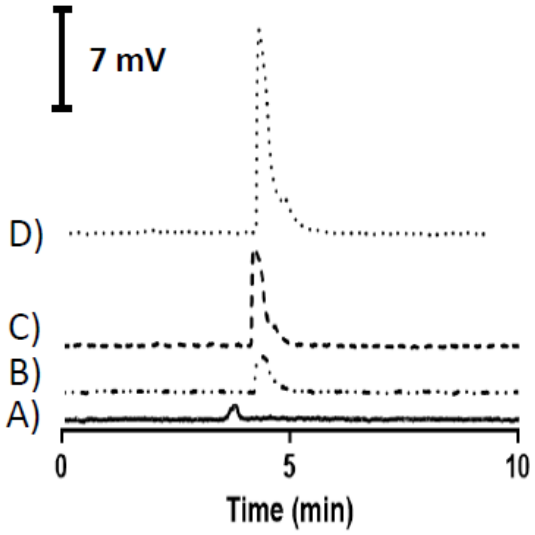

Fig. 5. DNA 300 bp fragments at different concentrations purified off-line, then on-line eluted, labelled and electrokinetically preconcentrated prior to CE-LEDIF analysis. (A) Dye in water (blank); CE-LEDIF of dsDNA 300 bp at (B) 2,5 ng/µL; (C) 5 ng/µL; (D) 10 ng/µL. Other CE conditions as in Fig. 3. Note that the dye gives the fluorescent signal only when it intercalates in the DNA fragment, therefore there is no peak of free dye.

In the second stage, all steps in the protocol (steps 1-7 of Fig. 1) were subsequently realized in the capillary, where the 300 bp DNA fragment was captured, released, labelled, and electrokinetically preconcentrated prior to CE separation. A flow of the DNA standard solution (3 µL) was flushed through the circulating magnetic beads in the capillary for magneto-extraction of target DNA fragments (stage 1). Indeed, to circulate the magnetic beads and to avoid the permanent falling of beads onto the capillary wall, the sample flow should be high enough so as the hydrodynamic force generated by the sample flow is stronger than the beads' gravity force. The sample flow therefore passes through the beads during their circulation. To assure high efficiency of DNA release and labeling at the same time, at the elution step (step 5 in Fig. 1) the same plug of dye in water (0.5 µL) was flushed back-and-forth 4 times inside the capillary through the trapped magnetic beads. The magnetic beads were then released upon triggering of the LVSS process (stage 2). The elution volume in the on-line in-capillary mode was 0.5 µL, compared to 60 µL in the off-line batchwise operation. Fig. 6 shows the electropherograms obtained from this on-line dual-stage preconcentration process for the target DNA fragment at different concentrations, with satisfactory linearity (R of 0.987 for peak areas, see Fig. S8 in the ESI).

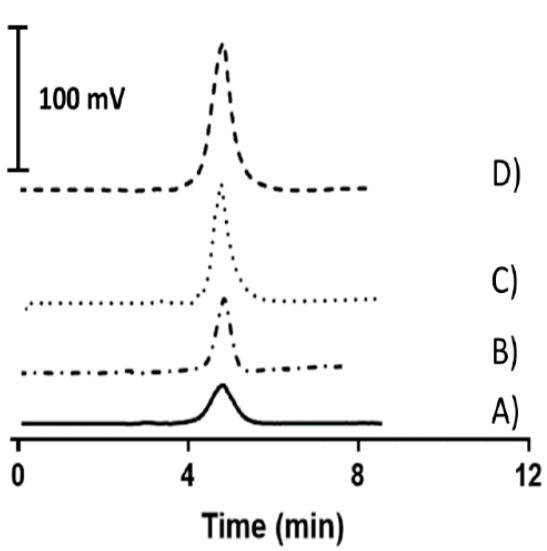

Fig. 6. Electropherograms for CE-LEDIF analysis of the dsDNA 300 bp fragment at different concentrations (3 – 5 – 7 – 10 ng /μL) after on-line extraction, elution, fluorescent labeling and electrokinetic preconcentration. Other CE conditions as in Fig. 3.

Each concentration was repeated three times, and the repeatability for peak areas was satisfactory (RSDs < 9 % for all tested concentrations, see Fig. S8), considering that these RSD values were due to the accumulation of all operational variations from different on-line steps.

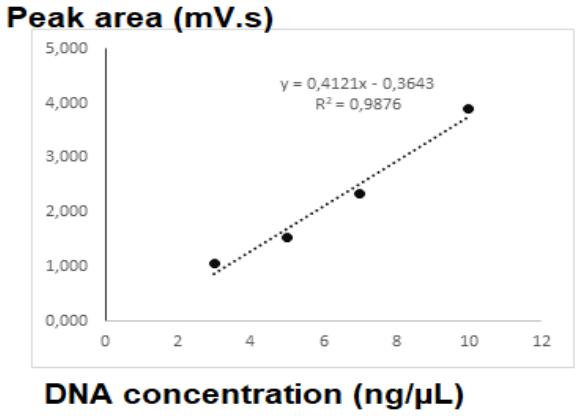

DNA concentration (ng/µL)	Peak area 1	Peak area 2	Peak area 3	RSD %
10	4.25	3.55	3.91	8.96
7	2.52	2.37	2.15	7.93
5	1.60	1.62	1.41	7.53
3	1.08	1.02	1.09	3.56

Fig. S8. Calibration obtained with electropherograms for online dual-stage enrichment of dsDNA 300 bp fragment at different concentrations and the respective repeatability data

A preconcentration factor of 125 was achieved with our approach, compared to CE of dsDNA without LVSS (calculated from the ratios of peak area *vs.* DNA concentration). To further demonstrate the applicability of our approach, the dual-stage enrichment protocol was applied for extraction and detection of dsDNA 300 bp fragment spiked in the cerebrospinal fluid (CSF) and cell culture supernatant matrices (Fig. S9 in the ESI). Detection of target DNA in CSF helps improve the diagnosis of central nervous system tumors [36], whereas analysis of cell-free DNA in cell culture supernatant allows understanding of the physical and biological characteristics of DNA in human biology [37].

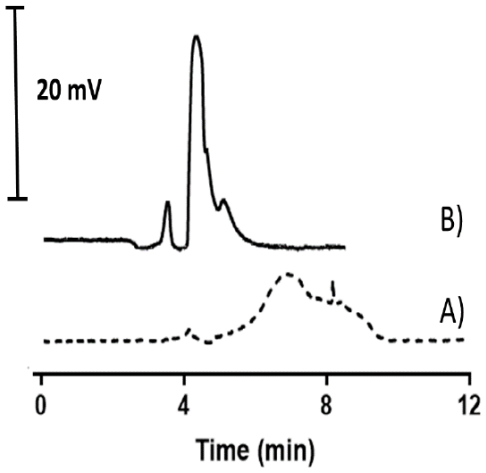

Fig. S9. Electropherogram for online dual-stage enrichment of dsDNA 300 bp fragment (3ng/µL) spiked in diluted cell culture supernatant (A) and cerebrospinal fluid (B) matrices. BGE: Diethanolamine / CHES at IS of 40 mM and pH 8.4. Other CE conditions as in Fig. S3.

The DNA peaks were clearly observed, demonstrating successful magneto-extraction and electrokinetic preconcentration of the target DNA even with the complexity of the media. Compared with the DNA peaks obtained with DNA standards (Fig. 6), those from spiked biological samples were more broadened, with the more pronounced for the cell culture supernatant one. This degradation of the CE separation performance is probably due to adsorption of matrix compounds (notably proteins) on to the capillary wall, which would occur when working with biological samples. This is indeed an inherent problem of the CE technique, regardless of the on-line preconcentration methods used. Forefront protein depletion and / or further investigation on capillary coating strategies would be needed to eliminate / alleviate this challenge. These optimizations nevertheless are envisaged in another subsequent bio-application work. It is worthy to note that the signal achieved with Fig. 6 is almost 10-fold higher than that obtained with Fig. 5 for the same DNA concentration of 5 ng/µL. This difference indeed reflects perfectly the performance superiority of the proposed dual-stage preconcentration approach over conventional solid-phase-extraction (SPE) one. Fig. 6 was obtained with all steps (DNA capture, release, labelling, enrichment, and CE separation) carried out on-line in the same capillary, therefore the totality of the released DNA was preconcentrated without any loss. For Fig. 5, the capture of DNA on magnetic beads was done off-line, and only part of the beads containing trapped DNA could be injected into the capillary for the subsequent on-line operations. This led to some loss of extracted DNA at the injection step, as encountered in conventional SPE protocol prior to CE separation. The total time for the entire procedure was around 75 min. Note that there is still some deadtime when

switching from one step to another using the actual stage of the purpose-made instrument. This could be improved in the next instrumental version when different modules can be piloted with the same control program.

4. Conclusions

The new on-line dual-stage preconcentration concept for CE and the associated instrument were developed and successfully demonstrated for on-line magneto-electrokinetic preconcentration, fluorescent labeling, and CE-LEDIF separation of the labeled target 300 bp DNA fragment. With our approach using circulating beads inside the CE capillary, the eluent stays inside the capillary for subsequent preconcentration and separation without any waste of pre-treated samples. Compared to other conventional on-line SPE methods, our approach with magnetic beads and tweezers offers higher flexibility and automated renewal of the solid support, which otherwise is not the case for packed particles (that required frits to hold the particles inside a capillary) nor monolithic columns (that require in situ monolithic synthesis inside a capillary). While the inaugural application was made for DNA at the actual stage of proof of concept, the proposed approach can be extended to other biomolecules (e.g., immuno-capture of proteins and peptides, precipitation of glycans), using relevant ligands to be grafted on magnetic beads. The effort is under progress to render this concept more robust and widespread used by integrating all steps in a commercial CE instrument.

Acknowledgements

This work has been financially supported by the ‘bourse d’excellence de l’ambassade de France’ (for PhD scholarship of N.V.T. Nguyen). The authors are grateful for the financial support from the Agence Nationale de la Recherche (ANR, France) with grant no. ANR-18-CE29-0005-01 and the program ‘Mobilité pour l'Elaboration de Réseaux de Recherche’ (MERR) from the Université Paris Saclay. We thank Dr. Francois Fay (Institut Galien Paris Saclay, France) for his help with the preparation of biological samples.

The authors have declared no conflict of interest.

References of PAPER 3

[1] G. Jarvas, A. Guttman, N. Miękus, T. Bączek, S. Jeong, D.S. Chung, V. Pätoprstý, M. Masár, M. Hutta, V. Datinská, F. Foret, Practical sample pretreatment techniques coupled with capillary electrophoresis for real samples in complex matrices, TrAC Trends in Analytical Chemistry, 122 (2020) 115702.

[2] M. Serra, D. Ferraro, I. Pereiro, J.L. Viovy, S. Descroix, The power of solid supports in multiphase and droplet-based microfluidics: towards clinical applications, Lab on a Chip, 17 (2017) 3979-3999.

[3] H.X. Chen, J.M. Busnel, G. Peltre, X.X. Zhang, H.H. Girault, Magnetic Beads Based Immunoaffinity Capillary Electrophoresis of Total Serum IgE with Laser-Induced Fluorescence Detection, Anal. Chem., 80 (2008) 9583-9588.

[4] P. Ramana, E. Adams, P. Augustijns, A. Van Schepdael, Trapping magnetic nanoparticles for in-line capillary electrophoresis in a liquid based capillary coolant system, Talanta, 164 (2017) 148-153.

[5] J. Schejbal, Z. Glatz, Immobilized-enzyme reactors integrated with capillary electrophoresis for pharmaceutical research, J. Sep. Sci., 41 (2018) 323-335.

[6] P. Ramana, J. Schejbal, K. Houthoofd, J. Martens, E. Adams, P. Augustijns, Z. Glatz, A. Van Schepdael, An improved design to capture magnetic microparticles for capillary electrophoresis based immobilized microenzyme reactors, Electrophoresis, 39 (2018) 981-988.

[7] J. Schejbal, R. Reminek, L. Zeman, A. Madr, Z. Glatz, On-line coupling of immobilized cytochrome P450 microreactor and capillary electrophoresis: A promising tool for drug development, J. Chromatogr. A, 1437 (2016) 234-240.

[8] T. Baciu, F. Borrull, C. Neusüß, C. Aguilar, M. Calull, Capillary electrophoresis combined in-line with solid-phase extraction using magnetic particles as new adsorbents for the determination of drugs of abuse in human urine, Electrophoresis 37 (2016) 1232-1244.

[9] L. Alexandre, A. Bendali, I. Pereiro, M. Azimani, S. Dumas, L. Malaquin, T.D. Mai, S. Descroix, Modular microfluidic system for on-chip extraction, preconcentration and detection of the cytokine biomarker IL-6 in biofluid, Sci. Rep., 12 (2022) 9468.

[10] T.D. Mai, D. Ferraro, N. Aboud, R. Renault, M. Serra, N.T. Tran, J.-L. Viovy, C. Smadja, S. Descroix, M. Taverna, Single-step immunoassays and microfluidic droplet operation: Towards a versatile approach for detection of amyloid-β peptide-based biomarkers of Alzheimer's disease, Sens. Actuators B, 255 (2018) 2126-2135.

[11] T.D. Mai, P.C. Hauser, S. Descroix, C. Crosnier de Lassichère, M. Taverna, C. Smadja, In-capillary immuno-preconcentration with circulating bio-functionalized magnetic beads for capillary electrophoresis, Anal. Chim. Acta, 1062 (2019) 156-164.

[12] L. Suntornsuk, O. Anurukvorakun, Sensitivity enhancement in capillary electrophoresis and their applications for analyses of pharmaceutical and related biochemical substances, Electrophoresis, In press (2022) 10.1002/elps.202100236.

[13] M.C. Breadmore, A.I. Shallan, H.R. Rabanes, D. Gstoettenmayr, A.S.A. Keyon, A. Gaspar, M. Dawod, J.P. Quirino, Recent advances in enhancing the sensitivity of electrophoresis and electrochromatography in capillaries and microchips (2010-2012), Electrophoresis, 34 (2013) 29-54.

[14] M. Pieckowski, P. Kowalski, T. Baczek, Combination of large volume sample stacking with polarity switching and cyclodextrin electrokinetic chromatography (LVSS-PS-CDEKC) for the determination of selected preservatives in pharmaceuticals, Talanta, 211 (2020) 120673.

[15] F. Kitagawa, S. Wakagi, Y. Takegawa, I. Nukatsuka, Highly Sensitive Analysis in Capillary Electrophoresis Using Large-volume Sample Stacking with an Electroosmotic Flow Pump Combined with Field-amplified Sample Injection, Ana. Sci., 35 (2019) 889-893.

[16] F. Kitagawa, T. Kawai, K. Otsuka, On-line Sample Preconcentration by Large-volume Sample Stacking with an Electroosmotic Flow Pump (LVSEP) in Microscale Electrophoresis, Anal. Sci., 29 (2013)

1129-1139.
[17] C.C. de Lassichere, T.D. Mai, M. Otto, M. Taverna, Online Preconcentration in Capillaries by Multiple Large-Volume Sample Stacking: An Alternative to Immunoassays for Quantification of Amyloid Beta Peptides Biomarkers in Cerebrospinal Fluid, Anal. Chem., 90 (2018) 2555-2563.
[18] A.H. Rageh, A. Kaltz, U. Pyell, Determination of urinary nucleosides via borate complexation capillary electrophoresis combined with dynamic pH junction-sweeping-large volume sample stacking as three sequential steps for their on-line enrichment, Anal. Bioanal. Chem., 406 (2014) 5877-5895.
[19] N.V.T. Nguyen, C. Smadja, M. Taverna, S. El Mousli, E. Secret, J.-M. Siaugue, L.T.H. Nguyen, T.D. Mai, Electroosmotic flow modulation for improved electrokinetic preconcentration: Application to capillary electrophoresis of fluorescent magnetic nanoparticles, Anal. Chim. Acta, 1161 (2021) 338466.
[20] T. Liénard--Mayor, B. Yang, N.T. Tran, A. Bruneel, A. Guttman, M. Taverna, T.D. Mai, High sensitivity capillary electrophoresis with fluorescent detection for glycan mapping, J Chromatogr A, 1657 (2021) 462593.
[21] F. Dusa, D. Moravcova, K. Slais, DNA puri fication and concentration by isotachophoresis in nonwoven fabric strip, Anal. Chim. Acta, 1117 (2020) 41-47.
[22] V. Datinska, I. Voracova, J. Berka, F. Foret, Preparative concentration of nucleic acids fragments by capillary isotachophoretic analyzer, J Chromatogr A, 1548 (2018) 100-103.
[23] V. Datinska, I. Voracova, U. Schlecht, J. Berka, F. Foret, Recent progress in nucleic acids isotachophoresis, J. Sep. Sci., 41 (2018) 236-247.
[24] S. Cheng, P. Wang, C. Tao, D. Zhang, Z. Li, Y. Yamaguchi, The effect of electrophoretic parameters on separation performance of short DNA fragments, Anal. Biochem., 556 (2018) 99-103.
[25] M. Frano, K. Dzuganova, P. Kois, M. Masar, DNA fragment separations by on-line combination of capillary isotachophoresis-capillary zone electrophoresis with UV detection, Electrophoresis, 37 (2016) 3084-3088.
[26] V. Datinska, P. Gheibi, K. Jefferson, J. Yang, S. Paladugu, C. Dallett, I. Voracova, F. Foret, Y. Astier, Epitachophoresis is a novel versatile total nucleic acid extraction method, Sci. Reports, 11 (2021) 22736.
[27] F. Foret, V. Datinska, I. Voracova, J. Novotny, P. Gheibi, J. Berka, Y. Astier, Macrofluidic Device for Preparative Concentration Based on Epitachophoresis, Anal. Chem., 91 (2019) 7047-7053.
[28] T. Liénard--Mayor, J.S. Furter, M. Taverna, H.V. Pham, P.C. Hauser, T.D. Mai, Modular instrumentation for capillary electrophoresis with laser induced fluorescence detection using plug-and-play microfluidic, electrophoretic and optic modules, Anal. Chim. Acta, 1135 (2020) 47-54.
[29] D. Ferraro, J. Champ, B. Teste, M. Serra, L. Malaquin, J.L. Viovy, P. de Cremoux, S. Descroix, Microfluidic platform combining droplets and magnetic tweezers: application to HER2 expression in cancer diagnosis, Sci. Rep., 6 (2016) 25540.
[30] D.S. Lian, X.Y. Chen, H.S. Zeng, Y.Y. Wang, Capillary electrophoresis based on nucleic acid analysis for diagnosing inherited diseases, Clin Chem Lab Med 59 (2021) 249-266.
[31] D.S. Lian, H.S. Zeng, Capillary Electrophoresis Based on Nucleic Acid Detection as Used in Food Analysis, Compr. Rev. Food Sci. Food Saf., 16 (2017) 1281-1295.
[32] A. Valdés, V. Garcia-Cañas, A. Cifuentes, CGE-laser induced fluorescence of double-stranded DNA fragments using GelGreen dye, Electrophoresis, 34 (2013) 1555-1562.
[33] M. Morani, T.D. Mai, Z. Krupova, P. Defrenaix, E. Multia, M.-L. Riekkola, M. Taverna, Electrokinetic characterization of extracellular vesicles with capillary electrophoresis: A new tool for their identification and quantification, Anal. Chim. Acta, 1128 (2020) 42-51.
[34] M. Morani, M. Taverna, T.D. Mai, A fresh look into background electrolyte selection for capillary electrophoresis-laser induced fluorescence of peptides and proteins, Electrophoresis 40 (2019) 2618-

2624.
[35] M. Serra, T.D. Mai, A.L. Serra, M.C. Nguyen, A. Eisele, L. Perié, J.L. Viovy, D. Ferraro, S. Descroix, Integrated droplet microfluidic device for magnetic particles handling: Application to DNA size selection in NGS libraries preparation, Sens. Actuators B, 305 (2020) 127346.

[36] A.E. McEwen, S.E.S. Leary, C.M. Lockwood, Beyond the Blood: CSF-Derived cfDNA for Diagnosis and Characterization of CNS Tumors, Front. Cell Dev. Biol., 8 (2020).
[37] A.J. Bronkhorst, V. Ungerer, S. Holdenrieder, Comparison of methods for the isolation of cell-free DNA from cell culture supernatant, Tumor Biology, 42 (2020) 1010428320916314.

Electronic supplementary data

On-line dual-layer enrichment via magneto-extraction and electrokinetic preconcentration: a new concept and instrumentation for capillary electrophoresis

Ngoc Van Thanh Nguyen[1], Claire Smadja[1*], Myriam Taverna[1,2], Lac Thuy Huu Nguyen [3], Stéphanie Descroix[4], Thanh Duc Mai[1*]

[1] *Université Paris-Saclay, CNRS, Institut Galien Paris-Saclay, 92296, Châtenay-Malabry, France.*

[2] *Institut Universitaire de France (IUF)*

[3] *Faculty of Pharmacy - University of Medicine and Pharmacy at Ho Chi Minh City - 41 Dinh Tien Hoang St., Ben Nghe Ward, District 1, Ho Chi Minh City, Vietnam*

[4] *Institut Curie, IPGG*

* Corresponding author

e-mail: thanh-duc.mai@universite-paris-saclay.fr

claire.smadja@universite-paris-saclay.fr

Keywords: Capillary electrophoresis, magneto-immunocapture, circulating magnetic beads, DNA; fluorescent detection;

Fig. S1. A) Photo of the purpose-made instrument for on-line dual-layer enrichment for CE-LEDIF analysis. B) Zoom in the setup of four pairs of magnetic tweezers for magnetic bead capture in a 50 µm I.D. capillary

A)

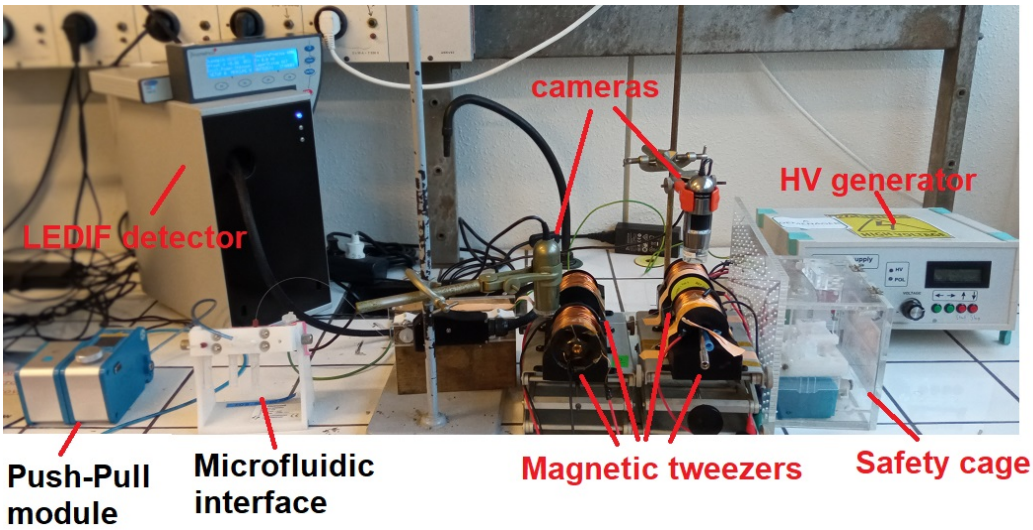

B)

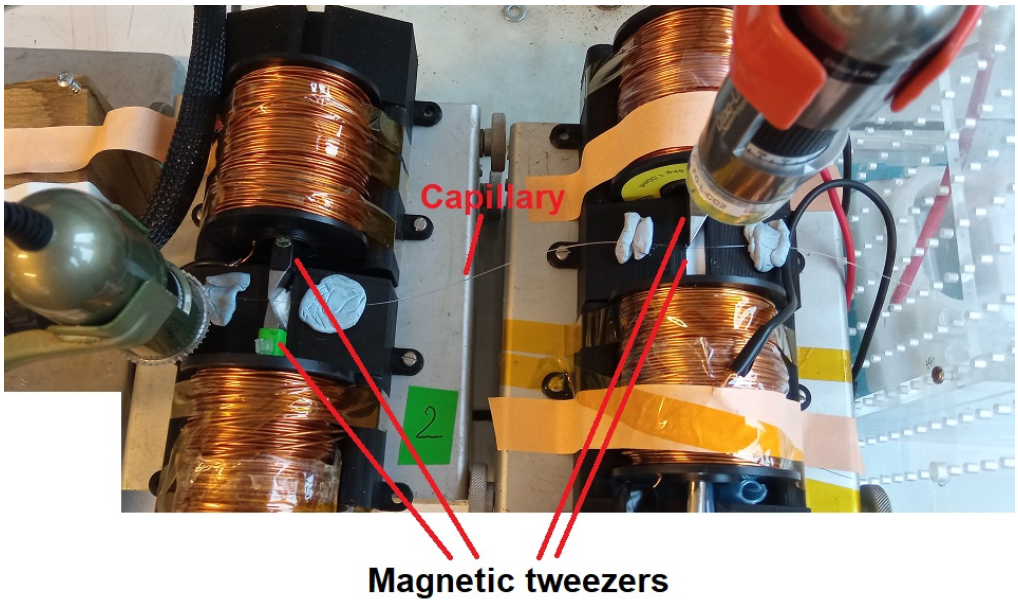

Fig. S2. Fluorescent intensity obtaining by FP-750 Spectrofluorometer for dsDNA ladder labeling conditions using GreenGel in term of different ratio volume V_{gel}: V_{dsDNA} (µl: µl).

A) Gelgreen;

B) Ratio volume V_{dye}: V_{dsDNA} (µl: µl) of 2:1;

C) Ratio volume V_{dye}: V_{dsDNA} (µl: µl) of 1:1;

D) Ratio volume V_{dye}: V_{dsDNA} (µl: µl) of 0.8:1;

E) Ratio volume V_{dye}: V_{dsDNA} (µl: µl) of 0.5:1;

F) Ratio volume V_{dye}: V_{dsDNA} (µl: µl) of 0.2:1

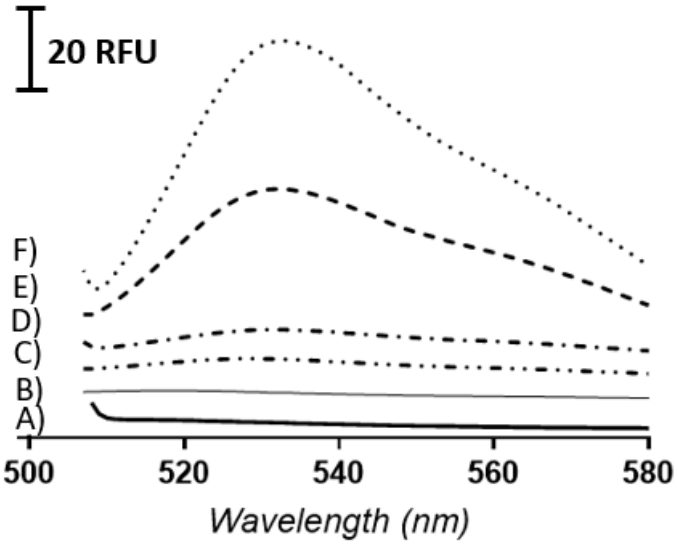

Fig. S3. CE-LEDIF separation of dsDNA ladders using different BGE compositions. CE conditions: uncoated fused silica capillary of 50 µm I.D., 50 cm effective length and 60 cm total length; HV of 25 kV; detection at excitation / emission wavelengths of 480 and 520 nm, respectively. A) Tris-CHES 50 mM pH 8,4; B) Diethanolamin-MOPS 40 mM pH 7.2; C) Diethanolamin-CAPS 50 mM pH 9.2; D) Diethanolamin-CHES 40Mm pH 8.4; E) Triethanolamin-CHES 40mM pH 8.4.

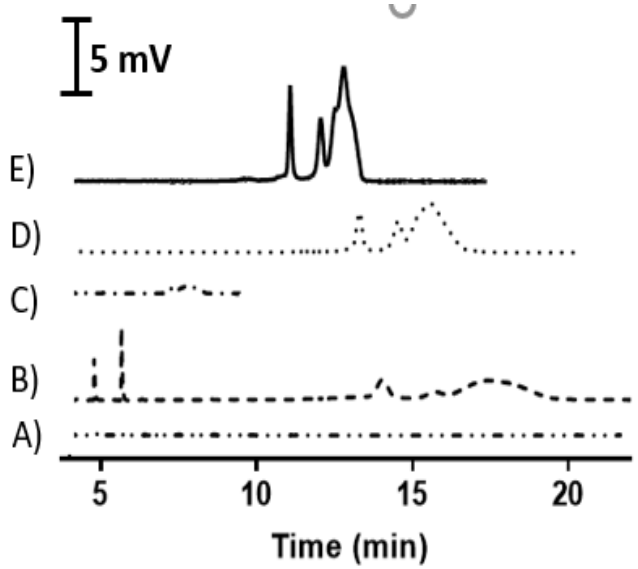

Fig. S4. Workflow for DNA purification using the Ampure XP beads. For more information, refer to the instructions for use provided by BeckmanCoulter

https://www.beckman.fr/reagents/genomic/cleanup-and-size-selection/pcr/performance

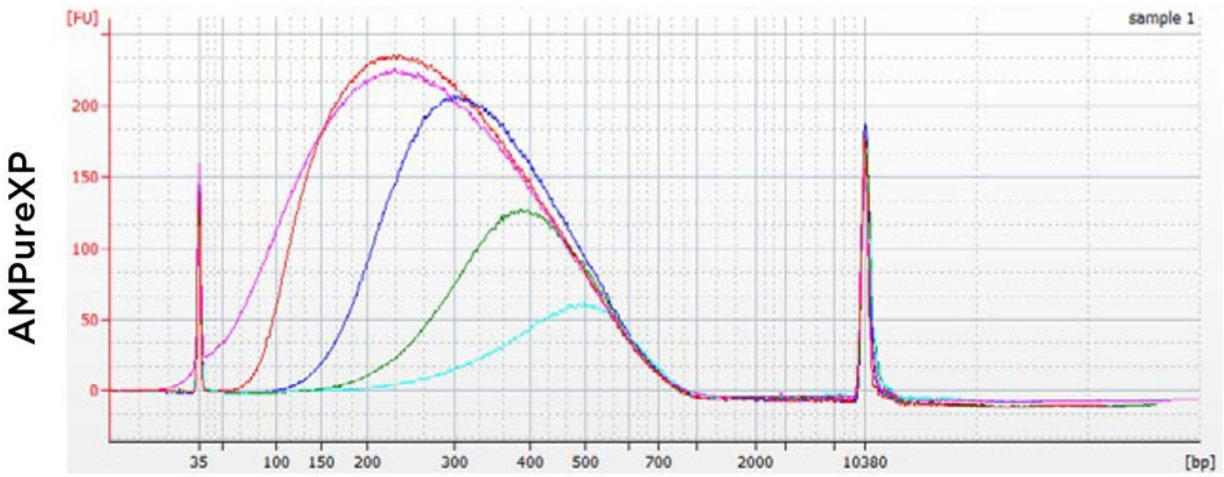

CHART COLOR	BEAD/SAMPLE RATIO
PINK	Input/Reference
RED	1.8X
BLUE	0.9X
GREEN	0.7X
AQUA	0.6X

Fig. S5. Electropherograms for electrokinetic preconcentration of DNA eluents using LVSS with polarity switching and CE-LEDIF separation of the enriched DNA fragments. A) The sample containing a 300 bp DNA fragment at different concentrations, purified with Ampure XP at the ratio of 0.9X; A.1) Blank; A.2) 0.01 ng/µL; A.3) 0.05 ng / µL

B) The sample containing DNA ladder (100-700 bp) at different concentrations, purified with Ampure XP at the ratio of 0.9X. BGE: Diethanolamine / CHES at IS of 40 mM and pH 8.4. B.1) Other CE conditions as in Fig. S3.

C) and D) Calibration curves obtained for the tests (A) and (B), respectively.

A)

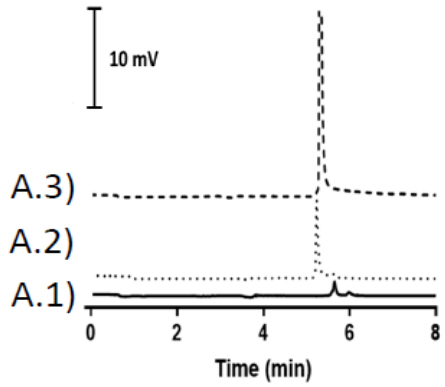

B)

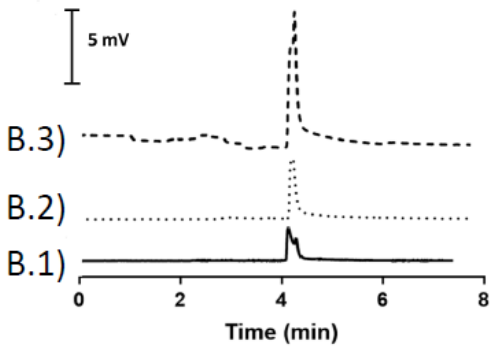

C)

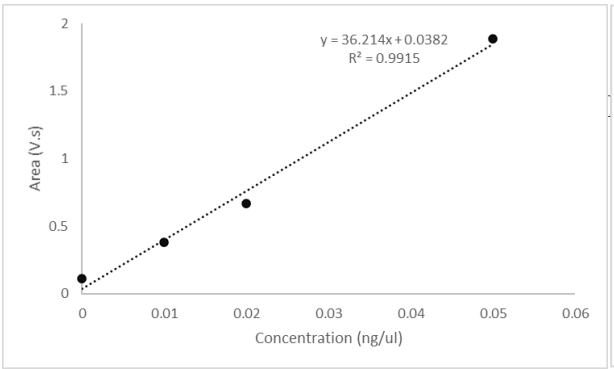

D)

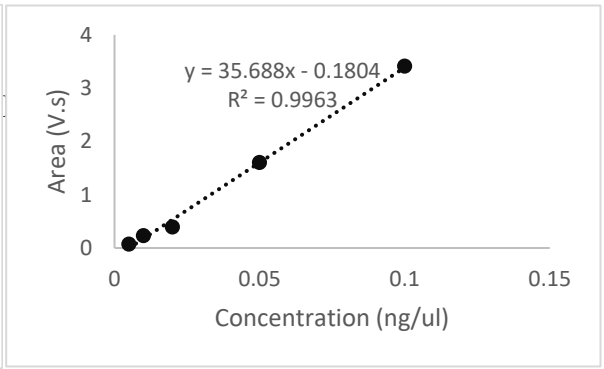

Fig. S6. LVSS of DNAs after in-capillary release from trapped magnetic beads. A) Most of magnetic beads were trapped with dual pairs of magnetic tweezers during the elution step; B) Magnetic beads were partially trapped with dual pairs of magnetic tweezers during the elution step; and C) Magnetic beads were not well retained using only one single pair of magnetic tweezers during elution. Failure of LVSS was more evident with the cases (B) and (C) where with several scattered peaks were observed.

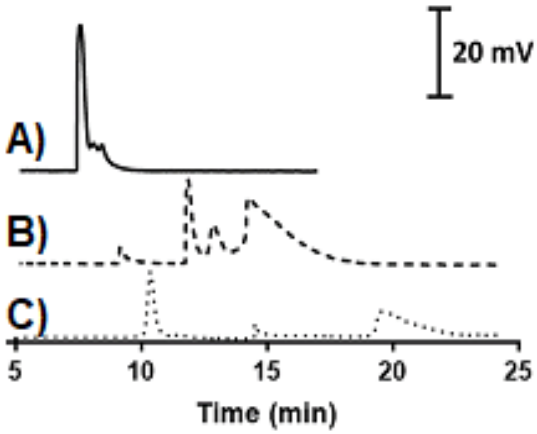

Fig. S7. Behavior of trapped magnetic beads during LVSS of released DNA fragments. A) All beads were trapped at pair of tweezers. B) A back-flow appeared during LVSS, pushed the beads'blog to inlet. C) The blog of beads was broken and the failure of LVSS.

A)

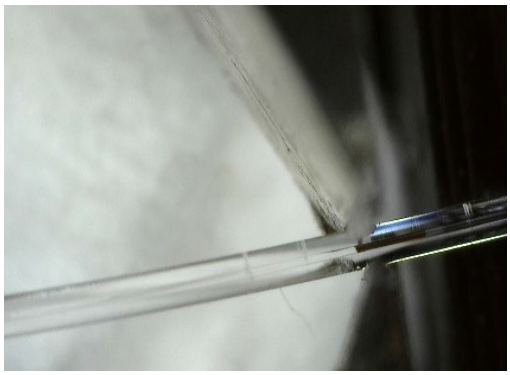

B)

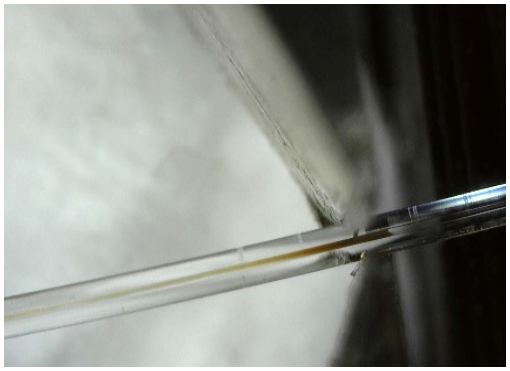

C)

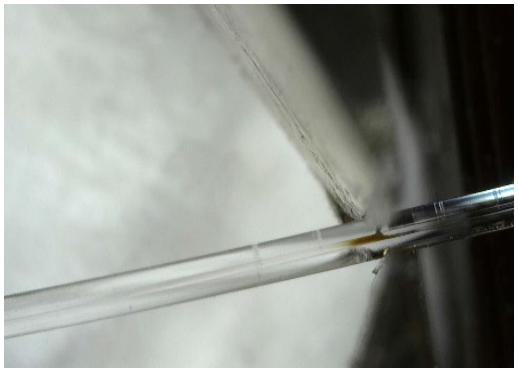

Fig. S8. Calibration obtained with electropherograms for online dual-stage enrichment of dsDNA 300 bp fragment at different concentrations and the respective repeatability data

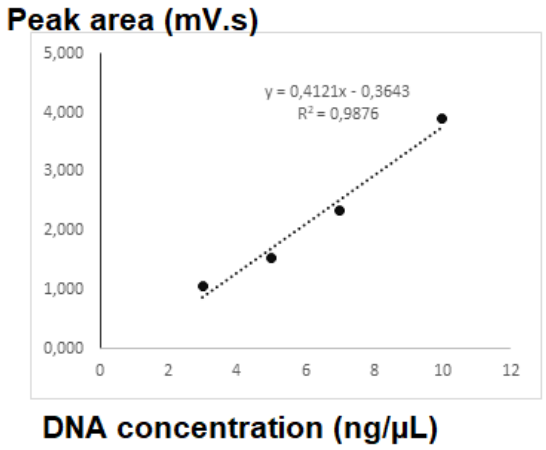

DNA concentration (ng/µL)	Peak area 1	Peak area 2	Peak area 3	RSD %
10	4.25	3.55	3.91	8.96
7	2.52	2.37	2.15	7.93
5	1.60	1.62	1.41	7.53
3	1.08	1.02	1.09	3.56

Fig. S9. Electropherogram for online dual-stage enrichment of dsDNA 300 bp fragment (3 ng/µL) spiked in diluted cell culture supernatant (A) and cerebrospinal fluid (B) matrices. BGE: Diethanolamine / CHES at IS of 40 mM and pH 8.4. Other CE conditions as in Fig. S3.

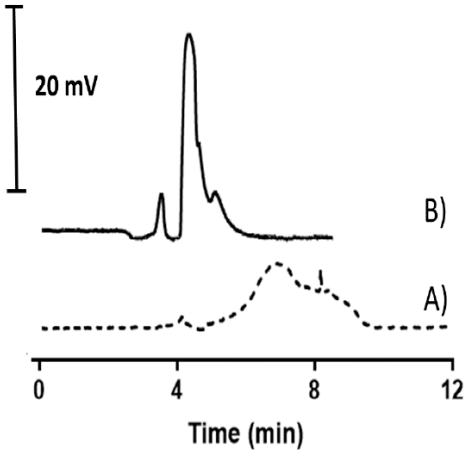

5.2 CONCLUSIONS

The new on-line concept and associated instrument of dual stage enrichment based on magneto extraction with the circulation of beads and electrokinetic preconcentration, followed by CE-LEDIF separation were successfully developed for DNA extraction and preconcentration. Our approach with magnetic beads and tweezers offers higher flexibility, robustness and automated renewal of the solid support, compared to conventional extraction methods. The extended applications for other biomolecules are envisaged.

CONCLUSIONS AND PERSPECTIVES

In this thesis, I successfully developed two innovative methods to characterize the MPs and their interaction with different (bio)molecules. One on-line extraction and enrichment approach based on the combinaison of MPs and CE was also investigated.

First, the enzymatic stratergy, SEC-LIF condions and grating protocols were developed and optimized for the immobilisation, digestion and analyse of NAB228 antibody on magnetic beads. Under the optimized conditions, more than 70 % antibodies was defined grafting in right orientation on Tosyl-activated and protein G beads. Regarding the immunoassay based on magnetic bead support for amyloid beta peptide, the antibody grafted on Protein G beads showed better performance and LOD reached 10 ng/mL. The enzymatic and SEC approach can be used for further applications targeting biomarkers. Note that the compatibility of digestion enzyme and antibody as well as magnetic beads should be take into account for each target molecule. However, the LOD is still far from the concentration of Aβ in real biosample (<1ng/mL). The size and charge of magnetic beads as well as the interaction between MPs and IgG should be optimized to increase the captured density of paptide, down to pg.

Second, a new EOF-assisted preconcentrate method was developed based-on weakly charged ions, contributes to MPs and amyloid beta 1-42 peptide enrichment prior to CE separation. The sensitivity improvement compared to CE-UV method were 340 and 18-fold, respectively. The approach could be widely applied for many purposes, such as preconcentrating biomolecules (e.g., DNA in chapter 5) or monitor the interaction of MNPs with drug at low abundant (20 µM). And the separation should be optimized when using the BGEs at very low EOF.

Third, the novel concept of dual-stage enrichment online was demontrated based on the circulation forth-and-back of MPs inside the capillary and EOF-assisted preconcentrate method (developed in chapter 4). The LOD of dsDNA 300 bp reached 3 ng/µL and enrichmnet factor was 125 folds, compared to traditional CE- LIF.

For overall perspective, these developed methods will be investigated on extraction, separation and detection of molecules in real biosamples (e.g, DNA from cellular supernatant or plasma, amyloid beta 1-42 from blood of healthy people and AD patients). The EOF-assisted preconcentration and detection by CE- LIF for Aβ1-42 peptide (chapter 4) will be used to detect the peptide eluted from antibody NAB228 immobilized on beads (chapter 3). Thus, the comparison of LOD and

reproducibility between ELISA and CE- LIF will be envisaged. For chapter 5, the optimization of homemade system to be smaller, more automatic and robust are envisaged in next step. The temperature control will be invested to achieve higher reproducibility of peak form and enrichment factor.